Investigating the Molecular Mechanisms of MPS1 localisation to Mammalian Kinetochores

Emile Roberts

Lincoln College

University of Oxford

Thesis submission for the degree of DPhil Molecular Cell Biology in Health and Disease

Michaelmas 2023

Acknowledgements

Multiple people contributed to the work presented in this thesis. Work that is not solely that of the candidate, or that has already been submitted for the candidate's undergraduate dissertation, is outlined below. All data not produced by the candidate is reproduced with the consent of those who produced it.

- Figures 1 and 3 are reproduced from the candidate's undergraduate dissertation.
- Dr Daniel Hayward solely performed the work presented in figures 2, 4, 13, 15 and 33. These data are reproduced from a joint-first author paper between him and the candidate published during the course of this study [1].
- Dr Daniel Hayward conducted the work presented in figure 14, after jointly generating the cell lines with the candidate.
- Vanessa Enoguanbhor helped to generate the cell lines shown in figure 25 and conducted preliminary experiments with helped to produce the data shown in figure 26.
- Mia Holloway generated the specific clones and Western blot used in figure 35

I am immensely grateful to Professor Ulrike Gruneberg for providing an environment for my growth and development as a scientist. The support and guidance from her and Dr Daniel Hayward has been incredibly valuable. The whole of the Gruneberg lab; Ulli, Daniel, Iona, Izzy, Zoe, James, Loki, Manton, Rhiannon, Renaud, and Christy have been wonderful to work alongside, and I am deeply grateful for their help and company. In addition, the provision of expertise by other scientists at the Sir William Dunn School of Pathology and department of Biochemistry has saved

weeks of my time, and I greatly appreciate their eagerness to assist me. Chief amongst these are Alan, Lior, Francis, Michela, Kasia, Roberto, Marion, Adam, Struan, and JL.

My family: Susie, Joe, and Oscar, have been endlessly supportive of me throughout this journey, and I do not think I would be in the place I am today without their continued love and support. It is a shame they would not understand anything written in this thesis. Additional thanks to my wonderful housemates: Emily, Lucrezia, Violaine, and Bertie who have listened to unending complaints and kept me smiling.

Finally, I would like to thank Josie. She has been astronomically supportive to me throughout my PhD and beyond. Despite not reading any of this document, it would be a lot worse without her.

Abstract

The accurate segregation of the genome during mitosis is necessary for successful cell division. Prior to anaphase the cell must ensure that all chromosomes are properly attached, via large proteinaceous structures called kinetochores, to microtubules of the mitotic spindle. Two related processes, spindle assembly checkpoint signalling and error correction, have an essential role in promoting the formation of proper microtubule attachments prior to anaphase onset. The kinase Monopolar Spindle 1 (MPS1) dynamically localises to kinetochores to initiate spindle checkpoint signalling in the absence of stable microtubule attachment, and additionally promotes error correction at improperly attached chromosomes. This thesis explores how the control of MPS1 localisation is controlled by kinase and phosphatase activity, and microtubule binding, to fulfil its role in checkpoint signalling and error correction. A new paradigm for how MPS1 localisation is coupled to microtubule binding is established wherein the balance between Aurora B kinase and Protein Phosphatase 2A-B56 determines MPS1 recruitment downstream of microtubule binding. Furthermore, the molecular mechanisms of MPS1 binding to the kinetochore are investigated, finding that auto-phosphorylation of the N-terminus of MPS1 controls its steady-state levels at kinetochores without microtubules bound. Beyond the mechanisms of MPS1 localisation to kinetochores, a detailed view of the involvement of MPS1 in error correction is developed. New evidence is provided that MPS1 participates directly in error correction, but that this attachment-destabilising function is balanced by MPS1-dependent recruitment of PP2A-B56. These findings highlight a complex interplay between MPS1, Aurora B, and PP2A-B56 which serves to control checkpoint signalling and microtubule attachment stability.

List of abbreviations

ANA	Anaphase
APC	Anaphase Promoting Complex
BUB	Budding Uninhibited by Benzimidazoles
CCAN	Constitutive Centromere Associated Network
CDC20	Cell Division Cycle 20
CDK	Cyclin Dependent Kinase
CENP	Centromere protein
CH	Calponin homology (domain)
CPC	Chromosomal Passenger Complex
ENSA	Endosulfine α
FKBP	FK506 Binding Proteins
FRAP	Fluorescence Recovery After Photobleaching
FRB	FKBP Rapamycin Binding (domain)
FRET	Förster Resonance Energy Transfer
GFP	Green Fluorescent Protein
GST	Glutathione S-Transferase
HEC1	Highly Expressed in Cancer 1
HURP	Hepatoma Up-Regulated Protein
IF	Immunofluorescence
INCENP	Inner Centromere Protein
IP	Immunoprecipitation
KD	Kinase-Dead
KMN	KNL-1/Mis12 complex/Ndc80 complex (network)
KNL1	Kinetochore null lethal 1
KT	Kinetochore
MAD	Mitotic Arrest Deficient
MALS	Multi-Angle Light Scattering
MCC	Mitotic Checkpoint Complex
MIM	MAD2-Interacting Motif
Mis12	Missegregation 12
MPS1	Monopolar Spindle 1
MR	Middle Region
MT	Microtubule
NDC80-C	Nuclear division cycle 80 - complex
NEBD	Nuclear Envelope Break-Down
NMR	Nuclear Magnetic Resonance
NOC	Nocodazole
NTE	N-Terminal Extension
PICH	PLK1-Interacting Checkpoint Helicase
PYT	Phosphotyrosine Picked Threonine Kinase
RZZ	Rod–Zw10–Zwilch (complex)
SAC	Spindle Assembly Checkpoint
SD	Standard Deviation
SEC	Size-Exclusion Chromatography
SEM	Standard Error of the Mean

SKA	Spindle And Kinetochore Associated (complex)
SKAP	Small Kinetochore-Associated Protein
STLC	S-trityl-l-cysteine
TAF	Template Activating Factor
TEV	Tobacco Etch Virus
TPR	Tetratricopeptide Repeat (domain)
UTR	Untranslated Region
WT	Wildtype

Contents

Introduction

An overview of mitosis

The ability of a cell to make new copies of itself is essential for life. In Eukaryotes, mitosis is the form of cell division which gives rise to two genetically identical daughter cells. This process is the basis for the growth, development, and maintenance of multicellular organisms. Dividing cells undergo cycles of growth and duplication of organelles and the genetic material in interphase, followed by partitioning of the replicated genome and organelles during mitosis and cytokinesis. This thesis will focus on how the replicated genome is accurately segregated during mitosis in human cells.

The nature of mitosis is the capture and segregation of chromosomes by the mitotic spindle, resulting in the separation of paired sister chromatids such that each daughter cell receives exactly one copy of each chromatid (Diagram 1). Mitosis occurs in several stages which were originally characterised by distinct morphologies of the mitotic spindle and chromatin [2–4].

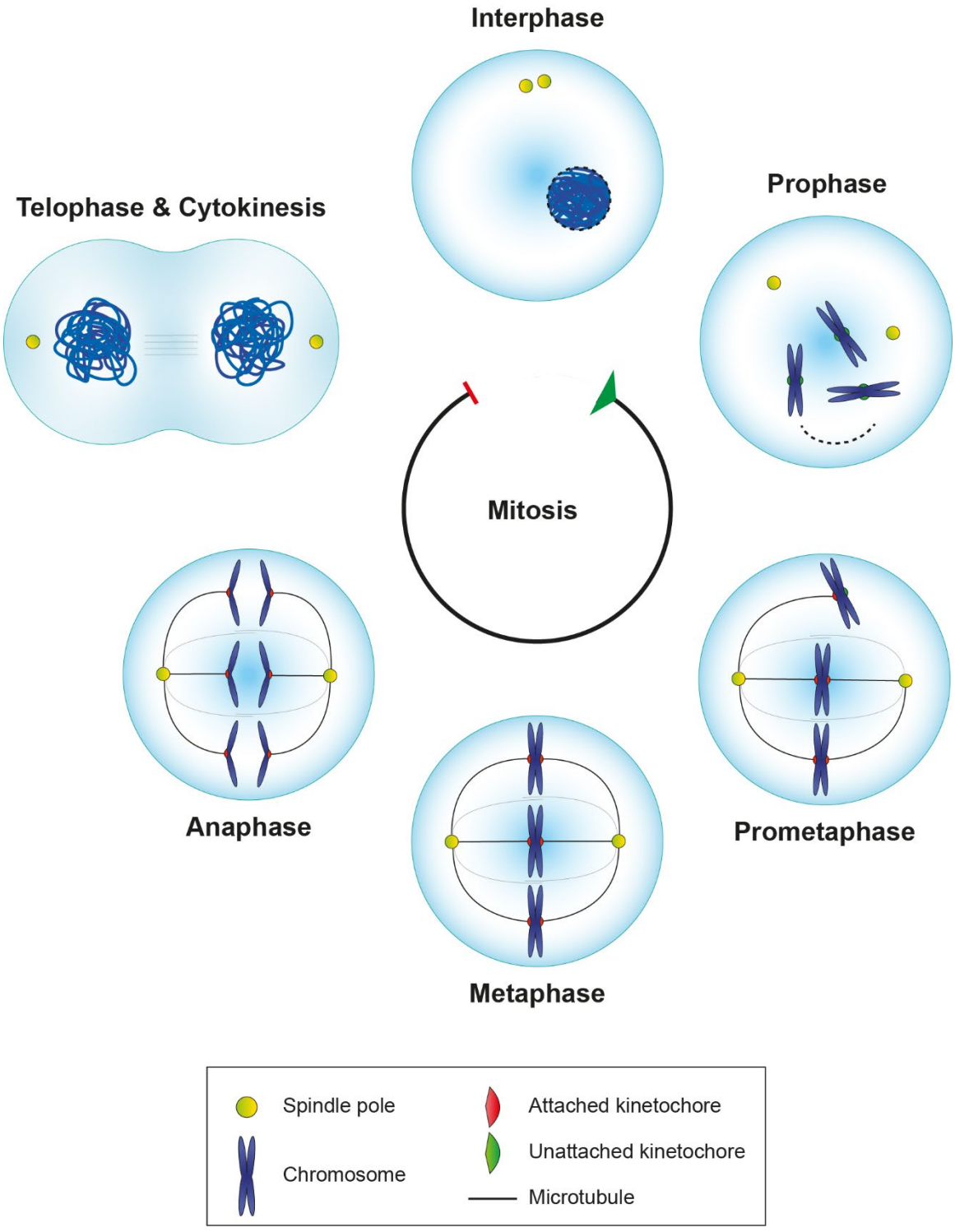

Diagram 1 – Overview of the stages of mitosis. See main text for full description.

As cells enter mitosis, in prophase, DNA condenses to form mitotic chromosomes which comprise two sister chromatids. Crucially, these replicated strands of DNA remain paired at the centromeres via topological entrapment by cohesin [5–7]. During this phase, the proteinaceous kinetochore (literally “moving place”) fully assembles atop the centromeres, such that each chromatid possesses one kinetochore. These kinetochores serve to mediate most of the interactions between the chromosomes and the mitotic spindle. The network of microtubules and other proteins known as the mitotic spindle begins to form in this phase, nucleated from two spindle poles. Additionally, in many organisms including humans, the nuclear envelope is completely disassembled allowing the contents of the nucleus to mix freely with the cytoplasm.

The extended period of pro-metaphase is characterised by the capture of chromosomes by the mitotic spindle, and their alignment at a central axis known as the metaphase plate. There are several mechanisms by which chromosomes are “congressed” to the metaphase plate which will be discussed later.

Metaphase describes the brief period during which all the chromosomes are congressed at the metaphase plate. This immediately precedes anaphase, during which cohesion between sister chromatids is lost [8] and each chromatid of a pair is pulled to opposing spindle poles by the mitotic spindle.

Telophase marks the end of mitosis – during which the chromosomes begin to decondense and the nuclear envelope reforms. This is swiftly followed by cytokinesis wherein the cell itself separates into two new cells.

The importance of attachment geometry

The importance of the correct geometry of chromosome capture by the mitotic spindle cannot be overstated. Attachment of each sister chromatid to opposing spindle poles (amphitelic attachment/biorientation) is the only geometry which ensures equal segregation of the genetic material (Diagram 2). Other states of attachment (no attachment, monotelic attachment, syntelic, and merotelic) may lead to missegregation events. Such errors are causative of structural and numeral aneuploidy, leading to cell death or tumorigenesis. Thus, it is vital that every chromosome achieves biorientation prior to anaphase onset. A mechanism known as error correction detects and rectifies incorrect attachment geometries.

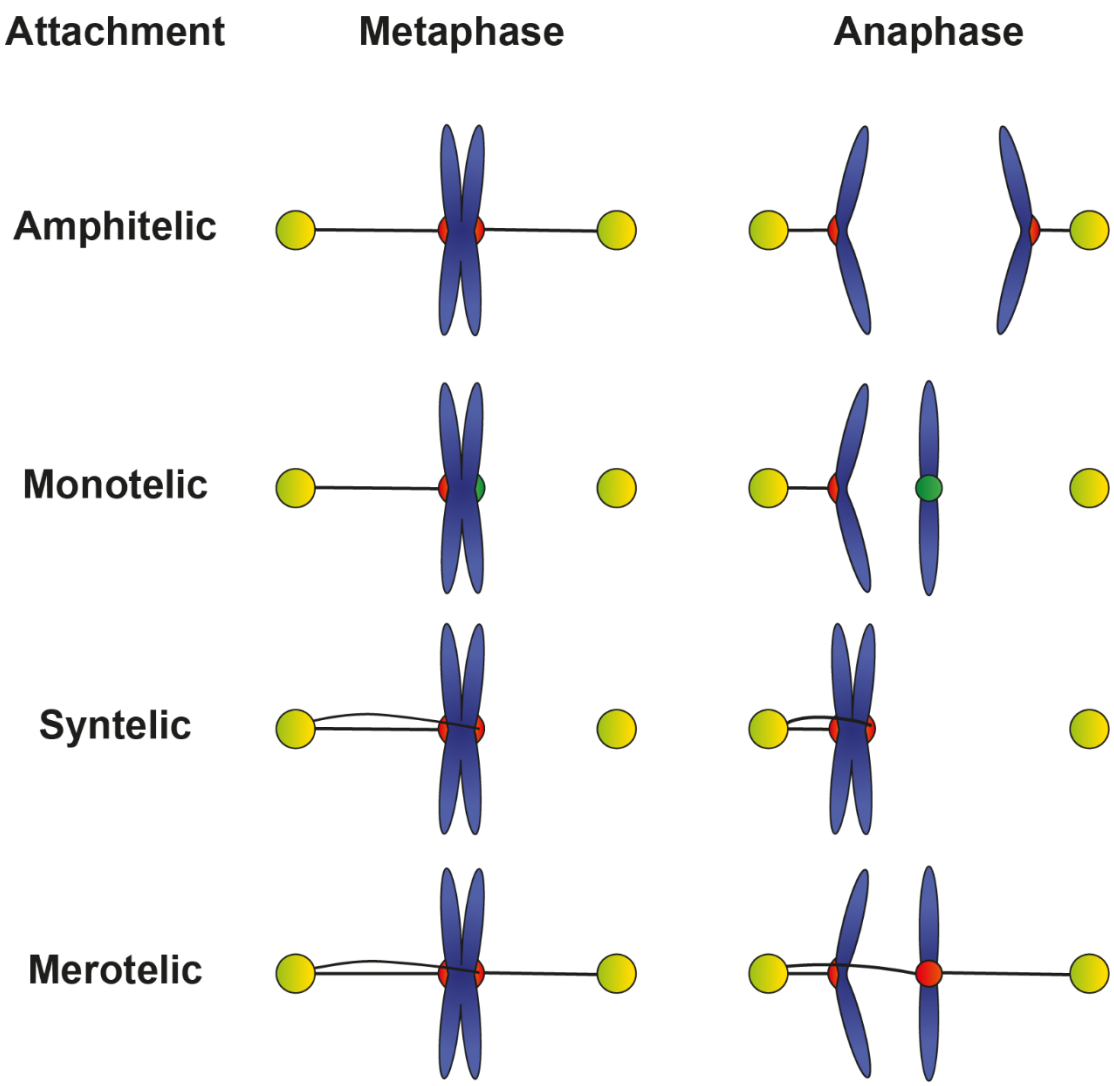

Diagram 2 - Possible attachment geometries of chromosomes to the spindle poles. Shown are the linkages between chromosomes and the spindle poles prior to anaphase onset (left) and the consequent segregation pattern of chromatids during anaphase (right).

Introduction to the spindle checkpoint

Temporal control of the phases of mitosis, as with all cell-cycle processes, is of great importance. If a cell were to enter anaphase prior to the biorientation of every single chromosome, then segregation errors would result (Diagram 3). A mechanism known as the spindle assembly checkpoint (SAC) serves to ensure that anaphase is only entered once metaphase has been achieved. Together, error correction and the spindle assembly checkpoint ensure that cells only progress into anaphase after all chromosomes are bioriented on the metaphase plate. These two processes form the focus of this thesis – specifically the involvement of a protein kinase known as monopolar spindle 1 (MPS1) in both.

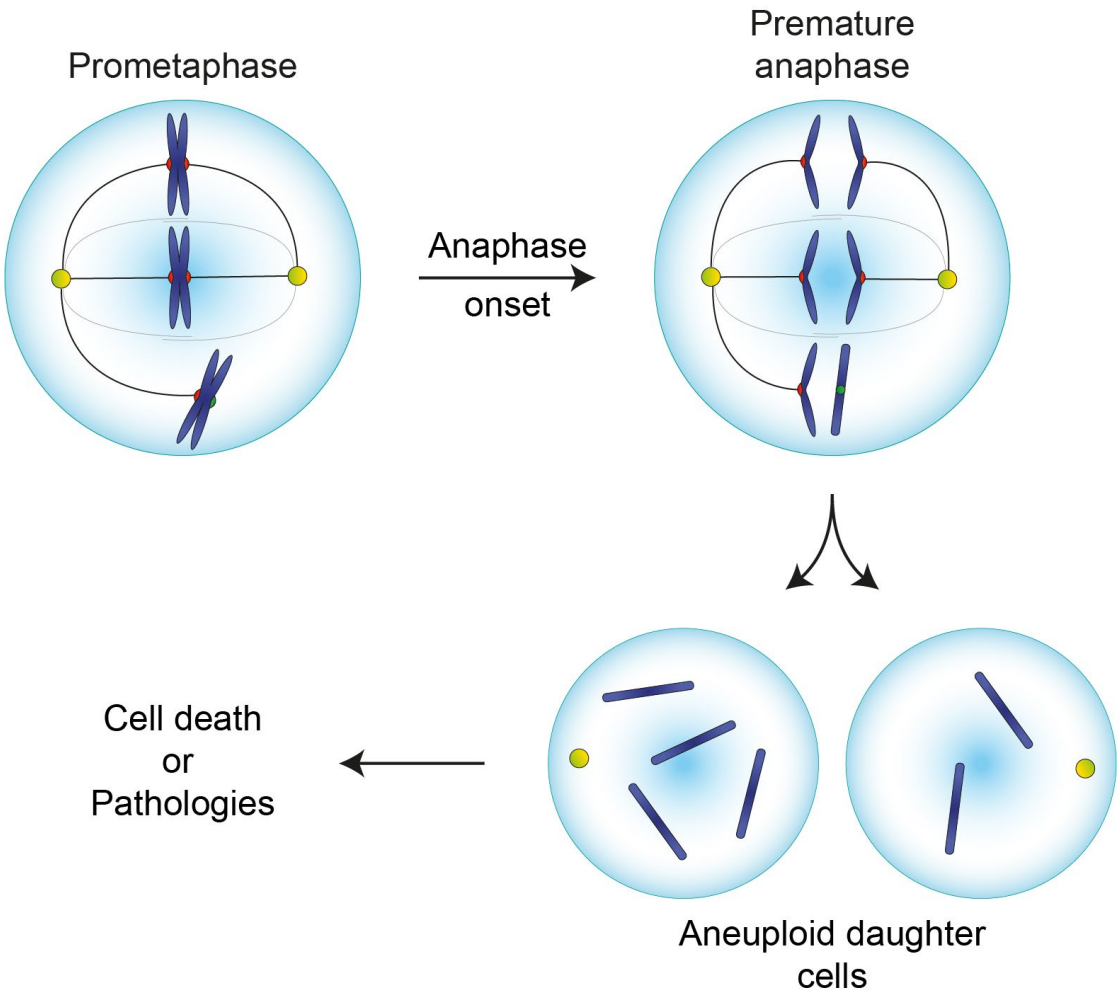

Diagram 3 – Premature entry into anaphase causes missegregation. If a cell with an unattached kinetochore (top left) were to enter anaphase (top right) the unattached chromatid would not be segregated to a specific spindle pole. As such, errors in chromosome copy number (bottom right) could arise from missegregaton, leading to cell death or pathologies.

Entry to, and exit from mitosis are controlled by CDK1-Cyclin B activity

Cyclin Dependent Kinase (CDK)-Cyclin holoenzymes are the kinases which drive transitions between cell cycle stages. The same is true for mitosis. Entry into mitosis is triggered by the steady accumulation of Cyclin B in G2 [9,10] (Diagram 4 ①). Once a high enough threshold of Cyclin B is reached, CDK1-Cyclin B complexes rapidly become active in a “switch-like” fashion which is the molecular basis of mitotic entry (Diagram 4②). The existence of positive [11] and double-negative [12] feedback loops controlling CDK1-Cyclin B activity is what causes this system to exhibit such bistability [13]. These feedback loops also imbue this bistable system with the property of hysteresis, meaning that the threshold of CDK1-Cyclin B activity required to transition between states is dependent on the directionality of the transition [14,15]. Therefore, once the transition to the high-activity state has occurred, Cyclin B levels must fall to a great extent to trigger a transition back into the low-activity state. The hysterestic bistability of CDK1-Cyclin B activation ensures entry to mitosis is both rapid and effectively unidirectional. Once active, CDK1-Cyclin B coordinates many of the events leading into mitosis – some of which will be highlighted in later sections.

CDK1-Cyclin B activity is reciprocally linked to the activity of several phosphatases, leading to a global state of high kinase activity and low phosphatase activity during mitosis (Diagram 2). This results in high levels of phosphorylation between mitotic entry and anaphase onset [16]. Protein Phosphastase 1 (PP1) subfamily phosphatases are directly phosphorylated by CDK1-Cyclin B, resulting in their inactivation [17]. In contrast, Protein Phosphatase 2A (PP2A) in complex with its regulatory subunit B55 (PP2A-B55) is inhibited indirectly by the ENSA-Greatwall

pathway. Here, the Greatwall kinase is activated by CDK1-Cyclin B phosphorylation [18,19], leading to the phosphorylation of Greatwall substrates ENSA [20] and Arpp19 [21]. It is the phosphorylated forms of ENSA and Arpp19 which bind to and thereby inhibit PP2A-B55. As PP2A-B55 and PP1 dephosphorylate CDK1 targets, this additional layer of control ensures that the cell stays in a state of high CDK1-Cyclin B activity during mitosis.

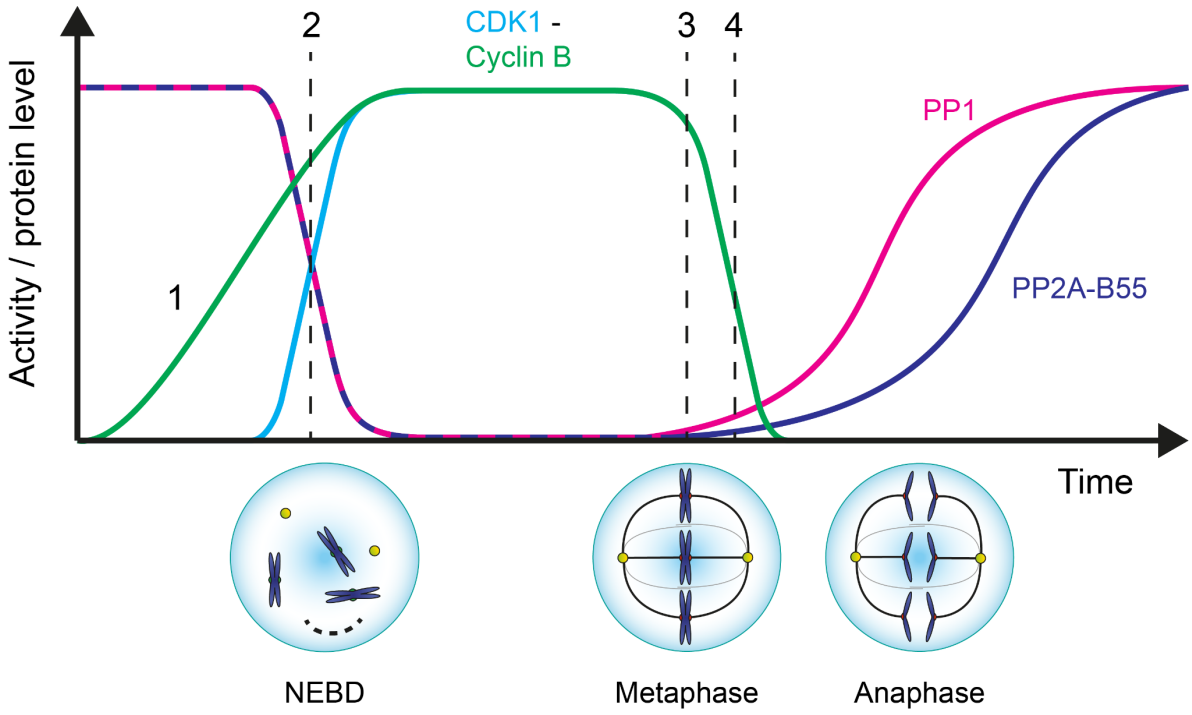

Diagram 4 – Mitosis is underpinned by changes in the activity of CDK1-Cyclin B and phosphatases. Prior to nuclear envelope breakdown (NEBD), in G2, Cyclin B protein levels (green) steadily accumulate ①. At some threshold of Cyclin B level, CDK1-Cyclin B holoenzymes rapidly become active (blue) in a switch-like fashion ②. This activation of CDK1-Cyclin B is reciprocally linked to the activity of PP1 and PP2A-B55 phosphatases (magenta and purple). This switch is the molecular basis for NEBD. Once chromosome biorientation is achieved at metaphase Cyclin B degradation begins, causing CDK1-Cyclin B activity to fall ③. At some level of Cyclin B degradation sister chromatid cohesion is lost marking the beginning of anaphase ④. The reactivation of PP1, then PP2A-B55, as anaphase progresses serves to guide mitotic exit.

Exit from mitosis, which is defined as anaphase entry onwards, is similarly linked to Cyclin B levels [22]. Anaphase onset and the subsequent stages of mitosis occur due to two related phenomena – loss of sister chromatid cohesion, and a switch into a state of low CDK activity and high phosphatase activity. In both cases these events are largely triggered by the proteasomal degradation of Cyclin B (Diagram 4③) [22]. Once a sufficient level of Cyclin B has been degraded, the cell enters anaphase (Diagram 4④). At the metaphase-to-anaphase transition, the proteolytic destruction of Cyclin B and Securin leads to cleavage of cohesin, permitting the loss of sister chromatid cohesion in early anaphase (Diagram 5). This proteasomal destruction is mediated by the ubiquitination of Cyclin B [23,24] and Securin [25], by the E3 ubiquitin ligase anaphase promoting complex/cyclosome (APC/C) in conjunction with its coactivator CDC20 [26,27]. Prior to their proteasomal degradation (i.e. before anaphase onset) Cyclin B and Securin maintain sister chromatid cohesion by binding to and inactivating a protease called Separase [28,29]. After Cyclin B and Securin are degraded, Separase can cleave the kleisin subunit of cohesin to abolish the linkage of sister chromatids [30]. Thus, as Securin and Cyclin B levels fall at the metaphase to anaphase transition, Separase is no longer inhibited and sister chromatid cohesion is lost.

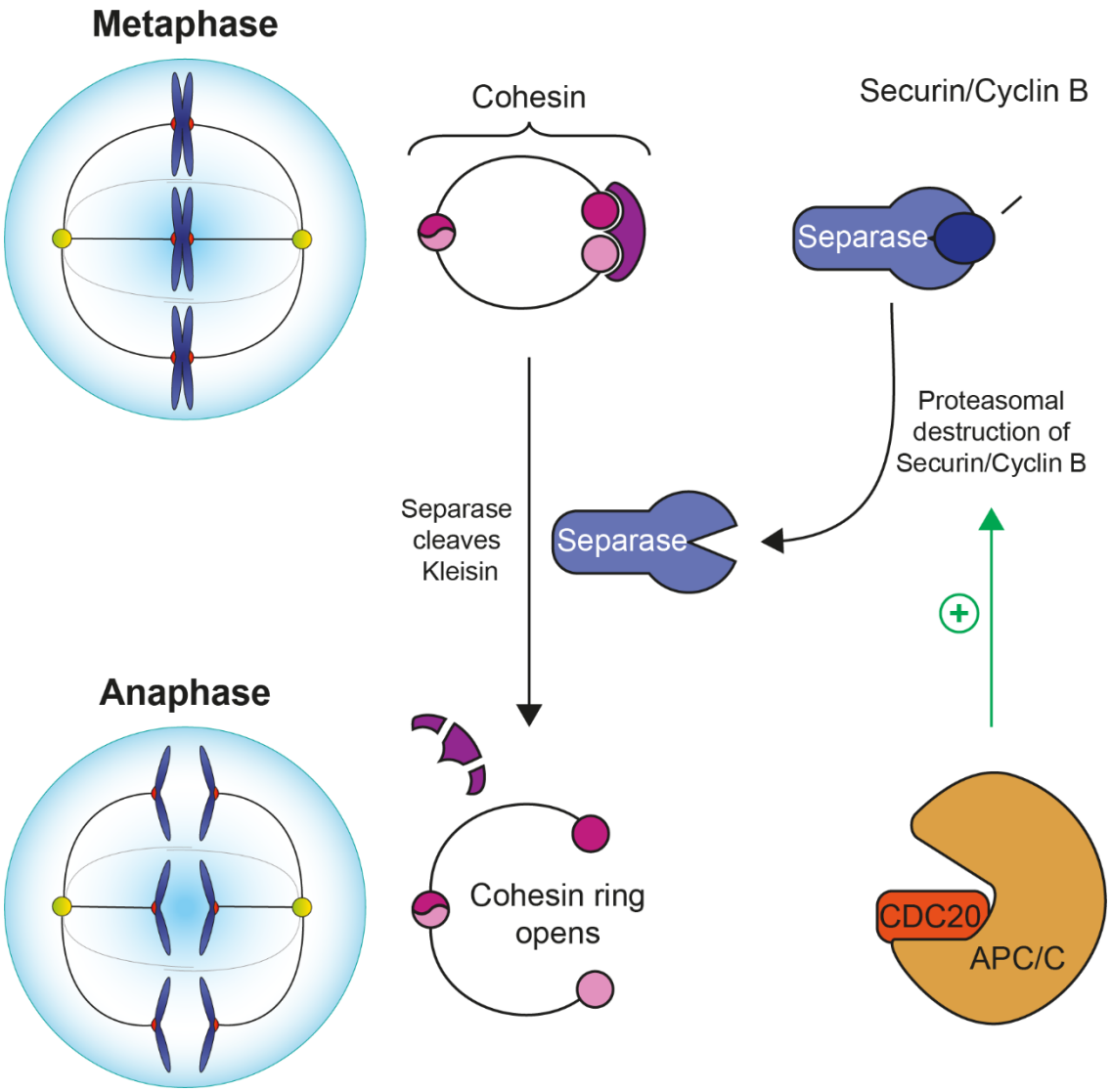

Diagram 5 – Anaphase onset is triggered by the degradation of Cyclin B and Securin. Prior to anaphase (top), Cyclin B and Securin directly inhibit the protease Separase. This inhibitory action ensures that centromeric cohesin remains closed to maintain sister chromatid cohesion. Following the destruction of Cyclin B and Securin by the proteasome following ubiquitination by APC/C^{CDC20} Separase is no longer inhibited. Separase cleaves the Kleisin subunit of cohesin (bottom) to cause the loss of sister chromatid cohesion and hence the onset of anaphase.

The events from late-anaphase onwards are coordinated by the ordered dephosphorylation of CDK1-Cyclin B targets. The inactivation of CDK1 at anaphase onset allows the global re-activation of PP1 and PP2A-B55, which serve to guide mitotic exit through anaphase, telophase, and cytokinesis. The activation of these enzymes is temporally distinct, given that the existence of the ENSA-Greatwall pathway causes a lag in PP2A-B55 activation [31] (Diagram 4). In addition to the difference in activation kinetics of PP1 and PP2A-B55, their substrates are dephosphorylated at different rates by virtue of differences in the motifs surrounding target phosphorylated residues [32–34]. This temporal control of phosphatase activation and substrate dephosphorylation forms the basis for ordering mitotic exit.

As with many CDK-Cyclin complexes, active CDK1-Cyclin B sets the stage for its own inactivation; via the destruction of Cyclin B. This occurs by direct phosphorylation of the APC/C by CDK1-Cyclin B, promoting its association with coactivator CDC20 [35–37]. It transpires that the activation of APC/C^{CDC20}, which controls mitotic exit, is a key control point during mitosis – forming the target of the spindle assembly checkpoint. Here, the spindle assembly checkpoint signalling results in the production of a soluble inhibitor of APC/C^{CDC20} called the mitotic checkpoint complex. This will be discussed in more detail in later sections.

Opposing its role in activating APC/C^{CDC20}, CDK1-Cyclin B also has major roles in keeping APC/C^{CDC20} inactive until the spindle checkpoint is satisfied. Namely CDK1-Cyclin B activity is required for spindle checkpoint signalling [38], and phosphorylation of CDC20 by CDK1-Cyclin B inhibits APC/C^{CDC20} holoenzyme assembly to prevent activity toward Cyclin B and Securin [38,39].

In summary, the entry to and exit from mitosis is controlled a hysteristic bistable switch controlling CDK1-Cyclin B activity. This is reciprocally linked to phosphatase activity, such that the stages of mitosis leading up to anaphase see high CDK1 activity and low phosphatase activity, followed by low CDK activity and high phosphatase activity post-anaphase. The switch to mitotic exit at the metaphase-to-anaphase transition is triggered by APC/C^{CDC20} activation, causing the destruction of Cyclin B and Securin. This culminates in the cleavage of cohesin and re-activation of PP1 and PP2A-B55 to drive mitotic exit. The activation of the APC/C is the functional target of the spindle checkpoint, which delays APC/C^{CDC20} activation to give chromosomes more time to achieve biorientation.

An introduction to the kinetochore

At the heart of chromosome capture is the kinetochore, which mediates interactions between chromatin and microtubules of the mitotic spindle. Additionally, it has major roles in error correction and the spindle checkpoint, as will be described in detail later. The kinetochore is a complex of ~100 different proteins, which in higher eukaryotes assemble in a regional fashion over centromeres. That is to say that many copies of kinetochore proteins are clustered together over centromeric DNA to form a surface with many binding sites for microtubules. Structurally and functionally, the kinetochore can be divided into inner and outer regions (Diagram 6). These regions can be observed as two electron-dense disks in electron micrographs, connected by a less dense layer [40]. The inner kinetochore binds to chromatin constitutively and forms a platform for the outer kinetochore to assemble on top of. The outer kinetochore assembles dynamically and serves as the point of attachment for microtubules, as well as playing host to the proteins implicated in the spindle assembly checkpoint, and some of the proteins implicated in error correction.

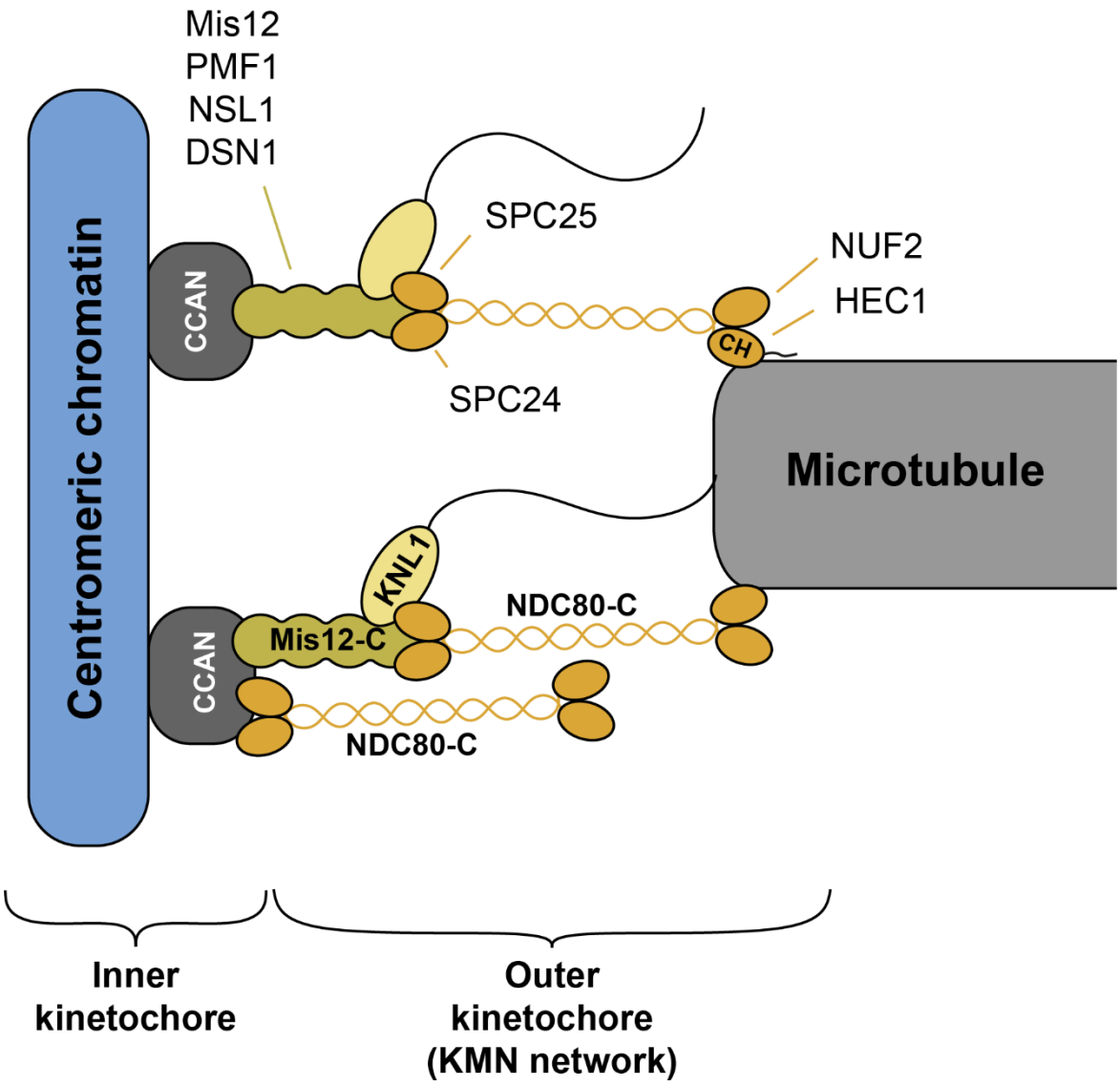

Diagram 6 – An overview of the organisation of the kinetochore. The CENP-C assembly pathway (top) and CENP-T assembly pathway (bottom) are shown. Contact between the kinetochore and microtubules is mediated by NDC80-C and KNL1.

The inner kinetochore, also known as the constitutive centromere associated network (CCAN) is assembled atop centromeres throughout the cell cycle [41]. Centromeres in higher eukaryotes are defined epigenetically through the presence of Histone H3 variant CENP-A [42]. The CCAN protein CENP-C directly binds CENP-A [43,44] and forms a flexible linker between CENP-A and the rest of CCAN,

which straddles and topologically entraps naked linker DNA [45,46]. This stable platform of proteins serves as a receptor for components of the outer kinetochore.

The outer kinetochore comprises a core unit of proteins which assemble on the inner kinetochore in late G2/prophase [47]. These proteins are kinetochore null lethal 1 (KNL1), and the missegregation 12 (Mis12) and nuclear division cycle 80 (NDC80) complexes [48]. The Mis12 complex contains Mis12, PMF1, NSL1, and DSN1. The NDC80 complex contains HEC1 (a.k.a. NDC80), NUF2, SPC24 and SPC25. These are collectively known as the KMN (KNL1, Mis12-C, NDC80-C) network. Assembly of the outer kinetochore occurs by two pathways in a cell-cycle controlled fashion. In one pathway, CENP-C binds to the MIS12 complex in a manner dependent on Aurora B phosphorylation of DSN1 [49,50]. In parallel pathway, the CCAN protein CENP-T is phosphorylated at multiple sites by CDK1–Cyclin B which promotes recruitment of the NDC80 and MIS12 complexes separately [51]. Thus, outer kinetochore assembly is linked to cell cycle progression. This regional assembly of the outer kinetochore results in the presence of ~240 NDC80-C at each human kinetochore [52].

The outer kinetochore forms the point of attachment to spindle microtubules [53]. This mode of binding is “end-on”, meaning that the KMN network binds to the dynamic tips (rather than the sides) of microtubules. It is the KMN network itself which harbours microtubule-binding functionality, via KNL1 and the NDC80-C [54]. The NDC80-C is the major site of microtubule attachment at the kinetochore [55], as evidenced by the observation that disruption of microtubule-NDC80-C interactions severely impairs the ability of kinetochores to form attachments [56]. Specifically, HEC1 binds microtubules through its globular calponin homology domain and unstructured positively charged N-terminal tail [57,58]. Quantitative

fluorescence microscopy and electron tomography data indicate that in human cells around 10 microtubules bind simultaneously to a single kinetochore [59,60], coordinated by ~14 NDC80-C each [52].

In mammals, a highly dynamic fibrous structure called the corona additionally assembles atop the outer kinetochore in the absence of microtubule attachment [61–63]. The corona is a highly interconnected mesh which is capable of self-expansion and comprises the RZZ-complex, MAD1-MAD2, CENP-F, and the motor proteins CENP-E and Dynein [64–68]. The corona assembles atop the KMN network, possibly due to the recruitment of MAD1 to KNL1-bound BUB1 [69]. The primary function of the corona is to produce a large surface which can facilitate the capture of spindle microtubules. Specifically, CENP-E and Dynein can mediate lateral attachment to and sliding along microtubules to promote chromosome congression (described below). Furthermore, CENP-E can facilitate the conversion of such lateral attachments into the more stable end-on configuration described previously [70].

Chromosome capture and congression

Chromosomes come together (congress) on the metaphase plate. To this end, several distinct mechanisms work together to achieve the movement of chromosomes (Diagram 7). Chromosomes which quickly find end-on, amphitelic attachment are pushed and pulled to the metaphase plate by microtubule polymerisation and depolymerisation [71–73]. Alternatively, chromosomes can slide laterally along microtubules toward the plus end at the metaphase plate in a manner dependent on the motor protein CENP-E [74–76]. This latter mechanism seems to be particularly important for chromosomes near the spindle poles.

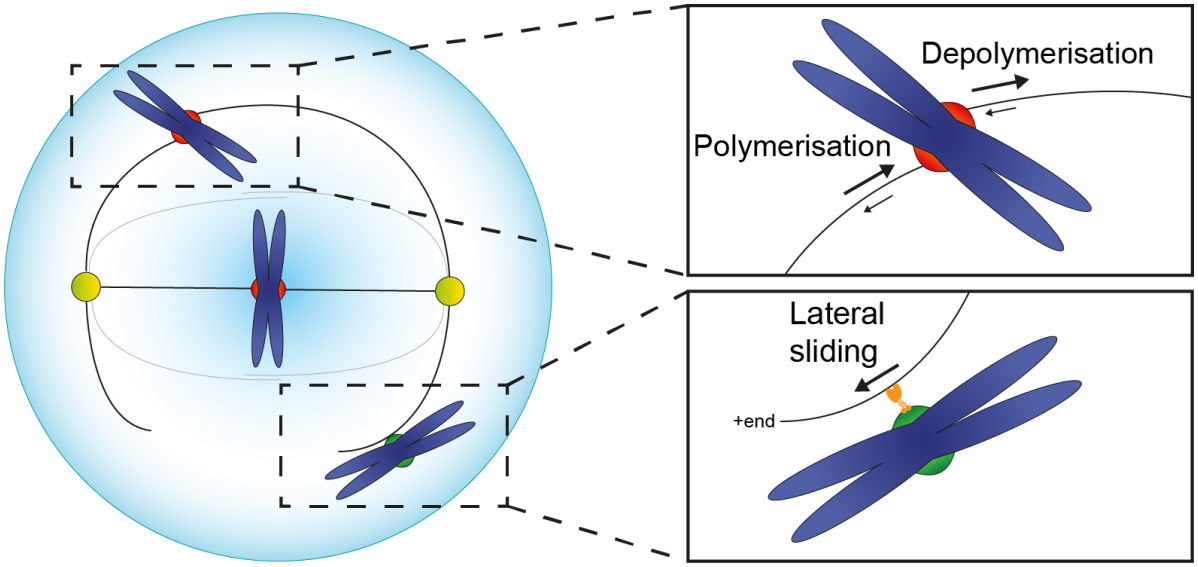

Diagram 7 – Chromosome congression occurs through distinct mechanisms. End-on attached chromosomes (top) are pushed and pulled to the metaphase plate by the polymerisation and depolymerisation of microtubules. Laterally attached chromosomes (bottom) can be moved along microtubules to the plus-end by the motor protein CENP-E.

The spindle assembly checkpoint

The spindle assembly checkpoint guards against the premature onset of anaphase by delaying APC/C^{CDC20} activation in response to the presence of kinetochores which are not end-on attached to microtubules [77]. In this way, mitotic progression is halted until all kinetochores are stably attached to microtubules. The spindle assembly checkpoint is triggered in a kinetochore-autonomous fashion – i.e. kinetochores act independently to initiate SAC signalling. This phenomenon is explained by the fact that each kinetochore can locally generate a diffusible inhibitor of the APC/C, called the mitotic checkpoint complex (MCC), which will freely diffuse through the cell. Assembly of the MCC, which comprises BUBR1, BUB3, MAD2 and CDC20, is largely orchestrated by the kinase MPS1 (Diagram 8).

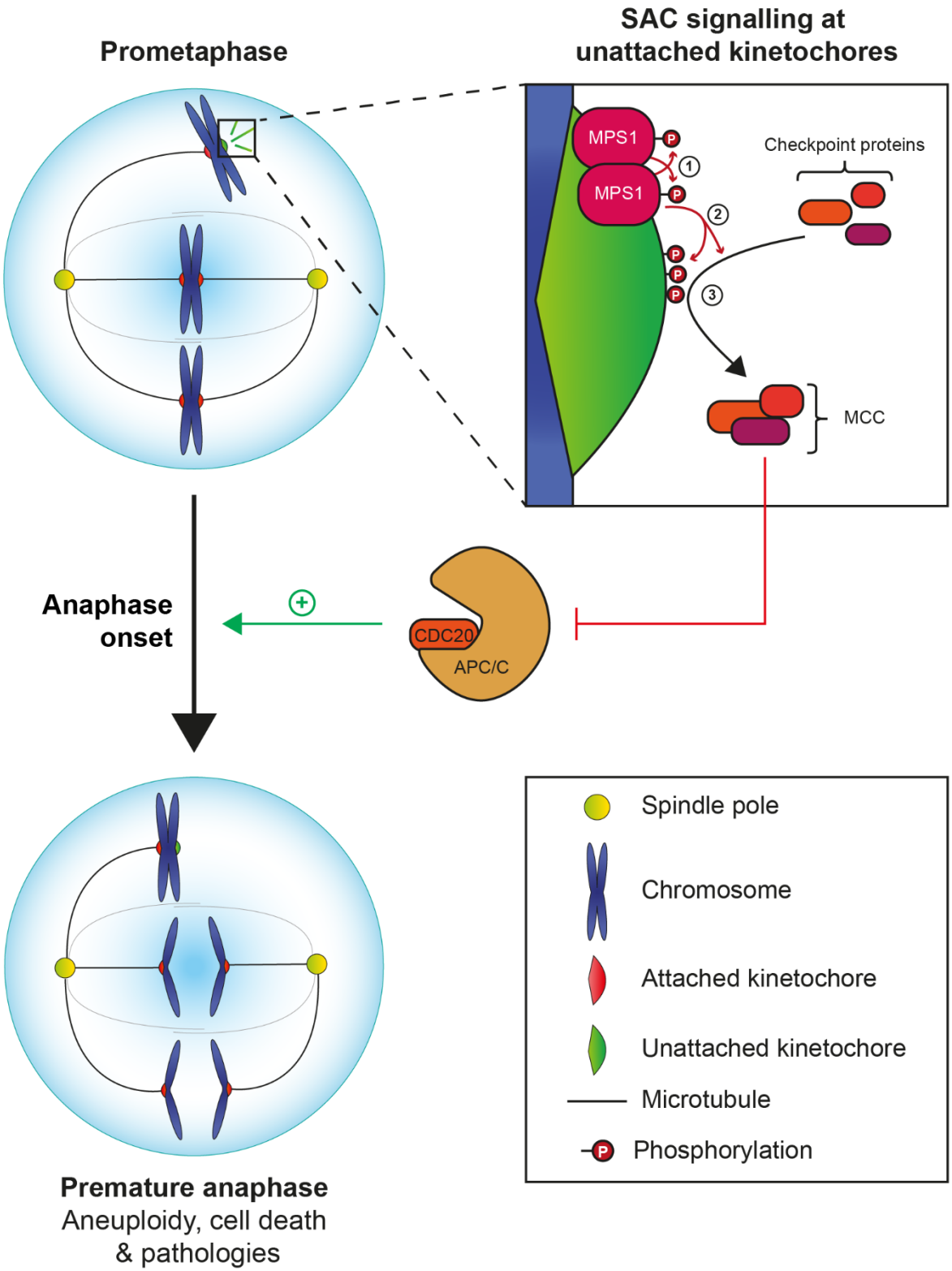

Diagram 8 – Kinetochores which are not end-on attached generate a diffusible inhibitor of APC/C^{CDC20} to delay anaphase onset. MPS1 localises to kinetochores which do not have end-on microtubule attachment and activates by trans auto-phosphorylation ①. Active MPS1 phosphorylates sites on the kinetochore which cause the accumulation of checkpoint proteins ②. Many of these checkpoint

proteins are also phosphorylated by MPS1, leading to their association into the MCC ③. The MCC freely diffuses throughout the cell to inhibit APC/C^{CDC20} activity toward Cyclin B and Securin, thus delaying anaphase onset.

The mechanism by which the MCC inhibits APC/C^{CDC20} is two-fold. The MCC itself contains CDC20 [78], the crucial co-activator of the APC/C required for cyclin B and securin ubiquitination. CDC20 in the MCC is unable to productively bind the APC/C, thus preventing assembly of active APC/C^{CDC20} [79,80]. Additionally, the MCC itself binds directly to the APC/C^{CDC20} as a pseudosubstrate inhibitor [81–84]. Thus, the presence of assembled MCC keeps APC/C^{CDC20} in an inactive state by sequestering CDC20 and directly inhibiting the APC/C.

The generation of MCC is catalysed by the local clustering and precise spatial positioning of several “checkpoint proteins” (including all members of the MCC) on the surface of the outer kinetochore. Many of these checkpoint proteins were discovered in two contemporaneous screens in *S. cerevisiae* for genes involved in maintaining a mitotic arrest in the presence of spindle-poisons (which led to the generation of unattached kinetochores). These screens revealed the mitotic arrest deficient (MAD) and budding uninhibited by bezimidazoles (BUB) proteins [85,86]. Additional checkpoint proteins are the APC/C co-activator and MCC member CDC20, which was discovered in an *S. cerevisiae* screen for mutants defective in the cell division cycle [87]. CDC20 mutants showed defects in anaphase onset because the APC/C cannot be fully activated [88]. This dual role of CDC20 – both an inhibitor and activator of the APC/C, explains why it did not show up in initial screens for checkpoint proteins. While MAD1, MAD2, BUB1, BUBR1, BUB3 and CDC20 are at the core of MCC assembly, several other factors are required to promote their clustering and productive association. Perhaps most importantly the

kinase activity of monopolar spindle 1 (MPS1) is essential for the mitotic checkpoint [89].

MPS1 localises to kinetochores where it initiates the recruitment of the other checkpoint proteins to the kinetochore and phosphorylates them to control their precise spatial positioning [90–93] (Diagram 9). Initially, phosphorylation of Met-Glu-Leu-Thr (MELT) motifs on KNL1 by MPS1 provide a docking site for the BUB1-BUB3 complex [94–96] (Diagram 9 ①). BUB1-BUB3 is already complex with BUBR1-BUB3 via a pseudo-symmetric interaction [97]. Thus, MPS1 phosphorylation of KNL1 causes the accumulation of BUB1-BUB3 – BUBR1-BUB3 at kinetochores. The association of BUB1 and BUBR1 tetratricopeptide repeat (TPR) domains with KI motifs on KNL1 serves to strengthen this interaction [98].

MAD1-MAD2 exists as a dimer-of dimers, and their recruitment to the kinetochore occurs via two separate pathways – via BUB1, and via the RZZ complex [99–102]. The main recruitment pathway relevant for checkpoint signalling is via a direct interaction between the RLK motif of MAD1 and BUB1 [69,103,104], which is promoted by MPS1 phosphorylation of the BUB1 conserved domain 1 (CD1) following a priming phosphorylation by CDK1 [104–106] (Diagram 9②). As mentioned, MAD1-MAD2 additionally forms part of the fibrous corona by association with the RZZ complex. This latter recruitment pathway only seems to be required for checkpoint function during prolonged mitotic arrest [101].

CDC20 is bound by both MAD1 and BUB1. MPS1 phosphorylates MAD1 at its C terminus to promote its interaction with the N-terminal tail of CDC20 [104,107] (Diagram 9③). Meanwhile, the C-terminal WD40 domain of CDC20 associates with the ABBA motif of BUB1 [108] (Diagram 9④). In this way, the C-terminal tail of

CDC20 is unfurled to reveal its MAD2-interacting motif (MIM), permitting MAD2 to bind to CDC20 to begin assembly of the MCC [109–111]. These phosphorylation-dependent associations between different checkpoint proteins result in the precise spatial positioning of CDC20 such that it is in a productive conformation for association with MAD2 [109–111] (Diagram 9⑤). This association with MAD2 is the rate limiting step in MCC formation [112,113] and requires the closure of a flexible loop domain around the MAD2 interaction motif (MIM) of CDC20. This loop-closure occurs via so-called templating, in which a molecule of MAD2 in the open conformation (O-MAD2) binds to the MAD1-bound MAD2 which is in the closed conformation (C-MAD2) [114]. This binding event induces the O-MAD2 to adopt the closed conformation. The CDC20 MIM is positioned adjacent to this constitutively associated C-MAD2 molecule, allowing for the simultaneous binding of O-MAD2 to CDC20 and C-MAD2 to produce a C-MAD2-CDC20 complex [109–111]. Once assembled, BUBR1-BUB3 rapidly associates with this subcomplex to compete MCC formation.

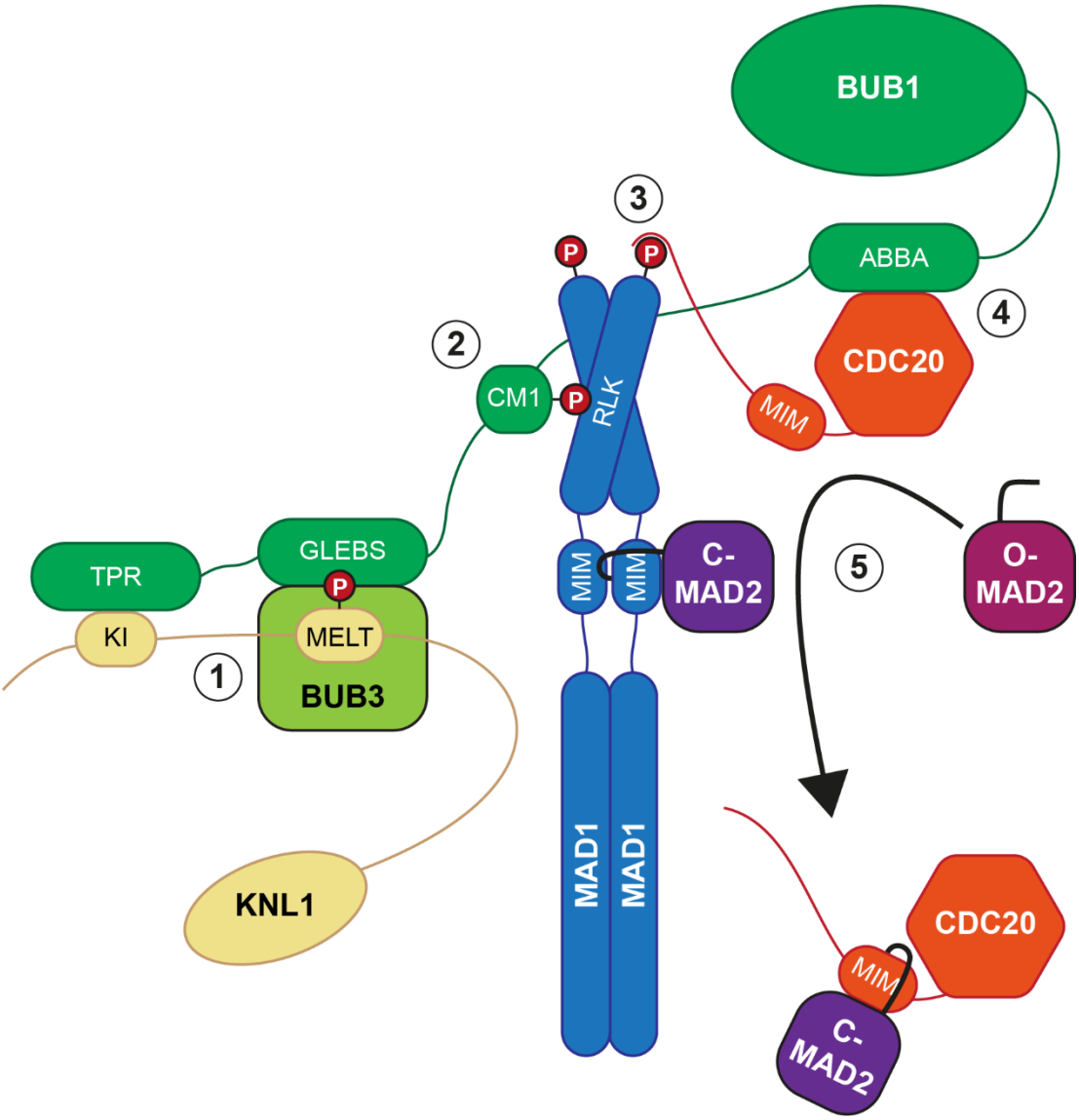

Diagram 9 – MPS1 phosphorylations direct the assembly of checkpoint proteins. See main text for full details.

Beyond MPS1 several other kinases have roles in checkpoint signalling, notably CDK1-Cyclin B and PLK1. The presence of these kinases at kinetochores is promoted by MPS1 activity, and through multiple positive feedback loops they mutually reinforce each other (Diagram 10). CDK1-Cyclin B localises to kinetochores via MAD1 [115,116], which in turn is dependent on MPS1 activity via phosphorylation of KNL1-MELT motifs and BUB1-T461. CDK1-Cyclin B feeds back to promote MPS1 localisation via phosphorylation of MPS1-S281[117], which will be discussed in further detail later. Additionally, CDK1-Cyclin B phosphorylates BUB1-S459 to prime the MPS1 BUB1-S461 phosphorylation [104–106] thereby promoting its own localisation. PLK1 localises to the kinetochore by binding to phosphorylated BUB1/BUBR1 [118–120]. MPS1 promotes PLK1 localisation via the phosphorylation of KNL1 MELT motifs to recruit BUB1/BUBR1. CDK1 phosphorylation of BUB1-pT609 then promotes the interaction between PLK1 and BUB1. Localised PLK1 activity then reinforces the activation of MPS1 by contributing to MPS1 T-loop phosphorylation and reinforces MELT motif phosphorylation by directly phosphorylating them alongside MPS1 [121–123]. Thus, MPS1 triggers recruitment of PLK1 and CDK1-Cyclin B to kinetochores, which all mutually reinforce one another’s localisation and function.

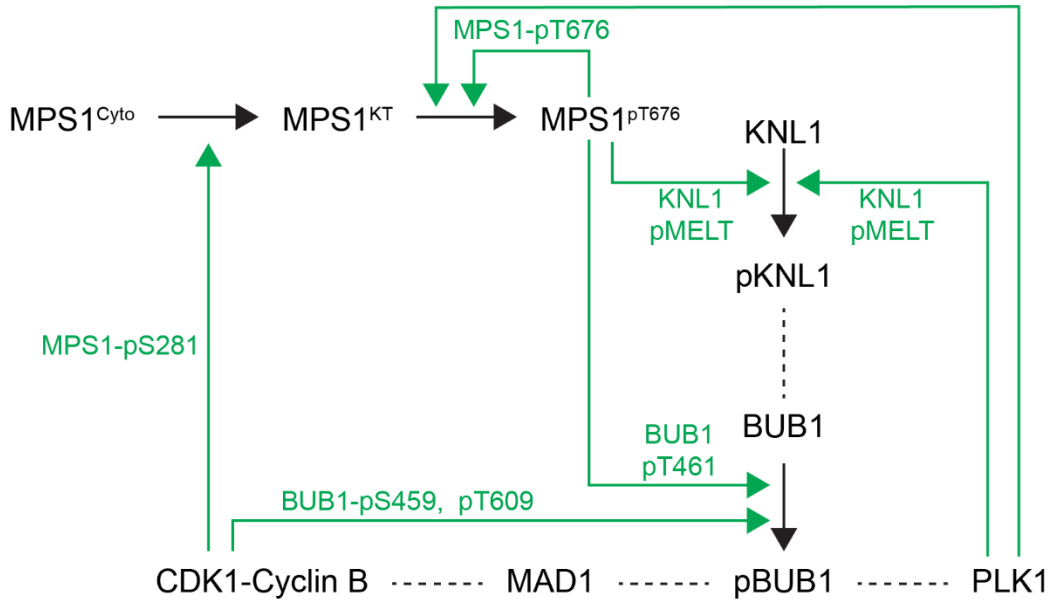

Diagram 10 – Positive feedback loops between MPS1, PLK1, and CDK1. See main text for full details.

As described above, MPS1 orchestrates spindle assembly checkpoint signalling at kinetochores. The importance of MPS1 localisation as a trigger for the rest of checkpoint signalling can be demonstrated by tethering MPS1 to kinetochores via fusion to MIS12. In this scenario kinetochores aberrantly localise checkpoint proteins and are unable to stop checkpoint signalling [124], highlighting the role of MPS1 as a principal regulator of checkpoint signalling. The control of spindle checkpoint signalling at individual kinetochores can thus be largely reduced to if MPS1 is localised to the kinetochore or not. Understanding how MPS1 localisation is controlled by end-on microtubule binding is therefore key to understanding how kinetochores make the decision to signal or not.

Everything MPS1

Discovery and structure

MPS1 was originally discovered in an *S. cerevisiae* screen for conditional mutants that were defective in centrosome replication [125]. Subsequently, two screens for dual-specificity kinases in humans identified MPS1 – naming the gene dual specificity kinase TTK (TTK), and phospho-tyrosine picked threonine kinase (PYT) [126,127]. MPS1 kinases are widely conserved throughout Eukaryotes, except for some nematode lineages [128]. Interestingly, PLK1 completely takes over the function of MPS1 in these nematodes to control the spindle checkpoint [128]. Many of the phosphorylation targets are unchanged, which is not surprising given that MPS1 and PLK1 have extremely similar consensus motifs [129].

MPS1 in humans is a 97kDa, 857 amino acid, dual specificity protein kinase [126,127] which phosphorylates serine and threonine residues *in vitro* at consensus E/D-x-**T** motifs [129,130]. MPS1 comprises several domains/regions; an N-terminal extension (NTE) [131], tetratricopeptide repeat (TPR) domain [131–133], middle region (MR) [134], and the highly-conserved C-terminal kinase domain [126,127] (Diagram 11). Most of MPS1 is predicted to be unstructured, except for the TPR and kinase domains – which are well folded [133,135].

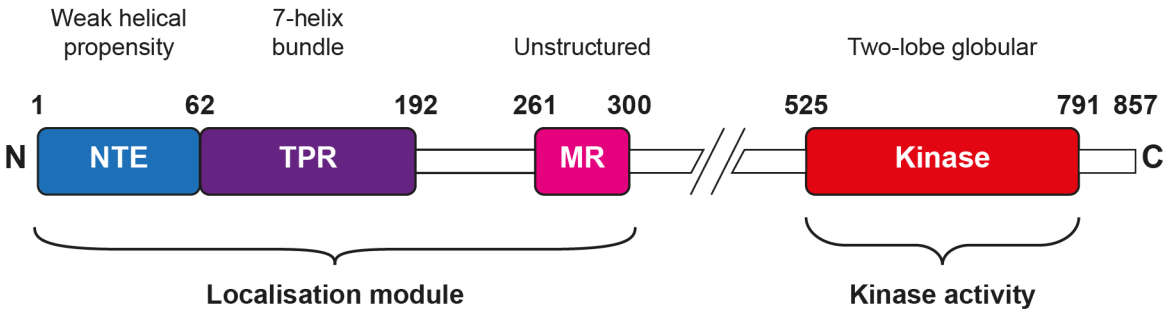

Diagram 11 – Human MPS1 comprises several functional domains. See main text for full details.

Involvement in the spindle checkpoint

The first hint that MPS1 was involved in the spindle checkpoint came from its initial discovery in *S.* cerevisiae, wherein conditional MPS1 mutants did not show a cell cycle arrest – unlike other mutants with spindle pole body duplication defects [125]. These observations were bolstered by experiments demonstrating that conditional MPS1 mutants could not maintain a mitotic checkpoint arrest in the presence of the spindle poison nocodazole, which should activate the spindle checkpoint [89]. Shortly thereafter, overexpression of MPS1 in *S. cerevisiae* was shown to induce a checkpoint arrest, which was dependent on the presence of the MAD and BUB checkpoint proteins [107]. The essential involvement of MPS1 homologues/paralogs in the spindle checkpoint were subsequently replicated in *S. pombe, X. laevis,* and human cell lines [136–138]. If MPS1 is required for centrosome duplication in human cells was a subject of debate for some years, concluding that this function of MPS1 is not conserved in humans [136,139,140].

Beyond depletion or conditional mutation of MPS1, a wealth of data has demonstrated that the kinase activity of MPS1 is required for its role in the spindle checkpoint. As with depletion of MPS1, chemical inhibition with a range of inhibitors abrogates the spindle assembly checkpoint [90,92,93,141–145]. Likewise, mutation of MPS1 to render it catalytically inactive also causes a failure of the spindle checkpoint [137,146]. Given the reliance of the spindle checkpoint on multiple MPS1 phosphorylations, this dependence on MPS1 activity is not surprising.

MPS1 localisation to the kinetochore is essential for its role in triggering robust checkpoint signalling. MPS1 has long been known to bind to kinetochores [136,137,147,148], where it has an extremely rapid turnover of a few seconds [149]. Specifically, MPS1 binds to unattached kinetochores [147]. For some years, there

was a debate as to if biorientation or mere microtubule attachment was required to silence checkpoint signalling at kinetochores. It is now widely accepted that end-on microtubule attachment is sufficient to cause kinetochores to stop localising MPS1 and to silence the spindle checkpoint [150–152]. Truncation of MPS1 to abolish kinetochore localisation drastically impairs spindle checkpoint function, highlighting the importance of local clustering of MPS1 for SAC signalling at the kinetochore [131]. This specific localisation of MPS1 to unattached kinetochores, and subsequent phosphorylation of key checkpoint targets, is widely considered the molecular basis for the initiation of checkpoint signalling. MPS1 recruitment thus serves to link the absence of end-on microtubule attachment to spindle checkpoint signalling.

Control of MPS1 activity

MPS1 localisation promotes MPS1 activation through trans-autophosphorylation. The activity of MPS1 is regulated by autophosphorylation – primarily of residues T676 and T686 in the T-loop of the kinase, which otherwise blocks the ATP-binding pocket [135,146,153,154]. Wildtype MPS1 was observed to phosphorylate a kinase-dead mutant at these residues, demonstrating that activation can occur in trans [92,146]. Furthermore, inducing the dimerization of MPS1 in solution is sufficient to cause auto-activation by this mechanism [146]. Together, these observations have resulted in a model in which the local clustering of MPS1 at unattached kinetochores promotes MPS1 activation through trans-autophosphorylation [146]. Mutation of T676 and/or T686 to alanine results in weakened, not absent, kinase activity [146,153–155]. Such mutants exhibit a weakened checkpoint - displaying chromosome missegregation defects and partial loss of the ability to hold an arrest in nocodazole [146,153,155]. Conversely, hyper-active MPS1 with a phospho-mimetic T-loop causes prolonged mitosis due to overactive checkpoint and error correction pathways [155]. The dynamic regulation of MPS1 activity is thus linked to MPS1 localisation and is important for ensuring normal checkpoint and error correction function.

Dynamic phosphorylation regulates MPS1 localisation to kinetochores

The localisation of MPS1 to unattached kinetochores is regulated by dynamic phosphorylation events (Diagram 12). CDK1 – Cyclin B activity controls the temporal window in which MPS1 can localise to kinetochores. CDK1 targets 4 sites in human MPS1 [129]. Of these, serine 281 phosphorylation has been seen to be required for MPS1 localisation – as mutation of this residue severely reduced the ability of MPS1 to localise to unattached kinetochores [117]. Without CDK1-Cyclin B phosphorylation of S281, cells demonstrate an impaired spindle checkpoint and slower kinetics of MPS1 kinetochore-localisation immediately following nuclear envelope breakdown [115,117]. This phosphorylation is removed by PP2A-B55, which only becomes active after the metaphase-to-anaphase transition – thus tying the ability of MPS1 to localise and activate the spindle checkpoint to the activity of CDK1-Cyclin B [117].

The kinase activity of Aurora B is an essential pre-requisite for MPS1 recruitment. Inhibition of Aurora B prevents MPS1 recruitment to and subsequent activation at kinetochores in a nocodazole arrest, causing a failure of the spindle assembly checkpoint [156,157]. Partial inhibition of Aurora B combined with depletion of HEC1 were seen to synergise to abolish MPS1 recruitment and impair checkpoint function, suggesting that Aurora B and HEC1 operate in the same pathway to recruit MPS1 [156,157]. The proposed molecular details of this pathway will be presented later in this section with a view to the molecular interactions between MPS1 and the kinetochore. MPS1 kinase activity feeds back on to MPS1 localisation. Inhibited MPS1 accumulates on kinetochores [92,124] – demonstrating that MPS1 kinase activity somehow opposes MPS1 kinetochore localisation. Both MPS1 and Aurora

B phosphorylations at the kinetochore are opposed by the phosphatases PP2A-B56, with contributions from PP1 [155,158–162].

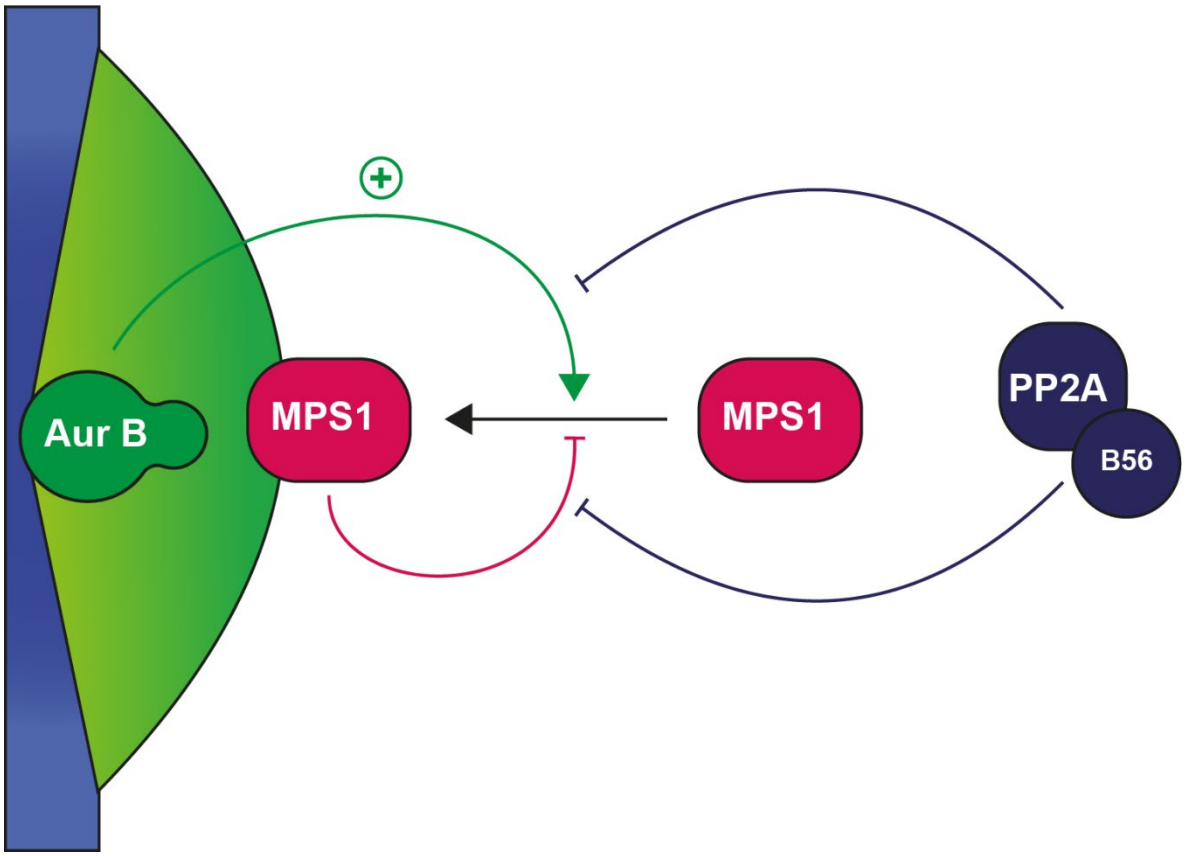

Diagram 12 – Kinase and phosphatase activity influence MPS1 localisation to unattached kinetochores. Aurora B activity is required for robust MPS1 localisation. MPS1 activity negatively feeds back onto MPS1 kinetochore localisation. PP2A-B56 opposes the activity of both Aurora B and MPS1.

MPS1 binds HEC1 and NUF2 through two different regions

MPS1 binds the kinetochore through two distinct molecular interactions. Early truncation studies identified the first ~300 residues of MPS1, encompassing the NTE, TPR and MR, as necessary and sufficient for kinetochore binding [140,147]. This fragment of MPS1 was reported to require two regions at either end for robust kinetochore localisation. Specifically, loss of the first 55 amino acids (encompassing the NTE), or loss of the region 240-301 (encompassing the MR) greatly reduced the ability of this fragment to localise [147]. Knockdown of HEC1 or NUF2, either of which results in the loss of both proteins from the kinetochore, ablates MPS1 localisation [140,163]. Indeed, MPS1 binds to both HEC1 and NUF2 through different regions. The NTE binds HEC1 at its calponin homology domain [131]. The specific interaction surface was mapped by the mutating clusters of residues on HEC1 and observing the effect this had on MPS1 localisation or co-immunoprecipitation with HEC1 [134,164]. These two studies concluded that the NTE binds to HEC1 at, or immediately adjacent to, the patch of the HEC1 calponin homology domain which binds microtubules. Pulldown assays have demonstrated that the MR binds to the calponin homology domain of NUF2 [134]. Microtubule binding to the NDC80-C is reported to sterically block both HEC1 and NUF2 from binding MPS1 – leading to the so-called “competition model” of controlling MPS1 localisation in response to microtubule attachment [134,164]. This model will be discussed in detail later.

The relative importance of the NTE-HEC1 and MR-NUF2 interactions for MPS1 localisation are unclear. Additionally, there are conflicting data and models as to how these interactions are dynamically regulated by phosphorylation events. As mentioned, early studies found that disruption of either region severely reduced the

ability of a construct spanning amino acids 1-301 to localise to kinetochores [147]. One study reported that deletion of the MR had no effect on the localisation of otherwise wildtype MPS1, whereas the MR was required for the localisation of catalytically inactive MPS1 [165]. These findings are contradicted by a study in which similar MR deletion mutants had no effect on the localisation of inhibited MPS1 [134]. Finally, phosphorylation of the MR by CDK1-Cyclin B is a key requirement for MPS1 localisation to kinetochores [117]. How phosphorylation of the MR can be required if the whole domain is expendable for MPS1 localisation is puzzling, unless phosphorylation of the MR is required to relieve an auto-inhibitory effect. Regardless, the data on the importance of the MR for MPS1 localisation under different conditions is unclear.

The NTE-HEC1 interaction is now thought to be of primary importance for MPS1 localisation. Deletion of the NTE, or NTE and TPR together is reported to abolish the kinetochore localisation of inhibited MPS1 in nocodazole [131,134]. A different study reported that MPS1 lacking the first 100 amino acids (encompassing the NTE and part of the TPR) fails to localise to kinetochores in nocodazole [90]. However, endogenous MPS1 was not depleted in this study, hence it is possible that the presence of full length MPS1 could obscure the result. Finally, deletion of the NTE is reported to weaken, but not fully abolish, spindle checkpoint signalling as measured by the ability of cells to hold an arrest in nocodazole [90,131]. These data suggest that MPS1 kinetochore localisation may not be a pre-requisite for some low-level of spindle checkpoint signalling in cases where many kinetochores are unattached.

Molecular models of the control of MPS1 binding interactions

How the various phosphorylation events which control MPS1 localisation work at the molecular level is a subject of some debate. As mentioned, Aurora B kinase activity is an important prerequisite for MPS1 kinetochore binding, and two different mechanisms have been put forward for how this occurs.

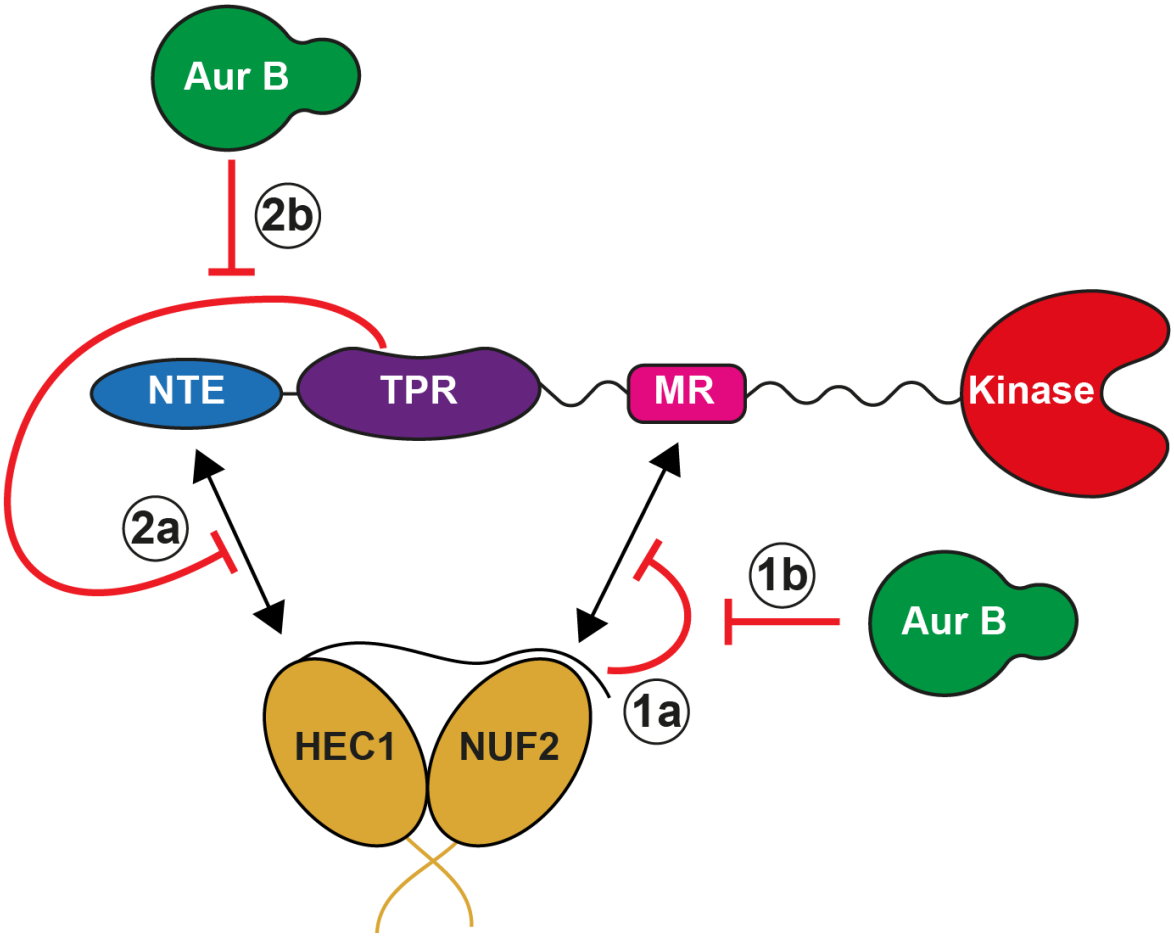

Diagram 13 – 2 models for how Aurora B activity supports MPS1 localisation. ① The N-terminal tail of HEC1 sterically blocks the interaction between the MR of MPS1 and NUF2 (a). Phosphorylation of the N-terminal tail of HEC1 frees NUF2 to interact with the MR (b). ② The TPR domain of MPS1 blocks the NTE of MPS1 from binding to HEC1 (a). Aurora B activity frees the NTE such that it can bind to HEC1 (b).

One model proposes that Aurora B phosphorylation impacts binding between HEC1 and the NTE of MPS1 (Diagram 13 ①). In this model, the TPR binds to the NTE and prevents its association with HEC1. Indeed, the NTE and TPR have been observed to interact by both NMR and chemical crosslinking [166,167]. Deletion of the TPR, or expression of an additional NTE was reported to render MPS1 localisation insensitive to Aurora B inhibition [131,166]. However, the observation that deletion of the TPR domain ablates the dependence of MPS1 localisation on Aurora B activity could not be replicated (Gruneberg lab, unpublished). Overall, this model posits that the binding of the NTE to the TPR and HEC1 are mutually exclusive and somehow linked to Aurora B phosphorylation. There are no known Aurora B phosphorylation sites on MPS1, and Aurora B does not phosphorylate MPS1 *in vitro* [129]. It has therefore been suggested that Aurora B phosphorylates an intermediate factor to control MPS1 localisation.

Another model (Diagram 13 ②) proposes that Aurora B phosphorylates the tail of HEC1 to promote MPS1 binding. *In vivo* the mutation of Aurora kinase consensus sites on HEC1 to alanine, mimicking constitutive dephosphorylation, were reported to drastically reduce MPS1 kinetochore localisation [168]. Conversely, mutation of these sites to aspartate were reported to increase MPS1 kinetochore localisation. However, these results could not be replicated by other groups [1,131,134]. *In vitro* there is evidence to suggest that the tail of HEC1 occludes the surface of NUF2 to which the MR of MPS1 binds. Deletion of the HEC1 tail, or phospho-mimetic mutation, greatly increased the ability of the MR to co-precipitate a soluble NDC80 complex [134]. The effect of the phosphorylation state of the HEC1 tail on MPS1 localisation remains controversial. In sum, there are mechanisms proposed for role

of Aurora B in regulating both the MR-NUF2 and NTE-HEC1 interactions, but their actual role in cells remains controversial.

The effect of MPS1 auto-phosphorylation on MPS1 kinetochore-affinity is controversial (Diagram 14). Classically, MPS1 inhibition results in the accumulation of MPS1 at unattached kinetochores [92,124]. There are both direct and indirect explanations for this phenomenon. MPS1 contains a great number of auto-phosphorylation sites, many of which cluster in the NTE [129,146,153,154,169,170]. There is contradictory evidence to suggest that auto-phosphorylation of some of these sites directly modulate MPS1 kinetochore affinity. One study found that auto-phosphorylation of MPS1 negatively regulated its ability to localise to kinetochores in cells [171]. Specifically, mutation of several sites outside the kinase domain to alanine caused a modest accumulation of MPS1 at kinetochores in a nocodazole arrest, whereas mutation to aspartate partially reduced the accumulation of inactive MPS1. These findings implicate auto-phosphorylation as a negative regulator of MPS1 localisation. In apparent contrast to this study, *in vitro* binding data from another publication showed that the first 240 amino acids of MPS1 (encompassing the NTE and TPR) only bound detectably to NUF2-HEC1 after being phosphorylated with recombinant MPS1 [164]. Such auto-phosphorylation of this region resulted in a strong binding affinity (K_D = 140nM) compared to no binding without phosphorylation. This latter result is surprising given that MPS1 inhibition, leading to loss of MPS1 autophosphorylation, does increase MPS1 localisation in cells. A recent study demonstrated that *S. cerevisiae* MPS1 binds NDC80 only weakly in pull-down assays when auto-phosphorylated [172]. While *S. cerevisiae* MPS1 has a very divergent N-terminus when compared to human MPS1, this study highlights

that in other organisms MPS1 auto-phosphorylation is a key mechanism for negatively regulating MPS1 kinetochore binding.

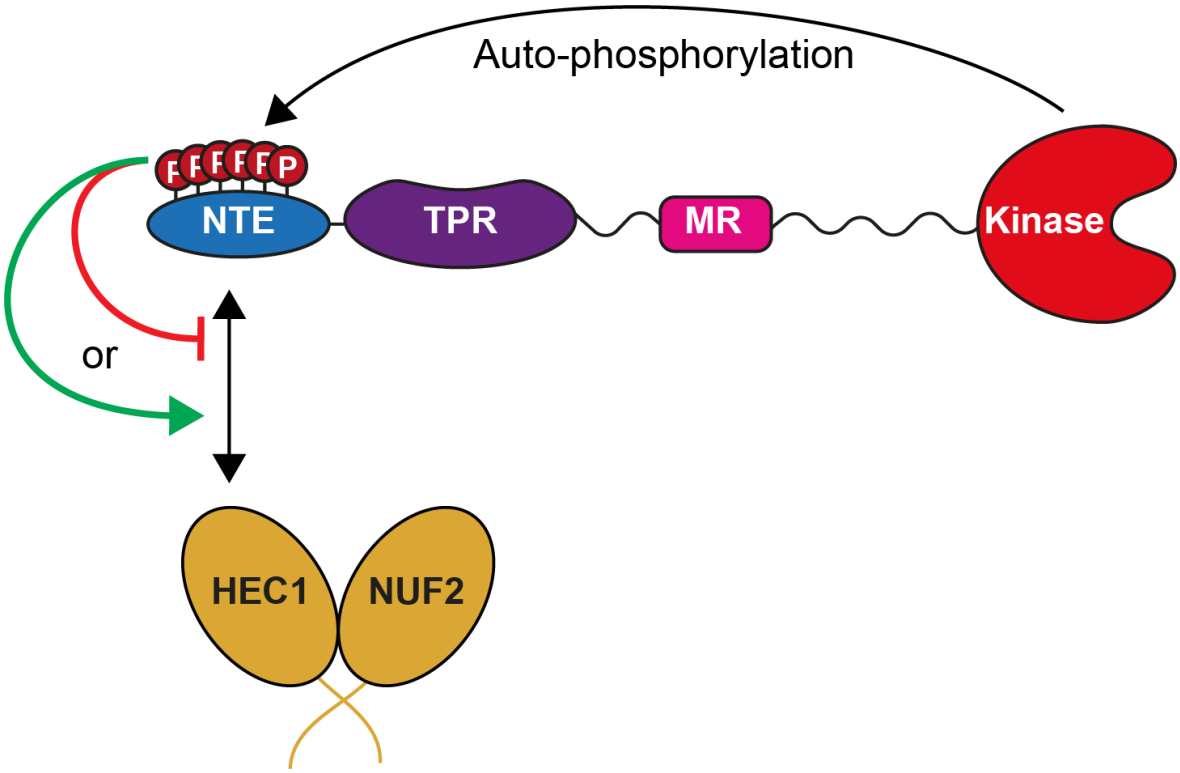

Diagram 14 – MPS1 auto-phosphorylation is proposed to positively and negatively regulate MPS1 localisation. See main text for full details.

MPS1 activity may indirectly affect its localisation by causing the accumulation of PP2A-B56 at kinetochores. As mentioned, MPS1 causes the accumulation of BUBR1 at kinetochores by phosphorylating MELT motifs on KNL1 [94–96]. A pool of PP2A-B56 binds BUBR1 directly via the BUBR1 KARD domain [158,173]. This interaction is promoted by CDK1 and PLK1 phosphorylation of the KARD domain. Thus, indirectly, MPS1 activity causes the accumulation of a BUBR1-localised pool of PP2A-B56. This specific pool of PP2A-B56 dephosphorylates Aurora B targets, the MPS1 T-loop, and MPS1 targets including KNL1-MELT motifs at the kinetochore [155,158,160,174]. Therefore, MPS1 activity-dependent recruitment of PP2A-B56 promotes the opposition of MPS1 activation and kinetochore-localisation.

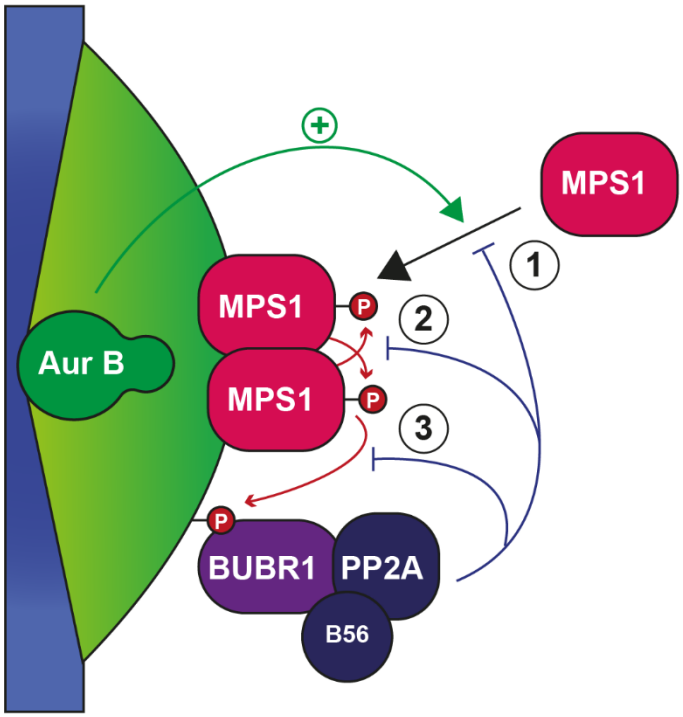

Diagram 15 – PP2A-B56 opposes MPS1 at multiple levels. Kinetochore recruitment of BUBR1-bound PP2A-B56 is MPS1 dependent. BUBR1-bound PP2A-B56 opposes:

① MPS1 recruitment by Aurora B

② MPS1 autoactivation

③ MPS1 phosphorylation of downstream targets

Finally, there may be crosstalk between MPS1 auto-phosphorylation and MPS1 kinase activity. The NTE contains a motif which is reported to inhibit MPS1 kinase activity unless phosphorylated [167]. This introduces the possibility that there is feedback between the auto-phosphorylation dependent and independent mechanisms by which MPS1 kinase activity regulates MPS1 localisation.

Turning off the spindle assembly checkpoint

Turning off the spindle assembly checkpoint requires the concentration of MCC to fall below some threshold to allow APC/C^{CDC20} activation. Two things must happen for this to occur - kinetochores must stop generating new MCC, and existing MCC must be disassembled. The disassembly of the MCC is continuous throughout mitosis and is catalysed by the opening of C-MAD2 by the AAA+ ATPase TRIP13 in concert with $p31^{comet}$ [175–179]. The silencing of the spindle checkpoint is thus largely determined by if any kinetochores are still actively generating MCC. To this end, multiple mechanisms contribute to removing checkpoint proteins from attached kinetochores to prevent MCC production.

A key feature of stopping MCC production at attached kinetochores is the removal of MPS1 from those kinetochores [124]. The leading model for how this occurs is via steric blocking of MPS1 binding sites at the kinetochore upon stable microtubule attachment. This model of direct competition between microtubules and MPS1 for kinetochore binding is supported by *in vitro* binding assays demonstrating mutually exclusive, competitive binding [134,164]. However, more recent data has shown that only around a third of NDC80-C are involved in binding microtubules at fully attached kinetochores [180], suggesting that additional mechanisms must be at play to result in the drastic reduction in MPS1 localisation observed upon microtubule binding. Additionally, there exists a report of MPS1 localising to attached kinetochores during anaphase if Aurora B localisation is maintained at centromeres – suggesting that MPS1 can bind to attached kinetochores under certain circumstances *in vivo* [181]. Finally, there is direct *in vitro* data showing that using purified yeast proteins, MPS1 can bind kinetochores which are end-on attached [182]. Together, these

observations call into question if competition alone can explain the changes in MPS1 localisation upon microtubule attachment.

Alongside removal of MPS1, the kinetochore substrates of MPS1, and Aurora B, must be dephosphorylated to prevent checkpoint localisation. In humans, this occurs primarily through the action of PP2A-B56 phosphatase, which removes phosphorylations on KNL1-MELT motifs to help stop MCC production [160]. This same pool of PP2A-B56 also dephosphorylates the T-loop of MPS1 to inactivate it [155]. Contributions to substrate dephosphorylation are also made by PP1 phosphatases, which localise to SILK/RVSF motifs in the N-terminus of KNL1 in a fashion opposed by Aurora B activity [161,162]. Thus, PP2A-B56 and PP1 contribute to the dephosphorylation of Aurora B and MPS1 substrates to stop kinetochores from producing MCC.

An additional mode of local checkpoint silencing is the physical removal of MAD1 - MAD2 complexes by the action of the motor protein Dynein in complex with the adaptor protein Spindly [183–185]. This phenomenon, known as dynein-mediated stripping, sees the MAD1-MAD2 physically carried away from attached kinetochores along the microtubule k-fibre. When this mechanism is disrupted, a delay in checkpoint silencing is seen [185].

A final mechanism implicated in preventing kinetochores from triggering the spindle checkpoint is the structural rearrangement of single kinetochores upon microtubule binding. Early studies proposing this model suggested that stretching within the kinetochore upon interaction with dynamic microtubules was a key mechanism regulating checkpoint activation [186–188]. Here, the average distance between an outer kinetochore component and an inner kinetochore/centromeric component was

measured with nm precision using light microscopy. This notion has since been called into question by subsequent studies showing that attachment of taxol-stablised (i.e. non-dynamic) microtubules to the kinetochore can silence the checkpoint, and studies which show that such measurements of intra-kinetochore stretch are majorly impacted by large-scale structural deformations of the kinetochore, hindering their interpretation [151,189,190]. There is, however, more legitimate evidence that certain components of the kinetochore undergo conformational changes upon microtubule binding (rather than being pulled by microtubule-associated forces). At yeast kinetochores, structural re-arrangements of KNL1 and HEC1 are proposed to physically separate Ndc80-bound MPS1 from reaching MELT motifs on KNL1 upon microtubule binding [191]. Similarly, in human cells, NDC80 has been reported to be pulled away from the inner kinetochore upon tensionless microtubule binding – raising the possibility that conformational changes of the kinetochore upon microtubule binding may contribute to controlling checkpoint signalling by separating regulatory components from one another [192].

The Aurora kinases

The Aurora kinases A, B, and C have prominent roles in mammalian cell division. Animals possess two mitotic Aurora kinases – A and B, which have core roles in coordinating mitosis. Aurora A has prominent roles in establishing and maintaining the mitotic spindle, whereas Aurora B is a key regulator of DNA condensation, kinetochore-microtubule interactions, and cytokinesis. As Aurora A and B share identical target consensus motifs, this difference in function is largely explained by differences in binding partners - which results in unique sub-cellular localisation. Aurora A is localised to the spindle poles and mitotic spindle by TPX2 [193]. Aurora B is localised by the so-called chromosomal passenger complex (CPC) to various regions as mitosis progresses (reviewed in [194]). Mammals additionally possess Aurora C which arose via gene duplication of Aurora B and has roles in meiosis rather than mitosis [195,196].

Aurora B forms an active complex with INCENP, Survivin and Borealin to form the CPC (Diagram 16). Aurora B is activated upon binding to the IN-box of INCENP, which causes allosteric restructuring of the Aurora B T-loop to ensure that Aurora B is only active when in complex with the rest of the CPC [197]. The non-catalytic subunits of the CPC are responsible for localising the complex [198]. INCENP, Survivin and Borealin oligomerise by forming a 3-helical bundle [199] and all three proteins bind work together to enrich CPC binding to centromeric DNA. Survivin directly binds Histone 3 phospho-T3 [200–202], which is enriched at centromeres through the activity of Haspin kinase. Borealin binds to Shugoshin [203], which is localised to the centromere by BUB1 phosphorylation of Histone 2A T120 [204]. Finally, INCENP harbours an acidic patch which binds to chromatin and microtubules [205,206]. These multivalent interactions reinforce each other to enrich

CPC at centromeric chromatin between nuclear envelope breakdown and anaphase onset, at which point the CPC is re-localised to the spindle midbody by MKLP2 to coordinate late-anaphase [207]. Notably this relocalisation to the spindle midbody requires that the CPC is first enriched at centromeres, allowing the recognition of INCENP by MLKP2 [205].

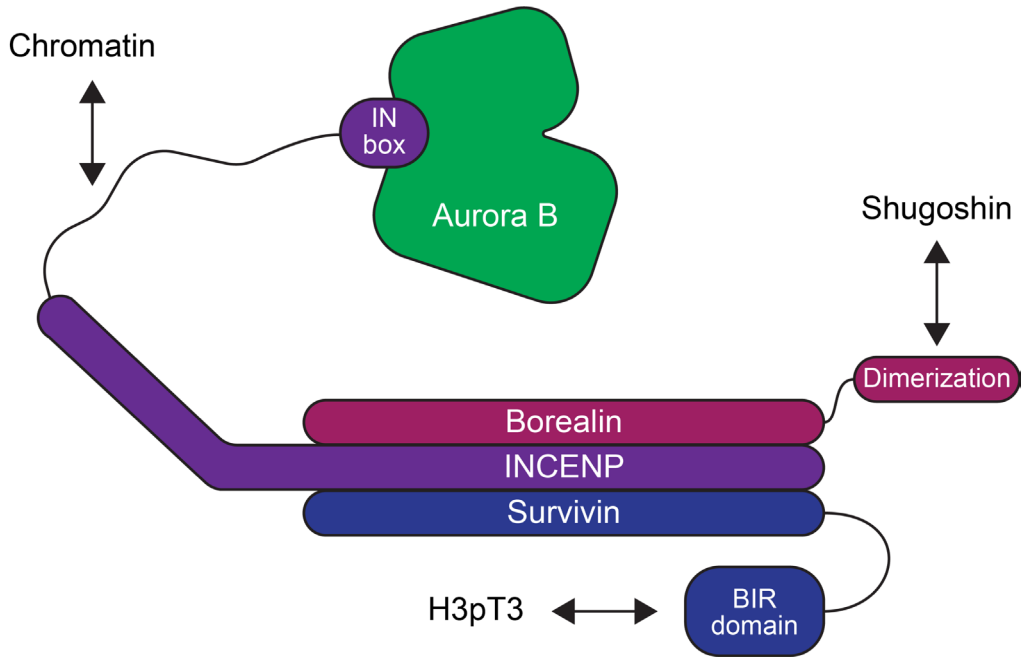

Diagram 16 – Schematic of the CPC. Borealin, INCENP, and Survivin form a 3-helical bundle, and contribute synergistically to the ability of the CPC to bind the centromere. The C-terminal IN-box of INCENP binds to and activates Aurora B.

The tension sensing model of error correction

While localised to the centromere, Aurora B is a key player in error correction and the spindle checkpoint. As mentioned, the only geometry of kinetochore-microtubule attachment which will result in error-free segregation is amphitelic. The first suggestion of how amphitelic attachments could be selectively stabilised was proposed by Dietz, who posited that this geometry alone allows chromosomes to be under “tension” [208]. The key idea is that by being pulled from opposite spindle poles, tension can be generated across the whole chromosome, which may act as the physical basis for sensing proper biorientation. Early evidence in support of this tension-sensing theory came from micromanipulation studies whereby syntellically attached chromosomes were tugged on to induce tension across the centromere [209]. Despite a lack of biorientation, such tensioned syntelic attachments were stable for hours (compared to minutes without tension). Since these experiments much molecular detail on the mechanisms of tension-sensing and error correction has been elucidated.

Aurora B activity destabilises kinetochore-microtubule attachments. Initial studies in *S. cerevisiae* demonstrated that without Aurora B or INCENP (Ipl1 and Sli15 in yeast) syntellic chromosomal attachments remained stable, implicating the CPC in tension-dependent error correction [210]. These observations were replicated in human cells by chemical inhibition of Aurora B – which highlighted its conserved role in checkpoint signalling and error-correction [211]. Aurora B phosphorylates multiple targets at the kinetochore, including many members of the KMN network [212,213]. The target of Aurora B which seems to have the largest effect on kinetochore-microtubule stability is HEC1 [54,57,214,215]. Early evidence for the direct regulation of kinetochore-microtubule attachments by Aurora B came from a

mix of cell biology and biochemistry. In microtubule pelleting assays between NDC80-C and microtubules, incubation with active Aurora B kinase was seen to weaken the interaction [54,57]. In cells, mutation of Aurora B target sites in the tail of HEC1 to alanine, simulating a lack of phosphorylation, was seen to render kinetochore-microtubule attachments unusually stable and resulted in the stabilisation of incorrect attachment geometries [214,216]. Conversely, mutation of the HEC1 tail to aspartate residues to mimic constitutive phosphorylation left cells unable to form more than a few stable kinetochore-microtubule attachments [216].

The regulation of kinetochore-microtubule stability by Aurora B and tension came together in the so-called spatial separation model [217,218] (Diagram 17). The central idea is that Aurora B, which is centromere-localised, can only phosphorylate HEC1 at the outer kinetochore in the absence of tension. Upon biorientation and the consequent establishment of tension the outer kinetochore is pulled away from the centromere – resulting in an inability of Aurora B to reach its outer-kinetochore substrates. Experiments tethering a FRET-sensor to different positions along the centromere-kinetochore axis demonstrated that when positioned at the outer kinetochore, the sensor was more highly phosphorylated in the absence of tension. Conversely, re-localising Aurora B so that it was closer to the outer kinetochore resulted in higher FRET-sensor phosphorylation and microtubule destabilisation [217].

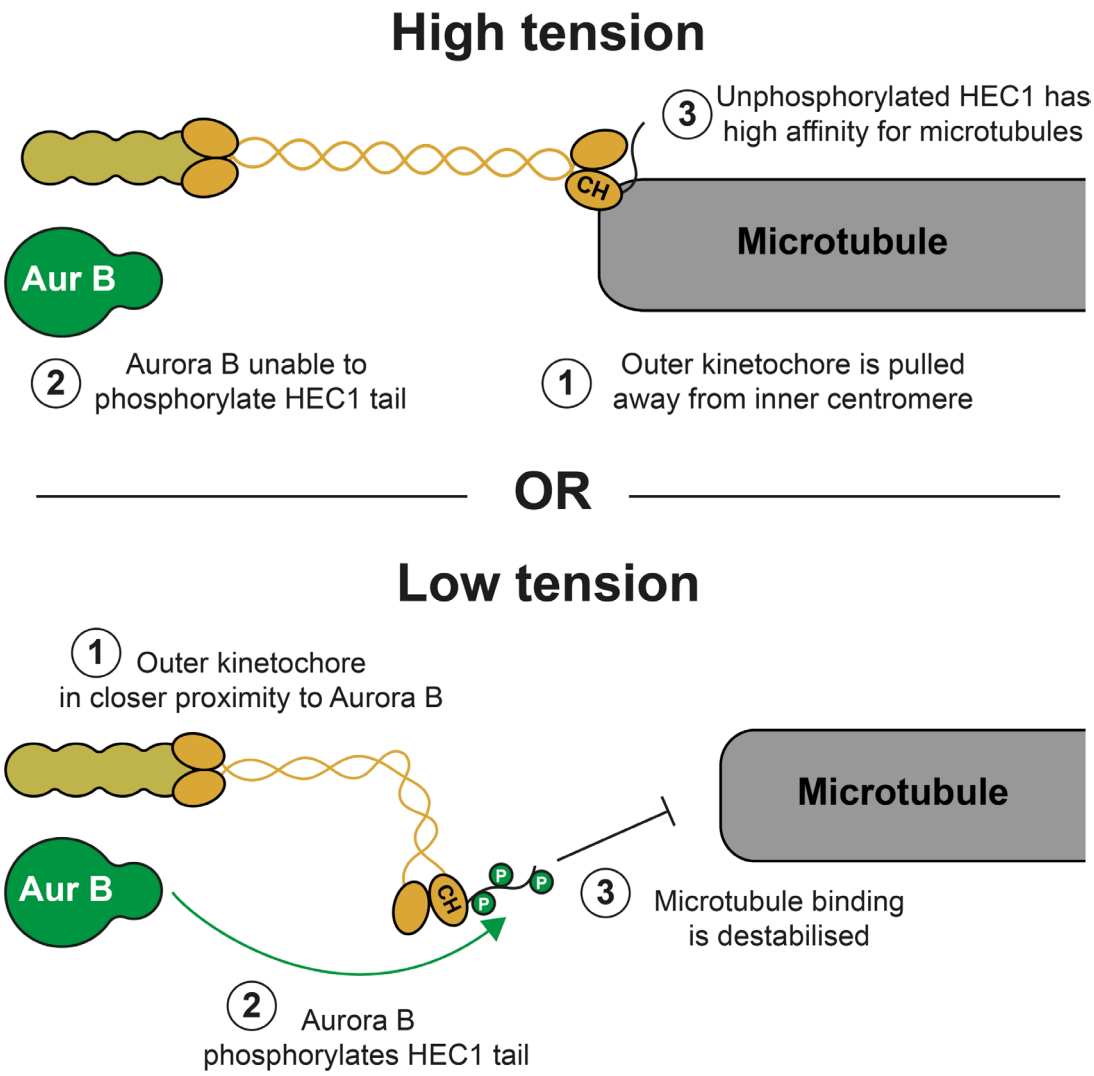

Diagram 17 – Spatial separation model of tension sensing. See main text for full details.

This model of spatial separation, wherein Aurora B at the centromere is unable to reach outer-kinetochore substrates upon tensioned attachment, is the most wide-spread model of tension sensing. However, since the inception of the spatial separation model, other possibilities for how tension stabilises microtubule attachment or regulates Aurora B have been put forward. These models will be briefly introduced below; their nuances are beyond the scope of this project but are reviewed in [219]. Even without Aurora B, *in vitro* experiments using purified yeast kinetochores showed that kinetochore-microtubule attachments are intrinsically

stabilised by tension [220]. Besides spatial separation, some models suggest that the deformation of tension-sensing molecules, namely INCENP, CENP-E, and/or PICH, at the kinetochore directly regulates the kinase activity of Aurora B [221–224]. In the opposing direction, the spatial separation of PP2A-B56 from the PP2A inhibitor SET/TAF1, localised at the centromere, is proposed to contribute to error-correction by changing the activity of the phosphatase which opposes Aurora B [225,226]. At odds with the idea that Aurora B is physically separated from outer-kinetochore targets, Aurora B has more recently been reported to localise to the outer kinetochore [227,228], which has led to the proposal that a kinetochore-localised pool of Aurora B is responding to tension [229]. In summary, many models now exist to explain how Aurora B and tension are linked to kinetochore-microtubule stability. While not all these models are mutually exclusive, this is an area of continued debate over 6 decades after the idea of tension-sensing was first introduced.

Additional determinants of kinetochore-microtubule stability

The regulation of microtubule-kinetochore stability depends on more than Aurora B phosphorylation of HEC1. Additional structural proteins, phosphatase activity, and kinases also play key roles in regulating attachment stability. MPS1 has long been reported to play a role in establishing biorientation. Depletion or inhibition of MPS1 in yeast and humans causes defects in chromosome biorientation [93,143,230,231]. In humans, the depletion of MPS1 was initially reported to cause the accumulation of polar chromosomes with syntelic attachments – suggesting that the defects in biorientation are specifically due to defects in error correction [231]. The mechanism by which MPS1 participated in error correction was believed to be via MPS1-dependent control of Aurora B activity [231], but this idea has since been called into question [93]. Subsequent studies have produced observations on the phenotype of MPS1 depletion or inhibition which conflict this original report as described in detail below [93,165].

A popular assay used to assess defects in error-correction is that of the monastrol washout [232–234] (Diagram 18). Here, the small-molecule inhibitor monastrol is used to inhibit Kinesin-5 (Eg5), resulting in the collapse of the spindle into a monopolar state [232]. Such spindles exhibit many chromosomes with a range of attachment states – including syntelic attachments. The removal of monastrol allows the spindle to re-establish bipolarity and continue mitosis as normal. The persistence of syntelic attachments following the washout of monastrol is indicative of an inability to correct erroneous kinetochore-microtubule attachments [234].

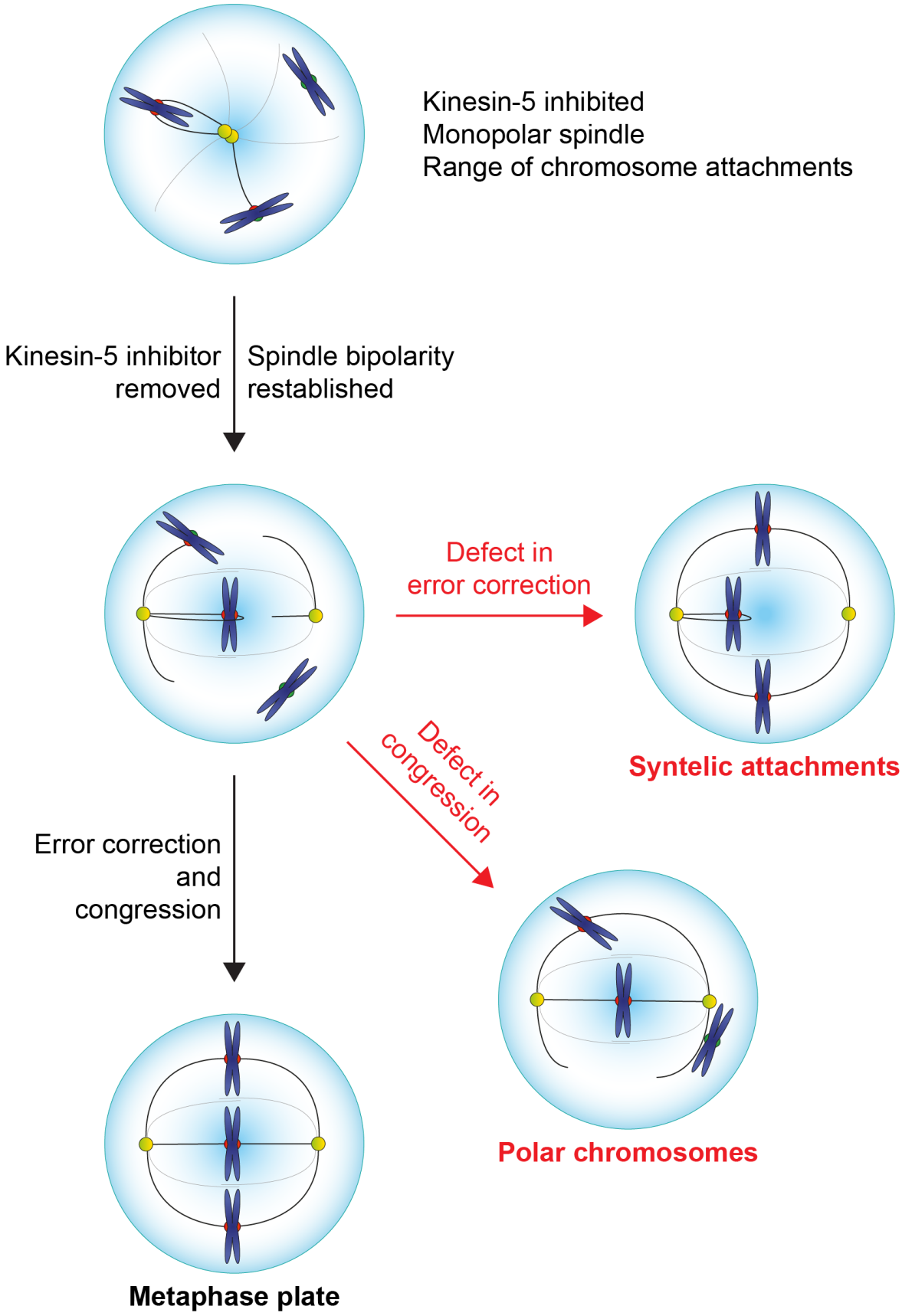

Diagram 18 – Schematic of a monastrol washout experiment. See main text for full details.

In such monastrol washout experiments, defects in chromosome biorientation are seen when MPS1 is inhibited [93,165]. However, the phenotype is not one in which syntelic attachments persist. Rather, unaligned chromosomes are seen which do not have end-on microtubule attachment – suggesting the biorientation defect is due to issues with chromosome congression, not error correction. Two explanations for this observation have been put forth. Firstly, Loss of MPS1 activity will cause defects in CENP-E recruitment, disrupting the CENP-E dependent lateral-sliding mechanism of chromosome congression [93,165]. In contrast to this idea, one study reported no loss of CENP-E upon MPS1 depletion [231]. Secondly, the accumulation of inactive MPS1 on unattached kinetochores has been proposed to block microtubule binding to prevent chromosome congression by end-on dependent mechanisms [165], consistent with the notion that MPS1 and microtubules compete for kinetochore binding [134,164]. Despite the main phenotype of MPS1 inhibition being congression defects, rapid targeting of MPS1 to the metaphase plate was seen to induce severe misalignment defects even when Aurora B was inhibited [235]. This observation, along with the identification of a molecular target for MPS1, SKA3, re-affirms the notion that MPS1 is involved in error correction [235]. How MPS1 inhibition or depletion does not produce defects in error correction is thus seemingly paradoxical. Additionally, how MPS1 exerts a local role in promoting error correction at attached kinetochores is incompatible with the idea that such kinetochores possess no free binding sites to localise MPS1.

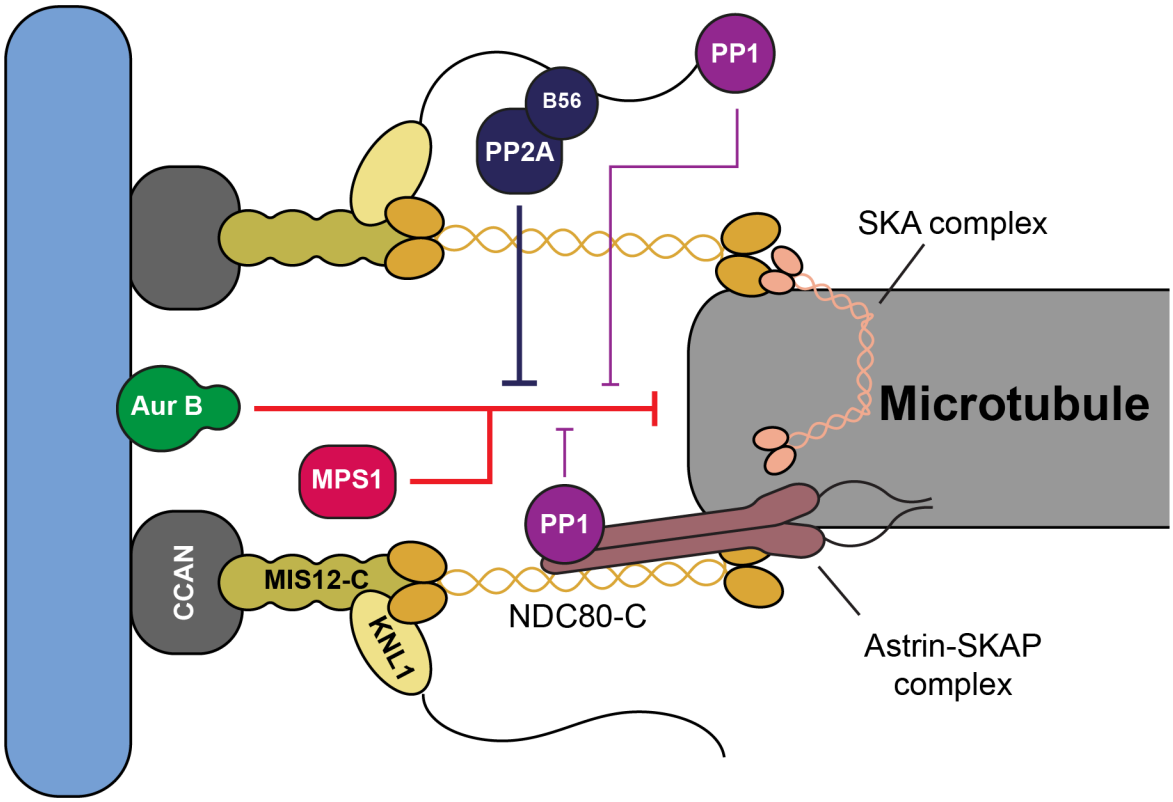

Diagram 19 – End-on attached microtubules are stabilised by a multitude of factors. The Astrin-SKAP and SKA complexes bolster the interaction between the NDC80-C and microtubules. PP1 and PP2A-B56 oppose the error-correcting activity of MPS1 and Aurora B kinases.

The Astrin-SKAP complex and the SKA complex localise to end-on attachments to stabilise them (Diagram 19). The SKA complex binds to both microtubules and HEC1 to strengthen microtubule-kinetochore attachments [236–238]. This crosslinking activity serves to strengthen the mechanical properties of the interaction between microtubules and the NDC80-C [237]. The localisation of the SKA complex has been linked to the activity of both error correcting kinases Aurora B and MPS1. Aurora B phosphorylation of HEC1 has been proposed to modulate kinetochore-microtubule stability via the SKA complex [239], whereas MPS1 phosphorylation of SKA3 itself is proposed to impair its residency time on microtubules [235]. Like the SKA complex, loss of the Astrin-SKAP complex compromises attachment stability [240]. The Astrin-SKAP complex also binds to both microtubules and HEC1 to

crosslink and stabilise kinetochore-microtubule attachments [241,242]. Aurora B is likewise responsible for opposing the localisation of Astrin-SKAP to microtubule-attached kinetochores [91,243].

Phosphatase activity stabilises kinetochore-microtubule attachment by dephosphorylating Aurora B and MPS1 targets which otherwise destabilise microtubule binding (Diagram 19). The BUBR1-localised pool of PP2A-B56 has major roles in stabilising microtubule binding, as loss of B56, or disruption from binding BUBR1, severely decreases the ability of cells to form stable kinetochore-microtubule attachments and congress chromosomes to the metaphase plate [158,173,174,244]. PP1 also contributes to attachment stability, though disruption of PP1 has much milder phenotypes than that of PP2A-B56 – suggesting it has a more minor role in human cells [161]. PP1 becomes enriched at attached kinetochores through several mechanisms. PP1 binds directly to SILK and RVSF motifs on KNL1 when Aurora B activity is low, and is brought by several binding partners, such as Astrin and KIF18A, to attached kinetochores [91,161,245]. Together, these phosphatases oppose Aurora B and MPS1 activity to stabilise attachments, similar to how they oppose Aurora B and MPS1 to silence local checkpoint signalling.

By localising PP2A-B56, the kinase activities of MPS1 and PLK1 promote attachment stability. As mentioned, the recruitment of BUBR1 to kinetochores is MPS1-dependent [94–96], and the interaction between BUBR1 and B56 is PLK1-dependent [120]. This dual role of MPS1 in both destabilising and stabilising kinetochore-microtubule attachments is seemingly paradoxical. This incoherent feed-forward loop likely constitutes a signal damping mechanism – increasing local PP2A-B56 at unattached kinetochores to oppose local Aurora B and MPS1 activity such that attachments can reform [235]. Additionally, this dual role of MPS1 may

explain why depletion of MPS1 does not result in an error-correction phenotype according to some studies [93,165]. Presumably the loss of MPS1 activity, which will stabilise attachments, also decreases the concentration of localised PP2A-B56, which will destabilise attachments.

Thesis aims

In summary, MPS1 has major roles in checkpoint signalling and error correction, yet many of the details are controversial or unclear. One key unsolved problem is how MPS1 recruitment to kinetochores is regulated. As MPS1 has core roles in initiating spindle checkpoint signalling and error correction, mechanistic detail of how MPS1 localisation is controlled will shed light on the molecular underpinnings of these processes. A model of direct competition seems insufficient to fully explain how sub-saturating microtubule binding can stop MPS1 localisation and silence local checkpoint signalling. The notion that microtubule occupancy alone is sufficient to stop MPS1 localisation will be re-addressed. How the activity of kinases and phosphatases may factor in to MPS1 localisation downstream of microtubule attachment will also be explored.

How MPS1, CDK1, and Aurora B elicit changes in the localisation of MPS1 is controversial. Direct (auto-phosphorylation) and indirect (recruitment of other factors) mechanisms may both explain how MPS1 kinase activity opposes its kinetochore localisation. Regarding Aurora B, the molecular target which is phosphorylated to promote MPS1 localisation remains unclear. Finally, the MR, which must be phosphorylated by CDK1-Cyclin B for MPS1 to localise, is apparently dispensable for MPS1 localisation This thesis will attempt to elucidate more molecular detail on how these three kinases control MPS1 localisation, and how their activities may integrate with one another.

There is clear evidence that MPS1 is involved in error correction. However, inhibition of MPS1 produces a different phenotype than that of Aurora B with regards to correcting syntelic attachments. This apparent discrepancy will be investigated. It is possible that the recruitment of PP2A-B56 by MPS1 may cause the stabilisation of

microtubule-kinetochore attachments – thus obscuring the role of MPS1 in error correction. Furthermore, the ability of MPS1 to localise to erroneous attachments to promote error-correction is not compatible with the idea that MPS1 cannot bind microtubule-attached kinetochores. By investigating the validity of the direct competition model, a new understanding of how MPS1 mechanistically participates in error correction will be generated.

Materials and methods

Molecular biology

Human MPS1, HEC1 and BUBR1 were amplified from Human testis cDNA (Marathon cDNA; Takara Bio Inc.) using Pfu polymerase (Promega). Mammalian expression constructs were made using pcDNA5/FRT/TO vectors (Invitrogen), modified to encode the EGFP- or mCherry-reading frames. To generate constructs with phospho-null (N8A) or phospho-mimetic (N8D, N8E) MPS1 autophosphorylation sites, the first 300 base pairs of MPS1 were synthesized by Twist Bioscience with the sites encoding amino acids Ser7, Thr12, Ser15, Thr33, Ser37, Thr45, Thr46 and Ser49 changed to encode either alanine (N8A), aspartic acid (N8D), or glutamic acid (N8E) residues. HiFi assembly (NEB) was then used to replace the first 300 base pairs of MPS1 with the synthetic fragments in expression vectors. All other mutations were performed using the Quikchange method (Agilent). Deletion of the MR (261-300) was performed by HiFi assembly (NEB).

Cell culture

HeLa cells, MPS1-GFP CRISPR HeLa cells [246,247], Parental HeLa Flp-In cells [248], and HEK293T cells were cultured in DMEM with 1% v/v GlutaMAX (Gibco) containing 10% v/v bovine calf serum (“plain DMEM”) at 37°C and 5% CO2. HeLa Flp-In TREx cell lines were maintained as above with the edition of 4 µg/ml blasticidine and 200 µg/ml hygromycin B. HeLa Flp-In TREx cell lines with endogenously tagged GFP-MPS1 were maintained with the edition of 0.2 µg/ml puromycin, 4 µg/ml blasticidine, and 200 µg/ml hygromycin B. HeLa cells expressing endogenously tagged MPS1-GFP as well as the rapamycin-dependent Aurora B kinetochore targeting system were grown in DMEM with 1% [vol/vol] GlutaMAX (Life

Technologies) containing 10% [vol/vol] bovine calf serum as well as 550 µg/ml geneticin and 1 µg/ml Puromycin.

Sf9 cells were cultured in Grace's Insect Media supplemented with 1% v/v GlutaMAX (Gibco) and 10% v/v bovine calf serum, or unsupplemented Sf-900 II SFM (Gibco). Cells were grown as either adherent mono-layer cultures at 27°C, or as suspension cultures in shaker flasks at 24°C. *E. coli* strains were grown in LB supplemented with appropriate antibiotics and grown at 16-37°C.

Table 1 – Cell lines used in this study.

Cell line	**Source**
HeLa S3	ATCC: CCL-2.2 RRID:CVCL_0058
HeLa S3 with MPS1 endogenously tagged with GFP at the C terminus	[117]
HeLa S3 with endogenously tagged with MPS1-GFP at with Aurora-B kinetochore targeting system integrated at AAVS1 locus	This study, made by Daniel Hayward
HeLa S3 Flp-In-TRex parental cells	[248]
HeLa S3 Flp-In-TREx GFP-MPS1 WT, KD, N8A, N8D, N8E, 3A, 3D, 3E	This study
HeLa S3 Flp-In-TREx GFP-MPS1 S281A, S281D, Δ60, ΔMR	[117], remade in conjunction with Vanessa Enoguanbhor
HeLa S3 Flp-In-TREx GFP-BUBR1 WT, LI/AA	[160], remade by Mia Holloway
HeLa S3 Flp-In-TREx B56 Delta	This study, made by Ulrike Gruneberg
HeLa S3 Flp-In-TRex parental cells with MPS1 endogenously tagged with GFP at the N terminus	This study, made by Daniel Hayward
HeLa S3 Flp-In-TREx mCherry-BUBR1 WT, LI/AA - with MPS1 endogenously tagged with GFP at the N terminus	This study, made in conjunction with Daniel Hayward
Sf9 cells	ATCC: CRL-1711
HEK 293T	ATCC: CRL-3216
E. coli DH5α	Invitrogen: 18258-012
E. coli JM109 pRIL	Homemade
E. coli BL21	NEB: C2530
E. coli BL21 DE3	NEB: C2527I

HeLa cell line generation

HeLa cell lines with single integrated copies of the desired transgene were created using the T-Rex doxycycline-inducible Flp-In system (Invitrogen, [248]) using pcDNA5/FRT/TO vectors as follows. Parental HeLa Flp-In T-REx cells [248] were seeded at 80,000 cells/well in plain DMEM in 6-well plates. After 24 hours wells were transfected with 100 µl of Optimem (Gibco) plus 3 µl of TransIT-LT1 (Mirus), 100 ng of the desired pCDNA5/RT/TO construct, and 900 ng of pOG44 (for expression of Flp-Recombinase). After 24 hours cells were trypsanised and plated onto 15 cm plates in plain DMEM. After a further 24 hours a media exchange into plain DMEM supplemented with 4 µg/ml blasticidine and 200 µg/ml hygromycin B was performed. Media was exchanged every 3-4 days until colonies had formed. Single colonies were picked and screened by fluorescence microscopy following 24 hour induction with doxycycline (2 µM). Positive, homogenous clones were further validated by Western blotting.

MPS1 was endogenously tagged at the N-terminus with GFP using CRISPR/Cas9 editing in HeLa cells already containing a single T-Rex doxycycline-inducible Flp-In integration site using a previously described method [115,117]. In brief, homology recombination cassettes containing the desired knock-in DNA with flanking regions of homology of 1075 bp to the target locus were co-transfected with a version of pSpCAS9(BB) (Addgene, #48139) containing the guide RNA sequence 5'-TCTTTGATGCTAGTTAAAGT-3' and modified to removed puromycin resistance. The knock-in sequences harbour a puromycin resistance marker followed by a glycine-serine rich flexible linker (GS), a P2A ribosome-skipping sequence, and the EGFP protein sequence followed by a glycine-serine rich flexible linker (GS).

Antibiotic-resistant clones were selected and successful modification was confirmed by western blotting.

INCENP kinetochore recruitment by rapamycin addition was achieved by editing a previously described system ([249], plasmid pERB109, Addgene #58280). This was adapted by placing miRFKBP5_Mis12-GFP-FKBP3 under doxycycline-inducible expression and replacing GFP with a Myc tag. INCENP 47-918 was inserted after mCh-FRB. 831 and 804 bp homology arms flanking the AAVS1 safe harbour locus were also added, and the system was stably integrated into the AAVS1 safe harbour locus of HeLa cells homozygously expressing MPS1 endogenously tagged with GFP at the C-terminus by CRISPR/Cas9 knock-in, using the guide RNA sequence 5'-GTTAATGTGGCTCTGGTTCT-3' ([250] Addgene constructs #72833 and #72834).

siRNA-mediated protein depletion and doxycycline-induced transgene expression

For siRNA cells were seeded at 50,000 cells/well in plain DMEM in 6-well plates. siRNA transfection was performed 24 hours after cells were seeded, and 48 hours before harvest/fixation. Transfection mixes were made as follows. Per well, 3-4 µl of 20 µM siRNA oligomers (Table 2) were added to Opti-MEM (Gibco) to a volume of 100 µl in an Eppendorf tube. In a separate tube, the equivalent volumes of oligofecctamine (Invitrogen) and Opti-MEM (Gibco) were mixed. After 5 minutes the two tubes were mixed together and incubated for a further 20 minutes before being added drop-wise to wells.

To induce expression of genes integrated at the Flp-In locus, doxycycline (InvivoGen) was added to 2 µM. For rescue experiments with MPS1, this was done

concomitantly with siRNA addition. For rescue experiments with HEC1, this was done 2 hours before siRNA addition. For rescue experiments with BUBR1, this was done 6 hours before siRNA addition. A second induction was performed 24 hours into the siRNA depletion.

Table 2 – Oligonucleotides used in this study.

Oligonucelotude	**Source**	**Cat#**
Control siRNA against GL2 (luciferase) (5'-CGUACGCGGAAUACUUCGAUU-3')	Dharmacon	Cat#D-001100-01-20
siRNA against MPS1 3'UTR (5'-UUGGACUGUUAUACUCUUGAA-3', 5'-GUGGAUAGCAAGUAUAUUCUA-3', and 5'-CUUGAAUCCCUGUGGAAAU-3')	[117]	N/A
siRNA against HEC1 5'UTR (5'-CCCUGGGUCGUGUCAGGAA-3')	[131]	N/A
siRNA against BUBR1 3'UTR (5'-GCAATCAAGTCTCACAGAT-3')	[160]	N/A
On-target plus Smartpool siRNA oligos against PPP2R5A (5'-GCUCAAAGAUGCCACUUCA-3', 5'-CAAUACAAGUGCCGAAUAA-3', 5'-UGAAUGAACUGGUUGAGUA-3', 5'-GGAAAUGAAUGGCAAGCUU-3')	Dharmacon	Cat#L-009352
On-target plus Smartpool siRNA oligos against PPP2R5B (5'-CGCAUGAUCUCAGUGAAUA-3', 5'-UCAAGUCGCUGUCUGUCUU-3', 5'-CAAACCAUCGUAUCACUGA-3', 5'-GAACAAUGAGUAUAUCCUA-3')	Dharmacon	Cat#L-009366
On-target plus Smartpool siRNA oligos against PPP2R5C (5'-GGAUUUGCCUUACCACUAA-3', 5'-GGAAGAUGAACCAACGUUA-3', 5'-CAUCAGAAUUUGUGAAGAU-3', 5'-CAGAAGUAGUCCAUAUGUU-3')	Dharmacon	Cat#L-009433
On-target plus Smartpool siRNA oligos against PPP2R5D (5'-GUACAUCGACCAGAAGUUU-3', 5'-UCCAUGGACUGAUCUAUAA-3', 5'-UGACUGAGCCGGUAAUUGU-3', 5'-GUAGGCAGAUCAACCACAU-3')	Dharmacon	Cat#L-009799

On-target plus Smartpool siRNA oligos against PPP2R5E (5'-UUAAUGAACUGGUGGACUA-3', 5'-GCACAGCUGGCAUAUUGUA-3', 5'-GACACGCUAUCUGAUCUUA-3', 5'-GGAUAAAGUAGACGGAUUU-3')	Dharmacon	Cat#L-008531
Silencer-Select siRNA oligo against BIRC5 (survivin) 5'-GCAGGUUCCUUAUCUGUCA-3'	ThermoFisher	Cat#4390824

Drug treatments

Drug treatments were performed by addition of 100 µl of working dilutions to ensure drugs were solubilised in water and could diffuse rapidly into cells.

Table 3 – Drugs used in this study.

Drug	**Supplier**	**Cat#**
AZ3146 – used at 2 µM, 10-60 min	Tocris Bioscience	Cat#3994
ZM447439 – used at 10 µM, 15-60 min	Tocris Bioscience	Cat#2458
Calyculin A – used at 25 nM, 6 min	Tocris Bioscience	Cat#1336
S-trityl-L-cysteine – used at 10 µM, 2 h	Sigma-Aldrich	Cat#164739-5G
Rapamycin – used at 500 nM, variable times	Sigma-Aldrich	Cat#R0395
MG132 – used at 20 µM, 30-90 min	Santa Cruz Biotechnology	Cat#sc-201270
Monastrol – used at 100 µM, 16 h	Tocris Bioscience	Cat#1305
5-iodotubercidin – used at 5 µM, 10-15 min	Tocris Bioscience	Cat#1745
AZD1152 – used at 10 µM, 60 min	Selleck	Cat#S1147
GSK923295 – used at 50 nM, 2 h	Cayman chemical	Cat#18389
Doxycycline – used at 2 µM, 48 h	Insight	Cat#sc-204743
SiR-Tubulin – used at 50 nM, 1 h prior to imaging	Spirochrome	Cat#SC002
SiR-DNA – used at 50 nM, 1 h prior to imaging	Spirochrome	Cat#SC007
Nocodazole – used at 0.6 – 6.6 µM, 5 min to overnight	Merck Chemicals Ltd	Cat#484728

Cold treatment

Mitotic cells were cold treated by placing cell dishes on ice and replacing the existing media with pre-chilled plain media. Cells remained on ice for 9 min and then were fixed at room temperature.

Western blotting

Cells from 6-well plates were harvested for Western blotting by scrapping. Media was transferred to 2 ml Eppendorf tubes and centrifuged at 800xg for 5 minutes. Pellets were washed in PBS twice. Cells were lysed for 50 minutes at 4^{o}C with lysis buffer (20 mM Tris-HCl pH 7.5, 150 mM NaCl, 1% v/v IGEPAL, 1:100 protease inhibitor cocktail (Sigma P8340), 1 mM PMSF). Lysates were centrifuged at 20,800xg for 15 minutes at 4^{o}C. Clarified lysates were diluted to the same concentration with lysis buffer and boiled in an appropriate volume of 5x sample buffer (Bio-rad) for 8 minutes.

Protein samples were separated on SDS-PAGE gels and transferred to nitrocellulose membranes using a Trans-blot Turbo system according to manufacturer's instructions (Bio-Rad). Membranes were blocked in blocking buffer (5% w/v milk powder or BSA, 0.1% v/v tween-20, in PBS) for 1 hour. Membranes were incubated with primary antibodies (Table 4) overnight at 4^{o}C, except for blots against Actin, which were blocked overnight. The following day membranes were washed 3 x 10 minutes in PBS + 0.1% tween and incubated with the appropriate HRP-conjugated secondary antibody (Jackson ImmunoResearch Laboratories Inc.) at 1 µg/ml for 45 minutes at room temperature. Blots against Actin were incubated with anti-actin HRP conjugated mAb (Abcam, [AC-15] (HRP)) for 45 minutes. Membranes were washed as previous and incubated with Amersham ECL Western

Blotting Detection Reagent according to manufacturer's instructions (GE Healthcare). Exposures were taken with Amersham Hyperfilm ECL (GE Healthcare).

Table 4 – Antibodies used in this study.

Antibody target	**Source**	**Cat# and RRID**
Astrin Rabbit pAb	[240] and this paper	N/A
BUB1 Rabbit pAb	Bethyl	Cat#A300-373A; RRID:AB_2065943
BUBR1 Rabbit pAb	Bethyl	Cat#A33-386A; RRID:AB_386097
CENP-C Guinea Pig pAb	MBL	Cat#PD030; RRID:AB_10693556
CREST Human pAb	Antibodies Inc.	Cat#15-234-0001; RRID:AB_2687472
HEC1 Mouse mAb (9G3.23)	GeneTex	Cat#GTX70268; RRID:AB_371632
MAD1 Rabbit pAb	GeneTex	Cat#GTX105079; RRID:AB_11173437
MPS1 Mouse mAb (N1)	Abcam	Cat#ab11108; RRID:AB_297757
Myc Mouse mAb (pE10)	Sigma-Aldrich	Cat#M4439; RRID:AB_439694
Phospho H3-T3 Rabbit pAb	Cell Signalling	Cat#9714; RRID:AB_491018
p-Histone H3 Ser10 – pH3S10 Mouse mAb (6G3)	Cell Signaling	Cat#9706S; RRID:AB_331748
Phospho H3-T120 Rabbit pAb	Active Motif	Cat#39392; RRID:AB_2744670
Phospho-Aurora Kinase B (Thr232) Rabbit pAb	ThermoFisher Scientific	Cat#600-401-677; RRID:AB_2061641
Aurora B Kinase (AIM1) Mouse pAb	Cell signalling	Cat#3094; RRID:AB_10695307
Phospho-TTK-T33/S37 Rabbit pAb	ThermoFisher Scientific	Cat#44-1325G; RRID:AB_2533594
Survivin Rabbit pAb	Abcam	ab76424; RRID:AB_1524459
Tubulin Mouse mAb (DM1A)	Sigma-Aldrich	Cat#T6199; RRID:AB_477583

Tubulin Rabbit mAb (EP1332Y)	Abcam	Cat#ab52866; RRID:AB_869989
HURP Sheep pAb	[242]	N/A
KNL1 pT875 (pMELT) pAb	[160]	N/A
KNL1 Sheep pAb	This paper	N/A
GFP Sheep pAb	Homemade Barr lab	N/A
Kinastrin Sh pAb	[240]	N/A
Beta Actin Mouse mAb (AC-15) HRP conjugate	Abcam	Cat#ab49900; RRID:AB_867494
Alexa Fluor® 647 AffiniPure Donkey Anti-Guinea Pig IgG (H+L)	Stratech	Cat#706-605-148; RRID:AB_2340476
Donkey anti-Mouse IgG (H+L) Highly Cross-Adsorbed Secondary Antibody, Alexa Fluor™ 555	ThermoFisher Scientific	Cat#A31570; RRID:AB_2536180
Donkey anti-Sheep IgG (H+L) Cross-Adsorbed Secondary Antibody, Alexa Fluor™ 555	ThermoFisher Scientific	Cat#A21436; RRID:AB_2535857
Donkey anti-Rabbit IgG (H+L) Highly Cross-Adsorbed Secondary Antibody, Alexa Fluor™ 555	ThermoFisher Scientific	Cat#A31572; RRID:AB_162543
Donkey anti-Mouse IgG (H+L) Highly Cross-Adsorbed Secondary Antibody, Alexa Fluor™ 350	ThermoFisher Scientific	Cat#A10035; RRID:AB_2534011
Donkey anti-Rabbit IgG (H+L) Highly Cross-Adsorbed Secondary Antibody, Alexa Fluor™ 350	ThermoFisher Scientific	Cat#A10039; RRID:AB_2534015
Donkey anti-Rabbit IgG (H+L) Highly Cross-Adsorbed Secondary Antibody, Alexa Fluor™ 647	ThermoFisher Scientific	Cat#A31573; RRID:AB_2536183
Donkey anti-Mouse IgG (H+L) Highly Cross-Adsorbed Secondary Antibody, Alexa Fluor™ 647	ThermoFisher Scientific	Cat#A31571; RRID:AB_162542
Donkey anti-Human IgG (H+L) Secondary Antibody [DyLight 350]	Bio-Techne Ltd.	Cat#NBP2-60667UV; RRID:AB_2556705
Peroxidase AffiniPure Donkey Anti-Rabbit IgG (H+L)	Stratech	Cat#711-035-152; RRID:AB_10015282
Peroxidase AffiniPure Donkey Anti-Mouse IgG (H+L)	Stratech	Cat#715-035-151; RRID:AB_2340771

Immunofluorescence staining

Cells seeded onto #1.5 thickness coverslips were fixed with PTEMF buffer (20 mM PIPES-KOH pH 6.8, 0.2% v/v Triton X-100, 10 mM EDTA, 1 mM MgCl2, 4% v/v formaldehyde) for 12 minutes at room temperature. Coverslips were incubated in

blocking buffer (3% w/v bovine serum albumin, 0.1% v/v Triton X-100 in PBS) for a minimum of 45 minutes. Coverslips were incubated face-down on 80 µl droplets of primary antibodies in a humidified chamber for 1 hour. Following primary antibody incubation coverslips were washed 3 x in PBS. Secondary donkey antibodies against mouse, rabbit, guinea pig, or sheep, labelled with Alexa Fluor 405, Alexa Fluor 555, or Alexa Fluor 647 (Molecular Probes) were used at 1:1000. Coverslips were incubated face-down on 80 µl droplets of diluted antibodies in a humidified chamber for 45 minutes. Coverslips were washed 3 x in PBS and 1 x in distilled deionised water. For dry-mounting, coverslips were left to dry completely before being mounted with 7 µl of Mowiol 4-88 (Sigma) according to manufacturer's instructions. For wet-mounting, coverslips were mounted onto droplets of Vectashield Plus (2bscientific) and sealed with clear nail polish.

Fixed cell imaging

For some figures, cells were imaged on a DeltaVision Core light microscopy system (GE Healthcare) using a 100×/1.4-NA objective fitted to an Olympus IX-71 microscope stand. Standard filter sets for DAPI (excitation 390/18, emission 435/48), FITC (excitation 475/28, emission 525/48), TRITC (excitation 542/27, emission 597/45), and Cy-5 (excitation 632/22, emission 676/34) were used to sequentially excite and collect fluorescence images on a CoolSnap HQ2 CCD camera (Photometrics) using the software package softWoRx (GE Healthcare). Cells were imaged using a 0.2 µm interval and a total stack of 2 µm and deconvolved for presentation using softWoRx. For quantification, imaging was performed using a 60×/1.35-NA oil-immersion objective on a BX61 Olympus microscope equipped with filter sets for DAPI, EGFP/Alexa Fluor 488, 555, and 647 (Chroma Technology

Corp.), a CoolSNAP HQ2 camera (Roper Scientific), and MetaMorph 7.5 imaging software (GE Healthcare).

For intrakinetochore distance measurements, samples seeded on #1.5 thickness coverslips were wet-mounted with Vectashield and imaged on an Olympus SoRa spinning disk confocal microscope using a 60x/1.5-NA objective fitted to an Olympus IX-83 microscope stand with 3.2 x optical zoom and a Yokogawa CSU-W1 SoRa super-resolution spinning disk. Solid state lasers emitting 405 nm, 488 nm, 561 nm and 633 nm were used. Images were captured with a Prime BSI sCMOS camera (photometrics) using Olympus cellSens software package. Images were acquired with a 0.24 μm interval over a total distance of 4.8 μm. Constrained iterative deconvolution was performed on cellSens.

Live cell imaging

For experiments with the Aurora B kinetochore-targetting system, cells seeded on circular glass bottom Fluorodish imaging dishes (World Precision Instruments) in Fluorobrite media (ThermoFisher Scientific) supplemented with 10% FBS and 1x GlutaMAX (ThermoFisher Scientific) were imaged at 37°C with 5% CO_2 on an Olympus SoRa spinning disk confocal microscope using a 60x/1.5-NA or 100x/1.45-sNA objective fitted to an Olympus IX-83 microscope stand with a Yokogawa CSU-W1 SoRa super-resolution spinning disk. Solid state lasers emitting 405 nm, 488 nm, 561 nm, and 633 nm were used. Images were captured with a Prime 95B sCMOS camera (photometrics) using Olympus cellSens software package. Kinetochores of STLC arrested cells were imaged using the 100x/1.45-NA objective as 1.3 μm stacks with intervals of 0.26 μm across a period of 15 minutes with 30 second intervals. STLC (10 μM) was added 4 hours prior to imaging. 10 μm stacks with intervals of 0.5 μm of MG132/Nocodazole arrested cells were imaged using the

60x/1.5-NA objective at intervals of 2 min over a total period of 22 minutes, with 100 ul PBS + Rapamycin added in the interval between the first a second timepoint. SiR-Tubulin (50 nM) and Hoechst (4 μM) were added 1 hour prior to imaging.

For determining mitotic timings of GFP-MPS1 Flp-In cell lines, cells were seeded on 6-well #1.5H glass-bottomed dishes (Cellvis) in Fluorobrite media (ThermoFisher Scientific) supplemented with 10% FBS and 1x GlutaMAX (ThermoFisher Scientific). Imaging was performed using a 20x/0.75 NA air objective on an EVOS M7000 (ThermoFisher) with software version 2.0.2094.0, equipped with an onstage incubator and DAPI, GFP, Texas Red, and Cy5 light cubes. Cells were imaged at 37°C under 5% CO2 every 5 minutes for 12 hours. At each time point and stage position a stack of 4 z-planes was taken spaced 3 μm apart were acquired. SiR-DNA was added 1 hour prior to imaging.

For FRAP measurements of GFP-MPS1 Flp-In cell lines, cells were seeded on 35mm Fluorodish imaging dishes (World Precision Instruments) in Fluorobrite media (ThermoFisher Scientific) supplemented with 10% FBS and 1x GlutaMAX (ThermoFisher Scientific). Imaging was performed using an IX81 (Olympus) coupled to an Ultraview Vox spinning disk confocal system (PerkinElmer) fitted with an EM-CCD camera (C9100-13; Hamamatsu Photonics) and on-stage incubator (Tokai Hit), using a 60×/1.42 NA oil immersion objective. Cells were imaged at 37°C under 5% CO_2. Nocodazole was added to cells 1 hour prior to imaging. A 488 nm (GFP) laser was used to image a single focal plane every 250 ms for 1 second prior to the bleach step. Following this, the 488nm laser was used to perform a 1 second bleach step at 100% power over a single kinetochore. Subsequently, images of the same focal plane were taken every 250 ms for 60 seconds using the 488 nm laser.

Immunoprecipitation

GFP-tagged WT, KD, N8A, N8D, and N8E MPS1 mutants, or GFP alone were expressed and purified from HEK 293T cells. Per 15 cm dish, 10^7 cells in plain DMEM were seeded. Cells were transfected 24 hours after seeding, and 36 hours prior to harvesting. Per dish, transfection mix was prepared by mixing 8 µg of the desired pCDNA5/RT/TO construct, 24 µl of TransIT-LT1 (Mirus Bio LLC, and 800 µl of Opti-MEM (Gibco). This mix was incubated for 15 minutes before being added drop-wise to cells. Nocodazole was added 12 hours prior to harvesting. Cells were harvested by mitotic shakeoff and centrifuged at 400xg for 5 minutes. Pellets were washed in PBS twice. Cells were lysed and the lysate clarified as described for the Flp-In cells. Clarified lysates were each incubated with 50 µl (packed volume) of Protein G Dynabeads (Invitrogen) and 8µg of sheep anti-GFP (homemade) per plate for 1 hour at 4°C. Immunoprecipitates were washed four times with 1 ml of lysis buffer, twice with 20 mM Tris-HCl pH 7.4, 300 mM NaCl, 0.1% v/v Triton X-100, and twice with 20 mM Tris-HCl pH 7.4, 300 mM NaCl.

To dephosphorylate immunoprecipitated material, the beads were resuspended in 50 µl of 1x PMP buffer (New England Biolabs), 1 mM $MgCl_2$ and 1 µl of λ-phosphatase (New England Biolabs) and incubated at 30°C for 30 minutes. Following this, beads were washed as previous, then twice in 1xMEB buffer. 5 µl aliquots (packed volume) of beads were made and stored as a 1:1 slurry in 1xMEB buffer with 50% v/v glycerol at -20°C.

Radiokinase assays

Aliquots of immunoprecipitated dephosphorylated GFP-MPS1 were resuspended in 20 µl of reaction buffer (200 µM ATP, 1 mM DTT, 50 mM KCl, 10 mM $MgCl_2$ 15 mM EGTA, 20 mM Na β-glycerophosphate, and 1 µCi [^{32}P]γ-ATP per reaction) plus 1 µg

of purified GST-KNL1$^{728-1200}$ per reaction. Reaction mixes were incubated at 30^{o}C for 60 minutes with agitation. At the end of the incubation the liquid phases were pipetted into separate tubes. Beads were resuspended in 50 µl of 1 x sample buffer and 12.5 µl of 5x sample buffer was added to the liquid phases. Samples were boiled for 8 minutes and run on SDS-PAGE gels. Gels were Coomassie stained with InstantBlue (Sigma-Aldrich) and dried. Exposures to reveal ^{32}P incorporation were taken using.

Purification of GST-KNL1$^{728-1200}$

A 1 l culture of LB plus 50 µg/ml ampicillin and 1% w/v D-glucose was inoculated with 10 ml of overnight culture of JM109 pRIL harbouring KNL1$^{728-1200}$ in pGEX-5X-1 and grown at 37^{o}C. At OD_{600} = 0.6 expression was induced by the addition of IPTG to 400 µM for 3 hours. Cells were harvested by centrifugation (4000xg, 15 min) and washed twice with PBS. Cells were resuspended in 20 ml of lysis buffer (50 mM Tris-HCl pH 7.4, 300 mM NaCl, 1.5% v/v N-lauryl sarcosine, 1 mM DTT, and 1 mM EDTA) supplemented with 1:100 protease inhibitor cocktail (Sigma P8340), lysozyme (20 U/ml, Merck), and 0.5 mg/ml lysozyme (Sigma) for 20 minutes on ice. Cells were lysed by homogenisation using an Emulsi Flex C5 (Avestin) by passing the suspension through 5 times with 15,000 psi backpressure. The lysate was clarified by centrifugation (35,000xg, 45 minutes, 4^{o}C) and mixed with 0.5 ml (packed volume) of Glutathione-Sepharose 4B (Cytiva). After 2 hours the beads were pelleted and transferred to a 20 ml gravity flow column (Econopak). The beads were washed with 60 bead volumes of lysis buffer, 40 bead volumes of wash buffer 1 (50 mM Tris-HCl pH 7.4, 300 mM NaCl, 0.1% v/v N-lauryl sarcosine, 1 mM DTT, and 1 mM EDTA), 80 bead volumes of wash buffer 2 (50 mM Tris-HCl pH 7.4, 300 mM NaCl, 1 mM ATP, 1 mM $MgCl_2$, 1 mM DTT, and 1 mM EDTA), and 40 bead

volumes of wash buffer 3 (50 mM Tris-HCl pH 7.4, 300 mM NaCl, 1 mM DTT, and 1 mM EDTA). Elution fractions were collected by incubating the beads for 10 minutes with 2 ml of elution buffer (50 mM Tris-HCl pH 7.4, 300 mM NaCl, 30 mM reduced glutathione) per fraction. Fractions of interest were pooled and dialysed overnight into 50 mM Tris-HCl pH7.4, 150 mM NaCl, and 1 mM DTT. Glycerol was added to 10% v/v to the dialysed fractions prior to concentrating to 0.18 mg/ml. Aliquots were made and snap-frozen prior to storage at -80^{o}C.

Purification of NDC80^{Bonsai}

A 1 l culture of LB plus 50 µg/ml ampicillin was inoculated with 10 ml of overnight culture of BL21 pRIL harbouring NDC80^{Bonsai} in a pST39 co-expression vector and incubated at 37^{o}C. At OD_{600} = 0.5 cells were transferred to 18^{o}C for 1 hour before expression was induced by the addition of IPTG to 100 µM for 18 hours. Cells were resuspended in 20 ml of lysis buffer (50 mM Tris-HCl pH 7.6, 300 mM NaCl, 1 mM DTT, and 1 mM EDTA) supplemented with with 1:100 protease inhibitor cocktail (Sigma P8340), lysozyme (20 U/ml, Merck), and 0.5 mg/ml lysozyme (Sigma) for 20 minutes on ice. Cells were lysed by homogenisation using an Emulsi Flex C5 (Avestin) by passing the suspension through 5 times with 15,000 psi backpressure. The lysate was clarified by centrifugation (35,000xg, 45 minutes, 4^{o}C) and mixed with 0.5 ml (packed volume) of Glutathione-Sepharose 4B (Cytiva). After 2 hours the beads were pelleted and transferred to a 20 ml gravity flow column (Econopak). The beads were washed with 30 bead volumes of lysis buffer and 10 bead volumes of cleavage buffer (50 mM Tris-HCl pH 7.6, 150 mM NaCl, 1 mM EDTA, 1 mM DTT). To elute by cleavage, beads were incubated overnight in 3 ml of cleavage buffer + 50U Prescission protease (Cytiva) at 4^{o}C. The following morning the flowthrough was collected, and the column washed with 2 bead volumes of cleavage buffer to

collect all cleaved protein. The elutions were pooled and glycerol added to 10% v/v. To further purify the complex by SEC, the sample was centrifuged (35,000xg, 45 minutes, 4°C) to remove precipitates prior to loading on a HiLoad Superdex 16/600 G75 pre-equilibrated with SEC buffer (25 mM Tris-HCl pH 7.6, 150 mM NaCl, 1 mM EDTA, 1 mM DTT, 5%(v/v) glycerol). 1 ml fractions of interest were pooled, aliquoted, and snap frozen prior to storage at -80°C.

Purification of NDC80^{Brocolli}

A 1 l culture of LB plus 50 µg/ml ampicillin and 1%(w/v) D-glucose was inoculated with 10 ml of overnight culture of BL21 DE3 harbouring NDC80^{Broccoli} in a pGEX-6P-2 co-expression vector and incubated at 37°C. At OD_{600} = 0.5 cells were transferred to 18°C for 1 hour before expression was induced by the addition of IPTG to 100 µM for 18 hours. Cells were resuspended in 20 ml of lysis buffer (20 mM Tris-HCl pH 8, 300 mM NaCl, 1%(v/v) Triton X-100, and 5 mM imidazole) supplemented with 1:100 protease inhibitor cocktail (Sigma P8340), lysozyme (20 U/ml, Merck), and 0.5 mg/ml lysozyme (Sigma) for 20 minutes on ice. Cells were lysed by homogenisation using an Emulsi Flex C5 (Avestin) by passing the suspension through 5 times with 15,000 psi backpressure. The lysate was clarified by centrifugation (35,000xg, 45 minutes, 4°C) and mixed with 0.5 ml (packed volume) of Ni-NTA agarose (Qiagen). After 1.5 hours the beads were pelleted and transferred to a 20 ml gravity flow column (Econopak). The beads were washed with 80 bead volumes of lysis buffer, 40 bead volumes of wash buffer 1 (50 mM Tris-HCl pH 8, 300 mM NaCl, 0.1%(v/v) Triton X-100, and 20 mM imidazole), and 20 bead volumes of wash buffer 2 (50 mM Tris-HCl pH 8, 300 mM NaCl, and 20 mM imidazole). Protein was eluted by multiple additions of 2 ml of IMAC200 (20 mM Tris-HCl, pH 8.0, 300 mM NaCl, and 200 mM imidazole). Elution fractions of interest were pooled and dialysed overnight into 20

mM Tris-HCl, pH 7.5, 150 mM KCl, and 1 mM DTT. Dialysed protein was concentrated to a total volume of 500 µl using a Vivaspin 20 10,000 MWCO concentrator and separated by SEC on a Superdex 200 10/300 GL column equilibrated with 20 mM Tris-HCl, pH 7.5, 150 mM KCl, and 1 mM DTT, collecting 0.3 ml fractions. Fractions of interest were pooled and concentrated to 0.25 mg/ml, aliquoted, and snap-frozen prior to storage at -80^{o}C.

MPS1 full-length purification from insect cells

Recombinant baculoviruses encoding His-TEV-MPS1 constructs were generated (Expression systems) and used to infect 8 x 15 cm dishes containing 2 x 10^{7} insect cells each. 66 hours after infection cells were harvested by knocking and centrifuged at 500xg for 4 minutes. Pellets were washed twice in PBS then lysed in 8 ml each of lysis buffer (IMAC5 (20 mM Tris-HCl, pH 8.0, 300 mM NaCl, and 5 mM imidazole) plus 1% v/v Triton X-100, 1:100 protease inhibitor cocktail (Sigma P8340), 0.2 mM PMSF, 40 mM Na β-glycerophosphate, 10 nM calyculin A, and 100 nM okadaic acid) for 20 minutes at 4^{o}C. Lysates were centrifuged at 20,800xg for 20 minutes. Clarified lysates were incubated with 2 ml of Ni-NTA agarose beads (Qiagen) for 1 hour 30 minutes at 4^{o}C. Bead-lysate mixes were transferred to 20 ml gravity-flow columns (Econopak) and washed once with lysis buffer, once with IMAC5 plus 1% v/v Triton X-100, once with IMAC20 (20 mM Tris-HCl, pH 8.0, 300 mM NaCl, and 5 mM imidazole) plus 1% v/v Triton X-100, and four times with IMAC20. Protein was eluted by multiple additions of 2 ml of IMAC200 (20 mM Tris-HCl, pH 8.0, 300 mM NaCl, and 5 mM imidazole). Elution fractions of interest were pooled and dialysed overnight into 20 mM Tris-HCl, pH 8.0, 300 mM NaCl, and 1 mM DTT in the presence of 10 U of TEV protease (New England Biolabs). Glycerol was added to the dialysed samples to 10% v/v. Samples were concentrated to a volume of 150 µl using a

Vivaspin 20 50,000 MWCO concentrator and separated by SEC on an analytical Superose 6 10/300 GL column equilibrated with 20 mM Tris-HCl, pH 8.0, 300 mM NaCl, 1 mM DTT and 10% v/v glycerol, collecting 0.5 ml fractions. Fractions of interest were pooled and concentrated as previous before snap-freezing. Samples, previously purified by SEC, were diluted to 1 mg/ml and analyzed by SEC-MALS. Experiments were performed at room temperature during SEC on an analytical Superose 6 10/300 GL column, equilibrated with 20 mM Tris-HCl, pH 8.0, 300 mM NaCl, and 1 mM DTT. Elution was monitored via static light-scattering (DAWN HELEOS 8+; Wyatt Technology), differential refractive index (Optilab T-rEX; Wyatt Technology) and UV (SPD-20A; Shimadzu) detectors. Data were analysed using the ASTRA software package (Wyatt Technology).

Purification of GST-MPS1$^{1-305}$

A 1 l culture of LB plus 50 µg/ml ampicillin was inoculated with 10 ml of overnight culture of BL21 pRIL harbouring MPS1$^{1-305}$ in pGEX-5X-1 and grown at 37^{o}C. At OD_{600} = 0.6 expression was induced by the addition of IPTG to 400 µM for 3 hours. Cells were harvested by centrifugation (4000xg, 15 min) and washed twice with PBS. Cells were resuspended in 20 ml of lysis buffer (50 mM Tris-HCl pH 7.4, 300 mM NaCl, 1.5% v/v N-lauryl sarcosine, 1 mM DTT, and 1 mM EDTA) supplemented with 1:100 protease inhibitor cocktail (Sigma P8340), lysozyme (20 U/ml, Merck), and 0.5 mg/ml lysozyme (Sigma) for 20 minutes on ice. Cells were lysed by homogenisation using an Emulsi Flex C5 (Avestin) by passing the suspension through 5 times with 15,000 psi backpressure. The lysate was clarified by centrifugation (35,000xg, 45 minutes, 4^{o}C) and mixed with 0.5 ml (packed volume) of Glutathione-Sepharose 4B (Cytiva). After 2 hours the beads were pelleted and transferred to a 20 ml gravity flow column (Econopak). The beads were washed with 60 bead volumes of lysis buffer, 40 bead volumes of wash buffer 1 (50 mM Tris-HCl pH 7.4, 300 mM NaCl, 0.1% v/v N-lauryl sarcosine, 1 mM DTT, and 1 mM EDTA), 80 bead volumes of wash buffer 2 (50 mM Tris-HCl pH7.4, 300 mM NaCl, 1 mM ATP, 1 mM $MgCl_2$, 1 mM DTT, and 1 mM EDTA), and 40 bead volumes of wash buffer 3 (50 mM Tris-HCl pH 7.4, 300 mM NaCl, 1 mM DTT, and 1 mM EDTA). Elution fractions were collected by incubating the beads for 10 minutes with 2 ml of elution buffer (50 mM Tris-HCl pH 7.4, 300 mM NaCl, 30 mM reduced glutathione) per fraction. Fractions of interest were pooled and dialysed overnight into 50mM Tris-HCl pH 7.4, 150 mM NaCl, and 1 mM DTT. Glycerol was added to 10% v/v to the dialysed fractions prior to concentrating to 4 mg/ml. Aliquots were made and snap-frozen prior to storage at -80^{o}C.

Image processing and analysis

Image processing and analysis was performed using the Fiji distribution of ImageJ [251]. For figures, images acquired on a DeltaVision Core light microscopy system or Olympus BX61 microscope, were deconvolved and maximum-projected. Channels were subject to linear contrast adjustment. Within each figure contrast adjustment of each channel is the same between conditions and merges.

Quantification of kinetochore-localised signals were performed on images of cells from a BX61 Olympus microscope which were cropped to 250 x 250 px and sum projected. Kinetochore intensities for each fluorescence channel were determined by placing 8 px-diameter circular ROIs at the maxima of individual non-overlapping kinetochores and measuring the mean pixel intensity of each channel within said selections. Where possible 20 kinetochores were measured per cell. Background measurements were derived by taking an equivalent number of pixels as were in the ROI which were as close as possible to the ROI without overlapping with kinetochores. In brief, a binary mask of kinetochore signal was generated by performing a tophat transform of the CENP-C channel and thresholding using an iterative intermeans method [252]. Pixels were radially selected from outside the kinetochore ROI and, if not overlapping with signal in the binary kinetochore mask, added to a new background ROI. Once 52 px had been incorporated into the background ROI the mean pixel intensity of each channel within said ROI was measured.

To measure the total amount of signal on chromatin a binary mask of chromatin based on Hoechst staining was generated. The area of this mask and mean signal was measured, as was the average signal in an adjacent area of cytoplasm. The mean background signal was subtracted from that within the chromatin mask and

multiplied by the total area of chromatin. To measure the amount of signal with respect to kinetochores, the position of kinetochores as determined by the same method as described in the previous paragraph, was used to generate a Euclidian distance map. Distances from this map were measured based on a binary chromatin mask, as was the signal in fluorescence channels. After substracting background signal, the intensities at each pixel could be extracted, alongside the distance from a kinetochore as per measurements from the Euclidian distance map.

Data analysis was performed in Rstudio [253] using the Tidyverse collection of packages [254]. Kinetochore signal intensities were background-adjusted by subtracting the background signal on a channel-by-channel basis. Next, the mean intensity of the channel of interest was divided the mean intensity of the CENP-C channel on a per-kinetochore basis. The mean kinetochore localization intensities were then calculated for each cell. Normalization was performed within repeats by dividing each cell's mean kinetochore localization intensity by that of the group which was being normalized to.

Analysis of kinetochore MPS1-GFP and mCherry-FRB-INCENP$^{47\text{-}918}$ from live imaging was performed by placing five 8 pixel-diameter circular ROIs over MPS1 positive kinetochores at the first timepoint they were visible. The same ROIs were then measured at previous timepoints. ROIs were moved where needed at subsequent timepoint to track the same kinetochores. Background measurements were taken from 5 chromatin free cytoplasmic regions. Where no MPS1 positive kinetochores were visible, ROIs were taken from 5 points of the mitotic plate, as defined by Hoechst staining. Chromosome misalignment was measured by generating a rectangular ROI at timepoint 0 which covered the metaphase plate as defined by Hoechst staining, and measuring the intensity of Hoechst staining. A

second measurement was taken of the total level of Hoechst staining in the cell (the cell boundary defined by cytoplasmic GFP signal). A third measurement was made of the average background intensity outside of the cell, which was multiplied by the area of either the metaphase plate ROI of whole cell ROI, and subtracted from those values. A percentage of chromatin outside of the metaphase plate could then be ascertained and reported as percent of chromosomes that are misaligned. This was performed for each timepoint, with the rectangular ROI measuring the area of the metaphase plate moved where needed to be covering what remained of the metaphase plate and so as to be perpendicular with the spindle axis, as defined by SiR-Tubulin staining. Where chromosome misalignment was severe and SiR-Tubulin staining demonstrated that no microtubules remained in the vicinity of the area previously occupied by the metaphase plate, the level of chromosome misalignment was set as 100%.

Analysis of GFP-MPS1 mitotic timings on live cell data was performed on maximum projections of movies. DNA morphology was used to record at which timepoints cells entered NEBD or anaphase.

Analysis of GFP-MPS1 FRAP measurements was performed using an in-house ImageJ macro. Movies in which the kinetochores drifted out of the focal plane at any point were discarded. At each timepoint, following background correction, the signal from the bleached ROI was divided by that of the whole cell to correct for general photobleaching. This metric was then normalised to the average of that from the 4 pre-bleach timepoints. A single exponential fit was used to determine $t_{1/2}$ timings.

Statistical analysis

All statistical analysis was performed using GraphPad Prism version 9.2.0 for Windows (GraphPad Software, San Diego, California USA, www.graphpad.com). Each cell measured was considered as a biological replicate (n), hence mean measurements calculated for each cell were used for statistical analysis. At least three independent repeats of each experiment were performed, with statistical analysis performed using a sum of biological replicates from all independent experiments. The precise n numbers (where n is the number of cells analysed) is indicated in the figures.

Data sets were tested for normal distribution via a D'Agostino-Pearson omnibus K2 test. If all groups in an experiment were normally distributed, then the means were compared using a parametric statistical test as follows. If only two groups were compared then an unpaired 2 tailed t-test was used (with Welch's correction if the groups had unequal standard deviations). If more than two groups were compared with equal standard deviations a one-way ANOVA was used, which if rejected was followed by a Tuckey's multiple comparisons test. If more than two groups were compared with unequal standard deviations a Brown-Forsythe ANOVA was used, which if rejected was followed by a Dunn's multiple comparisons test.

If all groups did not exhibit a normal distribution then medians were compared using a non-parametric statistical test as follows. If only two groups were compared then a Mann-Whitney test was used. If more than two groups were compared then a Kruskal-Wallis test was used, which if rejected was followed by a Dunn's multiple comparisons test. Graphs display the mean± SEM. p-values are shown on graphs as follows: $p > 0.05$ = not significant (n.s.), $p \leq 0.05$ = *, $p \leq 0.01$ = **, $p \leq 0.001$ = ***, $p \leq 0.0001$ = ****.

Results 1 – MPS1 recruitment is controlled by kinases and phosphatases

The removal of MPS1 from kinetochores upon microtubule attachment is a crucial mechanism to stop SAC signalling [124]. The leading model is that microtubules physically compete with MPS1 for kinetochore binding, and thus sterically block MPS1 binding sites at attached kinetochores [134,164]. This model alone does not account for the observation that sub-saturating microtubule occupancy can satisfy checkpoint signalling, or that only a third of NDC80-C molecules are involved in directly binding microtubules at attached kinetochores [180,255]. It is therefore likely that additional mechanisms couple MPS1 recruitment to microtubule occupancy, possibly involving the network of kinases and phosphatases which is already known to control MPS1 localisation to unattached kinetochores (Diagram 12). This chapter will explore the importance of these additional mechanisms for regulating MPS1 localisation, especially regarding the response to end-on microtubule attachment.

MPS1 and microtubules can simultaneously bind kinetochores

A model where microtubule occupancy is sufficient to prevent MPS1 localisation is falsifiable by the observation of end-on attached kinetochores which recruit MPS1. To this end, the amount of kinetochore-localised MPS1 was measured by fluorescence microscopy in HeLa cells expressing endogenously tagged MPS1-GFP [115,117]. Due to the resolution limit of light microscopy and the dense packing of microtubules within the mitotic spindle, simply observing tubulin immunostaining is not sufficient to confidently assign the attachment status of kinetochores. End-on attached microtubules exhibit increased stability in comparison to other spindle microtubules, which can be exploited to selectively depolymerise microtubules

which are not stably bound by kinetochores [256]. Therefore, to ensure that the end-on attachment status of kinetochores could be confidently assigned, cells were chilled on ice for 9 minutes prior to fixation to remove non-k fibre microtubules. Cells were then stained for tubulin to visualise k-fibres, and CENP-C to visualise kinetochores. To create a variety of kinetochore-microtubule attachment statuses, cells were treated with the following drugs prior to cold-treatment and fixation. Nocodazole causes the depolymerisation of microtubules and was used to generate a scenario in which all kinetochores are unattached [257]. MG132 is a short synthetic peptide which inhibits the proteasome [258]. In the context of this assay, MG132 prevents destruction of Cyclin B which results in an enrichment of cells at metaphase when all kinetochores are end-on attached.

Without cold-treatment, MPS1-GFP displayed the expected localisation in response to microtubule attachment. In nocodazole-treated cells, where all kinetochores are unattached, MPS1 robustly localised to kinetochores (Figure 1A, B). Conversely, in MG132-treated cells, where all kinetochores are end-on attached, MPS1 levels were drastically reduced to near undetectable levels (Figure 1A, B). Remarkably, in cells which were cold-treated prior to fixation, MPS1 readily localised to kinetochores to an equal level, regardless of microtubule attachment status. The localisation of MPS1 to end-on attached kinetochores is in direct conflict with a model in which microtubule occupancy alone stops kinetochores from binding MPS1 [134,164].

To investigate the localisation behaviour of MPS1 in response to microtubule attachment and cold treatment in the same cell, cells were arrested with monopolar spindles. This was achieved through use of the small molecule inhibitor STLC to prevent Kinesin-5 from producing pushing forces at antiparallel spindle microtubules [259]. Thus, the bipolar spindle collapses into a monopole. Such monopolar spindles

exhibit a wide range of chromosome attachment states, as the absence of tension across sister kinetochores results in repeated cycles of microtubule binding and release [232]. Due to the mix of attachment statuses, an alternative method of assigning attachment status without cold treatment was required. Therefore, the binding of Astrin to kinetochores was used as a marker of end-on attachment [91,240]. In cells which were not cold treated, MPS1-GFP localised clearly to Astrin-negative (i.e. unattached) kinetochores, and was weakly localised at Astrin-positive (i.e. end-on attached) kinetochores (Figure 1C, D). As previous, following cold treatment MPS1 localised to an intermediate level to all kinetochores, regardless of the presence of Astrin (Figure 1C, D). Together, these results demonstrate that competition with microtubules is not the only mechanism which prevents a kinetochore from localising MPS1. Therefore, additional mechanisms must exist to couple microtubule occupancy to MPS1 binding.

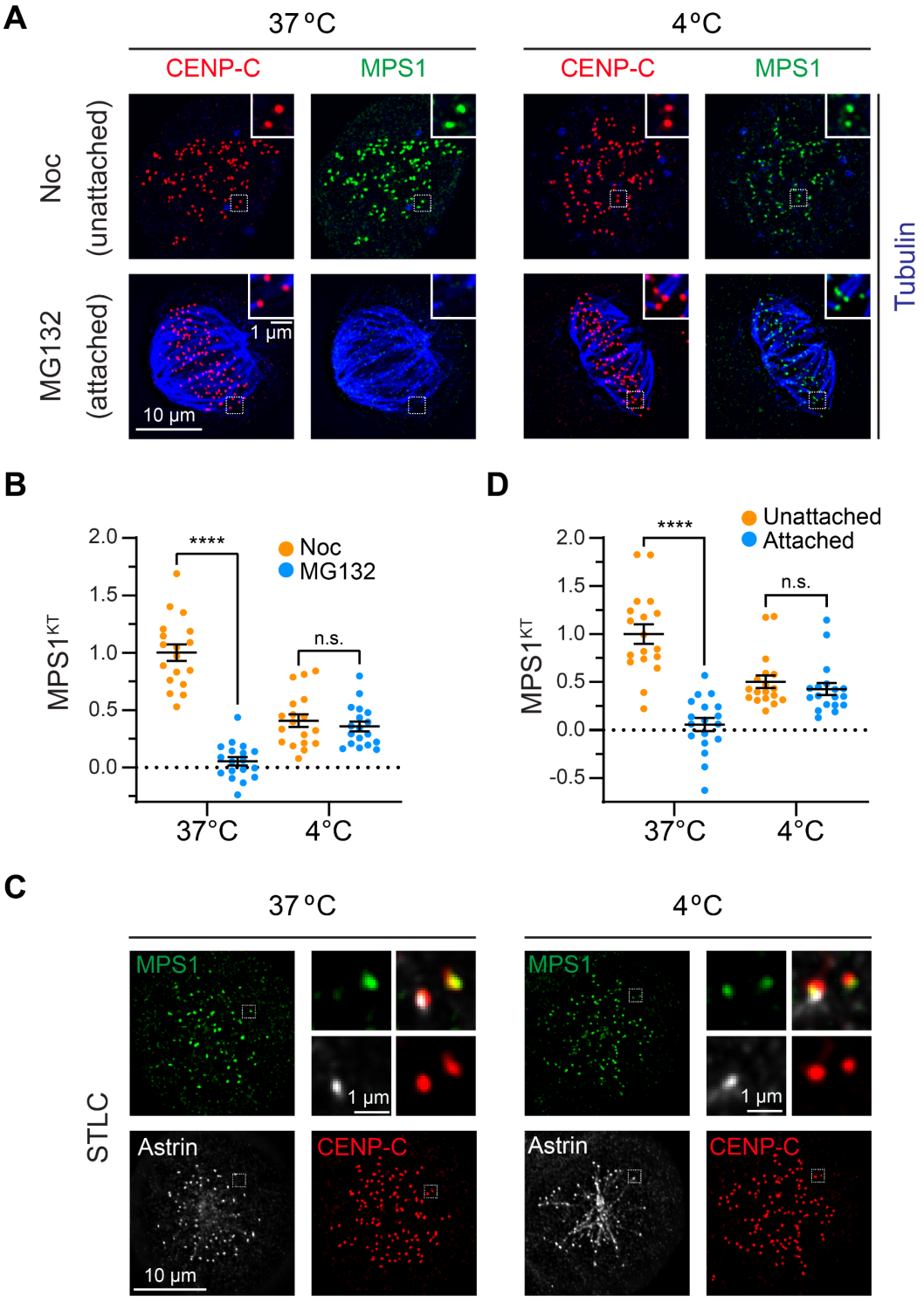

Figure 1 – **MPS1 and microtubules can simultaneously bind kinetochores**

A) HeLa cells expressing endogenously tagged MPS1-GFP were arrested with nocodazole (2 h, 0.6 µM) or MG132 (30 min, 20 µM) and fixed (37ºC) or incubated on ice for 9 min and then fixed (4ºC). Cells were immunostained for CENP-C and tubulin.

B) Quantification of the mean amount of MPS1 kinetochore localisation of cells in (A). Each dot represents one cell, data pooled from 3 biological repeats. Bars show mean± S.E.M.

C) HeLa cells expressing endogenously tagged MPS1-GFP were arrested with STLC (2 h, 10 µM) and fixed (37ºC) or incubated on ice for 9 min and then fixed (4ºC). Cells were immunostained for CENP-C and Astrin.

D) Quantification of the mean amount of MPS1 kinetochore localisation of cells in (C). Each dot represents one cell, data pooled from 3 biological repeats. Bars show mean± S.E.M.

If microtubule attachment is just the initial step in preventing MPS1 localisation to kinetochores, a short-lived intermediate state of end-on attached kinetochores which still localise MPS1 should be rarely observable in unperturbed mitosis. To this end, HeLa MPS1-GFP cells were fixed and stained for Astrin and CENP-C. Cells in late pro-metaphase were imaged and the amount of kinetochore-localised MPS1 measured in relation to the presence of Astrin – indicating end-on attachment. At Astrin-negative kinetochores, MPS1 was robustly localised (Figure 2). At Astrin-positive kinetochores, many kinetochores exhibited greatly reduced MPS1 signal. However, a small subset which clearly had Astrin foci robustly localised MPS1 – suggesting the presence of the postulated transition state (Figure 2). This observation is consistent with a model in which additional steps control MPS1 localisation downstream of microtubule attachment.

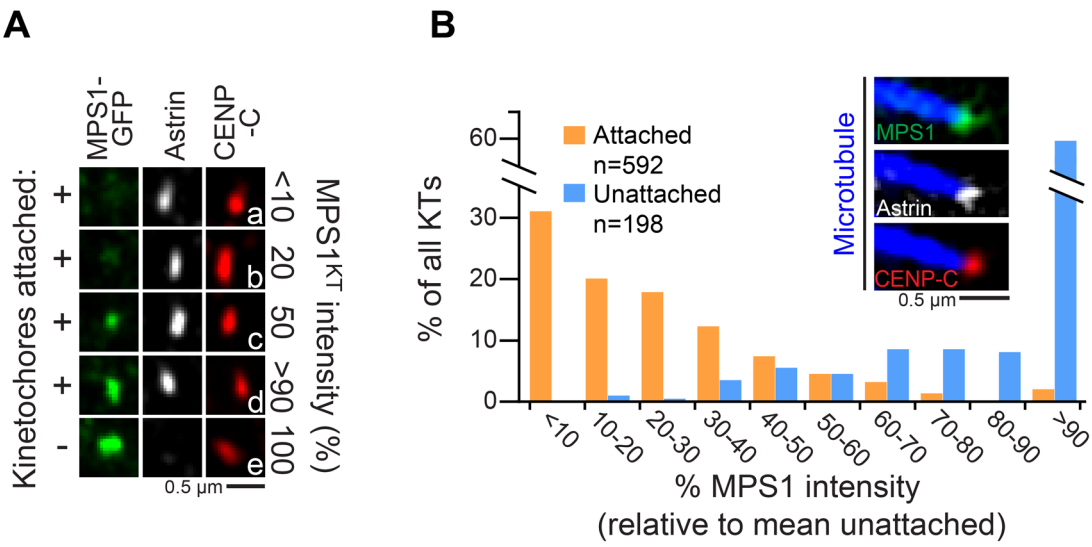

Figure 2 – **Astrin-positive kinetochores which robustly localise MPS1 can be rarely observed in unperturbed mitosis**

A) Example kinetochores from a late-prophase HeLa cell expressing endogenously tagged MPS1-GFP and immunostained for CENP-C and Astrin. End-on attachment is assigned by the presence of Astrin.
B) Histogram of MPS1 levels at individual kinetochores from cells as in (A), categorised by the presence or absence of Astrin foci.

MPS1 auto-activation is suggested to be intrinsically linked to kinetochore-localisation and checkpoint signalling [135,146,153,154]. Indeed, tethering MPS1 to kinetochores produces aberrant checkpoint signalling [124]. This raises the possibility that the MPS1 localised to attached kinetochores in cold-treated cells is active and can promote checkpoint signalling. To investigate this idea, cells were treated with nocodazole, MG132, or STLC, cold treated, and fixed. Staining of MPS1-pT676 was used to address the activation status of MPS1, as phosphorylation of the T-loop indicates active MPS1 [124]. Staining of the checkpoint protein MAD1 was used to address the ability of MPS1 to localise checkpoint proteins. Surprisingly, MPS1 at attached kinetochores displayed markedly lower pT676 staining than at unattached kinetochores (Figure 3A, B). Likewise, while MAD1 was robustly localised to unattached kinetochores, it was undetectable at attached kinetochores (Figure 3C, D). Together, these observations suggest that although MPS1 is localised to attached kinetochores in cold-treated cells, it is not fully active and cannot robustly localise checkpoint proteins. This observation suggests that MPS1 localisation and activation may be separable phenomena. A caveat of using MAD1 to assess checkpoint protein localisation is that dynein-mediated stripping should still occur in this scenario. Therefore, looking at the localisation of the BUB proteins, which are not subject to stripping, would have been a better readout of checkpoint protein localisation.

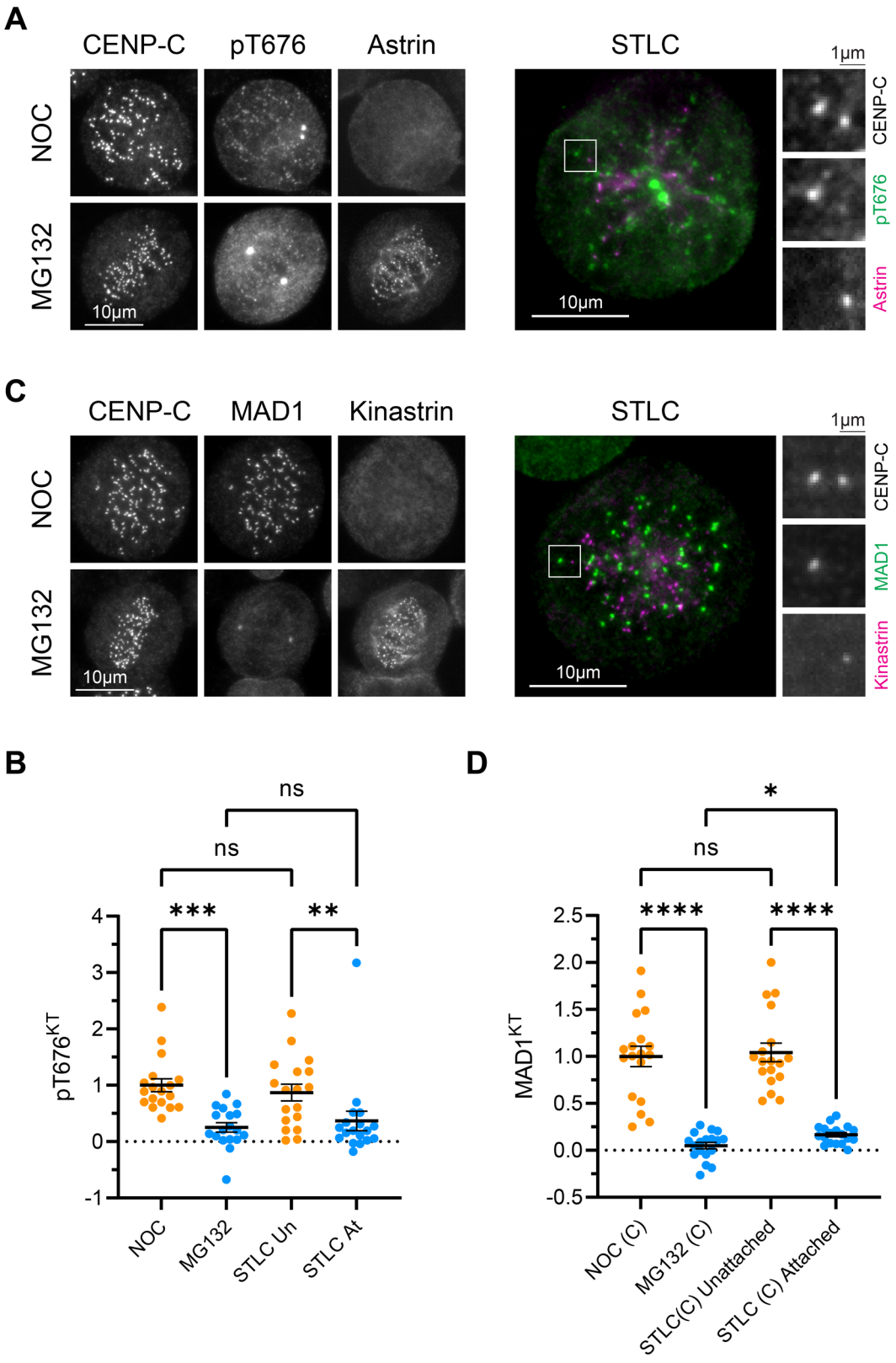

Figure 3 – **In cold treated cells MPS1 is less active at attached kinetochores**

A) HeLa cells expressing endogenously tagged MPS1-GFP were arrested with nocodazole (2 h, 0.6 µM), MG132 (30 min, 20 µM), or STLC (2 h, 10 µM) prior to cold treatment and fixation. Cells were immunostained for MPS1-pT676, CENP-C, and Astrin.

B) Quantification of the mean amount of pT676 kinetochore signal of cells in (A). Each dot represents one cell, data pooled from 3 biological repeats. Bars show mean± S.E.M.
C) Cells as treated in (A) stained for MAD1, CENP-C, and Kinastrin.
D) Quantification of the mean amount of MAD1 kinetochore signal of cells in (C). Each dot represents one cell, data pooled from 3 biological repeats. Bars show mean± S.E.M.

The direct observation of a state in which end-on attached kinetochores localise MPS1 show that steric competition alone does not prevent MPS1 localisation upon microtubule attachment. Additional mechanisms must be involved. As discussed (Diagram 12), there are several enzymes which control MPS1 localisation to unattached kinetochores. Namely, MPS1 itself, Aurora B, CDK1-Cyclin B, and PP2A-B56 [92,117,124,155–157,159,160]. It is conceivable that changes to the network of these factors is what ultimately controls if a kinetochore will localise MPS1 or not. If this is true, then perturbation of these kinases and phosphatases should re-produce the observation of MPS1 at end-on attached kinetochores, without cold treatment. The observation that temperature strongly affects the localisation behaviour of MPS1 is consistent with the idea that chemical reactions are involved in ultimately controlling MPS1 binding. Another possibility is that low-temperature favours a particular conformational state of the kinetochore which prevents MPS1 removal. The rest of this chapter explores the perturbation of MPS1, PP2A-B56, and Aurora B in turn, and the effect of this on MPS1 localisation to unattached and end-on attached kinetochores.

Exploring the contribution of MPS1 kinase activity to localisation

Chemical inhibition of MPS1 causes its accumulation at unattached kinetochores [92,124]. To investigate the contribution of MPS1 activity to MPS1 localisation in the context of microtubule attachment, MPS1-GFP HeLa cells were arrested with nocodazole, MG132 or STLC and subject to a short treatment with MPS1 inhibitor prior to fixation. Astrin was used as a marker for end-on attachment. As previously reported, MPS1 at unattached kinetochores accumulated upon inhibition (Figure 4A, B). At attached kinetochores, MPS1 localisation was also increased by inhibition – to levels equivalent to uninhibited MPS1 at unattached kinetochores (Figure 4A, B). MPS1 levels under conditions of inhibition were still sensitive to microtubule attachment, suggesting that MPS1 activity feeds into, but does not solely determine, the loss of MPS1 from kinetochores upon microtubule binding.

There are two pathways by which MPS1 activity could feed back onto MPS1 localisation (Figure 4C) – directly via auto-phosphorylation [171,172], and indirectly via recruitment of downstream checkpoint proteins - for example BUBR1-bound PP2A-B56 [94–96,158,173]. To isolate the influence of auto-phosphorylation, the strategy of mutating residues in MPS1 to alanine (to mimic constitutive dephosphorylation) or glutamate or aspartate (to mimic constitutive phosphorylation) was used (Figure 4D). The NTE is reported to be the main kinetochore-binding domain of MPS1 *in vivo* [131,134], and it contains 8 autophosphorylation sites [129,171] (Figure 4D). N-terminal autophosphorylation at a subset of these sites has shown to modulate MPS1 localisation [172,260]. This mechanism could explain why inactive MPS1 accumulates at unattached kinetochores [124], and why inactive MPS1 localises to attached kinetochores (Figure 4A, B). To investigate these possibilities, all 8 auto-phosphorylation sites in

the NTE were mutated to either alanine (N8A), aspartate (N8D) or glutamate (N8E) (Figure 4D).

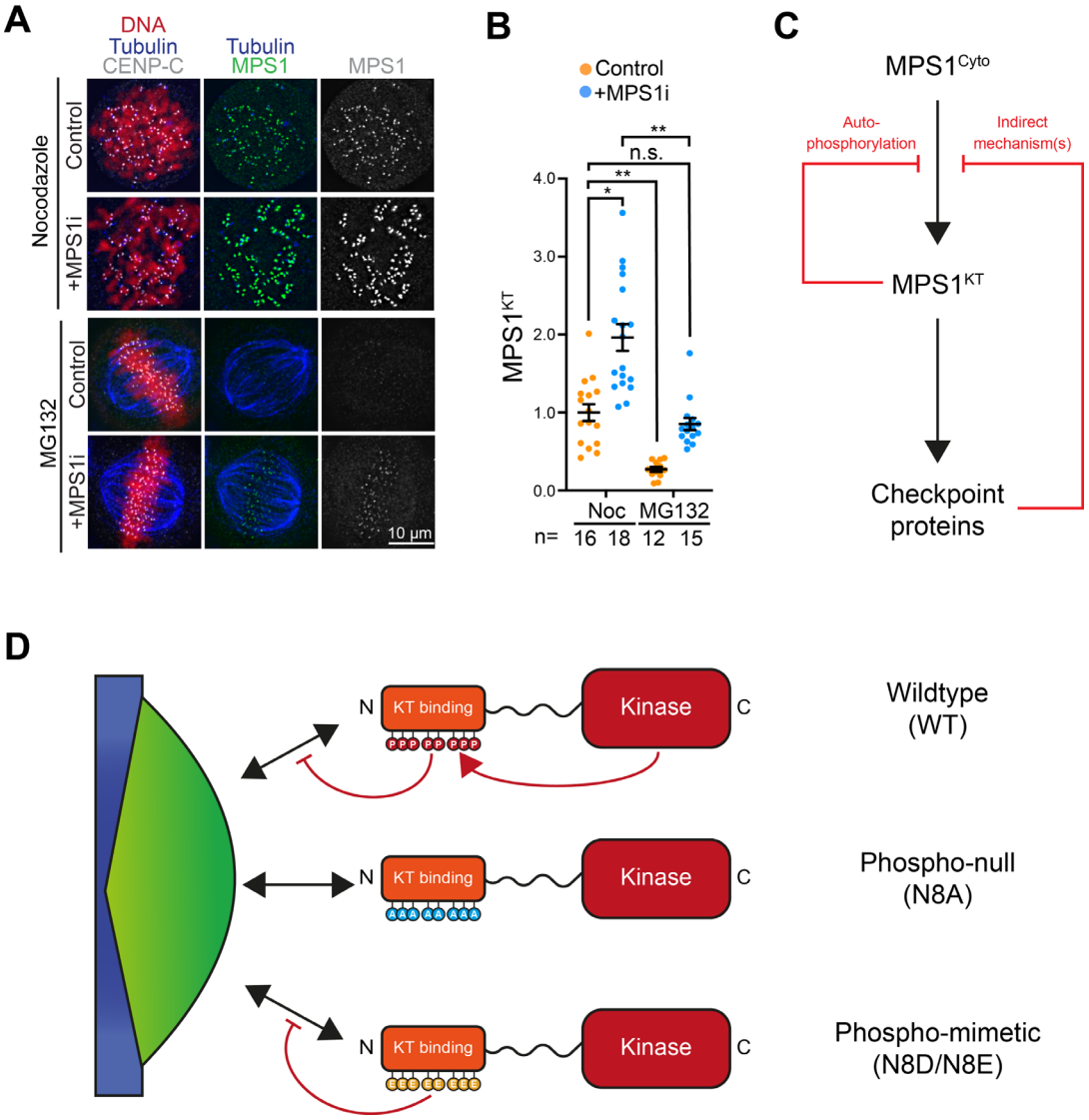

Figure 4 – **Inhibited MPS1 localises to end-on attached kinetochores**

A) HeLa cells expressing endogenously tagged MPS1-GFP were arrested with nocodazole (2 h, 0.6 µM) and MG132 (30 min, 20 µM) (Noc condition), or MG132 alone (30 min, 20 µM) (MG132 condition), and treated with or without MPS1i (AZ3146, 10 min, 2 µM). Cells were fixed and immuno-stained for CENP-C and Tubulin.

B) Quantification of the mean amount of MPS1 kinetochore localisation of cells in (A). Each dot represents one cell, data pooled from 2 biological repeats. Bars show mean± S.E.M.

C) Schematic demonstrating how MPS1 kinase activity my directly (through auto-phosphorylation) or indirectly (through the recruitment of downstream checkpoint proteins) may feed back onto MPS1 kinetochore localisation.

D) Schematic showing the principle behind mutation of MPS1 N-terminal auto-phosphorylation sites.

Stable, inducible, HeLa cell lines were made using the Flp-In TREx system [145] to express wildtype (WT), kinase-dead (KD) or the phospho-mutant GFP-tagged transgenes from a single genomic locus. Experiments using these cells utilise an "RNAi rescue" strategy, wherein endogenous MPS1 is depleted through siRNA and replaced by induction of GFP-tagged MPS1 mutants. Cells were treated with siMPS1 (targeting the 3' UTR) or siControl (targeting luciferase, GL2), and with or without doxycycline induction (Figure 5A). In all cell lines endogenous MPS1 was efficiently depleted by siMPS1 (Figure 5A, +siMPS1), and GFP-MPS1 mutants were efficiently expressed upon induction (Figure 5A, +dox). Thus, these cell lines and this experimental setup can be used to replace endogenous MPS1 with GFP-tagged MPS1 mutants within a short period of time.

If phosphorylation of the N-terminus does alter MPS1 binding to the kinetochore, the steady-state levels of MPS1 at unattached kinetochores should be altered upon their mutation. Furthermore, mutation of these sites should over-ride the increase in MPS1 localisation upon inhibition. To test these hypotheses, an RNAi rescue strategy was employed as described. Cells were arrested in mitosis in the absence of microtubules by treatment with the spindle-poison nocodazole, prevented from entering anaphase with the proteasome inhibitor MG132, and treated with or without MPS1 inhibitor prior to fixation. Cells were fixed and stained for the kinetochore protein CENP-C (Figure 5B).

In the absence of MPS1 inhibitor (Figure 5B top panel, C orange dots), $MPS1^{WT}$ was clearly visible at kinetochores. $MPS1^{KD}$ localised 3 times as strongly as $MPS1^{WT}$, as previously reported [92,124]. $MPS1^{N8A}$ localised as strongly as $MPS1^{KD}$, suggesting that dephosphorylation of the NTE does increase MPS1 localisation. Conversely, $MPS1^{N8D}$ to around 80% the level of $MPS1^{WT}$, though this

difference was not significant. MPS1^{N8E} localised to around 50% the level of MPS1^{WT}. These data re-affirm the idea that phosphorylation of these sites modulates MPS1 localisation. The difference between the D and E mutants could be a result of how well these sites mimic phosphorylated S/T.

It is possible that other MPS1-activity dependent mechanisms modulate MPS1 localisation to unattached kinetochores, specifically localisation of PP2A-B56 [94–96,158,173] and the feedback of NTE phosphorylation onto MPS1 kinase activity [167]. The addition of MPS1 inhibitor (MPS1i, Figure 5B lower panel, C blue dots) allowed this possibility to be explored. Upon addition of MPS1i, MPS1^{WT} localised to the same extent as MPS1^{KD}, confirming the effectiveness of the inhibition. For MPS1^{KD} there was no further increase in localisation upon inhibition – as expected given this mutant is already inactive. MPS1^{N8A} displayed the same phenotype as MPS1^{KD}. This observation alone does not rule-out other effects of MPS1 inhibition, as MPS1^{N8A} may already saturate kinetochore-binding sites such that no further increase in localisation can be observed. Crucially, MPS1$^{N8D/E}$ showed no change in localisation upon MPS1 inhibition – strongly suggesting that N-terminal autophosphorylation is the main factor which causes the accumulation of inactive MPS1 at unattached kinetochores (Figure 5B, C).

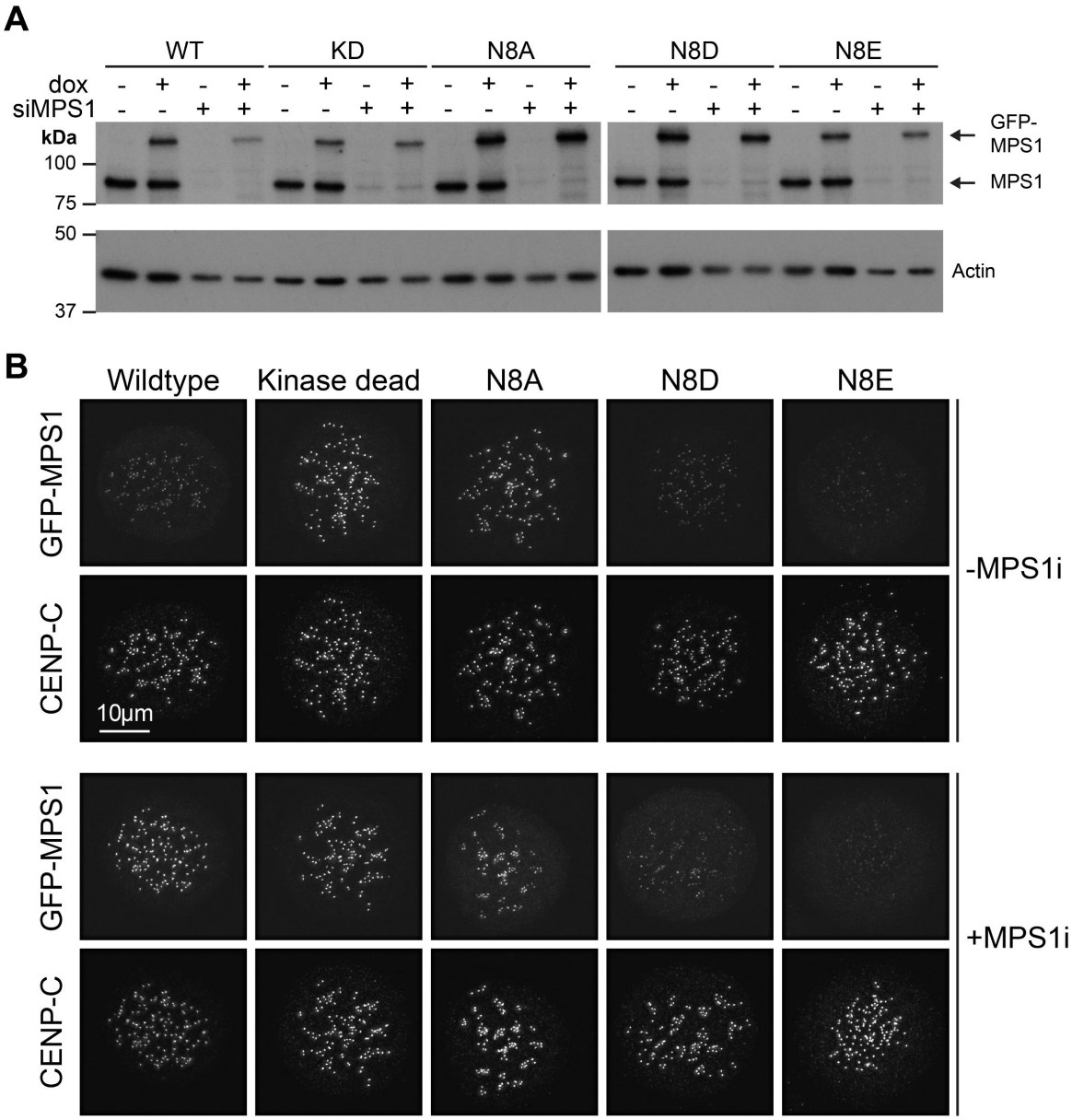
A
WT
KD
N8A
N8D
N8E
dox
siMPS1
kDa
100
75
50
37
GFP-MPS1
MPS1
Actin
B
Wildtype
Kinase dead
N8A
N8D
N8E
GFP-MPS1
CENP-C
10μm
-MPS1i
+MPS1i
C
MPS1KT
12
10
8
6
4
2
0
***
n.s.
n.s.
n.s.
n.s.
-MPS1i
+MPS1i
WT
KD
N8A
N8D
N8E

Figure 5 – **MPS1 N-terminal autophosphorylation modulates MPS1 recruitment to unattached kinetochores**

A) Anti-MPS1 Western blot of HeLa Flp-In TREx cells treated with siMPS1 or siControl and ± doxycycline (2 μM) to induce GFP-MPS1 transgene expression for 48 hours. Actin is used as a loading control.
B) HeLa Flp-In TREx cells depleted of endogenous MPS1 and expressing GFP-MPS1 transgenes were arrested with nocodazole (2 h, 0.6 μM) and MG132 (30 min, 20 μM) and treated with or without MPS1i (AZ3146, 10 min, 2 μM). Cells were fixed and immuno-stained for CENP-C.
C) Quantification of the mean amount of MPS1 kinetochore localisation of cells in (B). Each dot represents one cell, data pooled from 3 biological repeats. Bars show mean± S.E.M.

It has been suggested that inactive MPS1 does not require the kinase activity of Aurora B to localise to kinetochores [171], but contradictory observations have been made by other groups [93]. To investigate if Aurora B activity is required for the localisation of inactive MPS1, HeLa cells expressing endogenously tagged MPS1-GFP were arrested in nocodazole and MG132 to trap cells in mitosis with unattached kinetochores. Cells were then treated with combinations of MPS1 and Aurora kinase inhibitors (Figure 6A). MPS1 or Aurora B inhibition alone had the expected results – MPS1 levels increased upon MPS1 inhibition and were greatly decreased upon Aurora B inhibition (Figure 6A, B). The combination of MPS1 and Aurora B inhibition resulted in extremely weak MPS1 localisation to the same level as Aurora B inhibition alone (Figure 6A, B). Thus, MPS1 seems to require Aurora B activity regardless of its activity state.

To investigate if the strongly-localising $MPS1^{N8A}$ and $MPS1^{KD}$ still required Aurora B activity to localise, an RNAi rescue assay was used to express $MPS1^{WT/KD/N8A}$ in the absence of endogenous MPS1. Cells were arrested with nocodazole and MG132 to trap cells in a state with no attachments, and treated with or without Aurora kinase inhibitor. Staining for Aurora B target H3pS10 [261] was used to confirm successful inhibition of Aurora B (Figure 6D). $MPS1^{KD/N8A}$ localised ~2.5x more strongly than $MPS1^{WT}$ (Figure 6D, E), as previously observed (Figure 6B, C).

As expected, all constructs localised weakly upon Aurora kinase inhibition (Figure 6D, E), confirming that their localisation is still dependent on Aurora B activity. These observations are consistent with the idea that MPS1 auto-phosphorylation acts downstream of Aurora B activity to control MPS1 localisation.

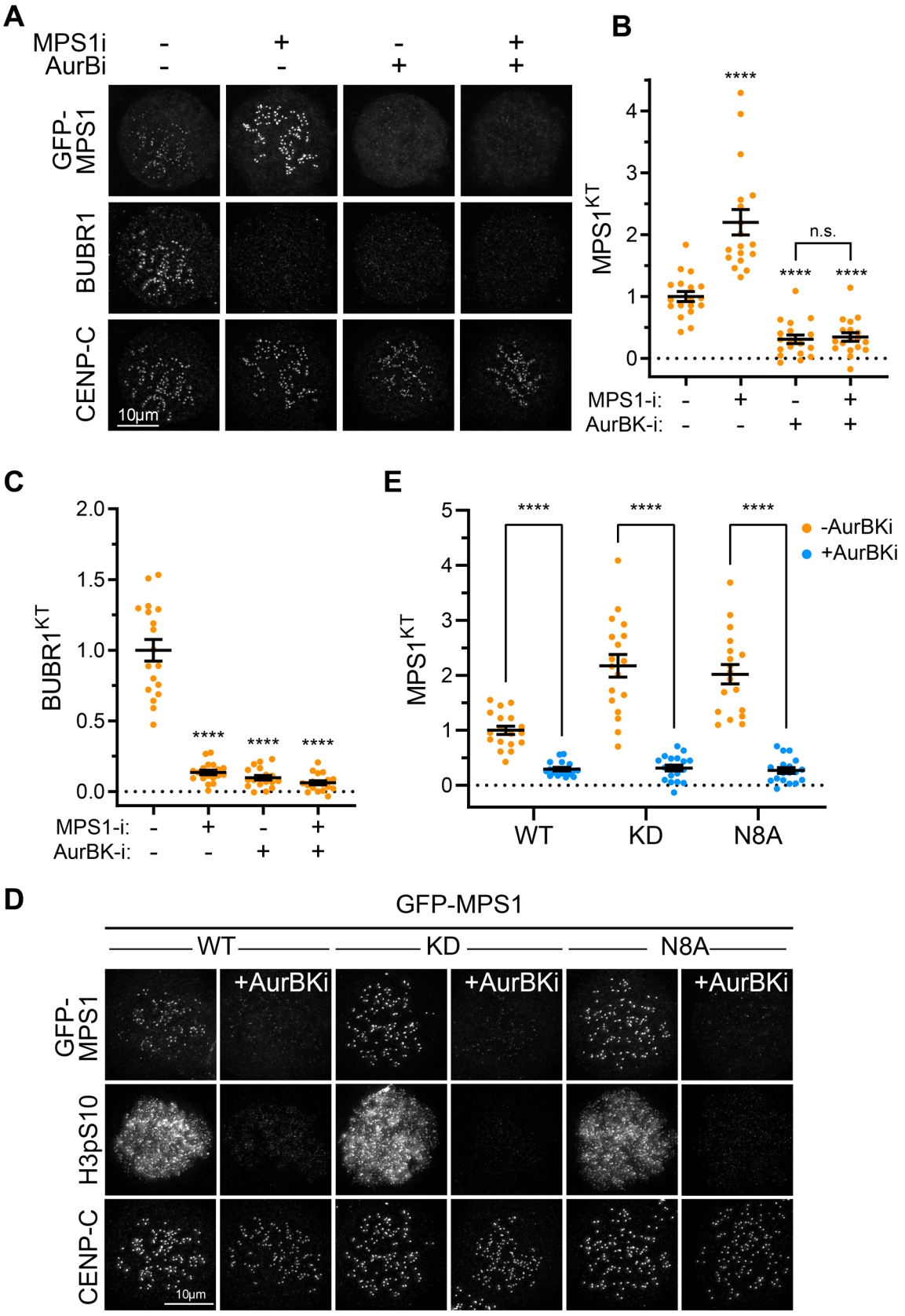

Figure 6 – **The localisation of inactive MPS1 and N-terminal mutants is subordinate to Aurora B**

A) HeLa cells expressing endogenously tagged MPS1-GFP were arrested with nocodazole (2 h, 0.6 μM) and MG132 (30 min, 20 μM) and treated with or without MPS1i (AZ3146, 15 min, 2 μM) and with or without AurBKi (ZM447439, 15 min, 10 μM). Cells were fixed and immunostained for CENP-C and BUBR1
B) Quantification of the mean amount of MPS1 kinetochore localisation of cells in (A). Each dot represents one cell, data pooled from 3 biological repeats. Bars show mean± S.E.M.
C) Quantification of the mean amount of BUBR1 kinetochore localisation of cells in (A). Each dot represents one cell, data pooled from 3 biological repeats. Bars show mean± S.E.M.
D) HeLa Flp-In TREx cells depleted of endogenous MPS1 and expressing GFP-MPS1 transgenes were arrested with nocodazole (2 h, 0.6 μM) and MG132 (30 min, 20 μM) and treated with or without AurBKi (ZM447439, 15 min, 10 μM). Cells were fixed and immunostained for CENP-C and histone 3 phospho-serine 10.
E) Quantification of the mean amount of MPS1 kinetochore localisation of cells in (D). Each dot represents one cell, data pooled from 3 biological repeats. Bars show mean± S.E.M.

It is possible that the inhibition of MPS1 may have consequences for the localisation and/or activity of Aurora B. MPS1 has been proposed to directly regulate the kinase activity of Aurora B [231]. Additionally, the inhibition of MPS1 would be expected to interfere with one of the pathways by which the CPC is enriched at the centromere. One centromeric mark which supports the localisation pattern of Aurora B is H2ApT120. This phosphorylation is carried out by BUB1 and creates a binding site for Shugoshin [262] – which in turn binds to the Borealin subunit of the CPC [263]. As BUB1 kinetochore recruitment is MPS1 activity-dependent [94–96], loss of MPS1 activity may ultimately lead to a loss of the centromeric enrichment of the CPC. To investigate these possibilities, cells arrested in nocodazole were treated with DMSO, MPS1 inhibitor, or Aurora B inhibitor as previous. Immunostaining was used to assess the level of H2A-pT120 phosphorylation. Upon inhibition of MPS1 or Aurora B, the level and centromeric-enrichment of H2A-pT120 was drastically reduced, presumably due to the loss of BUB1 localisation (Figure 7A, B). Despite this loss of H2A-pT120, the centromeric enrichment of Aurora B was unaffected (Figure 7C, D). The total amount of Aurora B on chromatin was not decreased upon inhibition of MPS1 or Aurora B – rather it went up by a small, but statistically significant amount upon MPS1 inhibition (Figure 7C, E). Thus, despite the loss of H2A-pT120 upon

MPS1 inhibition, there was no loss of Aurora B localisation under these assay conditions. The activity status of Aurora B was assessed by staining the T-loop of Aurora B and the phosphorylation of Aurora B target H3-S10 [261]. Unlike inhibition of Aurora B, inhibition of MPS1 caused no change in Aurora B activation, as assessed by T-loop staining, or Aurora B activity, as assessed by H3-S10 phosphorylation (Figure 7C, G-H). Thus, under these assay conditions MPS1 inhibition does not decrease or grossly alter Aurora B localisation.

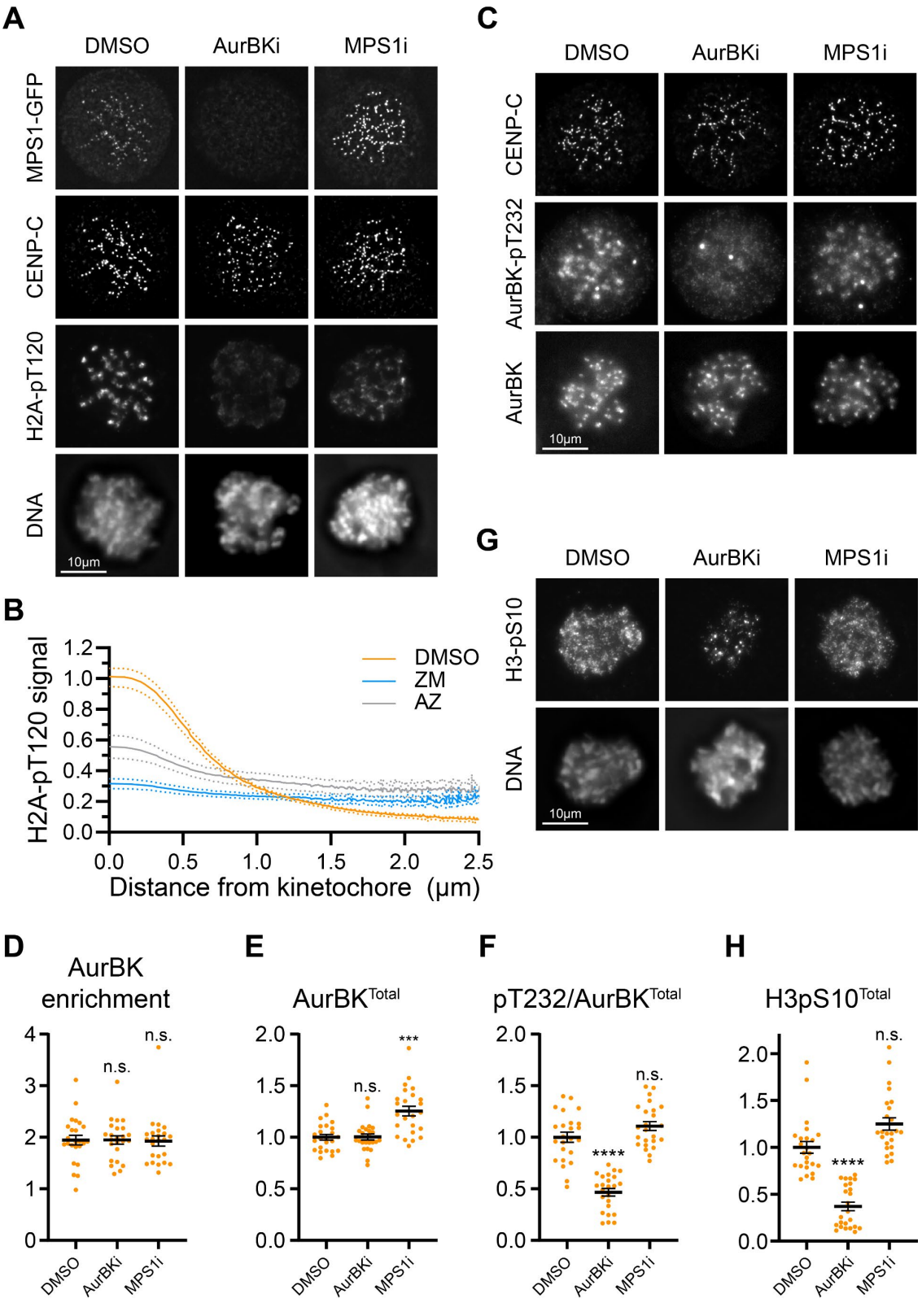

Figure 7 – **MPS1 inhibition does not compromise the localisation or activity of Aurora B**

A) HeLa cells expressing endogenously tagged MPS1-GFP were arrested with nocodazole (2 h, 0.6 µM) and MG132 (30 min, 20 µM) and treated with or without MPS1i (AZ3146, 15 min, 2 µM) and with or without AurBKi (ZM447439, 15 min, 10 µM). Cells were fixed and immunostained for CENP-C and H2A-pT120.

B) Plot of the Aurora B signal on chromatin as a function of distance from a kinetochore from cells in (A).
C) HeLa cells expressing endogenously tagged MPS1-GFP were arrested with nocodazole (2 h, 0.6 μM) and MG132 (30 min, 20 μM) and treated with or without MPS1i (AZ3146, 15 min, 2 μM) and with or without AurBKi (ZM447439, 15 min, 10 μM). Cells were fixed and immuno-stained for Aurora B and Aurora B-pT232.
D) Quantification of (C). The ratio of the mean Aurora B signal within 1 μm of a kinetochore to that >1μm from a kinetochore. Each dot represents one cell, data pooled from 3 biological repeats. Bars show mean± S.E.M.
E) Quantification of (C). The total amount of Aurora B on chromatin is plotted. Each dot represents one cell, data pooled from 3 biological repeats. Bars show mean± S.E.M.
F) Quantification of (C). The total amount of Aurora B-pT232 adjusted to the total amount of Aurora B is plotted. Each dot represents one cell, data pooled from 3 biological repeats. Bars show mean± S.E.M.
G) HeLa cells expressing endogenously tagged MPS1-GFP were arrested with nocodazole (2 h, 0.6 μM) and MG132 (30 min, 20 μM) and treated with or without MPS1i (AZ3146, 15 min, 2 μM) and with or without AurBKi (ZM447439, 15 min, 10 μM). Cells were fixed and immuno-stained for H3pS10.
H) Quantification of (G). The total amount of H3-pS10 signal is plotted. Each dot represents one cell, data pooled from 3 biological repeats. Bars show mean± S.E.M.

The observations so far demonstrate that N-terminal autophosphorylation decreases the ability of MPS1 to localise to unattached kinetochores. Hence, it may play a role in preventing MPS1 accumulation at attached kinetochores – as seen upon inhibition of MPS1 (Figure 4). To examine this possibility, the localisation of the MPS1 transgenes was observed in cells which have both end-on attached and unattached kinetochores. Cells were arrested in mitosis in the presence of a monopolar spindle, fixed, and stained for the kinetochore protein CENP-C and Astrin.

$MPS1^{WT}$ was present at unattached but not attached kinetochores as expected (Figure 8A, B). All other mutants showed similar sensitivity to microtubule binding (Figure 8A, B). This demonstrates that microtubule binding prevents MPS1 localisation upstream of N-terminal autophosphorylation. In contrast to $MPS1^{N8A}$, $MPS1^{KD}$ still localised to attached kinetochores to the same level as $MPS1^{WT}$ at unattached kinetochores, as has previously been observed (Figure 8A, B). This suggests that the kinase activity of MPS1 may have some role in preventing MPS1

localisation to attached kinetochores which is separate to N-terminal auto-phosphorylation. Further supporting the idea that MPS1 auto-phosphorylation is subordinate to microtubule attachment, $MPS1^{N8A}$, like $MPS1^{WT}$ does not localise to bioriented kinetochores at the metaphase plate (Figure 8C, D).

Inactive MPS1 has a different phenotype than $MPS1^{N8A}$ – namely it localises to attached kinetochores (Figure 4, Figure 8A, B). Additional evidence that $MPS1^{KD}$ has a different behaviour to $MPS1^{N8A}$ was observed by measuring the turnover of the MPS1 mutants in nocodazole arrested cells by FRAP. $MPS1^{N8A}$ ($t_{1/2}$ = 3.7s) displayed insignificant differences in turnover from $MPS1^{WT}$ ($t_{1/2}$ = 2.9s), whereas the turnover of $MPS1^{KD}$ ($t_{1/2}$ = 6.4s) was almost double, as previously reported [124] (Figure 8E). The difference in half-lives between $MPS1^{KD}$ and $MPS1^{N8A}$ suggests that additional mechanisms are at play in regulating the dynamics of MPS1 binding to kinetochores, seemingly without altering the steady-state levels which these mutants localise to. Together, these observations demonstrate that the localisation of inactive MPS1 to attached kinetochores, and the decreased turnover of inactive MPS1, are not due to N-terminal auto-phosphorylation. Therefore, some other target of MPS1 must be responsible for these phenomena – possibly the MPS1-dependent kinetochore pool of PP2A-B56 (Diagram 15). The contribution of PP2A-B56 recruitment will be addressed later in the chapter.

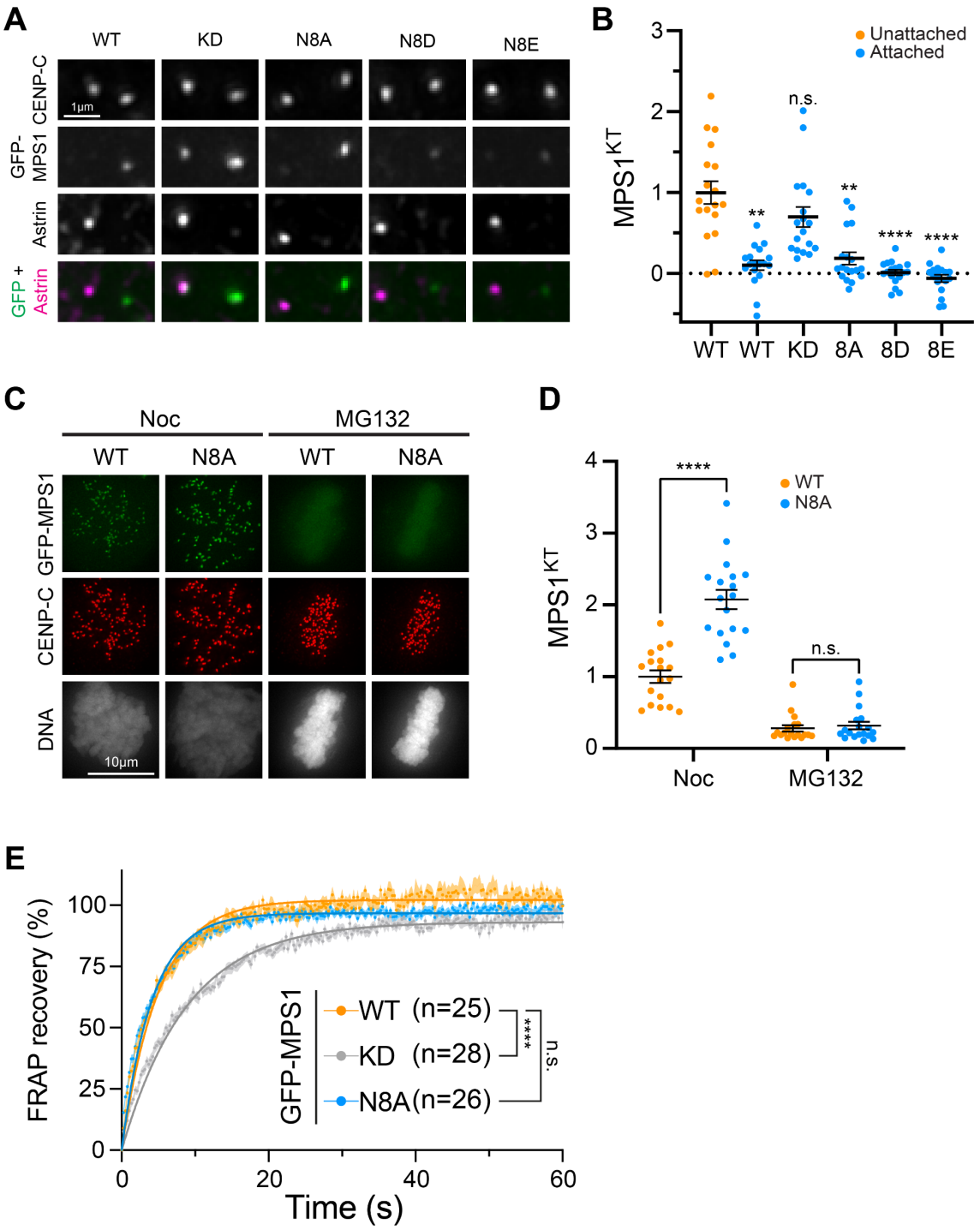

Figure 8 – **MPS1 N-terminal auto-phosphorylation acts downstream of end-on attachment**

A) Monotelic kinetochore pairs. HeLa Flp-In TREx cells depleted of endogenous MPS1 and expressing GFP-MPS1 transgenes were arrested with STLC (2 h, 10 μM) and MG132 (30 min, 20 μM). Cells were fixed and immuno-stained for CENP-C and Astrin.

B) Quantification of (A). The mean amount of MPS1 kinetochore localisation at Astrin-positive (attached) kinetochores are plotted and compared to Astrin-negative (unattached) kinetochores in WT-expressing cell. Each dot represents one cell, data pooled from 3 biological repeats. Bars show mean± S.E.M.

C) HeLa Flp-In TREx cells depleted of endogenous MPS1 and expressing the indicated GFP-MPS1 transgene were arrested with nocodazole (2 h, 0.6 μM) and MG132 (30 min, 20 μM)

(Noc condition), or MG132 alone (30 min, 20 μM) (MG132 condition). Cells were fixed and immuno-stained for CENP-C.

D) Quantification of the mean amount of MPS1 kinetochore localisation of cells in (C). Each dot represents one cell, data pooled from 3 biological repeats. Bars show mean± S.E.M.

E) Plots of averaged fluorescence recovery after photobleaching of single kinetochores. HeLa Flp-In TREx cells depleted of endogenous MPS1 and expressing the indicated GFP-MPS1 transgene were arrested with nocodazole (2 h, 0.6 μM) and MG132 (30 min, 20 μM). Single kinetochores from cells were bleached and fluorescence recovery recorded. Data pooled from 3 biological repeats.

Physiological consequences of altered MPS1 levels

The data so far suggest that N-terminal autophosphorylation fine-tunes the level to which MPS1 will accumulate at unattached kinetochores but does not alter the behaviour of MPS1 localisation in response to microtubule attachment. Functionally, it is unclear what advantage localising MPS1 to a specific level to checkpoint-active kinetochores might have. To explore potential functional consequences of perturbing N-terminal auto-phosphorylation, mitotic progression of the Flp-In cells expressing different MPS1 mutants was observed by live-cell imaging following RNAi rescue (Figure 9A, B). The median time from nuclear envelope breakdown to anaphase onset was measured based on DNA morphology. Upon siMPS1, NEBD-ANA was reduced from the usual 45 minutes to 25 minutes, demonstrating an abrogated checkpoint resulting from knockdown of MPS1 (Figure 9A, B). Rescue with $MPS1^{WT}$ gave the expected time of 45 minutes. Rescue with $MPS1^{KD}$ decreased mitotic timing to 15 minutes – indicative of a complete loss of the spindle checkpoint (Figure 9A, B). In this situation, mitotic timing was even shorter than in non-rescued cells; possibly because $MPS1^{KD}$ may compete any residual endogenous MPS1 away from kinetochores, causing a further loss of checkpoint. $MPS1^{N8A/D}$ did not have significantly different timings than $MPS1^{WT}$. However, $MPS1^{N8E}$, which localises to 50% the level of $MPS1^{WT}$ showed a significant decrease in median mitotic timing to 35 minutes (Figure 9A, B). This suggests a largely functional checkpoint (as some rescue is observed compared to MPS1 depletion alone), but a subtle decrease in the strength of the checkpoint.

It is possible that a 2-fold reduction in MPS1 levels, seen in for $MPS1^{N8E}$, would decrease the strength of the checkpoint. To test the effect of altered MPS1 levels on

spindle checkpoint signalling, the recruitment of checkpoint protein BUBR1 to kinetochores was studied. It has been suggested that the concentration of checkpoint proteins in a cell can be limiting for MCC production [264]. That is to say that when multiple kinetochores are unattached, there is no increase in the overall rate of MCC production as more kinetochores initiate SAC signalling. To avoid a scenario in which free checkpoint proteins are limiting, cells were arrested such that a small subset of kinetochores were not attached to microtubules. This was achieved by inhibiting the motor protein CENP-E, which causes a few chromosomes to become stuck at the spindle poles by preventing lateral chromosome congression [265] (Figure 9C). As anticipated, at unattached kinetochores with no rescue, rescue with $MPS1^{KD}$, or at attached kinetochores in rescue with $MPS1^{WT}$, the levels of BUBR1 were significantly reduced compared to unattached kinetochores in the rescue with $MPS1^{WT}$ (Figure 9C, D). BUBR1 localisation at unattached kinetochores was the same between $MPS1^{N8A}$ and $MPS1^{WT}$, demonstrating that increases in MPS1 level do not increase the levels of BUBR1. There was no significant reduction in the levels of BUBR1 at unattached kinetochores between rescue with $MPS1^{N8D/E}$ and $MPS1^{WT}$. These data suggest that BUBR1 can reach similar steady-state levels regardless of the weakened or enhanced localisation of the MPS1 NTE phospho-mutants. Given that multiple checkpoint proteins need to be phosphorylated by MPS1 for efficient MCC production (Diagram 9), the idea that decreased levels of MPS1 could slow MCC production and thereby weaken the checkpoint is still possible.

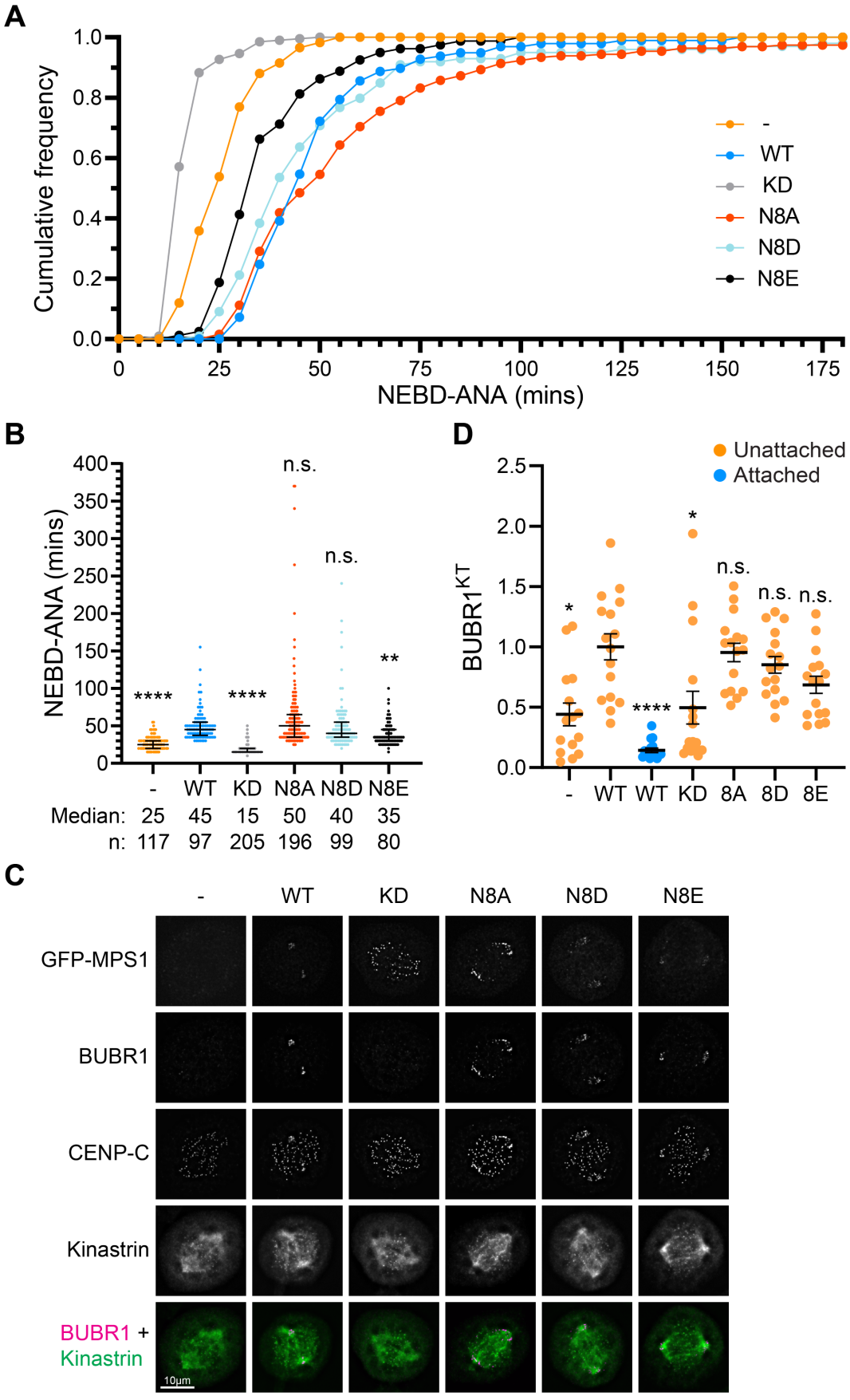

Figure 9 – **Perturbation of MPS1 auto-phosphorylation sites has subtle effects on mitotic progression**

A) Dot plot of mitotic timings (nuclear envelope break down to anaphase) in HeLa Flp-In TREx cells depleted of endogenous MPS1 (- condition) or depleted of endogenous MPS1 and expressing the indicated GFP-MPS1 transgene. Each dot represents one cell, data pooled from 3 biological repeats. Bars show median and interquartile range.
B) Cumulative frequency plot of data in (F) within the first 3 hours of NEBD.
C) HeLa Flp-In TREx cells depleted of endogenous MPS1 and expressing the indicated GFP-MPS1 transgene were arrested with CENP-E inhibitor (GSK923295, 2 h, 50 nM) and MG132 (30 min, 20 μM). Cells were fixed and immune-stained for CENP-C, BUBR1, and Astrin.
D) Quantification of the mean amount of BUBR1 kinetochore localisation of cells in (D). Each dot represents one cell, data pooled from 2 biological repeats. Bars show mean± S.E.M.

N-terminal auto-phosphorylation does not modulate MPS1 kinase activity

It has been suggested that autophosphorylation of the N-terminus of MPS1 regulates the kinase activity of MPS1 [167]. In this model, the NTE inhibits the kinase activity of MPS1 when unphosphorylated. Upon phosphorylation, inhibition is relieved and MPS1 is proposed to become fully active. This model predicts that N8A will display decreased kinase activity, and N8D and E will display increased kinase activity. To test these hypotheses, the kinase activity of MPS1 was assayed *in vitro*. For a physiologically relevant substrate for MPS1, a fragment of KNL1 containing 8 MELT motifs (amino acids 728-1200) [160] was purified from bacteria as a GST-fusion protein (Figure 10A, B).

To obtain purified MPS1 protein, GFP-MPS1 constructs were overexpressed in mitotic HEK293T cells and purified by immunoprecipitation with anti-GFP antibodies (Figure 10C). This resulted in clean GFP-MPS1 bound to Dynabeads (Figure 10C, Pre λ-PPase). As the MPS1 mutants display different levels of MPS1 kinetochore localisation, they may have different initial activation states in the lysate of mitotic HEK293T cells. To overcome this confounding variable, the immunoprecipitated GFP-MPS1 was dephosphorylated completely prior to the kinase assay. λ-PPase treatment efficiently removed phosphorylations on GFP-MPS1, evidenced by a downshift of the band in SDS-PAGE (Figure 10C, Post λ-PPase). The beads were then washed thoroughly to remove λ-PPase prior to the kinase assay.

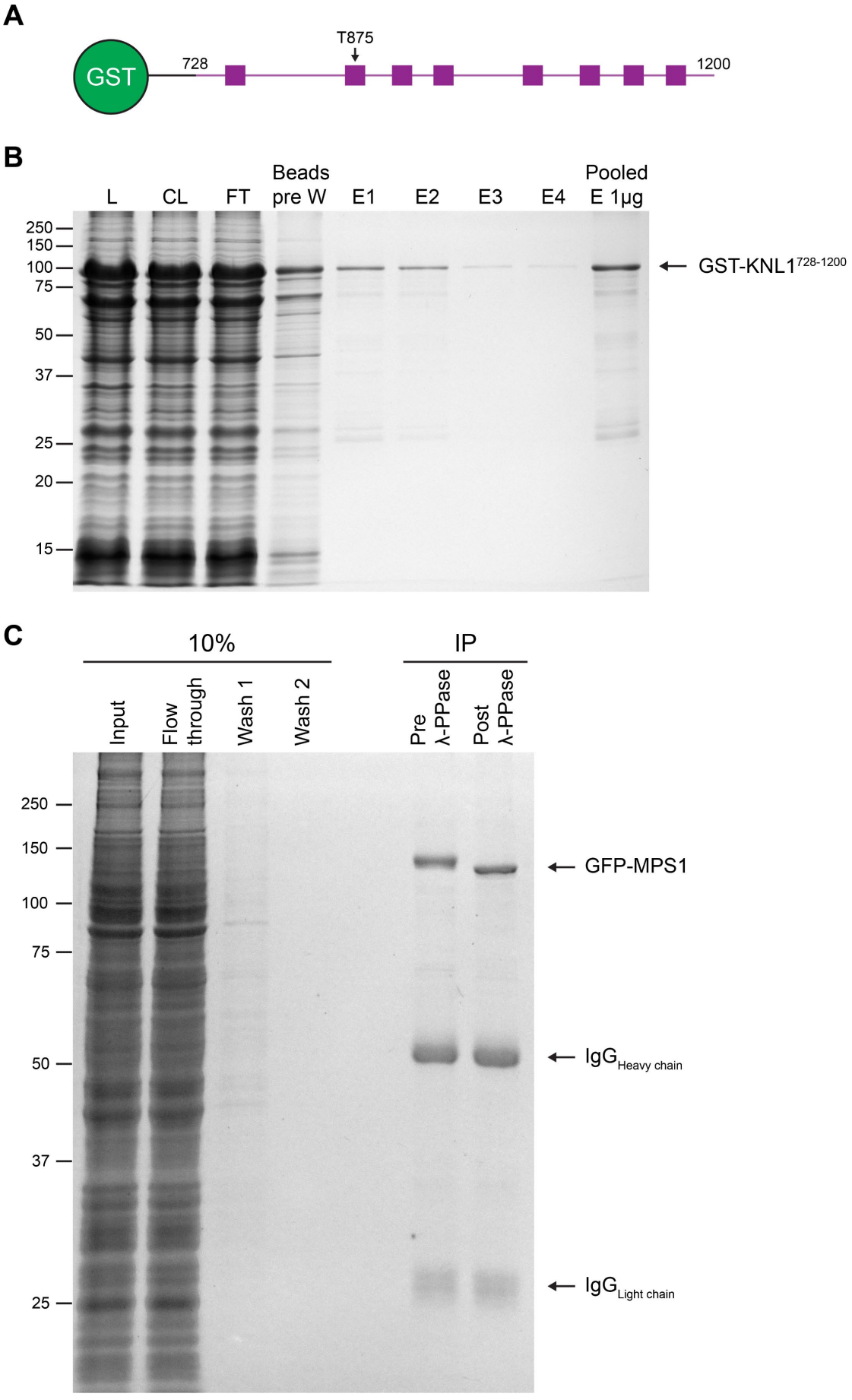
A
GST
728
T875
1200
B
L
CL
FT
Beads pre W
E1
E2
E3
E4
Pooled E 1µg
250
150
100
75
50
37
25
20
15
GST-KNL1728-1200
C
10%
IP
Input
Flow through
Wash 1
Wash 2
Pre λ-PPase
Post λ-PPase
250
150
100
75
50
37
25
GFP-MPS1
IgGHeavy chain
IgGLight chain

Figure 10 – **Preparation of purified GST-KNL1$^{728-1200}$ and GFP-MPS1 for kinase assays**

A) Schematic showing GST-KNL1$^{728-1200}$**.** MELT motifs in KNL1 are indicated by purple squares. T875 at one such MELT motif is indicated as a phospho-specific antibody against this site exists.
B) Coomassie gel of affinity purification of GST-KNL1$^{728-1200}$ from bacteria with glutathione agarose. Elutions were performed by addition of reduced glutathione. Equivalent volumes of each fraction are loaded on the gel, except for the final lane in which 1µg of the pooled elution fractions is loaded.
C) Coomassie gel of anti-GFP IP from mitotic HEK293T cells expressing GFP-MPS1^{WT}. After IP beads were treated with lambda-phosphatase to dephosphorylate MPS1 before copious washing to remove phosphatase.

To check that the phosphatase treated GFP-MPS1 could still become active and phosphorylate targets in cis and trans, a kinase assay comparing non-dephosphorylated and dephosphorylated WT MPS1 was carried out (Figure 11A, B). Purified GFP-MPS1, pre-treated with or without phosphatase, was mixed with GST-KNL1 and incubated in the presence or absence of ATP. In the absence of ATP, western blotting for MPS1-pT33/S37 confirmed the efficacy of the lambda phosphatase treatment (Figure 11B). Upon incubation with ATP, the GFP-MPS1 without phosphatase pre-treatment efficiently phosphorylated itself – seen by an upshift of the band by Coomassie staining (Figure 11A) and an increase in MPS1-pT33/S37 signal (Figure 11B). Furthermore, this GFP-MPS1 was able to phosphorylate KNL1 weakly but detectably at T875. GFP-MPS1 pre-treated with phosphatase was also able to phosphorylate itself and KNL1, albeit to a lesser extent (Figure 11A, B). This experiment verified that the phosphatase-treated GFP-MPS1 could still become active under these assay conditions.

To compare the kinase activity of the various GFP-MPS1 constructs, they were immunoprecipitated and dephosphorylated as previous (Figure 10C). The ability of the treated GFP-MPS1 proteins to auto-phosphorylate and phosphorylate GST-KNL1$^{728-1200}$ was assayed by ^{32}P incorporation (Figure 11C-E). MPS1^{WT} phosphorylated itself and GST-KNL1$^{728-1200}$ as expected (Figure 11C-E). The lack of

phosphorylation by MPS1^{KD} demonstrated that this kinase activity was due to MPS1, and not a contaminating kinase (Figure 11C-E). As the NTE phospho-mutants have a different number of phosphorylatable residues, the substrate concentration of unphosphorylated residues is different from that of WT. Therefore, it is most pertinent to compare these mutants to each other, and to a construct lacking the entire NTE (MPS1$^{\Delta 60}$), rather than to MPS1^{WT}. There were no large differences in the extent of MPS1 auto-phosphorylation or phosphorylation of GST-KNL1$^{728\text{-}1200}$ (Figure 11C-E). These data suggest that the mutation or deletion of the N-terminal autophosphorylation sites in MPS1 does not affect MPS1 kinase activity.

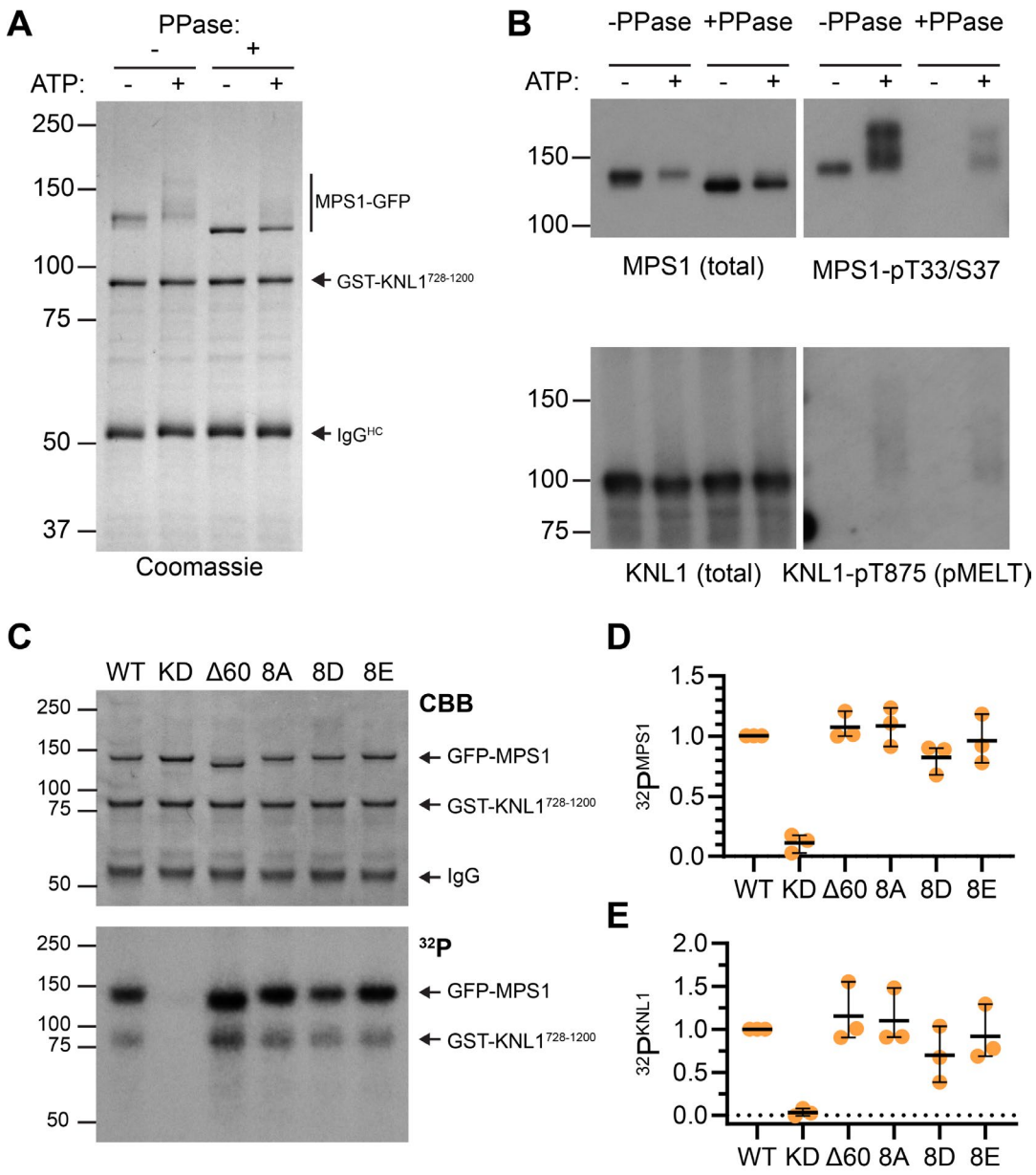

Figure 11 – **Mutation of NTE auto-phosphorylation sites does not grossly alter kinase activity**

A) Coomassie gel of cold kinase assay (90 min, 30°C) with immunoprecipitated GFP-MPS1 pre-treated with or without lambda-phosphatase and purified GST-KNL1$^{728-1200}$. Reaction mixes were incubated with or without ATP.

B) Western blots of samples in (A) for total MPS1, pT33/S37-MPS1, total KNL1, and pT835-KNL1 (pMELT).

C) Coomassie gel (top) and autoradiogram (bottom) of radioactive kinase assay between indicated GFP-MPS1 proteins and GST-KNL1$^{728-1200}$. GFP-MPS1 proteins were immunoprecipitated from mitotic HeLa cells and dephosphorylated on-bead by lambda phosphatase treatment as in 3B. GFP-MPS1 on-beads was incubated with GST-KNL1$^{728-1200}$ for 1 h at 30°C in the presence of γ-^{32}P ATP.

D) Quantification of ^{32}P signal from MPS1 normalised to total MPS1 from 3 technical replicates.

E) Quantification of ^{32}P signal from GST-KNL1$^{728-1200}$ normalised to total MPS1 from 3 technical replicates.

The opposing activities of PP2A-B56 and Aurora B control MPS1 localisation in response to end-on attachment

MPS1 and PP2A-B56 participate in a negative feedback loop via BUBR1

MPS1 participates in a negative feedback loop with BUBR1-bound PP2A-B56 (Diagram 15). Thus, MPS1 indirectly recruits a pool of kinetochore-localised PP2A-B56 which stabilises microtubule-kinetochore attachments and opposes SAC signalling and MPS1 localisation [155,158–160]. One explanation for the appearance of inhibited MPS1 at attached kinetochores is a reduction in kinetochore-localised PP2A-B56. To investigate the relationship between MPS1 activity, attachment status, and BUBR1 localisation, HeLa cells expressing endogenously tagged MPS1-GFP were arrested in STLC and MG132 to trap cells in mitosis with attached and unattached kinetochores (Figure 12A). Without MPS1 inhibitor, MPS1 and BUBR1 localised to unattached kinetochores as expected (Figure 12A-D). At Astrin positive kinetochores, MPS1 localised weakly, and BUBR1 levels were decreased to 50% (Figure 12A-D). Upon MPS1 inhibition, MPS1 localised ~2.5x as strongly as expected, and BUBR1 levels were further reduced to ~25% regardless of attachment status (Figure 12A-D). These data confirm that BUBR1 localisation can still be decreased upon MPS1 inhibition at attached kinetochores and suggest that PP2A-B56 levels will be similarly affected.

To verify that PP2A-B56 levels at kinetochores follow that of BUBR1, the localisation of BUBR1 and B56δ was measured in HeLa Flp-In cells transiently expressing GFP-B56δ. Cells were arrested with nocodazole and treated with or without MPS1 inhibitor prior to fixation and staining for CENP-C and BUBR1 (Figure 12E). As previous, BUBR1 levels were reduced to ~25% upon MPS1 inhibition (Figure 12E,

F). GFP-B56δ localised weakly to kinetochores without MPS1 inhibition and fell to ~25% upon MPS1 inhibition (Figure 12E, G). To probe how attachment status fits with PP2A-B56 levels, the experiment was repeated with a monopolar spindle (Figure 12H). It was observed that GFP-B56δ localised much more weakly to unattached kinetochores in STLC than in nocodazole, despite no obvious change in BUBR1 level. This was not formally quantified, so remains an anecdotal observation. The changes in BUBR1 localisation mirrored that previously seen (Figure 12A, D, H, I). Upon microtubule attachment B56δ levels fell to ~50% (Figure 12H, J). Upon MPS1 inhibition, GFP-B56δ levels fell further to ~25% (Figure 12H, J). Together, these data demonstrate that even though BUBR1 and PP2A-B56 recruitment decreases upon microtubule attachment, their levels are decreased even further without the activity of MPS1. Thus, the appearance of MPS1 at attached kinetochores upon inhibition or inactivation (Figure 4, Figure 8) could be due to a reduction in PP2A-B56 at these attached kinetochores.

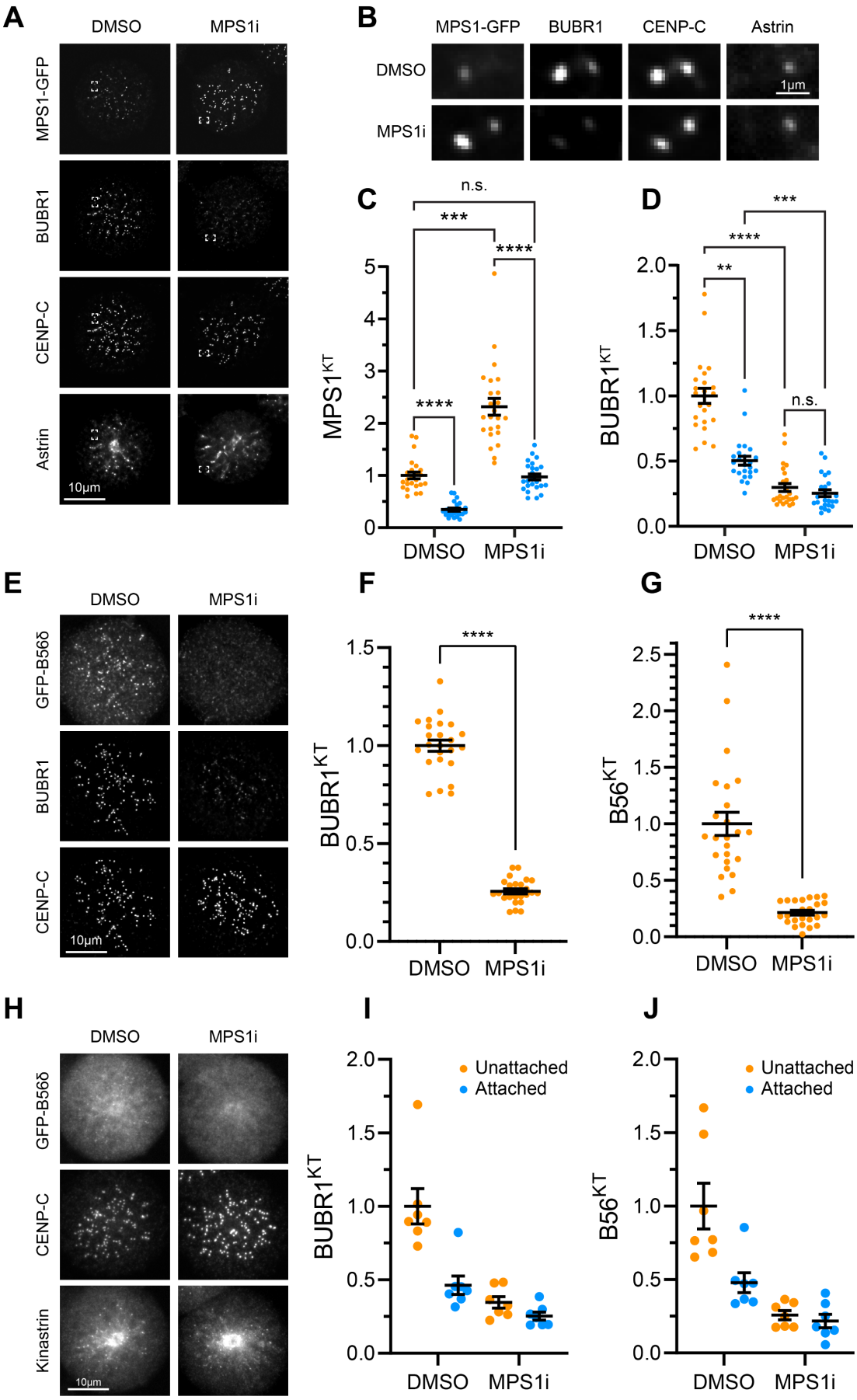
A
DMSO
MPS1i
MPS1-GFP
BUBR1
CENP-C
Astrin
10μm
B
MPS1-GFP
BUBR1
CENP-C
Astrin
DMSO
MPS1i
1μm
C
n.s.
***
****
****
MPS1KT
DMSO
MPS1i
D
***
****
**
n.s.
BUBR1KT
DMSO
MPS1i
E
DMSO
MPS1i
GFP-B56δ
BUBR1
CENP-C
10μm
F
****
BUBR1KT
DMSO
MPS1i
G
****
B56KT
DMSO
MPS1i
H
DMSO
MPS1i
GFP-B56δ
CENP-C
Kinastrin
10μm
I
Unattached
Attached
BUBR1KT
DMSO
MPS1i
J
Unattached
Attached
B56KT
DMSO
MPS1i

Figure 12 – **MPS1 activity is required to localise BUBR1 and B56 to attached kinetochores**

A) HeLa cells with endogenously tagged MPS1-GFP were arrested with STLC (2 h, 10 μM) and MG132 (30 min, 20 μM) and treated with or without MPS1i (AZ3146, 10 min, 2 μM). Cells were fixed and immuno-stained for CENP-C, Astrin, and BUBR1.
B) Enlarged monotelic kinetochore pairs from (A).
C) Quantification of (A). The mean amount of MPS1 kinetochore localisation at Astrin-positive (attached) or Astrin-negative (unattached) kinetochores is plotted. Each dot represents one cell, data pooled from 3 biological repeats. Bars show mean± S.E.M.
D) Quantification of (A). The mean amount of BUBR1 kinetochore localisation at Astrin-positive (attached) or Astrin-negative (unattached) kinetochores is plotted. Each dot represents one cell, data pooled from 3 biological repeats. Bars show mean± S.E.M.
E) HeLa Flp-In TREx cells expressing a GFP-B56δ transgene were arrested with nocodazole (2 h, 0.6 μM) and MG132 (30 min, 20 μM) and treated with or without MPS1i (AZ3146, 10 min, 2 μM). Cells were fixed and immuno-stained for CENP-C and BUBR1.
F) Quantification of the mean amount of BUBR1 kinetochore localisation of cells in (E). Each dot represents one cell, data pooled from 3 biological repeats. Bars show mean± S.E.M.
G) Quantification of the mean amount of GFP-B56δ kinetochore localisation of cells in (E). Each dot represents one cell, data pooled from 3 biological repeats. Bars show mean± S.E.M.
H) HeLa Flp-In TREx cells expressing GFP-B56 δ were arrested with STLC (2 h, 10 μM) and MG132 (30 min, 20 μM) and treated with or without MPS1i (AZ3146, 10 min, 2 μM). Cells were fixed and immuno-stained for CENP-C, Kinastrin, and BUBR1.
I) Quantification of the mean amount BUBR1 kinetochore localisation of cells in (H) at Kinastrin-positive (attached) or Kinastrin-negative (unattached) kinetochores. Each dot represents one cell, 1 biological repeat. Bars show mean± S.E.M.
J) Quantification of the mean amount of GFP-B56δ kinetochore localisation of cells in (H) at Kinastrin-positive (attached) or Kinastrin-negative (unattached) kinetochores. Each dot represents one cell, 1 biological repeat. Bars show mean± S.E.M.

PP2A-B56 is required to stop MPS1 localising downstream of microtubule attachment

One possible explanation for the accumulation of inactive MPS1 at attached kinetochores is that reduced levels of PP2A-B56 will be localised to said kinetochores (Figure 12), potentially resulting in an inability of the kinetochore to transition into a state which does not bind MPS1. To test the notion that phosphatase activity could be required to stop MPS1 localisation to attached kinetochores, the localisation of MPS1 with and without the PP1/PP2A-family inhibitor calyculin A was examined. HeLa cells expressing endogenously tagged MPS1-GFP were arrested with either nocodazole and MG132 or MG132 alone (Figure 13A). Following a brief treatment with or without calyculin A, cells were fixed and stained for CENP-C, tubulin, and DNA. Without Calyculin A, MPS1 was present at unattached kinetochores, and weakly localised to attached kinetochores (Figure 13A, B). However, upon calyculin A treatment, MPS1 localised to unattached and attached kinetochores to the same level (Figure 13A, B). This observation was confirmed in cells arrested with a monopolar spindle (Figure 13C, D). Together, these observations demonstrate that the activity of a PP1/PP2A phosphatase is required downstream of microtubule attachment to stop the kinetochore from binding MPS1.

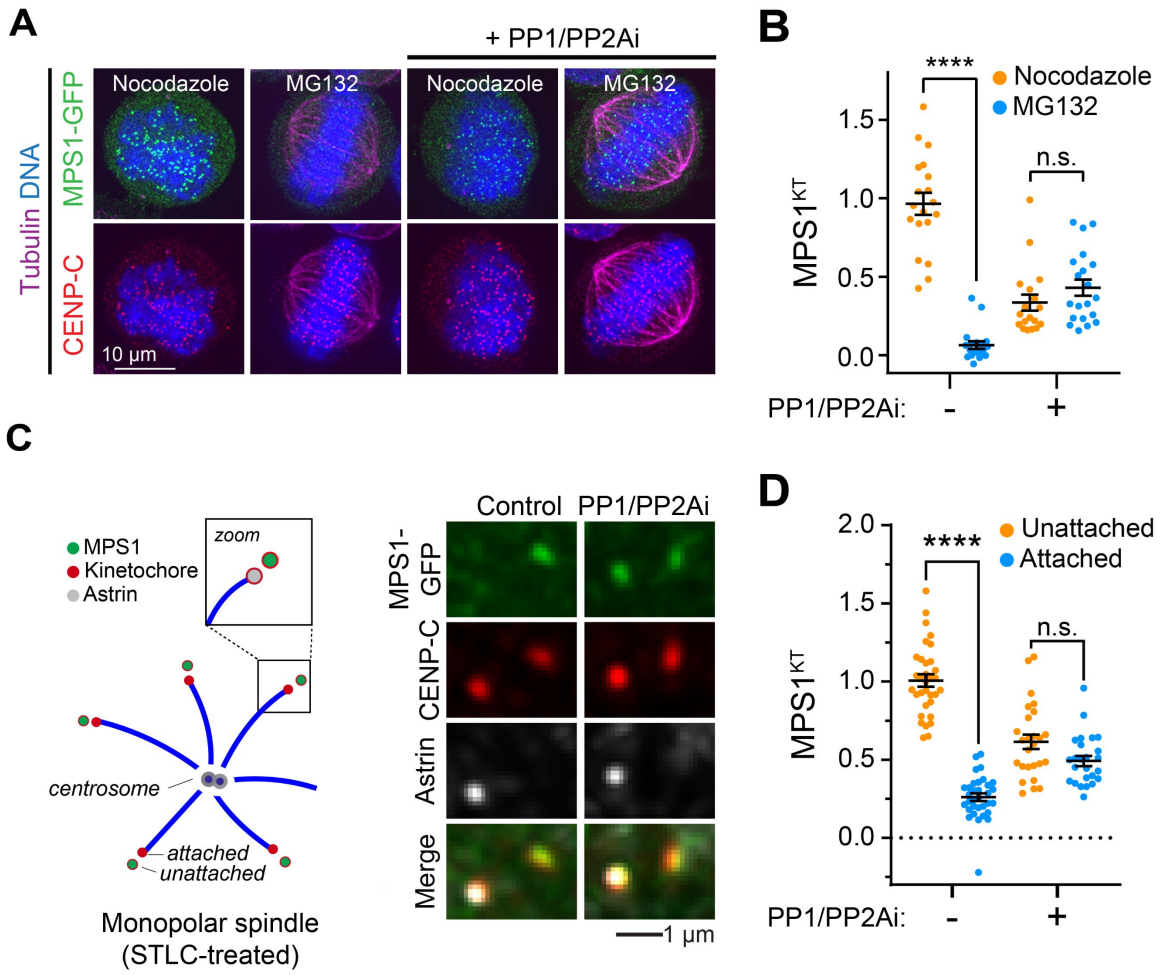

Figure 13 – **Phosphatase activity is required downstream of microtubule binding to prevent MPS1 localisation**

A) HeLa cells with endogenously tagged MPS1-GFP were arrested with nocodazole (2 h, 0.6 µM) and MG132 (30 min, 20 µM) (Noc condition), or MG132 alone (30 min, 20 µM) (MG132 condition) and treated with or without PP1/PP2Ai (Calyculin A, 6 min, 25 nM). Cells were fixed and immuno-stained for CENP-C and tubulin.

B) Quantification of the mean amount of MPS1 kinetochore localisation of cells in (A). Each dot represents one cell, data pooled from 3 biological repeats. Bars show mean± S.E.M.

C) HeLa cells with endogenously tagged MPS1-GFP were arrested with STLC (2 h, 10 µM) and MG132 (30 min, 20 µM) and treated with or without PP1/PP2Ai (Calyculin A, 6 min, 25 nM). Cells were fixed and immuno-stained for CENP-C and Astrin.

D) Quantification of (C). The mean amount of MPS1 kinetochore localisation at Astrin-positive (attached) or Astrin-negative (unattached) kinetochores is plotted. Each dot represents one cell, data pooled from 3 biological repeats. Bars show mean± S.E.M.

BUBR1-bound PP2A-B56 has been heavily implicated in dephosphorylating outer-kinetochore targets and opposing the activities of Aurora B and MPS1[155,158–160]. To investigate if the BUBR1-bound PP2A-B56 was the specific pool of phosphatase required for loss of MPS1 localisation upon microtubule attachment, HeLa-Flp-In cells with point mutations in BUBR1 which prevent it from binding B56 were made in an endogenously tagged GFP-MPS1 background. This BUBR1 mutant L669A, L672A (hereafter referred to as BUBR1^{LIAA}) does not detectable bind B56 [159,160]. An RNAi rescue assay was employed whereby endogenous BUBR1 was depleted, and induction of mCherry-BUBR1^{WT} or the B56-binding defective mCherry-BUBR1^{LIAA} was induced. Western blotting confirmed that endogenous BUBR1 could be depleted and mCherry-BUBR1 could be inducibly expressed as expected (Figure 14A). Cells were arrested with monopolar spindles prior to fixation and immunostained for CENP-C and Astrin, or CENP-C and HURP [266] (Figure 14B). In the wildtype rescue, MPS1 was localised as expected (Figure 14B, C). However, upon rescue with mCherry-BUBR1^{LIAA}, MPS1 localised to all kinetochores regardless of attachment status, to the same level as in the wildtype rescue at unattached kinetochores (Figure 14B, C). Furthermore, in cells expressing mCherry-BUBR1^{LIAA}, BUBR1 was recruited to attached kinetochores (Figure 14B, D). Presumably, this is because MPS1 is present at those kinetochores to phosphorylate MELT motifs, and PP2A-B56 is not present to dephosphorylate those MELT motifs. As this pool of PP2A-B56 has been reported to stabilise kinetochore-microtubule attachments [159], the binding defective mutant would be expected to have far fewer kinetochore-microtubule attachments. Indeed, there were far fewer attached kinetochores with the B56 binding mutant (Figure 14E). These data show

that the localisation of PP2A-B56 via BUBR1 is required for kinetochores to stop localising MPS1 downstream of microtubule attachment.

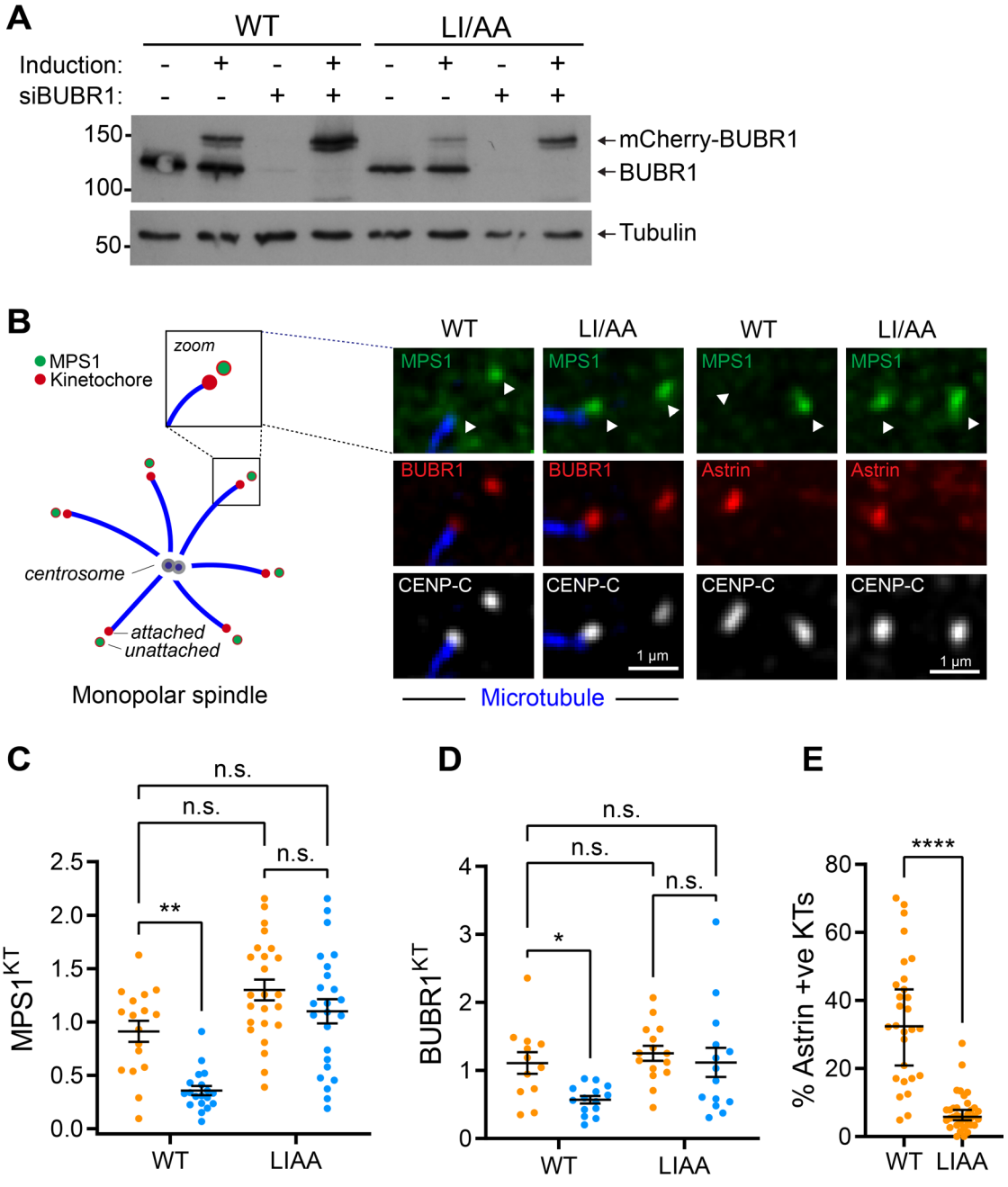

Figure 14 – **BUBR1-bound PP2A-B56 is required downstream of microtubule binding to prevent MPS1 localisation**

A) Anti-BUBR1 Western blot of HeLa Flp-In TREx cells with endogenously tagged GFP-MPS1 treated with siBUBR1 or siControl and ± doxycycline (2 µM) to induce mCherry-BUBR1 transgene expression for 48 hours. Actin is used as a loading control.

B) Monotelic kinetochore pairs. HeLa Flp-In TREx cells with endogenously tagged GFP-MPS1 depleted of endogenous BUBR1 and expressing mCherry-BUBR1 transgenes were arrested with STLC (2 h, 10 µM) and MG132 (30 min, 20 µM). Cells were fixed and immuno-stained

for CENP-C and HURP (a marker of stable k-fibres, left 2 columns) or CENP-C and Astrin (right 2 columns).

C) Quantification of (B). The mean amount of MPS1 kinetochore localisation at Astrin-positive (attached) or Astrin-negative (unattached) kinetochores is plotted. Each dot represents one cell, data pooled from 3 biological repeats. Bars show mean± S.E.M.

D) Quantification of (B). The mean amount of MPS1 kinetochore localisation at Astrin-positive (attached) or Astrin-negative (unattached) kinetochores is plotted. Each dot represents one cell, data pooled from 2 biological repeats. Bars show mean± S.E.M.

E) Quantification of (B). The percentage of kinetochores showing Astrin foci. Each dot represents one cell, data pooled from 3 biological repeats. Bars show mean± S.E.M.

Aurora B activity promotes MPS1 localisation downstream of microtubule attachment

The data gathered thus far suggest a model in which the ability of a kinetochore to localise MPS1 is determined downstream of microtubule attachment in a phosphorylation-dependent manner. BUBR1-localised PP2A-B56 appears to be the relevant phosphatase and is known to oppose both Aurora B and MPS1 phosphorylation at the kinetochore [155,158–160]. What is being dephosphorylated by PP2A-B56, and what this unknown target is being phosphorylated by remains to be determined. An obvious candidate for the kinase is Aurora B – as it is known that Aurora B activity is a crucial prerequisite for MPS1 localisation [156,157]. If Aurora B target phosphorylation does control MPS1 localisation, then increasing the level of Aurora B phosphorylation at kinetochores should over-ride the loss of MPS1 at attached kinetochores.

To increase the level of Aurora B substrate phosphorylation rapidly and transiently at attached kinetochores, a rapamycin-based system to recruit proteins of interest to kinetochore was used [249] (Figure 15A). This approach revolves around the use of rapamycin to hetero-dimerise the proteins FKBP and FRB. By fusing FKBP and FRB to different proteins, addition of rapamycin causes the dimerization of those proteins. In this experiment, FKBP was fused to MIS12, and FRB to an IN-box containing fragment of INCENP which lacked the first 46 amino acids required for centromere localisation [198] (Figure 15A). Thus, active INCENP-bound Aurora B can be rapidly localised to the outer kinetochore. If phosphorylation of an Aurora B target(s) controls MPS1 localisation downstream of microtubule binding, increasing Aurora B activity in this way at attached kinetochores should result in the appearance of MPS1. Cells expressing endogenously tagged MPS1-GFP,

alongside the rapamycin-based system, were arrested with MG132 (to enrich for metaphase plates) and treated with or without rapamycin for 2 minutes (Figure 15B). Addition of rapamycin was sufficient to recruit mCherry-FRB-INCENP$^{47-918}$ to the metaphase plate and resulted in a significant increase in the level of active Aurora B at kinetochores (Figure 15B, C). Thus, this system can successfully be used to rapidly recruit active Aurora B to kinetochores. Examining the localisation of MPS1-GFP in MG132-arrested cells upon rapamycin addition, it was seen that MPS1-GFP was recruited at a high level after 2 minutes of rapamycin edition in a fashion dependent on Aurora B activity (Figure 15D, E). Given the roles of Aurora B and MPS1 in error correction [210,211,231,235], it was important to test if end-on kinetochore-microtubule attachments were maintained in these conditions, and that the appearance of MPS1-GFP was not simply due to the generation of unattached kinetochores. Repeating the experiment with cold-treatment to selectively visualise stable microtubule attachments revealed no difference in the proportion of cells which maintained a cold-stable metaphase plate 2 minutes after rapamycin addition (Figure 15F, G). This observation confirmed that an increase in Aurora B activity at kinetochores can cause MPS1 accumulation, regardless of microtubule-occupancy.

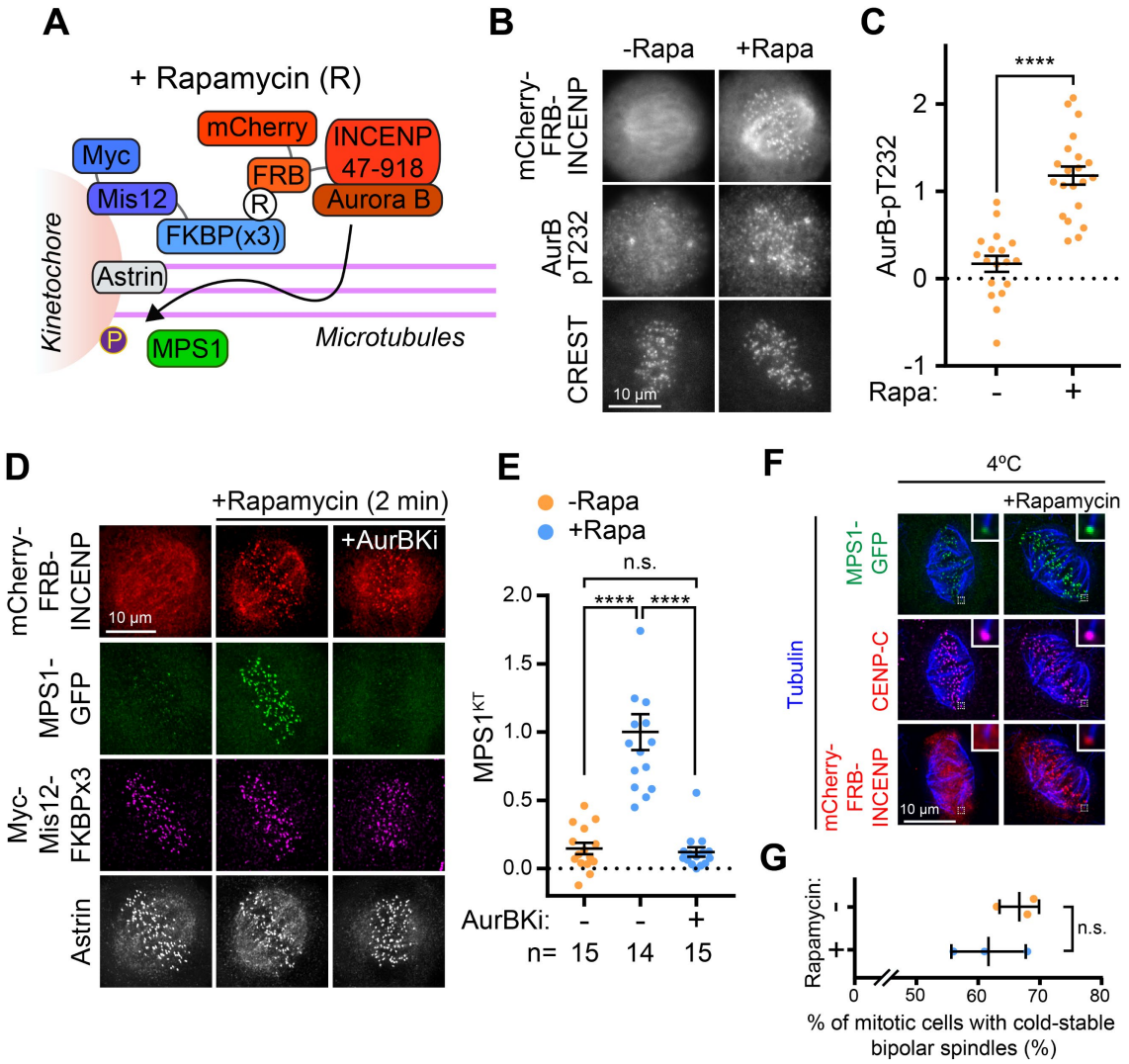

Figure 15 – **Aurora B activity controls MPS1 localisation downstream of MT attachment**

A) Schematic of the rapamycin-dimerisation system used to recruit active Aurora B to the outer kinetochore.

B) HeLa cells expressing endogenously tagged MPS1-GFP and the Aurora B kinetochore-targeting system were arrested with MG132 (30 min, 20 µM) and treated with or without rapamycin (2 min, 500nM). Cells were fixed and stained for Aurora B pT232 and CREST as a marker of kinetochores.

C) Quantification of (B). The total Aurora B-pT232 signal within 1um of a kinetochore. Each dot represents one cell, data pooled from 3 biological repeats. Bars show mean± S.E.M.

D) HeLa cells expressing endogenously tagged MPS1-GFP and the Aurora B kinetochore-targeting system were arrested with MG132 (30 min, 20 µM), treated with or without rapamycin (2 min, 500nM) and with or without AurBKi (ZM447439, 15 min, 20 µM). Cells were fixed and stained for Myc and Astrin.

E) Quantification of the mean amount of MPS1 kinetochore localisation of cells in (D). Each dot represents one cell, data pooled from 3 biological repeats. Bars show mean± S.E.M.

F) HeLa cells expressing endogenously tagged MPS1-GFP and the Aurora B kinetochore-targeting system were arrested with MG132 (30 min, 20 µM), treated with or without rapamycin (2 min, 500nM), incubated on ice for 9 min and fixed. Cells were stained for CENP-C.

G) Quantification of the percentage of cells in (F) with cold-stable bistable spindles.

Given that MPS1 was localised to attached kinetochores under these conditions, it was conceivable that spindle-checkpoint signalling could be initiated despite the presence of end-on microtubule attachment. To test this hypothesis, cells were arrested with either nocodazole or MG132, treated with or without rapamycin, and the localisation of checkpoint proteins BUB1, BUBR1, or MAD1 measured by immunostaining (Figure 16A-C). Without rapamycin, the checkpoint proteins localised robustly to kinetochores in nocodazole, whereas they localised significantly less (BUB1, BUBR1) or not at all (MAD1) in MG132 (Figure 16A-F). Upon addition of rapamycin, the checkpoint proteins were all seen to localise robustly to attached kinetochores in MG132 (Figure 16A-F). Therefore, MPS1 localisation and checkpoint signalling can both be decoupled from microtubule binding by increasing local Aurora B activity. These observations highlight the importance of removing MPS1 from kinetochores to stop localised MCC production.

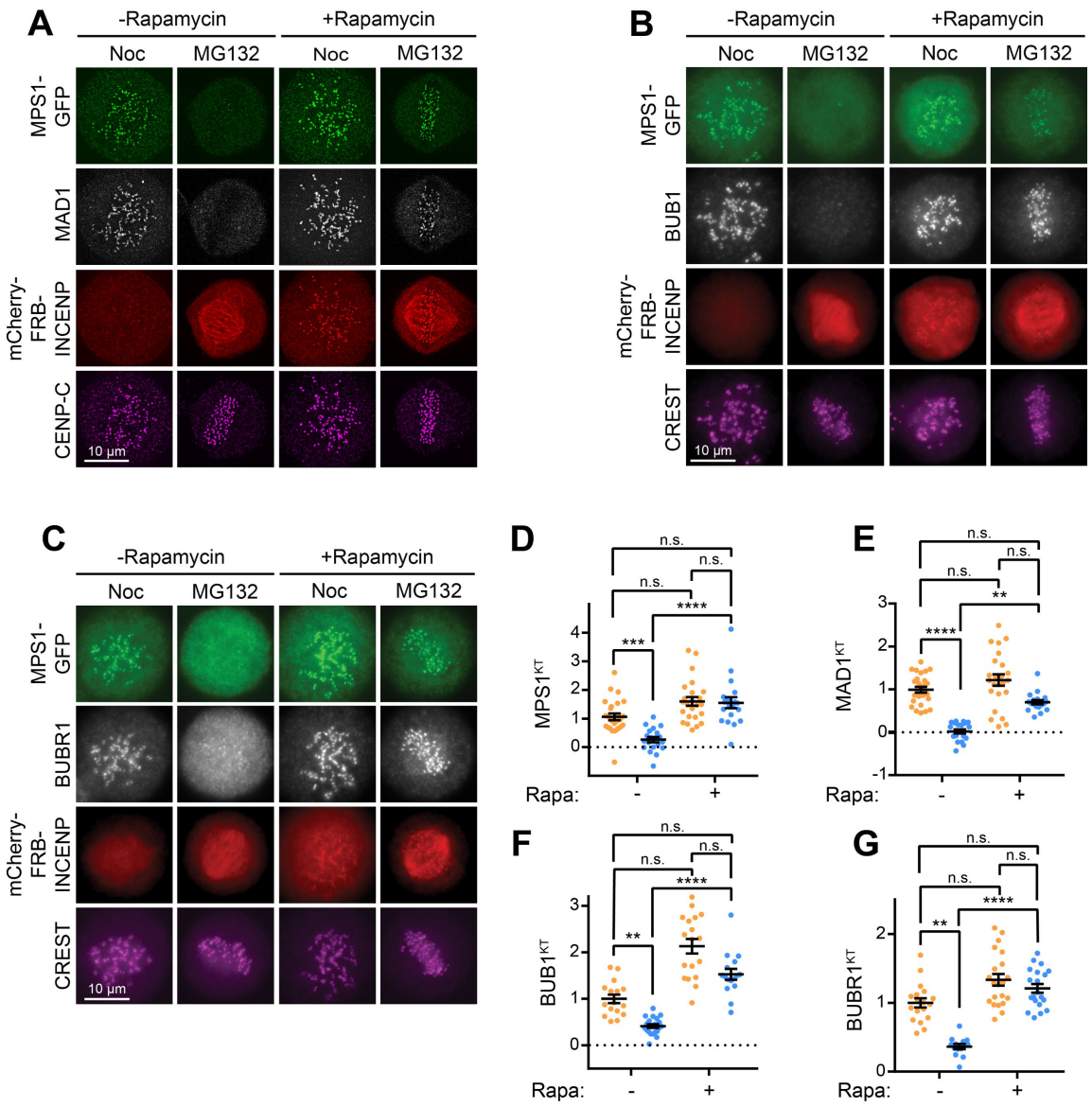

Figure 16 – **MPS1 at attached kinetochores can recruit checkpoint proteins**

A) HeLa cells expressing endogenously tagged MPS1-GFP and the Aurora B kinetochore-targeting system were arrested with nocodazole (2 h, 0.6 µM) or MG132 (30 min, 20 µM), and treated with or without rapamycin (2 min 500 nM). Cells were fixed and stained for CENP-C and MAD1.
B) Cells treated as in (A) stained for CREST and BUB1.
C) Cells treated as in (A) stained for CREST and BUBR1.
D) Quantification of the mean amount of MPS1 kinetochore localisation of cells in (A). Each dot represents one cell, data pooled from 3 biological repeats. Bars show mean± S.E.M.
E) Quantification of the mean amount of MAD1 kinetochore localisation of cells in (A). Each dot represents one cell, data pooled from 3 biological repeats. Bars show mean± S.E.M.
F) Quantification of the mean amount of BUB1 kinetochore localisation of cells in (B). Each dot represents one cell, data pooled from 3 biological repeats. Bars show mean± S.E.M.
G) Quantification of the mean amount of BUBR1 kinetochore localisation of cells in (C). Each dot represents one cell, data pooled from 3 biological repeats. Bars show mean± S.E.M.

What is the target of Aurora B which controls MPS1 localisation

Unveiling the identity of the molecular target of Aurora B / PP2A-B56 is vital to understanding how changes in microtubule binding are relayed to MPS1 binding and checkpoint activation. An attractive candidate is the N-terminal tail of MPS1 binding partner HEC1. HEC1 has been described as a target of Aurora B [54,57,214,215], and indeed phosphorylation of the tail has been published as the mechanism of recruiting MPS1 to kinetochores [168]. However, these observations have not been replicated by other groups [131]. During this study, the Gruneberg lab was also unable to replicate the observation that HEC1 tail phosphorylation impacts the localisation of MPS1, or the dependence of MPS1 localisation on Aurora B activity [1]. These data show that Aurora B must have other targets required for MPS1 recruitment. It is possible that there are multiple targets of Aurora B which are required for MPS1 localisation, and perturbation of a single target will not be sufficient to cause aberrant MPS1 behaviour. However, it has recently been confirmed that the HEC1 tail is predominantly a target of Aurora A kinase, not Aurora B, and that phosphorylation of these sites are rarely saturated [267]. Furthermore, some of these sites are more highly phosphorylated at end-on attached kinetochores [267,268]. Therefore, it is unlikely that phosphorylation of the HEC1 tail by Aurora B is a physiologically relevant target for controlling MPS1 localisation.

We noticed that there were 3 cryptic Aurora B consensus motifs on MPS1 itself which were phosphorylated on immunoprecipitated MPS1 (data not shown). These sites are adjacent to the middle region – S345, S346, and S393. To investigate the relevance of these sites for MPS1 localisation, phosphonull (3A) and phosphomimetic (3D, 3E) mutants were made and integrated into Flp-In cells. To validate the cell lines, cells were treated with siMPS1 or siControl, and with or

without doxycycline induction (Figure 17A). In all cell lines endogenous MPS1 was efficiently depleted by siMPS1 (Figure 17A, +siMPS1), and GFP-MPS1 mutants were efficiently expressed upon induction (Figure 17A, +dox). Cells were subject to RNAi rescue and arrested with nocodazole and MG132 to generate unattached kinetochores, and treated with or without Aurora kinase inhibitor. Cells were fixed and immunostained for CENP-C and H3pS10 to indicate Aurora B activity (Figure 17B). An internal experimental control demonstrated that RNAi depletion of endogenous MPS1 was efficient (Figure 17D). As expected, $MPS1^{WT}$ was present at kinetochores in the absence of Aurora B inhibitor (AurBKi), and weakly localised with its addition (Figure 17B, C). H3pS10 staining was lost in AurBKi conditions, indicating successful inhibition of Aurora B. All phosphomutants phenocopied $MPS1^{WT}$ – showing no change in MPS1 localisation when unperturbed, and a dependence on Aurora B activity (Figure 17B, C). These data suggest that these sites have no impact on the localisation behaviour of MPS1, and are likely not the physiologically relevant targets of Aurora B. Again, it is possible that there are several such targets and mutation of individual targets is not sufficient to override Aurora B dependence. Additionally, it is unclear whether these sites are phosphorylated by Aurora B, and no evidence exists which would suggest that Aurora B phosphorylates MPS1 *in vitro* [129].

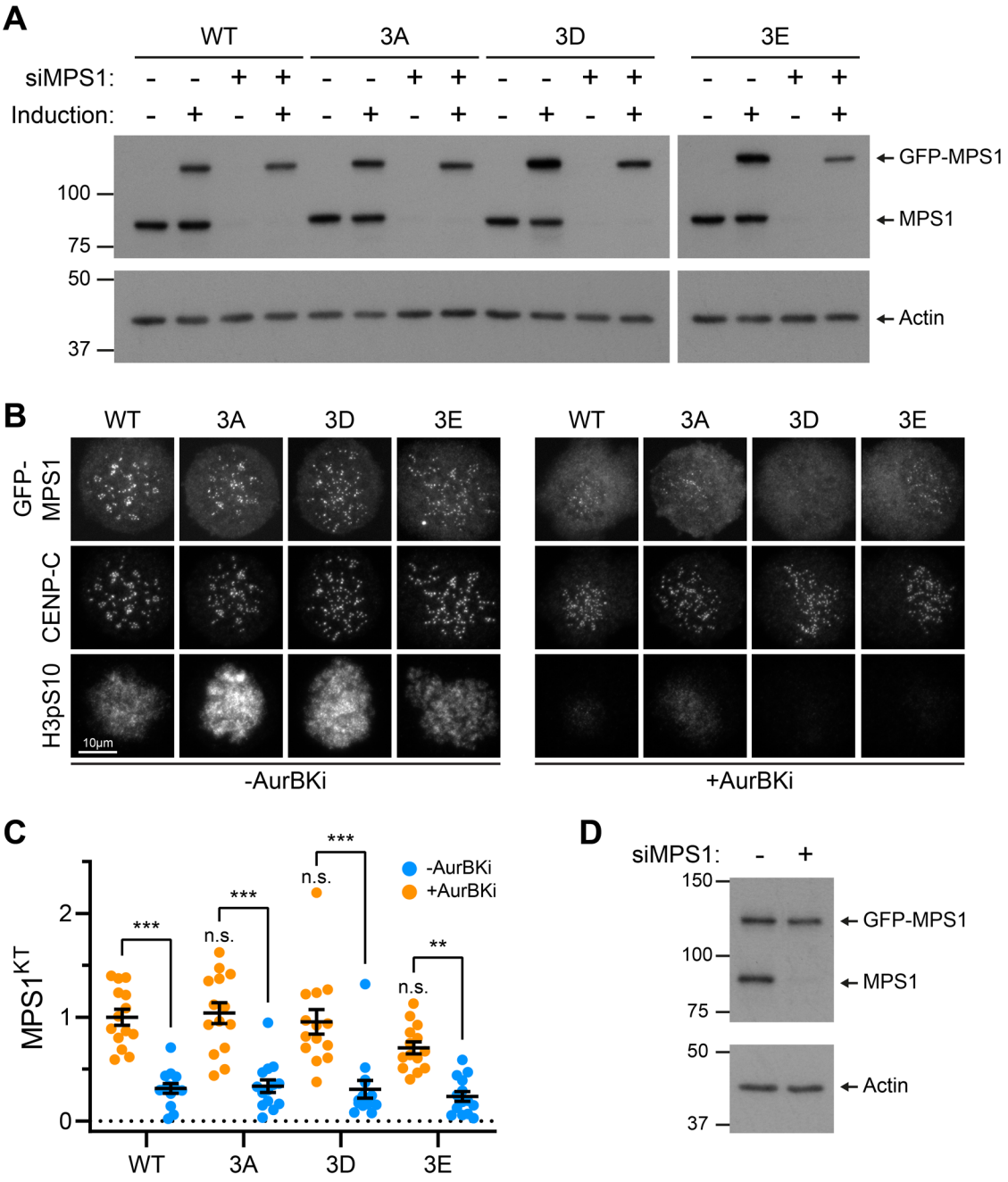

Figure 17 – **Mutation of putative Aurora B sites in MPS1 do not change MPS1 behaviour or dependency on Aurora B activity**

A) Anti-MPS1 Western blot of HeLa Flp-In TREx cells treated with siMPS1 or siControl and ± doxycycline (2 µM) to induce GFP-MPS1 transgene expression for 48 hours. Actin is used as a loading control.

B) HeLa Flp-In TREx cells depleted of endogenous MPS1 and expressing GFP-MPS1 transgenes were arrested with nocodazole (2 h, 0.6 µM) and MG132 (30 min, 20 µM) and treated with or without AurBKi (ZM447439, 15 min, 20 µM). Cells were fixed and immuno-stained for CENP-C and histone 3 phospho-serine 10.

C) Quantification of the mean amount of MPS1 kinetochore localisation of cells in (B). Each dot represents one cell, data pooled from 3 biological repeats. Bars show mean± S.E.M.

D) Internal control from (B). Anti-MPS1 Western blot of HeLa Flp-In TREx cells treated with siMPS1 or siControl and expressing GFP-MPS1^{WT} for 48 hours. Actin is used as a loading control.

Exploring the requirements of Aurora B localisation and activity for MPS1 kinetochore recruitment

How the spindle checkpoint is silenced, if not by direct competition between MPS1 and microtubules for kinetochore binding, is an open question. The data gathered in this project so far suggests that microtubule binding is somehow coupled to a change in the balance of Aurora B kinase and PP2A-B56 phosphatase activities. Prior to microtubule kinetochore attachment, the kinetochore is presumably in a state in which Aurora B activity is greater than that of PP2A-B56. Upon microtubule binding, the kinetochore will transition to a state in which PP2A-B56 activity predominates. There are several possibilities for how this might be mechanistically achieved:

- Changes in the local concentration of the enzymes
- Changes in the activity of the enzymes
- Changes in kinetochore conformation to change substrate accessibility

These possible mechanisms are not mutually exclusive. Regarding changes in local concentration of enzymes, BUBR1 and PP2A-B56 levels were seen to fall by 50% upon microtubule attachment (Figure 12). This is initially counterintuitive, given that one might expect PP2A-B56 levels to increase to favour substrate de-phosphorylation. It has been proposed that the higher levels of PP2A-B56 at unattached kinetochores serve as a signal-damping mechanism such that the checkpoint can be deactivated and microtubules can re-bind [235]. A long-standing model in the field is that of spatial separation of Aurora B from targets at the kinetochore upon tensioned microtubule attachment [217,218]. The idea being that the outer kinetochore is physically pulled away from Aurora B which is restricted to

the inner centromere, thereby preventing Aurora B from reaching its targets at the outer kinetochore. While this tension sensing mechanism does seem to be plausible for stabilising biorientation, stopping MCC generation at kinetochores does not require tension [151]. Indeed, microtubule attachment in the absence of tension, as in a monopolar spindle, is sufficient to cause the loss of MPS1 localisation (Figure 1). It has been suggested that microtubule binding to the kinetochore is sufficient to cause structural rearrangement, regardless of tension [192]. Therefore, the mere binding of microtubules to a kinetochore may favour a state in which Aurora B is separated from targets at the outer kinetochore. It should be stressed that this is different from the tension caused by pulling across sister kinetochores.

Regarding changes in the activity of the enzymes, models for modulating the activity of Aurora B and PP2A-B56 have been put forward in the context of tension sensing [219]. Some of these mechanisms may also be at play at tensionless attachments, given that the kinetochore is proposed to undergo structural rearrangement. However, this has not been investigated in this context.

To investigate the idea that a decrease in the local concentration of Aurora B might be the trigger for a transition into a PP2A-B56 dominant state, a strategy to rapidly deplete Aurora B from the centromere was devised. A major contribution to the centromeric enrichment of Aurora B, and the CPC, is the phosphorylation of histone 3 at threonine 3 by Haspin [200–202]. By inhibiting Haspin, H3pT3 should be rapidly dephosphorylated and the centromeric enrichment of Aurora B lost. If a decrease in the local concentration of Aurora B is sufficient to cause the loss of MPS1, then MPS1 localisation should be abolished. To test this hypothesis, HeLa cells expressing endogenously tagged MPS1-GFP were arrested with nocodazole and MG132 an treated with or without Haspin inhibitor prior to fixation. Cells were fixed

and immunostained for Aurora B (Figure 18A) or H3pT3 (Figure 18C). Without Haspin inhibition, H3pT3 was present on chromatin and Aurora B was enriched at centromeres (Figure 18A-E). Haspin inhibition reduced H3pT3 to nearly undetectable levels (Figure 18C) and caused Aurora B to localise diffusely to chromatin (Figure 18A, B, D). A metric for centromeric enrichment was calculated as the ratio of Aurora B within 1um of a kinetochore compared to that >1um from a kinetochore (Figure 18D), which showed a near-complete loss of centromeric enrichment upon Haspin inhibition. Additionally, the total level of Aurora B on chromatin fell to ~60% (Figure 18E). These observations confirm that Haspin inhibition causes the loss of centromeric Aurora B recruitment [200–202]. Notably, these observations contrast with reports that inhibition or knockout of Haspin causes Aurora B to re-localise from the centromere to the kinetochore [227,228]. This kinetochore localisation may only manifest upon loss of Haspin activity on longer timescales, as the inhibition period used in one study was 30minutes, compared to the 10 minutes used here [227].

Without Haspin inhibition, MPS1 localised clearly to kinetochores, and this localisation was not reduced upon Haspin inhibition (Figure 18A, F). Rather, the level of MPS1 at kinetochores increased by a small amount (Figure 18A, F). This data suggests that a reduction in Aurora B activity, by loss of centromeric enrichment, is not sufficient to cause unattached kinetochores to stop localising MPS1. Indeed, a recent paper found that centromeric enrichment of Aurora B was not required for a functional spindle checkpoint [228]. To validate these results, the experiment was repeated with monopolar spindles (Figure 18G). Again, the centromeric enrichment of Aurora B was virtually abolished upon Haspin inhibition (Figure 18G). Furthermore, there was a large increase in the percentage of Astrin-

positive kinetochores (Figure 18G, H), suggesting that the centromeric enrichment of Aurora B strongly contributes to destabilising kinetochore-microtubule attachments. Unattached kinetochores still localised MPS1 to the same level with Haspin inhibition as without (Figure 18G, I, J). Interestingly, these data suggest that the level of Aurora B required for MPS1 localisation may be lower than that required to destabilise microtubule attachments.

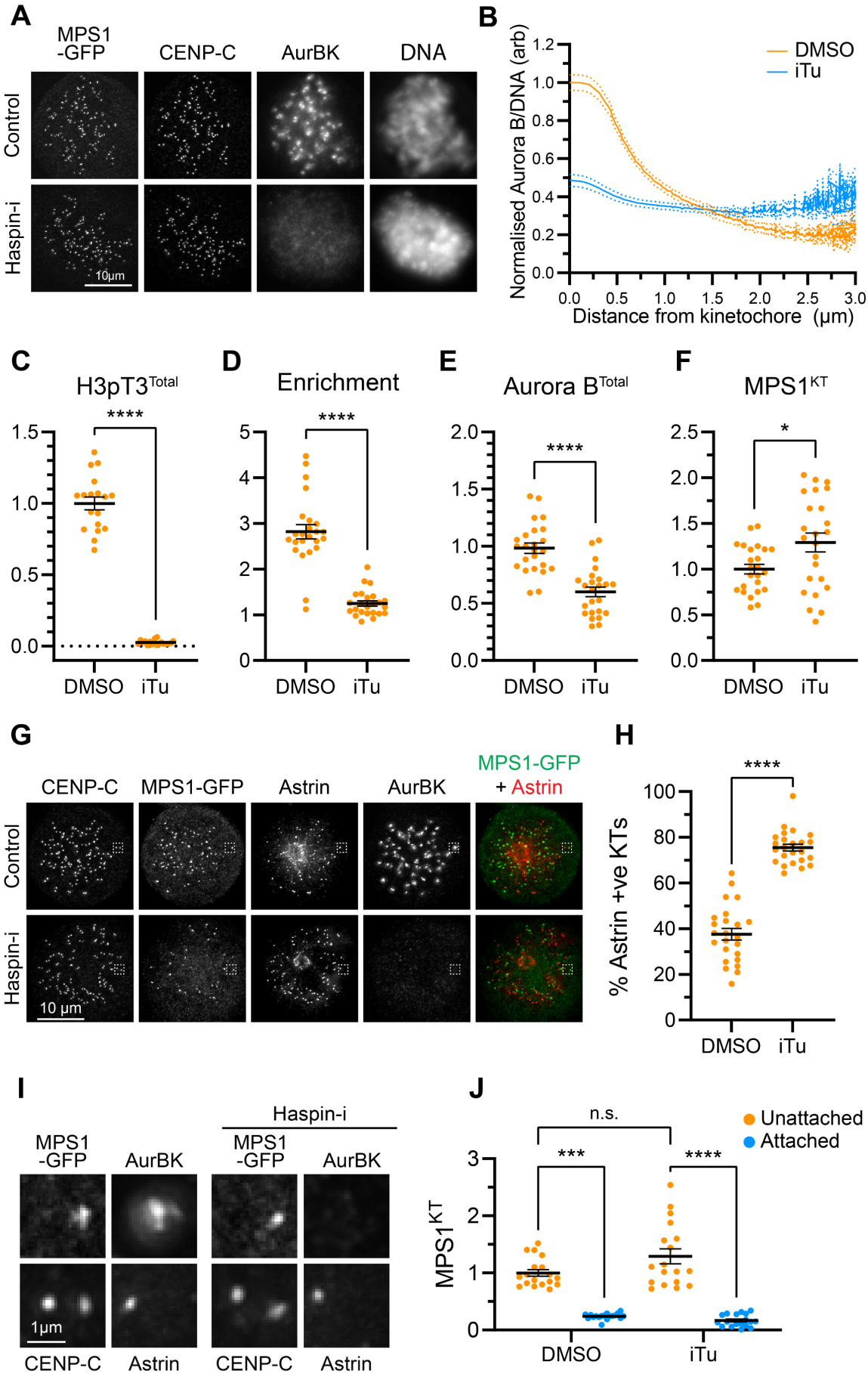
A
MPS1 -GFP
CENP-C
AurBK
DNA
Control
Haspin-i
10µm
B
DMSO
iTu
Normalised Aurora B/DNA (arb)
Distance from kinetochore (µm)
C
H3pT3Total
D
Enrichment
E
Aurora BTotal
F
MPS1KT
DMSO
iTu
G
CENP-C
MPS1-GFP
Astrin
AurBK
MPS1-GFP + Astrin
10 µm
H
% Astrin +ve KTs
I
Haspin-i
1µm
CENP-C
Astrin
J
n.s.
Unattached
Attached
MPS1KT

Figure 18 – **Loss of centromeric Aurora B enrichment is not sufficient to stop MPS1 localisation to unattached kinetochores**

A) HeLa cells with endogenously tagged MPS1-GFP were arrested with nocodazole (2 h, 0.6 μM) and MG132 (30 min, 20 μM) and treated with or without Haspin-I (5-iodotubercidin, 10 min, 10 μM). Cells were fixed and immuno-stained for AurBK and CENP-C.
B) Plot of the Aurora B signal on chromatin as a function of distance from a kinetochore from cells in (A).
C) Quantification of H3pT3 in cells treated as in (A). Each dot represents one cell, data pooled from 3 biological repeats. Bars show mean± S.E.M.
D) Quantification of (A). The ratio of the mean Aurora B signal within 1μm of a kinetochore to that >1μm from a kinetochore. Each dot represents one cell, data pooled from 3 biological repeats. Bars show mean± S.E.M.
E) Plot of the total Aurora B signal on chromatin from cells in (A). Each dot represents one cell, data pooled from 3 biological repeats. Bars show mean± S.E.M.
F) Quantification of the mean amount of MPS1 kinetochore localisation of cells in (A). Each dot represents one cell, data pooled from 3 biological repeats. Bars show mean± S.E.M.
G) HeLa cells with endogenously tagged MPS1-GFP were arrested with STLC (2 h, 10 μM) and MG132 (30 min, 20 μM) and treated with or without Haspin-i (5-iodotubercidin, 10 min, 10 μM). Cells were fixed and immuno-stained for AurBK, Astrin and CENP-C.
H) Quantification of the percentage of kinetochores showing Astrin staining in (C). Each dot represents one cell, data pooled from 3 biological repeats. Bars show mean± S.E.M.
I) Enlarged monotelic kinetochore pairs from (G).
J) Quantification of (G). The mean amount of MPS1 kinetochore localisation at Astrin-positive (attached) or Astrin-negative (unattached) kinetochores is plotted. Each dot represents one cell, data pooled from 3 biological repeats. Bars show mean± S.E.M.

When measuring the proportion of end-on attached kinetochores by examining cold-stable microtubule attachments, an increase in the level of attachments was observed upon Haspin inhibition (Figure 19A, B). However, it was noticed that the number of attachments produced by this metric was consistently lower than that by Astrin staining (Figure 19C). This was surprising given that cold-stability and Astrin-localisation should both be markers of end-on attachment. It is possible that during cold-treatment some end-on attachments are in fact lost. Leaving cells on ice for longer periods of time is known to reduce the number of attachments, to the extent that no microtubules will persist (Gruneberg lab, unpublished).

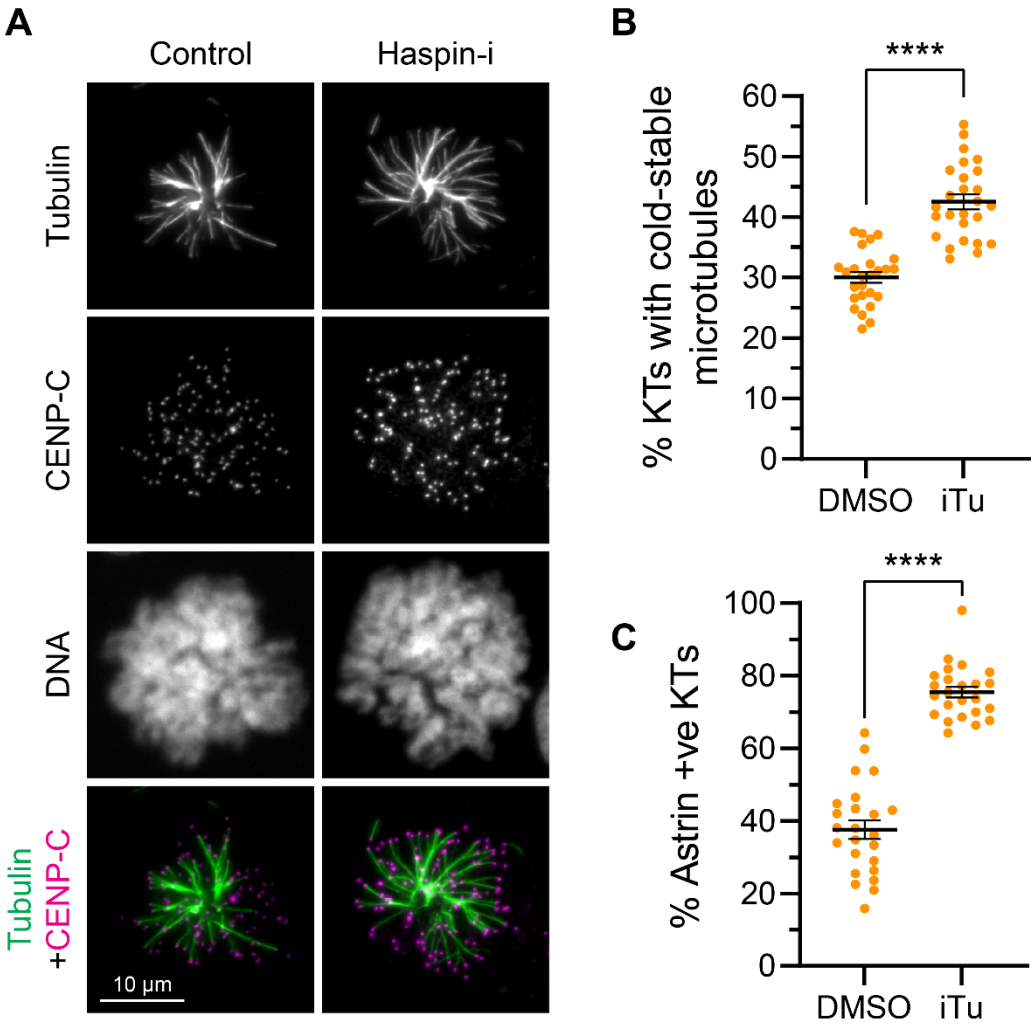

Figure 19 – **Haspin inhibition increases the level of kinetochores with cold-stable microtubules in a monopolar spindle**

A) HeLa cells with endogenously tagged MPS1-GFP were arrested with STLC (2 h, 10 µM) and MG132 (30 min, 20 µM) and treated with or without Haspin-i (5-iodotubercidin, 10 min, 10 µM). Cells were cold treated, fixed and immuno-stained for tubulin and CENP-C.

B) Quantification of the percentage of kinetochores showing with cold-stable microtubules in (A). Each dot represents one cell, data pooled from 3 biological repeats. Bars show mean± S.E.M.

C) Reproduced from Figure 18H. Quantification of the percentage of kinetochores showing Astrin staining from cells treated identically to (A) but without cold-treatment and stained for Astrin. Each dot represents one cell, data pooled from 3 biological repeats. Bars show mean± S.E.M.

To investigate the differences between these two metrics directly, the proportion of kinetochores with Astrin foci or cold-stable microtubules was quantified in the same STLC-arrested cells (Figure 20). Haspin and Aurora B inhibitions were used to generate different levels of end-on attached kinetochores to allow comparison across a range of values. As expected, the number of Astrin foci or cold-stable microtubules increased as Aurora B function was progressively perturbed by Haspin inhibition and direct inhibition (Figure 20A, B). The number of Astrin-positive foci was unchanged by cold-treatment in all cases (Figure 20A, B), suggesting that if the proportion of end-on attachments changes during cold treatment, this is not reflected by changes in Astrin localisation. Consistently, across cells and drug inhibitions, Astrin-foci were fewer than cold-stable microtubules (Figure 20A, D). Despite this, the two metrics correlated well. These results demonstrate that there are systematic differences between using cold-stable microtubule attachment and the presence of Astrin as a marker of end-on attachment. It is conceivable that some end-on attachments are lost during cold treatment, which do not lose Astrin staining.

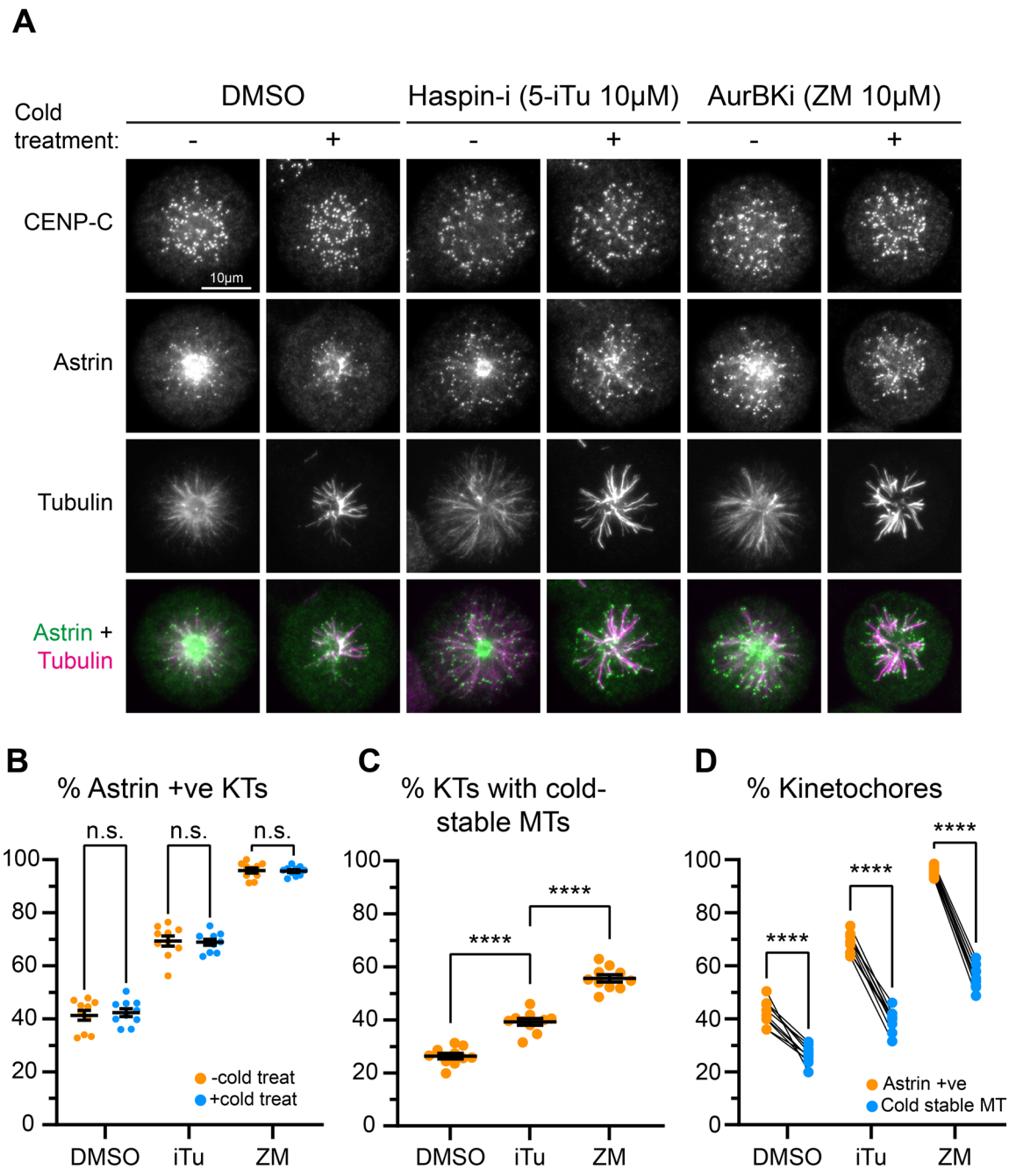

Figure 20 – **Astrin foci are consistently more numerous than cold-stable microtubules**

A) HeLa cells expressing endogenously tagged MPS1-GFP were arrested with STLC (2 h, 10 μM) and MG132 (30 min, 20 μM) and treated with DMSO, Haspin-I (5-iodotubercidin, 15 min, 10 μM), or AurBKi (ZM447439, 15 min, 10 μM). Cells were either fixed straight away (-cold treatment) or cold treated and then fixed (+cold treatment). Fixed cells were immuno-stained for tubulin, Astrin and CENP-C.

B) Quantification of the percentage of kinetochores showing Astrin staining in (A). Each dot represents one cell, data from 1 biological repeat. Bars show mean± S.E.M.

C) Quantification of the percentage of kinetochores with-cold stable microtubules in (A). Each dot represents one cell, data from 1 biological repeat. Bars show mean± S.E.M.

D) Quantification of the percentages of kinetochores with Astrin foci or cold-stable microtubules in (A). Each dot represents one cell, data from 1 biological repeat. Bars show mean ± S.E.M. Measurements from the same cell are paired, indicated by the lines between dots.

A decrease in local concentration of Aurora B by inhibiting Haspin was insufficient to stop MPS1 from localising to unattached kinetochores (Figure 18). This observation alone is not consistent with a model whereby conformational changes upon microtubule attachment to move Aurora B away from the outer kinetochore is solely responsible for stopping MPS1 localisation. To investigate a more extreme decrease in the level of Aurora B, the chromatin localisation of Aurora B can be completely abolished by depleting Survivin [201]. HeLa cells expressing endogenously tagged MPS1-GFP were treated with siGL2 or siSurvivin at different concentrations and for different lengths of time to establish optimal depletion conditions (Figure 21A). Survivin was efficiently depleted in all cases (Figure 21A). For subsequent experiments the 48-hour timepoint was chosen to try and minimise secondary effects of Survivin depletion. Following siRNA treatment, cells were arrested with nocodazole and MG132, fixed, and stained for CENP-C, Aurora B, and DNA (Figure 21B). As expected, Aurora B chromatin localisation was practically undetectable in cells treated with siSurvivin (Figure 21B, C). MPS1 levels were significantly reduced in cells treated with siSurvivin (Figure 21B, E), suggesting that the localisation of Aurora B to chromatin is important for supporting MPS1 localisation. Many cells treated with siSurvivin showed roughly doubled DNA content (Figure 21B, D), suggesting that Survivin was sufficiently depleted during the previous mitosis to cause cytokinesis to fail. The fact that these cells had already been through an aberrant mitosis prior to observation may have introduced confounding variables which could have affected MPS1 localisation. MPS1 levels did not decrease as drastically as when Aurora kinases were inhibited, or to the levels at end-on attached kinetochores. It would be interesting to inhibit Aurora B in a repeat of this experiment to see if MPS1 levels reduce further even when Aurora

B is not localised to chromatin. Together, these observations suggest that the spatial separation of Aurora B from substrates is not sufficient to control if a kinetochore will or will not localise MPS1. Interestingly, they also suggest that centromeric enrichment of Aurora B is not required for normal levels of MPS1 kinetochore localisation.

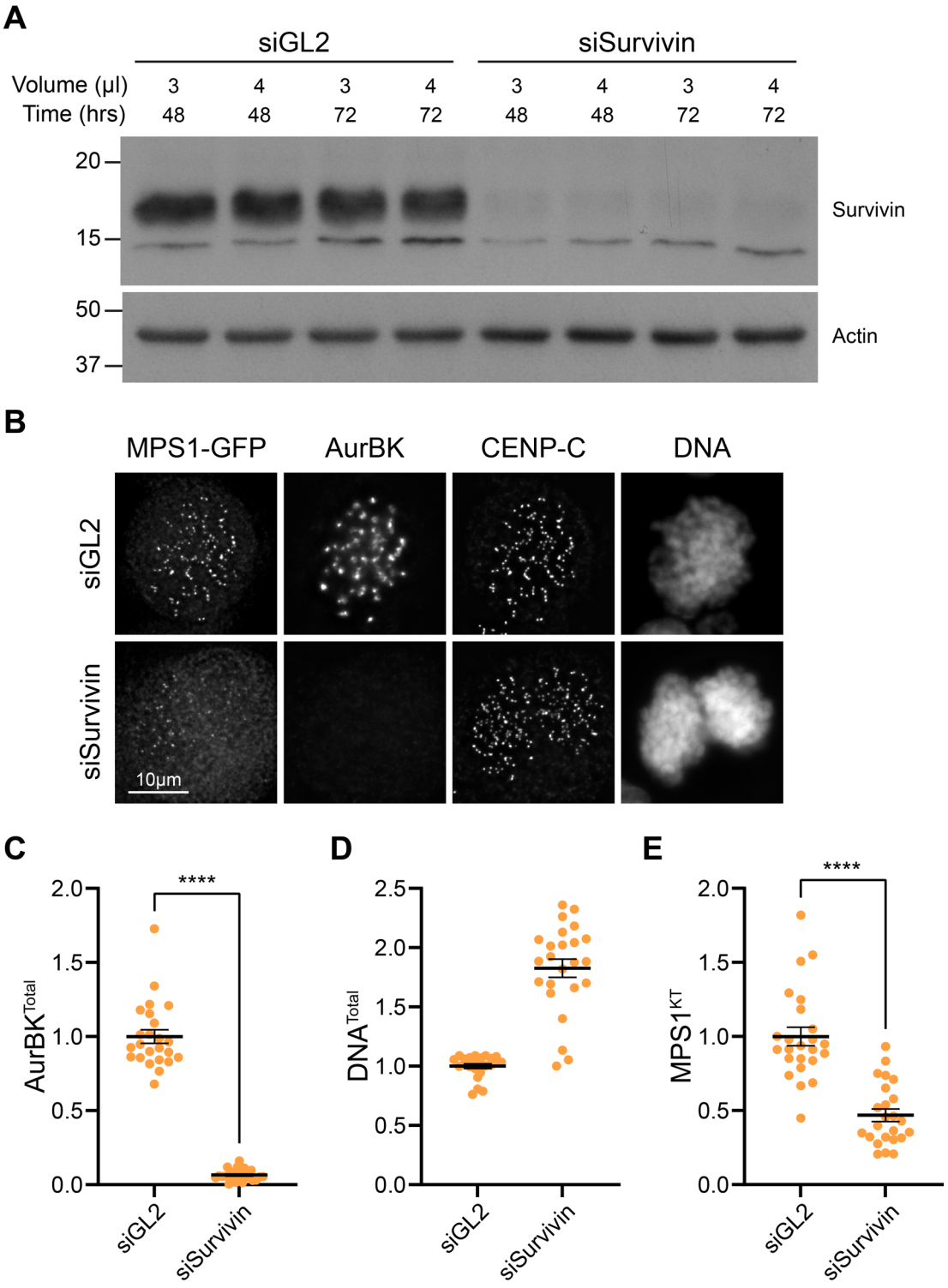

Figure 21 – **Mitotic chromatin-localisation of Aurora B is required for robust MPS1 recruitment to unattached kinetochores**

A) Western blot of HeLa cells treated with the indicated amount of siGL2 or siSurvivin for the indicated times. Membranes were probed for Survivin or Actin.

B) HeLa cells expressing endogenously tagged MPS1-GFP were treated with siGl2 or siSurvivin and arrested with nocodazole (2 h, 0.6 µM) and MG132 (30 min, 20 µM). Cells were fixed and stained for Aurora B, CENP-C and DNA.

C) Quantification of the total Aurora B signal on chromatin from cells in (B). Each dot represents one cell, data pooled from 3 biological repeats. Bars show mean± S.E.M.
D) Quantification of the total DNA signal from cells in (B). Each dot represents one cell, data pooled from 3 biological repeats. Bars show mean± S.E.M.
E) Quantification of the mean amount of MPS1 kinetochore localisation of cells in (B). Each dot represents one cell, data pooled from 3 biological repeats. Bars show mean± S.E.M.

The assays so far have addressed the importance of centromeric Aurora B enrichment for MPS1 recruitment at kinetochores which are already signalling. It is possible that the transition between signalling and non-signalling states exhibits hysteresis – requiring different thresholds of Aurora B activity depending on the direction of the transition. To investigate if centromeric enrichment of Aurora B is required for the rapid initiation of checkpoint signalling, a checkpoint-reactivation assay was used [117] (Figure 22A). Here, cells are treated with MG132 to arrest mitosis at metaphase. Following inhibitor treatment, a high dose of nocodazole is added to cells to ablate microtubule attachments. The ability of these kinetochores, which are transitioning from an attached to unattached state, to recruit MPS1 is then observed. Without any inhibition, MPS1 was robustly localised to kinetochores following nocodazole treatment (Figure 22B, C). Addition of Aurora B inhibitor prior to addition of nocodazole resulted in nearly undetectable levels of MPS1, as expected (Figure 22B, C). Inhibition of Haspin resulted in an intermediate level of MPS1 recruitment, suggesting that centromeric enrichment of Aurora B supports rapid and/or robust MPS1 recruitment at the initiation of checkpoint signalling. It would be interesting to observe the kinetics of MPS1 recruitment in this assay to see if there is a lag in recruitment and/or differences in the level of MPS1 recruited following nocodazole addition.

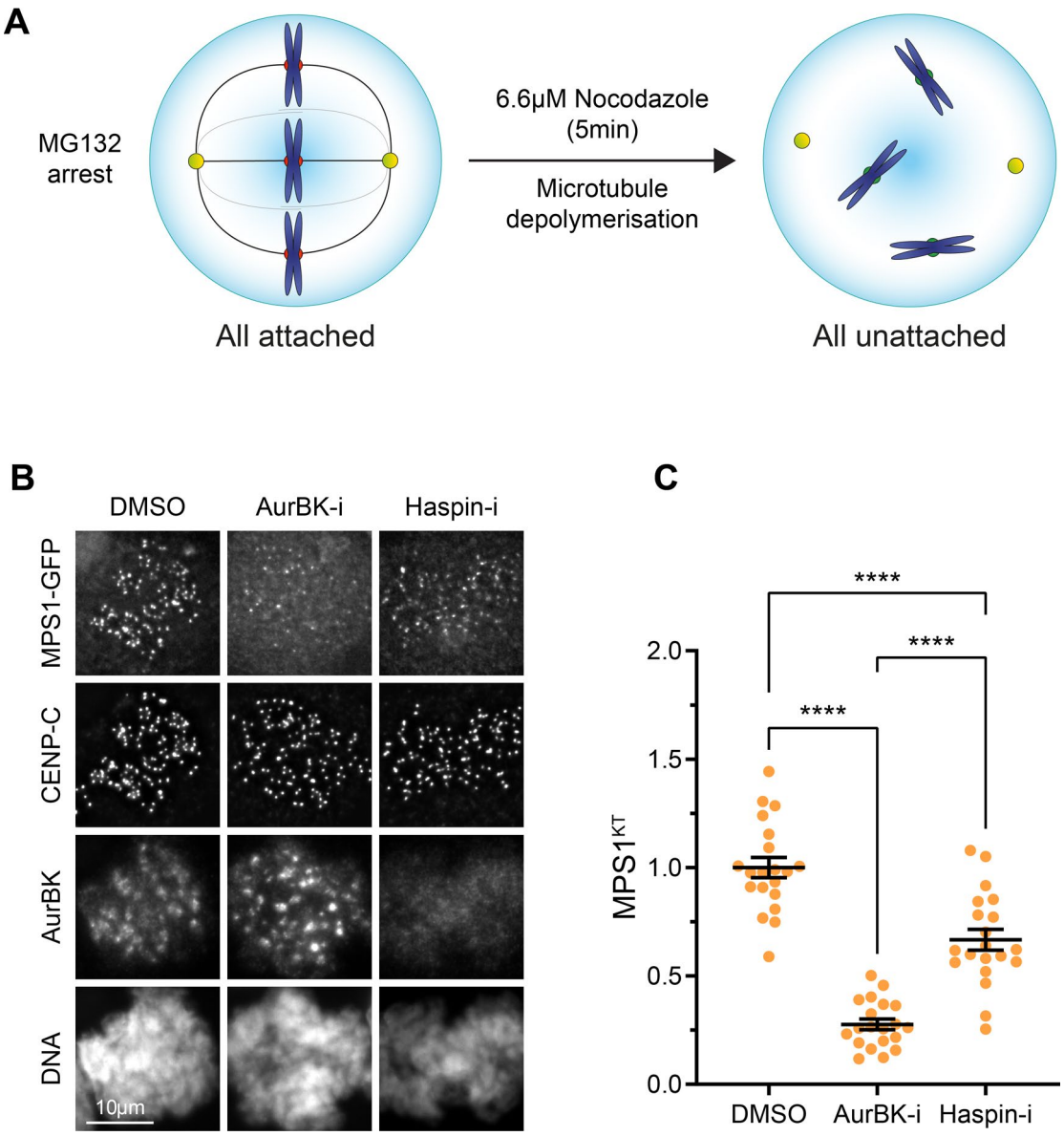

Figure 22 – **Centromeric enrichment of Aurora B is required for robust MPS1 localisation during the initiation of checkpoint signalling**

A) Schematic of experiment. Cells are arrested with attached kinetochores using MG132, and then treated with a high dose of nocodazole to rapidly generate unattached kinetochores.
B) HeLa cells with endogenously tagged MPS1-GFP were arrested with MG132 (90 min, 20 μM), treated with DMSO, AurBK-i (ZM447439, 10 min, 10 μM), or Haspin-i (5-iodotubercidin, 10 min, 10 μM), and subsequently treated with nocodazole (6.6 mM, 5 min). Cells were fixed and immuno-stained for and CENP-C.
C) Quantification of the mean amount of MPS1 kinetochore localisation of cells in (B). Each dot represents one cell, data pooled from 3 biological repeats. Bars show mean± S.E.M.

The previous observations raise the interesting possibility that different thresholds of Aurora B activity might be required for MPS1 localisation and destabilisation of kinetochore-microtubule attachments to occur. That is to say that lower levels of Aurora B activity seem to support localisation but alter the steady-state level of attachments in a monopolar spindle (Figure 18). If this is true, then increasing concentrations of Aurora B inhibitor should produce increases in kinetochore-microtubule attachments, and decreases in MPS1 localisation, at different thresholds. To this end, a titration of Aurora B inhibitor ZM447439 was performed on HeLa cells expressing endogenously tagged MPS1-GFP (Figure 23). As a readout for MPS1 localisation, cells were arrested in nocodazole and MG132 prior to inhibition to ensure microtubule attachment was not a confounding variable (Figure 23A). Cells treated in this manner were also stained for H3pS10 – a canonical Aurora B substrate, as independent confirmation of Aurora B inhibition. To assess the level of stable end-on attachments, cells were arrested in STLC and MG132 prior to Aurora kinase inhibition and stained for Astrin to allow the percentage of Astrin-positive kinetochores to be quantified (Figure 23B). As anticipated, increasing concentrations of ZM lead to the disappearance of H3pS10 signal (Figure 23A, C) with an IC_{50} of ~2uM (Figure 23C). MPS1 levels also decreased as ZM concentration increased (Figure 23A, B, C) with an IC_{50} of ~3uM (Figure 23C). Interestingly, increases in the number of kinetochore-microtubule attachments were apparent from a very low level of Aurora B inhibition, with an IC_{50} of ~0.6uM (Figure 23B, C). These data support the idea that different thresholds of Aurora B activity may be required for error correction and MPS1 localisation. However, it should be noted that ZM447439 will also inhibit Aurora A at higher concentrations. This may in turn influence kinetochore-microtubule attachments as Aurora A has important roles in

regulating spindle size [267]. Therefore, this line of inquiry warrants further investigation with more specific Aurora B inhibitors before drawing firm conclusions.

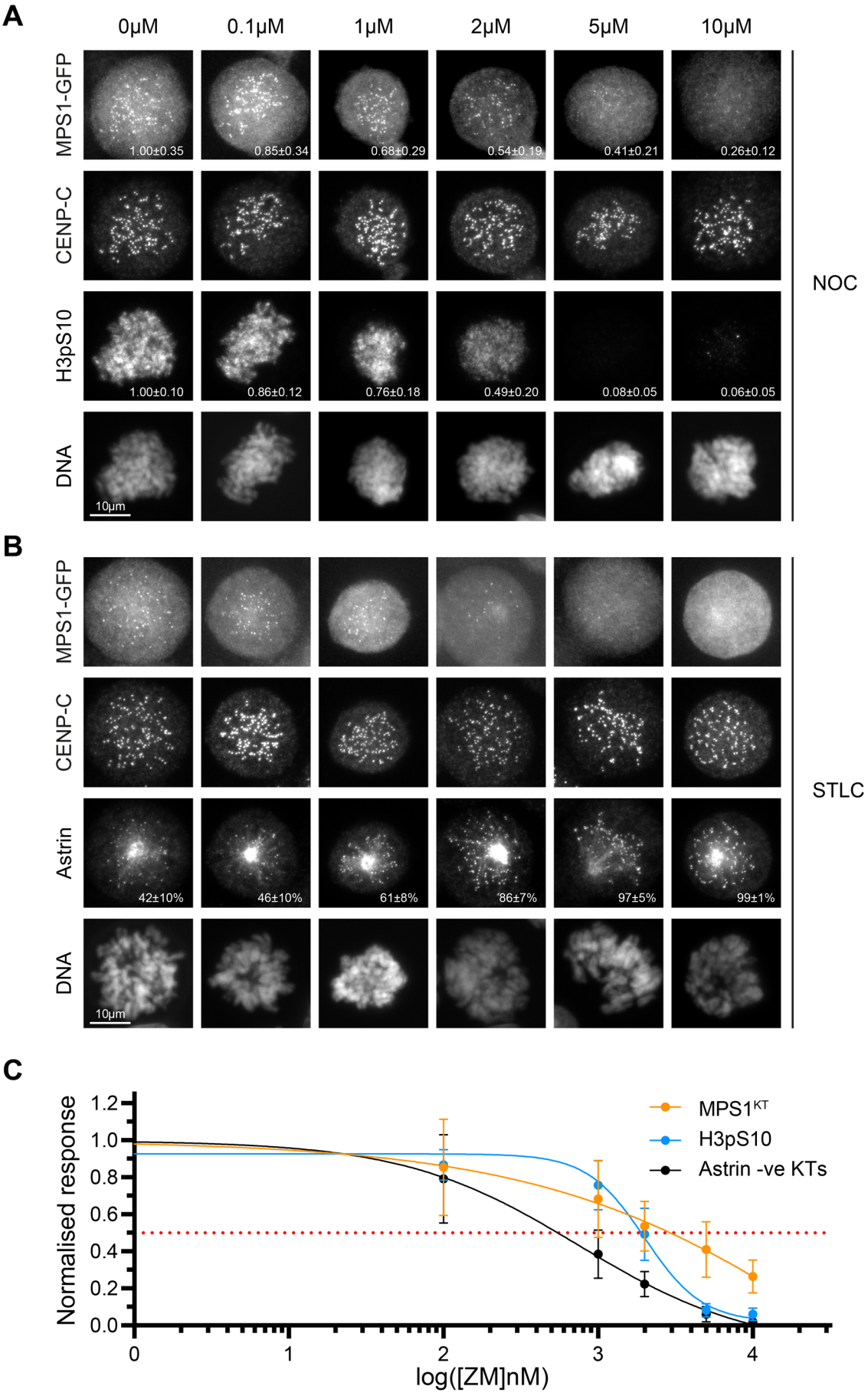
A
0μM
0.1μM
1μM
2μM
5μM
10μM
MPS1-GFP
1.00±0.35
0.85±0.34
0.68±0.29
0.54±0.19
0.41±0.21
0.26±0.12
CENP-C
H3pS10
1.00±0.10
0.86±0.12
0.76±0.18
0.49±0.20
0.08±0.05
0.06±0.05
DNA
10μm
NOC
B
MPS1-GFP
CENP-C
Astrin
42±10%
46±10%
61±8%
86±7%
97±5%
99±1%
DNA
10μm
STLC
C
Normalised response
1.2
1.0
0.8
0.6
0.4
0.2
0.0
0
1
2
3
4
log([ZM]nM)
MPS1KT
H3pS10
Astrin -ve KTs

Figure 23 – **The steady-state level of end-on attachments is more sensitive to Aurora B inhibition than MPS1 localisation is**

A) HeLa cells expressing endogenously tagged MPS1-GFP were arrested with nocodazole (2 h, 0.6 μM) and MG132 (30 min, 20 μM). Cells were treated with the indicated concentration of ZM447439 for 15 min prior to fixation and staining for H3pS10, CENP-C and DNA. Them mean±S.D. of $MPS1^{KT}$ or total H3pS10 signal per condition is shown within the relevant image.
B) HeLa cells expressing endogenously tagged MPS1-GFP were arrested with STLC (2 h, 10 μM) and MG132 (30 min, 20 μM). Cells were treated with the indicated concentration of ZM447439 for 15 min prior to fixation and staining for Astrin, CENP-C and DNA. The mean±S.D. percentage of kinetochores with Astrin staining is shown within the relevant image.
C) Dose-response curves from (A) and (B).

The basis by which microtubule attachment causes MPS1 to stop localising to kinetochores remains unclear. The data thus far suggest that a simple reduction in the local levels of Aurora B, as might be expected by a conformational change of the kinetochore upon microtubule binding, is insufficient to stop MPS1 recruitment. Additional changes based around a conformational change of the kinetochore, such as regulation of substrate availability, or changes in PP2A-B56 activity, could also participate in the loss of MPS1. What is different between those rarely observable end-on attached kinetochores which recruit MPS1 and those which don't may be insightful (Figure 2). To investigate if end-on attached kinetochores with MPS1 display conformational differences from those which do not recruit MPS1, the average distance between CENP-C and the N-terminal CH domain of HEC1 was measured at individual kinetochores. This technique has been used to show that microtubule binding alone is sufficient to induce conformational changes in HEC1 [192] (Figure 24A).

These distances (sub-100nm) are well below the diffraction limit of light microscopy. Thus, the technique relies on labelling 2 kinetochore proteins with different fluorophores and finding the centroids of the resulting diffraction-limited foci. These centroids can be determined with nm-scale precision, and thus used to determine the average distance between the 2 populations of proteins at single kinetochores. Chromatic aberrations heavily impact the precision of this technique, and the data presented here was corrected for chromatic aberrations using the software Chromagnon [269,270]. Here, samples with the same target labelled in two different channels are used to calculate differences in translation, rotation, and magnification between the two channels. The resultant transform can then be applied to raw images to counteract the relative positional error between channels caused by

chromatic aberrations. Furthermore, kinetochores which had a larger than 50nm displacement in the z-axis were discarded from analysis, due to the increased error introduced by the poor spatial resolution inherent to this axis.

To test the technique, HeLa cells expressing endogenously tagged MPS1-GFP were arrested with nocodazole (unattached kinetochores, no tension), MG132 (attached, tensioned kinetochores), and STLC (mix of attachment statuses, no tension). Cells were stained with a polyclonal CENP-C antibody, and a monoclonal antibody against the N-terminal CH domain of HEC1. A subset of coverslips were stained for HEC1 with secondary antibodies in both the red and far-red to correct for chromatic aberration. After correction, the mean distance between HEC1 and HEC1 in control cells was 29.6nm (Figure 24B). The expected value for this measurement is 0nm, and thus 29.6nm represents the noise floor of this technique. In the absence of microtubule attachment (a nocodazole arrest), the mean distance between CENP-C and HEC1 was 44.8nm (Figure 24B). At attached, tensioned kinetochores this distance was increased to 72.6nm (Figure 24B). This change of 27.8nm is very close to the 25.3nm change observed by a recent study using a state-of-the-art iteration of this technique [192]. In STLC, due to the mix of attachment states, one would expect to see a bimodal distribution of unattached (44.8nm) and attached (72.6nm) populations. Unfortunately, this was not the case, likely due to the high variance of the measurements. Rather the measurements from STLC-arrested cells were normally distributed, with a mean distance of 51.9nm (Figure 24B). Thus, trying to confidently assign the distance between CENP-C and HEC1 at the rare end-on attached MPS1-positive kinetochores is not feasible. The use of ultrastructure expansion microscopy [271] to physically enlarge kinetochores did not solve this

issue (data not shown). Consequently, this line of inquiry was deemed not worth pursuing.

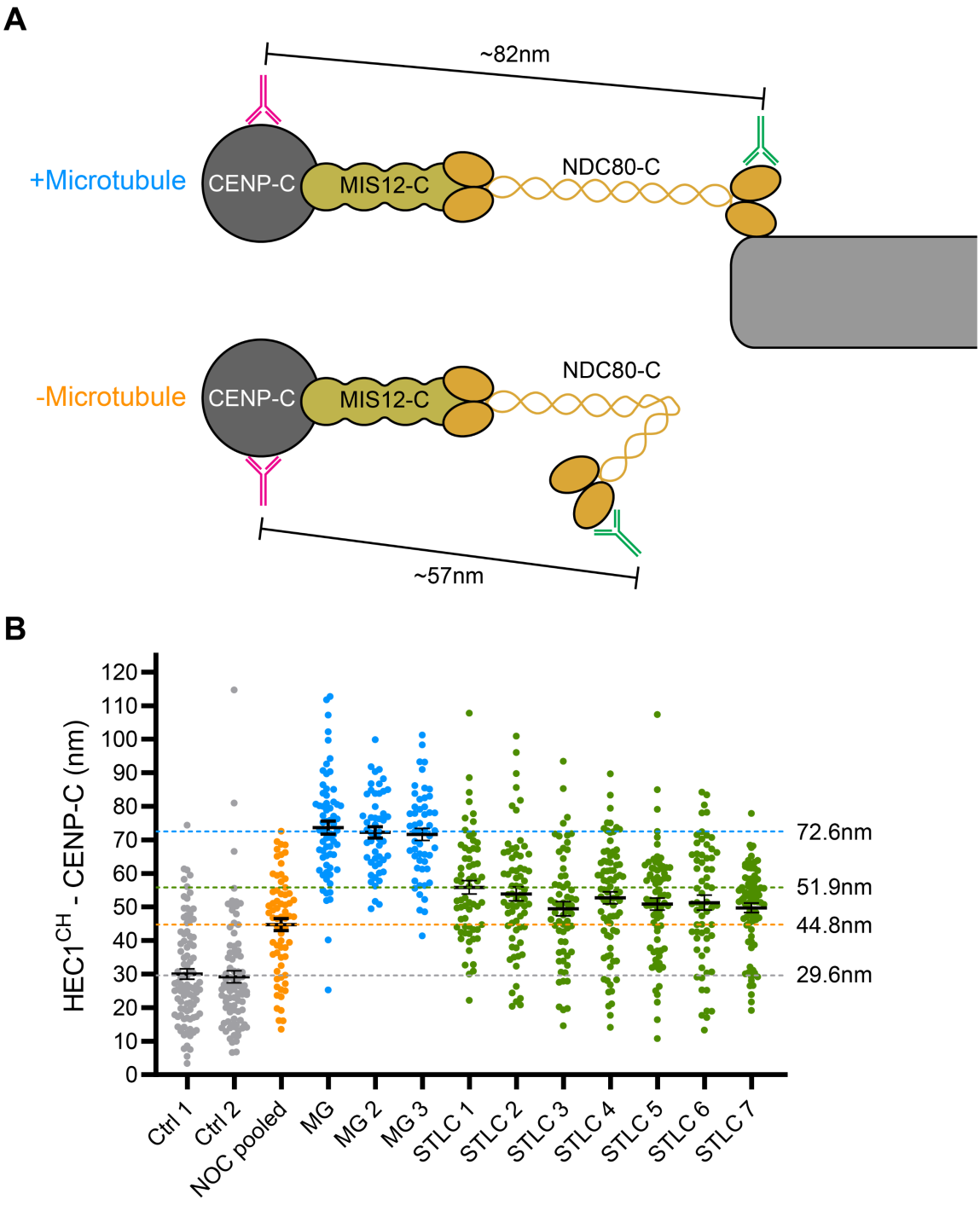

Figure 24 – **Intrakinetochore distance measurements**

A) Schematic showing conformational changes in HEC1 upon microtubule binding and the associated distances reported by [192].
B) Plot of distance measurements across conditions and cells. Each dot represents one kinetochore. Data from nocodazole arrested cells are pooled due to low n numbers of kinetochores aligned along the lateral plane in this condition. Bars show error ± S.E.M.

Results 2 - Revisiting the molecular mechanism of how MPS1 binds kinetochores

The relative binding contributions of the NTE and MR are activity dependent

Understanding the molecular detail of how MPS1 binds to kinetochores is necessary for understanding how MPS1 kinetochore-binding is regulated. Two separate molecular interactions have been implicated in how MPS1 binds to the kinetochore. The first interaction is between the NTE and HEC1, and the second interaction is between the MR and NUF2 [134,164,168]. As HEC1 and NUF2 are obligate binding partners, and the NTE and MR are distinct domains, it is theoretically possible for both interactions to occur simultaneously. *In vivo* the interaction between the NTE and HEC1 is thought to be the most important [131,134]. Indeed, the deletion of the entire MR has been reported to have no effect on MPS1 localisation [134]. The seeming lack of requirement for the MR is puzzling, given that phosphorylation of S281 in the MR by CDK1-Cyclin B is a pre-requisite for MPS1 localisation [117]. There are two solutions to this apparent contradiction. One is that the MR inhibits MPS1 localisation unless it is phosphorylated – thus deletion of the MR or phospho-mimetic mutation of S281 would support MPS1 localisation. The other solution is that there are different requirements for the MR depending on the activity status of MPS1. This is because experiments whereby the MR was deleted were done in the presence of MPS1 inhibitor reversine, whereas experiments with S281A mutants were done without MPS1 inhibition. Therefore, it would be insightful to directly compare MPS1 constructs lacking the MR ($MPS1^{\Delta MR}$), NTE ($MPS1^{\Delta 60}$), or with

S281A mutations (MPS1^{S281A}, MPS1^{S281D}), in the presence or absence of MPS1 inhibitor (Figure 25A).

As in previous experiments, an RNAi rescue assay was performed to replace endogenous MPS1 with these various GFP-MPS1 transgenes. As expected, endogenous MPS1 could be successfully replaced with the GFP-MPS1 transgenes (Figure 25B). Additionally, two clones of each mutant were tested for induction and subsequently used in future experiments (Figure 25C). The efficacy of MPS1 depletion was assessed by treating cells with siControl or siMPS1. Cells were arrested with nocodazole and MG132, fixed, and stained for BUBR1 (Figure 25D). Depletion of MPS1 was very effective – evidenced by the large reduction in BUBR1 kinetochore localisation to ~25% in almost all cells (Figure 25D, E).

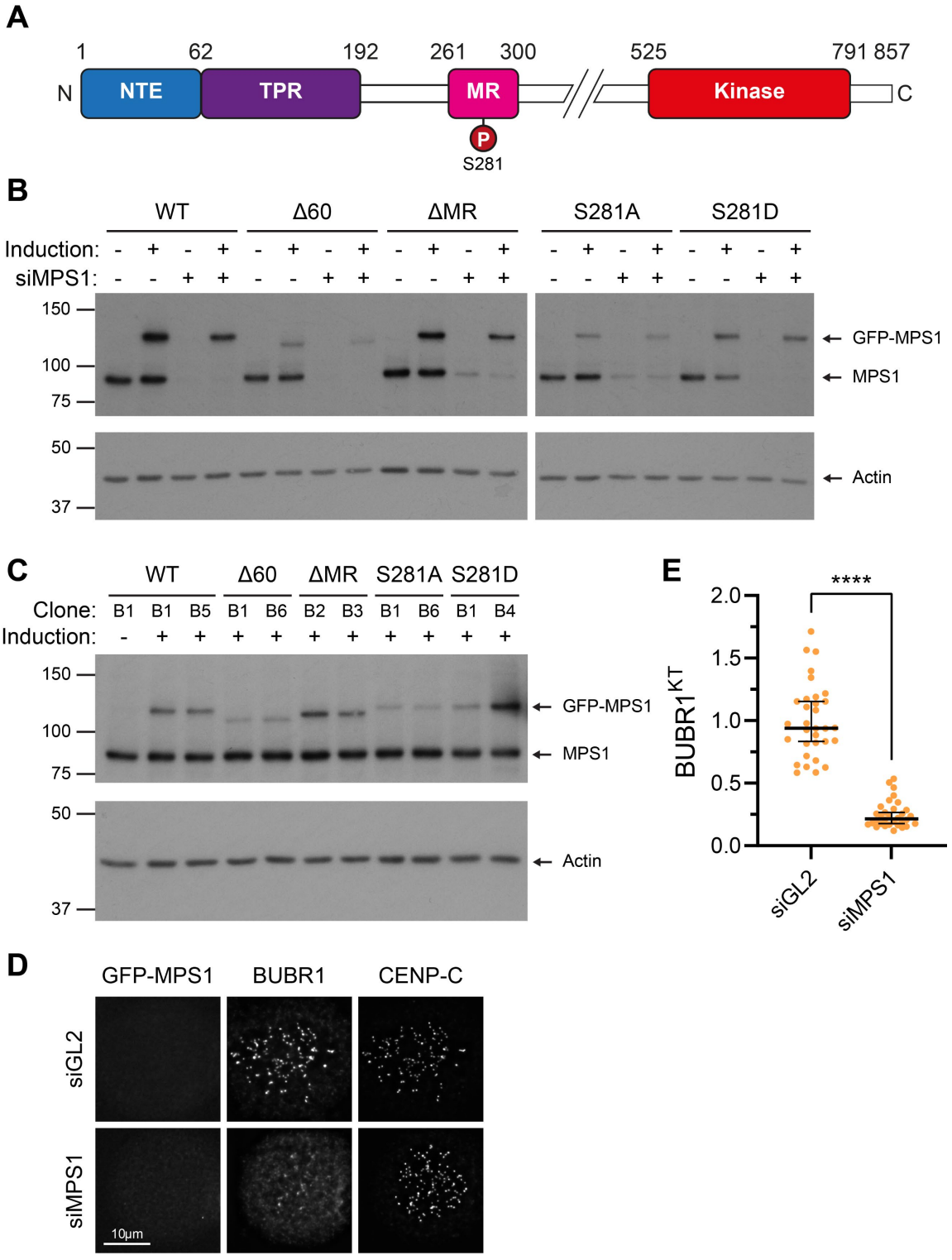

Figure 25 – **Generation of MPS1 deletion and S281A phospho-mutant Flp-In cells**

A) Schematic showing the main domains of MPS1 and location of S281. Domain boundaries are indicated by amino acid number.

B) Anti-MPS1 Western blot of HeLa Flp-In TREx cells treated with siMPS1 or siControl and ± doxycycline (2 μM) to induce GFP-MPS1 transgene expression for 48 hours. Actin is used as a loading control.

C) Anti-MPS1 Western blot of HeLa Flp-In TREx cells treated with ± doxycycline (2 μM) to induce GFP-MPS1 transgene expression for 48 hours. Actin is used as a loading control.

D) HeLa Flp-In TREx cells were treated with siMPS1 or siControl for 48 hours. Cells were arrested with nocodazole (2 h, 0.6 μM) and MG132 (30 min, 20 μM), fixed, and stained for BUBR1 and CENP-C
E) Quantification of the mean amount of BUBR1 kinetochore localisation of cells in (D). Each dot represents one cell, data pooled from 3 biological repeats. Bars show mean± S.E.M.

The localisation of these mutants with and without MPS1 inhibitor to unattached kinetochores was examined by IF. Cells were arrested in mitosis in the absence of microtubules by treatment with nocodazole and MG132, and treated with or without MPS1 inhibitor prior to fixation (Figure 26). Cells were fixed and stained for the kinetochore protein CENP-C, and checkpoint protein BUBR1 to assess any potential downstream consequences of changes in MPS1 localisation (Figure 26A). For ease of comparison, the levels of kinetochore-localised MPS1 with and without MPS1 inhibitor are presented separately (Figure 26B, C) and together (Figure 26D).

Without MPS1 inhibitor, $MPS1^{WT}$ localised to kinetochores as expected (Figure 26A, B, D). Surprisingly, deletion of the NTE did not change the level of MPS1 localisation (Figure 26A, B, D). This result was unexpected given that the NTE has been reported to be necessary for MPS1 kinetochore-localisation [90,131,134,147] (albeit in truncated forms of MPS1 or under conditions of MPS1 inhibition). Conversely, deletion of the MR, or S281A mutation, showed a significant decrease in MPS1 levels (Figure 26A, B, D), as has previously been reported for $MPS1^{S281A}$[117]. There was no significant difference between $MPS1^{S281D}$ and $MPS1^{WT}$, as previously reported [117] (Figure 26A, B, D). All constructs were able to recruit BUBR1 to the same level (Figure 26A, E), suggesting that these changes in MPS1 localisation are not severe enough to prevent phosphorylation of MELT motifs. A construct lacking the entire kinetochore-binding domain (amino acids 1-305) would have been useful as a negative control for MPS1 kinetochore-localisation.

To investigate if the localisation pattern of the mutants was different in conditions of MPS1 inactivity, cells were treated with MPS1 inhibitor. Upon MPS1 inhibition, BUBR1 localisation was significantly reduced in all mutants, showing that MPS1 had been efficiently inhibited (Figure 26A, E). $MPS1^{WT}$ localised 2x as strongly with inhibitor, as expected (Figure 26A, C, D). $MPS1^{\Delta 60}$ localised more weakly under these conditions (Figure 26A, C, D). This observation is consistent with the idea that activity-dependent changes in MPS1 localisation are mediated through auto-phosphorylation of the NTE. Strikingly, both $MPS1^{\Delta MR}$ and $MPS1^{S281A}$ localised strongly upon addition of MPS1 inhibitor, despite extremely weak localisation in the absence of MPS1 inhibitor (Figure 26A-D). This localisation was not as strong as inhibited $MPS1^{WT}$, although this was only significantly different for $MPS1^{S281A}$. Inhibited $MPS1^{S281D}$ localised to the same extent as inhibited $MPS1^{WT}$ (Figure 26A, C, D).

These data show that seemingly conflicting data on the requirement for S281 phosphorylation, and the dispensability of the MR, and are reconcilable through the conditions under which the experiments were performed – namely with or without MPS1 inhibition. In unperturbed conditions (no MPS1 inhibitor), the presence and phosphorylation of the MR contribute greatly to MPS1 localisation, whereas the NTE appears dispensable. Alone, these observations would implicate the MR as the main kinetochore-binding domain. However, the addition of MPS1 inhibitor shows the MR to be dispensable for kinetochore localisation, whereas the NTE appears to be the main kinetochore-binding domain. This difference in the contribution of the NTE and MR is potentially explainable by the status of NTE phosphorylation. Under non-inhibited conditions, MR-binding seems to predominate, perhaps as the NTE exhibits a level of phosphorylation which decreases its affinity for the kinetochore

(Figure 5). Conversely, in conditions of MPS1 inhibition the dephosphorylated NTE may bind the kinetochore more strongly, to the extent that contributions from the MR are no longer needed.

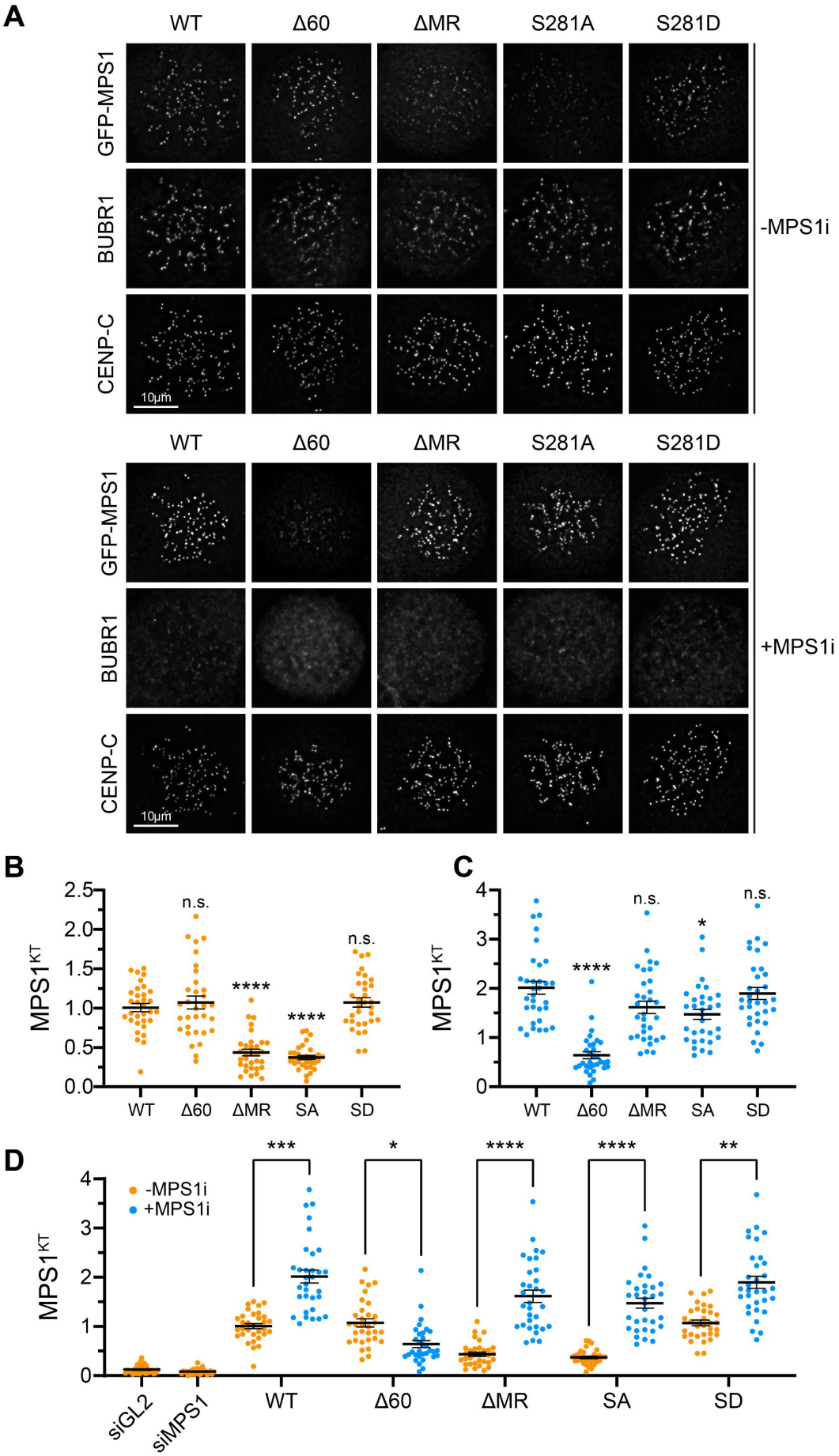
A
WT
Δ60
ΔMR
S281A
S281D
GFP-MPS1
BUBR1
CENP-C
10μm
-MPS1i
+MPS1i
B
C
MPS1KT
n.s.
****
*
WT
Δ60
ΔMR
SA
SD
D
-MPS1i
+MPS1i
***
**
siGL2
siMPS1

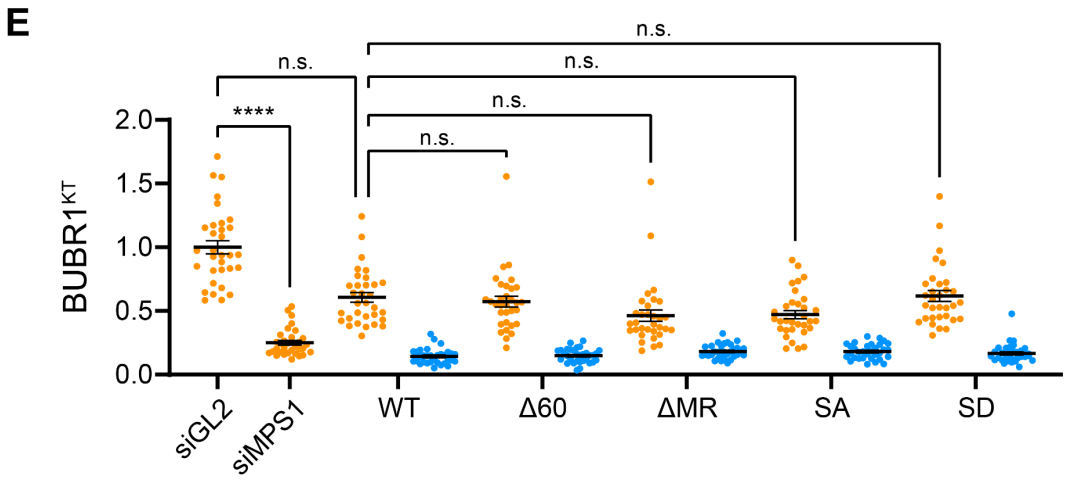

Figure 26 – **Kinetochore-binding domain contributions to MPS1 localisation are activity-dependent**

A) HeLa Flp-In TREx cells depleted of endogenous MPS1 and expressing GFP-MPS1 transgenes were arrested with nocodazole (2 h, 0.6 μM) and MG132 (30 min, 20 μM) and treated with (bottom) or without (top) MPS1i (AZ3146, 10 min, 2 μM). Cells were fixed and immuno-stained for CENP-C and BUBR1.

B) Quantification of the mean amount of MPS1 kinetochore localisation of cells in (A) treated without MPS1 inhibitor. Each dot represents one cell, data pooled from 3 biological repeats. Bars show mean± S.E.M.

C) Quantification of the mean amount of MPS1 kinetochore localisation of cells in (A) treated with MPS1 inhibitor. Each dot represents one cell, data pooled from 3 biological repeats. Bars show mean± S.E.M.

D) Quantification of the mean amount of MPS1 kinetochore localisation of cells in (A). Each dot represents one cell, data pooled from 3 biological repeats. Bars show mean± S.E.M.

E) Quantification of the mean amount of BUBR1 kinetochore localisation of cells in (B). Each dot represents one cell, data pooled from 3 biological repeats. Bars show mean± S.E.M.

Investigating binding between MPS1 and the NDC80-C in vitro

To further investigate the contributions of the various domains and their phosphorylation status, *in vitro* binding assays between MPS1 and the NDC80 complex would be insightful. Other studies have used purified HEC1 or NUF2, or truncated NDC80-C constructs. The two most widely used truncated NDC80-C constructs are “bonsai” and “broccoli”. Bonsai comprises fusions of HEC1-SPC25, and NUF2-SPC24, such that their globular domains are linked by truncated coiled-coil domains [57] (Figure 27A). Broccoli contains HEC1 and NUF2, with their C-terminal coiled-coiled region slightly truncated [272] (Figure 28A). $NDC80^{Bonsai}$ was successfully purified to a high level of purity from E. coli (Figure 27). Size exclusion chromatography revealed that the two peptides formed a soluble complex as expected (Figure 27B, C).

$NDC80^{Broccoli}$ was purified in a similar manner, although suffered a major contaminant at ~70kDa – most likely HSP70 (Figure 28). Moving forward, it was decided that the pure, soluble $NDC80^{Bonsai}$ would be preferable to use in binding assays.

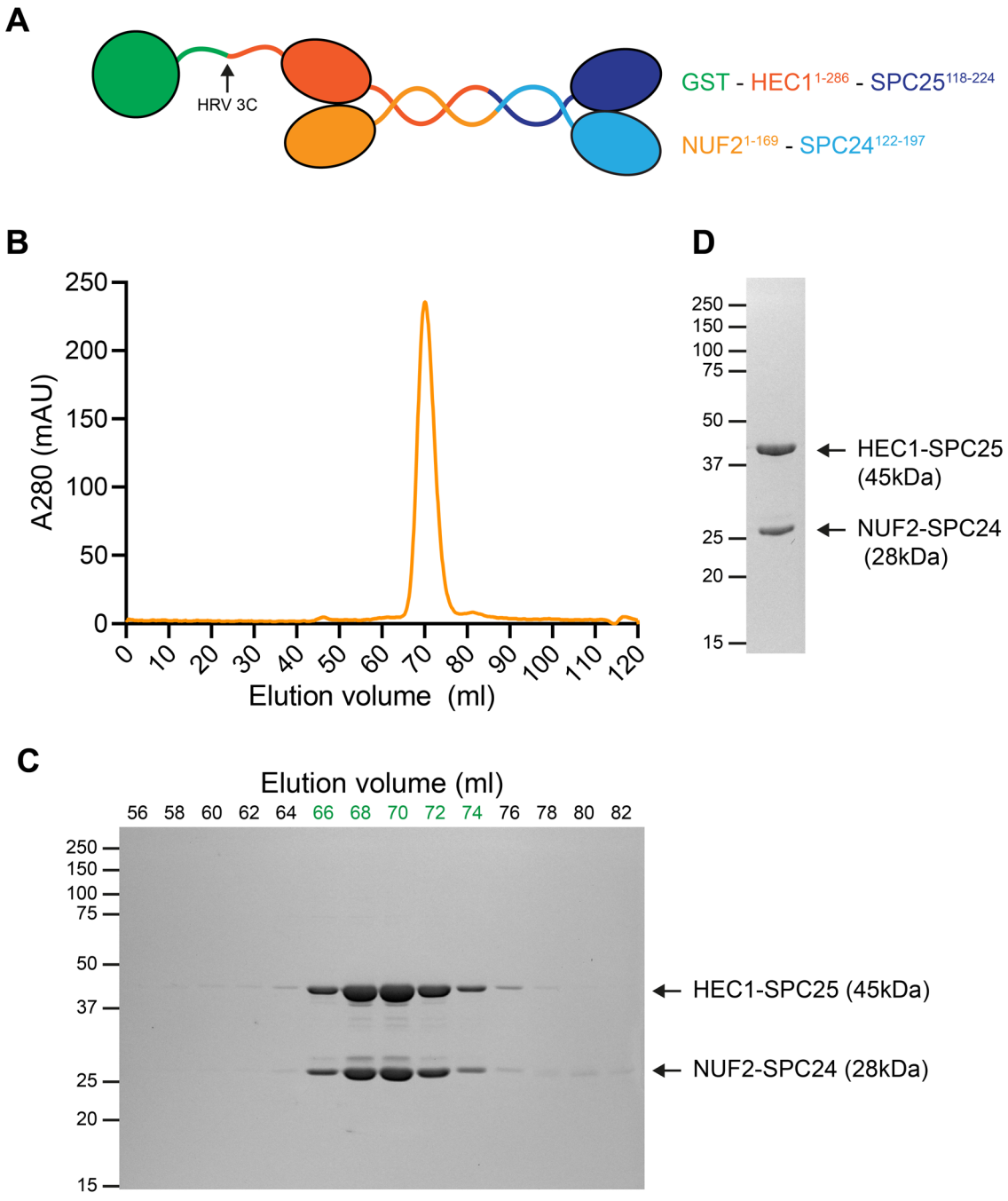

Figure 27 – **Purification of NDC80-C^{Bonsai}**

A) Schematic of the GST-NDC80-C^{Bonsai} construct.
B) Chromatogram of affinity-purified NDC80-C^{Bonsai}. GST-NDC80-C^{Bonsai} was affinity purified from *E. coli* on glutathione-sepharose, eluted by on-bead cleavage with Prescission protease, and subject to size exclusion chromatography on a HiLoad Superdex 16/600 G75 column.
C) Coomassie gel of fractions collected at the indicated elution volume from (B). Fractions indicated in green were pooled and concentrated.
D) Coomassie gel of 2 µg of SEC purified NDC80-C^{Bonsai} from (C).

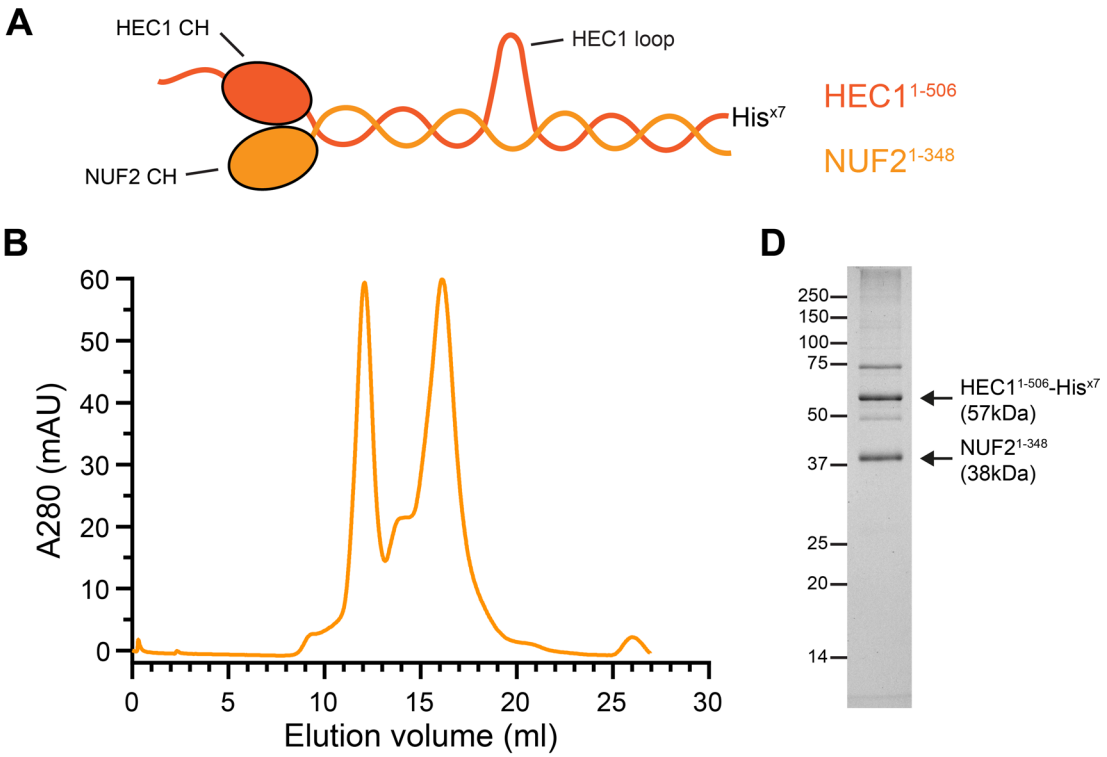
A
HEC1 CH
HEC1 loop
NUF2 CH
His^x7
HEC1^1-506
NUF2^1-348
B
A280 (mAU)
Elution volume (ml)
D
HEC1^1-506-His^x7
(57kDa)
NUF2^1-348
(38kDa)
C
Elution volume (ml)
Fraction: C5 C6 C7 C8 C9 C10 C11 C12 D1 D2 D3 D4 D5 D6
HEC1^1-506-His^x7
(57kDa)
NUF2^1-348
(38kDa)
Elution volume (ml)
D7 D8 D9 D10 D11 D12 E1 E2 E3 E4 E5 E6 E7 E8

Figure 28 – **Purification of NDC80-C^{Broccoli}**

A) Schematic of the NDC80-C^{Broccoli} construct.
B) Chromatogram of affinity-purified NDC80-C^{Broccolii}. NDC80-C^{Broccoli} was affinity purified from *E. coli* on Ni-NTA agarose, eluted with imidazole, dialysed overnight, and subject to size exclusion chromatography on Superdex 200 10/300 column.
C) Coomassie gel of fractions collected at the indicated elution volume from (B). Fractions indicated in green were pooled and concentrated.
D) Coomassie gel of 2 µg of SEC purified NDC80-C^{Broccoli} from (C).

The *in* vivo assays presented so far show that auto-phosphorylation of the NTE alter the level to which MPS1 localises to unattached kinetochores (Figure 5). Similarly, differences in localisation strength were observed for MPS1^{S281A} and constructs lacking the NTE or MR (Figure 26). It would therefore be expected that such constructs would have different binding strengths for HEC1 and/or NUF2. To investigate the ability of MPS1 constructs to bind NDC80-C, a pulldown assay between immunoprecipitated GFP-MPS1 constructs and purified NDC80^{Bonsai} was performed, like other studies [134,165]. GFP-MPS1 constructs, or GFP alone, was immunoprecipitated on Protein G Dynabeads as previous (Figure 10). Following blocking or no blocking with BSA, beads coated in the GFP species were incubated with NDC80^{Bonsai} at a 10:1 molar ratio, before gentle washing and analysis by SDS-PAGE. From the input lanes, the various GFP constructs were immunoprecipitated with roughly equal efficiency (Figure 29A, Inputs). Unfortunately, in all cases, including the negative control, NDC80^{Bonsai} (indicated by bands for HEC1-SPC24 and NUF2-SPC25) bound strongly to the beads (Figure 29A, IP lanes). These results indicate that the beads are likely too sticky for this assay, and an alternative approach should be used. Other studies have used NDC80-C^{Bonai} as bait in such assays with more success [165].

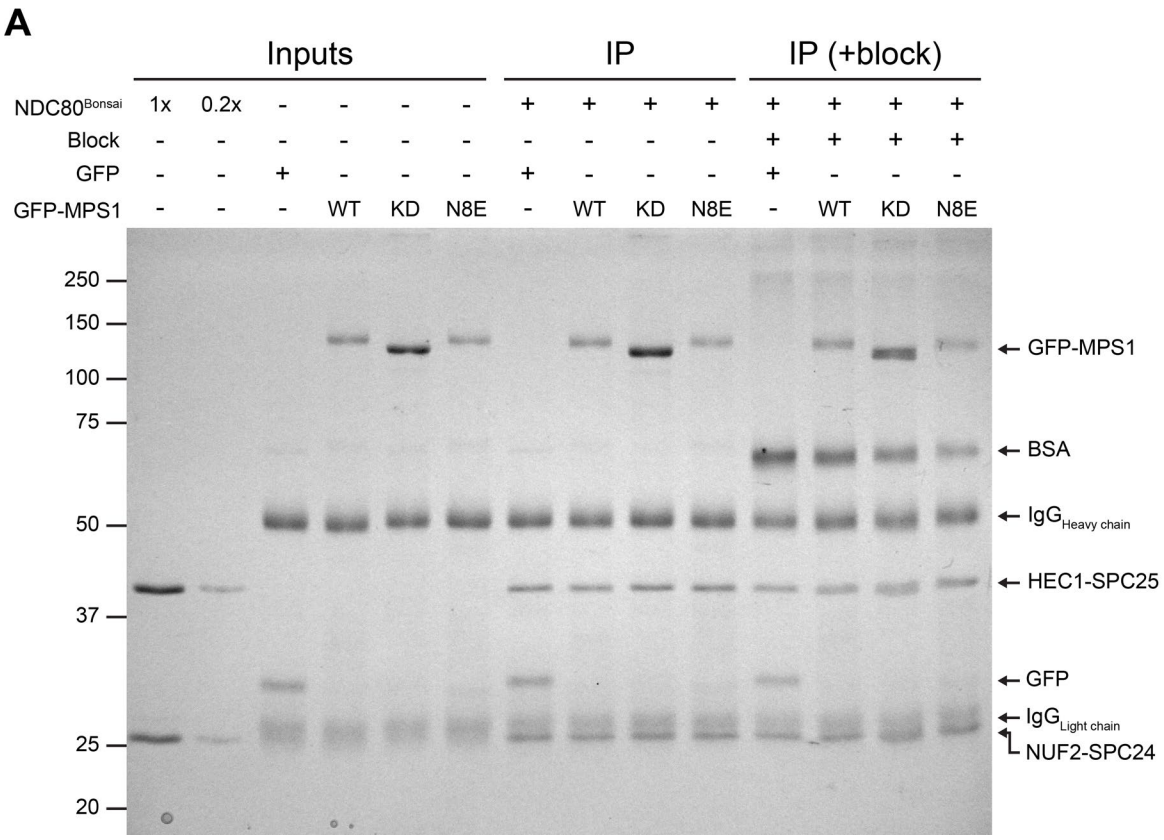

Figure 29 – **Attempt at co-immunoprecipitation assay using purified GFP-MPS1 and NDC80-C^{Bonsai}**

A) Protein G Dynabeads were used to immunoprecipitate the indicated GFP construct from mitotic HEK293T cells as in Figure 9. Beads coated in GFP/GFP-MPS1 were incubated at a 10:1 molar ratio with purified NDC80-C^{Bonsai} for 2 hours at 4°C. After washing, beads were boiled in sample buffer, run on and SDS-PAGE gel, and bound proteins were visualised by Coomassie stain. The assay was performed with or without pre-incubation of the GFP-coated beads with BSA as a blocking step.

To generate MPS1 constructs with different, or no, tags for use in binding assays, full-length MPS1 or the kinetochore-binding domains (amino acids 1-305) of MPS1 were purified. $MPS1^{1-305}$ was purified from *E. coli* as a GST-fusion protein to a moderate level of purity (Figure 31). Full-length $MPS1^{WT}$ and $MPS1^{KD}$ was successfully purified from insect cells (Figure 32). SEC-MALS of $MPS1^{WT}$ revealed possible monomeric and dimeric populations of MPS1, consistent with the notion that MPS1 can dimerise [92,132] (Figure 32B, C). The purification of these soluble MPS1 constructs lay the groundwork for future work investigating the binding interactions between MPS1 and NDC80-C.

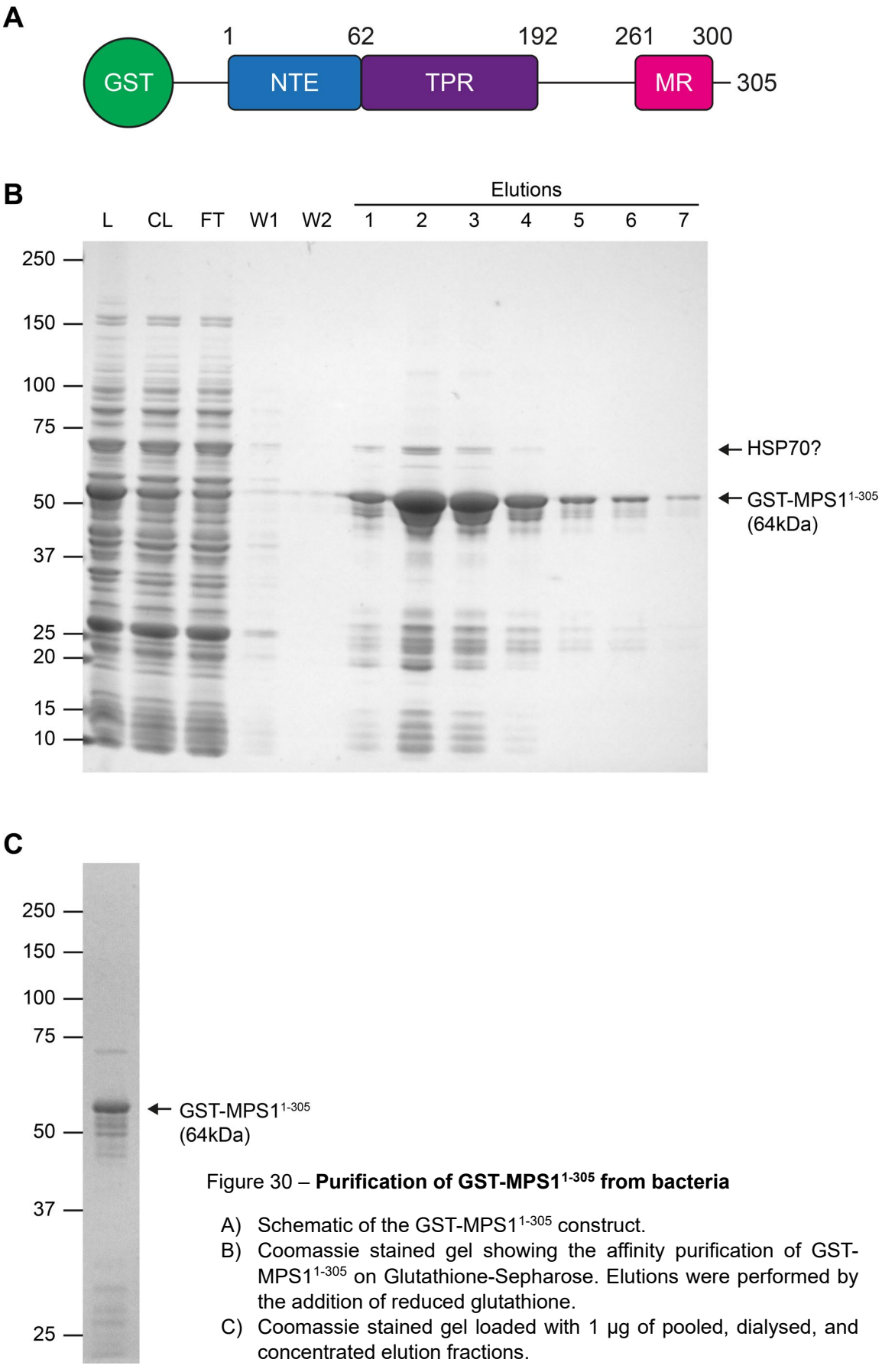

Figure 30 – **Purification of GST-MPS1$^{1-305}$ from bacteria**

A) Schematic of the GST-MPS1$^{1-305}$ construct.
B) Coomassie stained gel showing the affinity purification of GST-MPS1$^{1-305}$ on Glutathione-Sepharose. Elutions were performed by the addition of reduced glutathione.
C) Coomassie stained gel loaded with 1 µg of pooled, dialysed, and concentrated elution fractions.

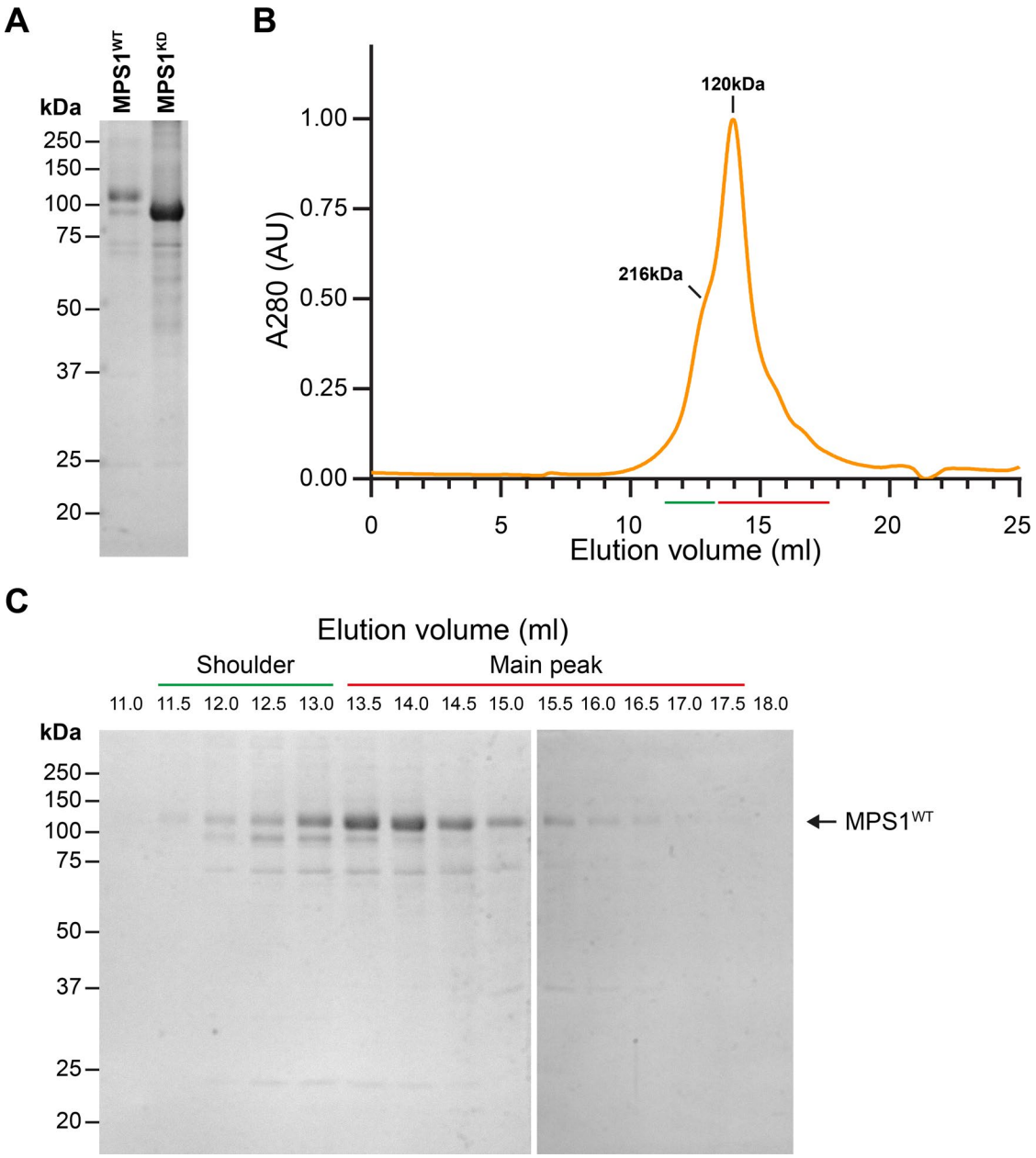

Figure 31 – **Purification of MPS1^{WT} and MPS1^{KD} from insect cells**

A) Coomassie stained gel loaded with MPS1^{WT} and MPS1^{KD} purified from insect cells. Sf9 cells transfected with baculovirus to cause expression of His-MPS1^{WT} or His-MPS1^{KD} were lysed and centrifuged to remove cell debris. His-tagged proteins were purified by affinity chromatography on Ni-NTA agarose. Elutions were performed by addition of imidazole. Elution fractions were pooled and dialysed overnight in the presence of TEV protease to remove the His-tag. Dialysed samples were concentrated and purified further by size exclusion chromatography on a Superose 6 10/300 GL column. Fractions of interest were pooled and concentrated.

B) MPS1^{WT} from (A) was analysed by SEC-MALS on a Superose 6 10/300 GL. The elution profile is plotted, with corresponding molecular weights of eluting species as determined by MALS.

C) Coomassie gel of fractions collected at the indicated elution volume from (B).

Revisiting the role of MPS1 in error correction

MPS1 inhibition does not produce a phenotype which suggests defects in error correction

The role of MPS1 in error correction is not fully clear. The first report of a role for MPS1 in error correction in human cells was that inhibition of MPS1 led to the stabilisation of syntelic attachments [231]. In subsequent studies using monastrol washout assays (Diagram 18), inhibition or depletion of MPS1 has been reported to cause phenotypes more reminiscent of defects in congression than error-correction [93,165] - namely, uncongressed chromosomes without microtubule attachments. Despite this, MPS1 has been shown to have a direct role in error correction when ectopically recruited to attached kinetochores [235].

To verify the phenotype of MPS1 inhibition on error-correction a monastrol washout experiment was performed [232–234] (Figure 32). Here, cells are arrested using monastrol – which like STLC inhibits kinesin 5 to arrest cells with a monopolar spindle [232]. Consequently, cells exhibit a range of attachment geometries (Figure 32A). The monastrol is then removed by washing the cells with media – allowing spindle bipolarity to recover in the presence of MG132 to prevent anaphase entry. The ability of chromosomes to congress to the metaphase plate, and for the aberrant attachment geometries to be corrected, can then be assessed (Figure 32A). As a positive control for the assay, cells were released into DMSO such that error correction and congression could occur unperturbed. As a negative control, cells were released into Aurora B inhibitor. Release in the absence of inhibition resulted in the formation of metaphase plates with few unaligned or unattached kinetochores (Figure 32B-D). Inhibition of Aurora B predictably caused massive defects in error

correction [234]. While most kinetochores were attached to microtubules, an abundance of these attachments were to the same spindle pole – causing misalignment of these chromosomes with syntelic attachments (Figure 32B-D). Release into MPS1 inhibitor resulted in the alignment of most chromosomes to the metaphase plate, but a small proportion of kinetochores remained at the spindle poles, without microtubule attachment (Figure 32B-D). This phenotype is reminiscent of a CENP-E inhibition as has been previously noted [93,165]. Together these observations confirm that simple inhibition of MPS1 does not produce defects in error correction, despite the clear evidence for the direct involvement of MPS1 in error correction in other situations.

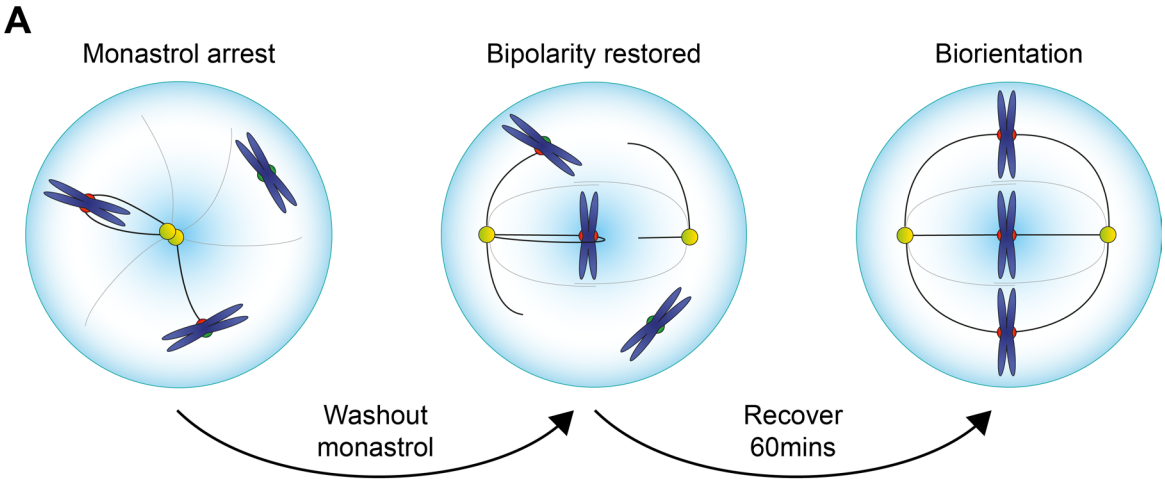
A
Monastrol arrest
Bipolarity restored
Biorientation
Washout
monastrol
Recover
60mins

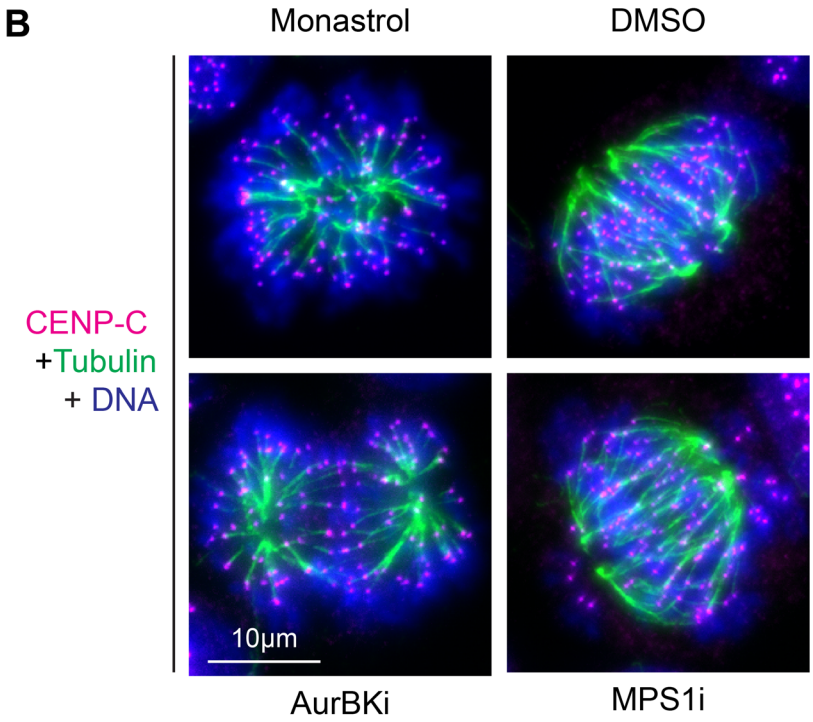
B
Monastrol
DMSO
CENP-C
+Tubulin
+ DNA
10μm
AurBKi
MPS1i

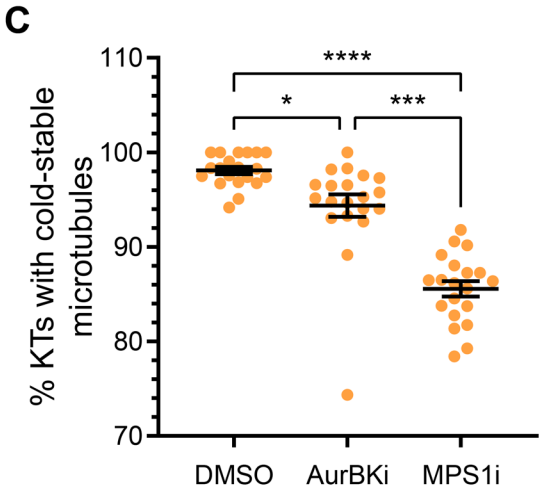
C
% KTs with cold-stable microtubules
110
100
90
80
70
****
*
***
DMSO
AurBKi
MPS1i

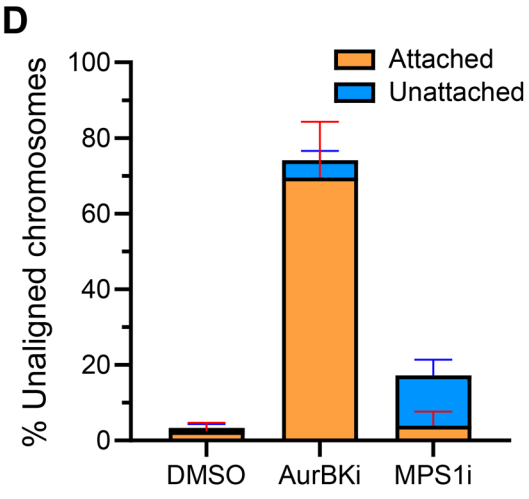
D
% Unaligned chromosomes
100
80
60
40
20
0
Attached
Unattached
DMSO
AurBKi
MPS1i

Figure 32 – **Different phenotypes from perturbation of MPS1 and Aurora kinases in a monastrol washout**

A. Schematic showing the principle behind a monastrol washout experiment. Monopolar spindles generate attachment errors. After washout of monastrol, spindle bipolarity recovers and the ability of cells to congress chromosomes and correct attachment errors is assessed.
B. HeLa cells were arrested in monastrol (100 μM, 16 h). The proteasome was inhibited with MG132 (30 min, 20 μM) prior to several rounds of media replacement to remove monastrol. Cells were released into media containing the indicated drug and allowed to recover for 60 minutes before cold treatment, fixation, and staining for CENP-C, Tubulin, and DNA.
C. Quantification of the number of kinetochores with cold-stable microtubules from cells in (B). Data pooled from 2 biological repeats. Bars show mean ± S.E.M.
D. Quantification of the number of unaligned kinetochores and their attachment status. Data pooled from 2 biological repeats. Bars show mean ± S.E.M. n = 20.

MPS1 and Aurora B cooperate to destabilise kinetochore-microtubule attachments

Direct evidence for the role of MPS1 in error-correction comes from experiments where it was rapidly ectopically localised to MIS12 [235]. In such an instance, the metaphase plate was seen to quickly fragment as MPS1 destabilised kinetochore-microtubule attachments [235]. The observation that MPS1 can be localised to attached-kinetochores through its endogenous binding partner via rapamycin-mediated recruitment of Aurora B provided another system to examine this phenomenon (Figure 15). HeLa cells expressing endogenously tagged GFP-MPS1 and the INCENP rapamycin-targeting system were arrested at metaphase and then treated with rapamycin. The recruitment of INCENP and GFP-MPS1, and the subsequent stability of the metaphase plate was observed by live cell imaging (Figure 33A). Recruitment of INCENP and GFP-MPS1 was near instantaneous upon addition of rapamycin, as previously established with fixed cell imaging (Figure 33A, B). After a few minutes, the metaphase plate fragmented as microtubule-kinetochore attachments were destablised (Figure 33A, B). This is unsurprising given that both Aurora B and MPS1 promote error correction. Curiously, chromosomes typically stayed attached to one spindle pole and were pulled toward said spindle pole (data not shown). This observation is in line with a report suggesting that Aurora B only promotes the release of microtubules at kinetochores under tension – instead promoting microtubule depolymerisation at tensionless/monotelic attachments [273].

To probe the role of MPS1 in this process of microtubule release, the experiment was repeated with and without MPS1 inhibitor (Figure 33C). As previous, in control cells the metaphase plate fragmented after a few minutes of rapamycin addition

(Figure 33C, D). This was markedly slowed when MPS1 was inhibited, demonstrating that even when large amounts of Aurora B were ectopically localised to the outer kinetochore, MPS1 activity still played a major role in destablising microtubule attachments (Figure 33C, D). These observations constitute further direct evidence that MPS1 works alongside Aurora B to cause microtubule turnover in a timely manner, alongside that already reported [235].

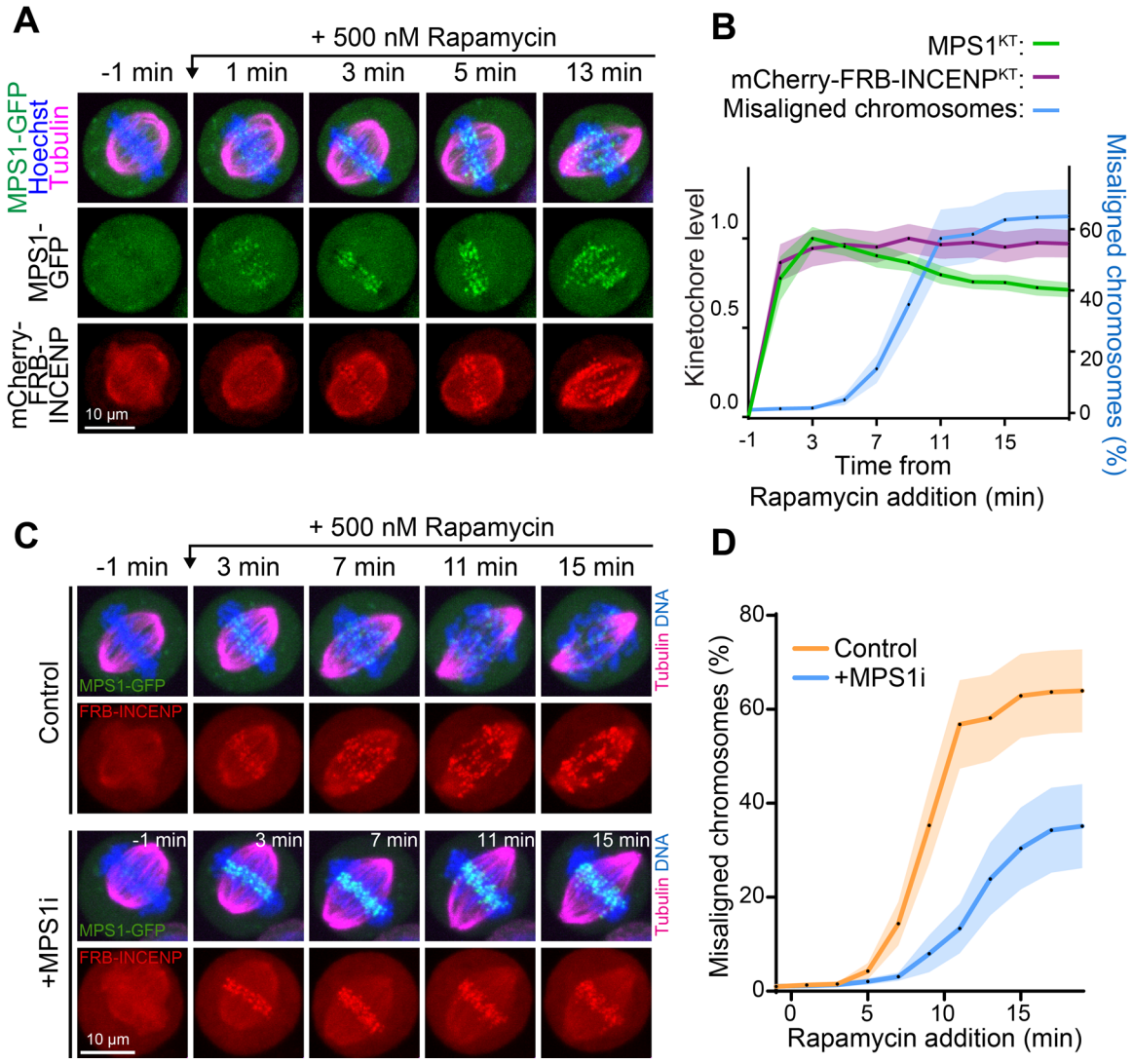

Figure 33 – **MPS1 acts in concert with Aurora B to destablise kinetochore-microtubule attachments**

A) HeLa cells expressing endogenously tagged MPS1-GFP and the Aurora B kinetochore-targeting system were arrested with MG132 (30 min, 20 µM) and imaged by live-cell microscopy. Tubulin and DNA were visualized with SiR-Tubulin and Hoechst. Rapamycin (500 nM) was added at the indicated timepoint.

B) Quantification of (A). The level of mCherry-FRB-INCENP or MPS1 at kinetochores, and the percentage of misaligned chromosomes are plotted over time as mean values ± S.E.M.
C) HeLa cells expressing endogenously tagged MPS1-GFP and the Aurora B kinetochore-targeting system were arrested with MG132 (30 min, 20 μM) and imaged by live-cell microscopy in the presence (+MPS1i) or absence (-MPS1i) of MPS1i (AZ3146, 2 μM). Tubulin and DNA were visualized with SiR-Tubulin and Hoechst. Rapamycin (500 nM) was added at the indicated timepoint.
D) Quantification of (C). The percentage of misaligned chromosomes over time are plotted as mean values ± S.E.M.

Changes in PP2A-B56 recruitment upon MPS1 inhibition counterbalance the microtubule-destabilising function of MPS1

Given that MPS1 clearly contributes to the destabilisation of kinetochore-microtubule attachments [235] (Figure 33), it is surprising that inhibition of MPS1 does not give rise to syntelic chromosomes in a monastrol washout [93,165] (Figure 32). This may be a result of other consequences of inhibiting MPS1 – specifically a drop in kinetochore-localised PP2A-B56 (Figure 12). Here, the loss of attachment-destabilising MPS1 activity would be counteracted by the loss of attachment-stabilising PP2A-B56 activity.

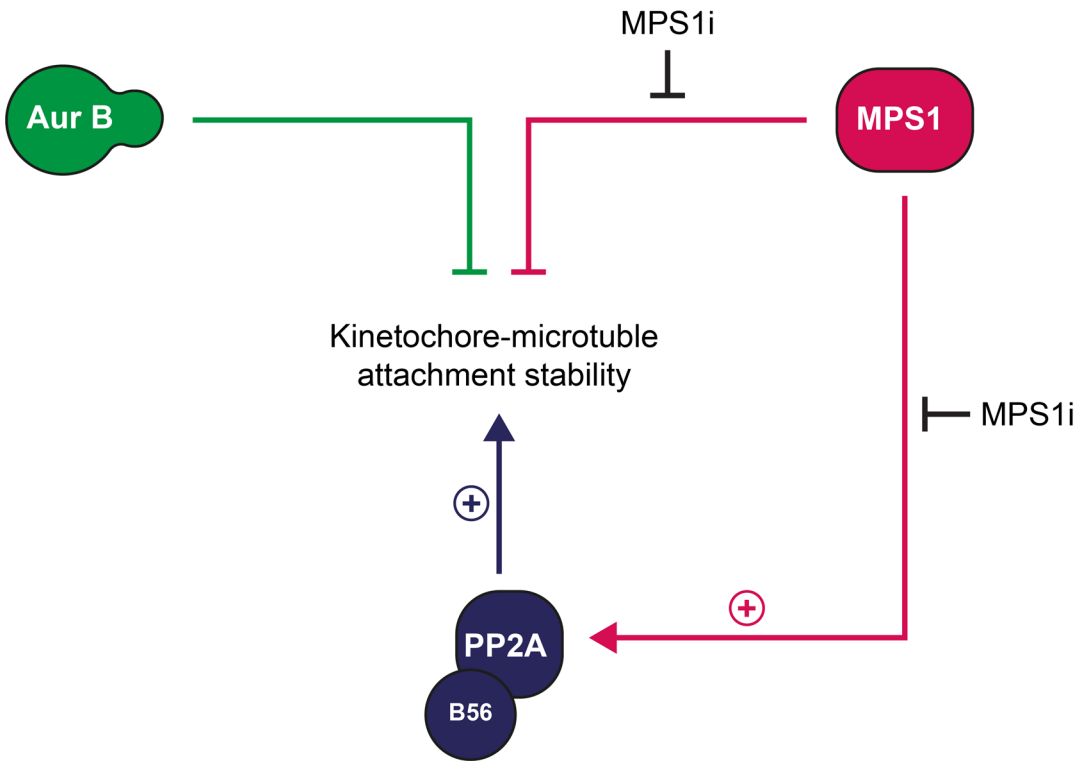

Diagram 20 – MPS1 inhibition may have both positive and negative effects on kinetochore-microtubule attachment stability. Aurora B and MPS1 activity destabilises kinetochore-microtubule attachments (top arrows). However, MPS1 activity causes the recruitment of PP2A-B56, leading to the stabilisation of attachments (bottom arrows). MPS1 activity may therefore have opposite effects on attachment stability via these two pathways, both of which would be affected by MPS1 inhibition.

To perturb the balance of MPS1 and PP2A-B56, it would be preferable to affect the activity of one enzyme more than the other without inhibiting MPS1. An increase in the total level of MPS1 activity will push the balance of MPS1 - PP2A-B56 toward MPS1 activity. This is essentially what has been observed for the ectopic recruitment of MPS1 to the metaphase plate [274]. A simple strategy to increase the level of MPS1 activity is to overexpress MPS1. HeLa cells with randomly integrated GFP-MPS1 under a doxycycline-inducible promoter were used to overexpress MPS1 (Figure 34). To assess the effect of overexpressing MPS1 on the steady-state levels of kinetochore-microtubule attachments, cells were arrested with a monopolar spindle with or without induction of GFP-MPS1 expression. The number of cold-stable microtubule attachments or Astrin-positive foci was used to quantify the percentage of end-on attachments (Figure 34). Using both metrics, the proportion of kinetochores with end-on attachments was significantly decreased upon induction of GFP-MPS1 overexpression (Figure 34). These observations provide further evidence that MPS1 contributes to the destabilisation of kinetochore-microtubule attachments. Furthermore, they support the notion that the increase in microtubule-attachment stability upon MPS1 inhibition is balanced by a decrease in stability from loss of PP2A-B56.

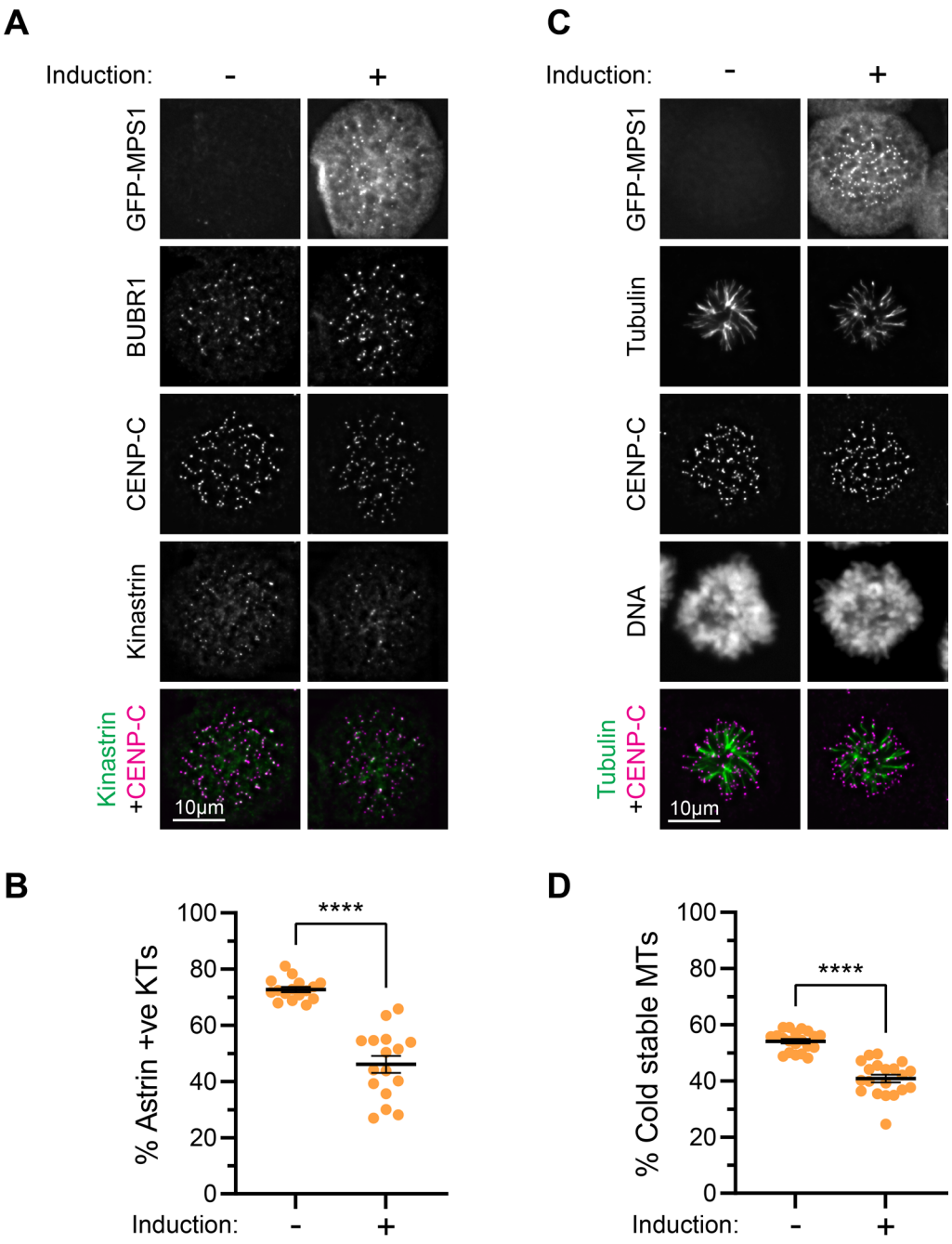

Figure 34 – **Overexpression of MPS1 is sufficient to disrupt the proportion of end-on attachments in a monopolar spindle**

A) HeLa cells harbouring randomly integrated, inducible GFP-MPS1 were treated with or without doxycycline (24 h, 2 µM) and arrested with monastrol (100 µM, 16 h) and MG132 (30 min, 20 µM). Cells were fixed and stained for BUBR1, CENP-C, and Kinastrin.
B) Quantification of the percentage of kinetochores with Astrin foci in (A).
C) HeLa cells harbouring randomly integrated, inducible GFP-MPS1 were treated with or without doxycycline (24 h, 2 µM) and arrested with monastrol (100 µM, 16 h) and MG132 (30 min, 20 µM). Cells were cold treated, fixed, and stained for Tubulin, CENP-C, and DNA.

D) Quantification of the percentage of kinetochores with cold-stable microtubules in (B).

An alternative, and more insightful strategy, to unpick the relative contributions of MPS1 and PP2A-B56 to attachment stability is to examine the effect of MPS1 inhibition on attachment stability in the absence of kinetochore-bound PP2A-B56. This approach removes the microtubule-stabilising PP2A-B56 pathway, allowing the effect of MPS1 inhibition on attachment stability to be isolated. To remove this factor, the BUBR1 B56-binding mutant can be used as previous (Figure 14). A summary of the different combinations of PP2A-B56 presence and MPS1 inhibition are outlined below.

In the absence of perturbations (wildtype BUBR1 and no MPS1 inhibition), Aurora B and MPS1 will destabilise attachments. MPS1-dependent recruitment of PP2A-B56 will oppose this activity of Aurora B and MPS1 (Diagram 21A). Inhibition of MPS1, in the presence of $BUBR1^{WT}$, will disrupt MPS1 destabilisation of attachments, and cause the loss of PP2A-B56 (Diagram 21B). The loss of PP2A-B56 will result in Aurora B activity being unopposed. Removing kinetochore-localised PP2A-B56 using $BUBR1^{LIAA}$ will disrupt PP2A-B56 opposition of Aurora B and MPS1, while maintaining the destabilising activity of these kinases (Diagram 21C). Inhibition of MPS1 in the presence of $BUBR1^{LIAA}$ will remove the MPS1 destabilising activity from the system (Diagram 21D). In summary, this experimental design enables the two opposing pathways by which MPS1 regulates attachment stability to be separated.

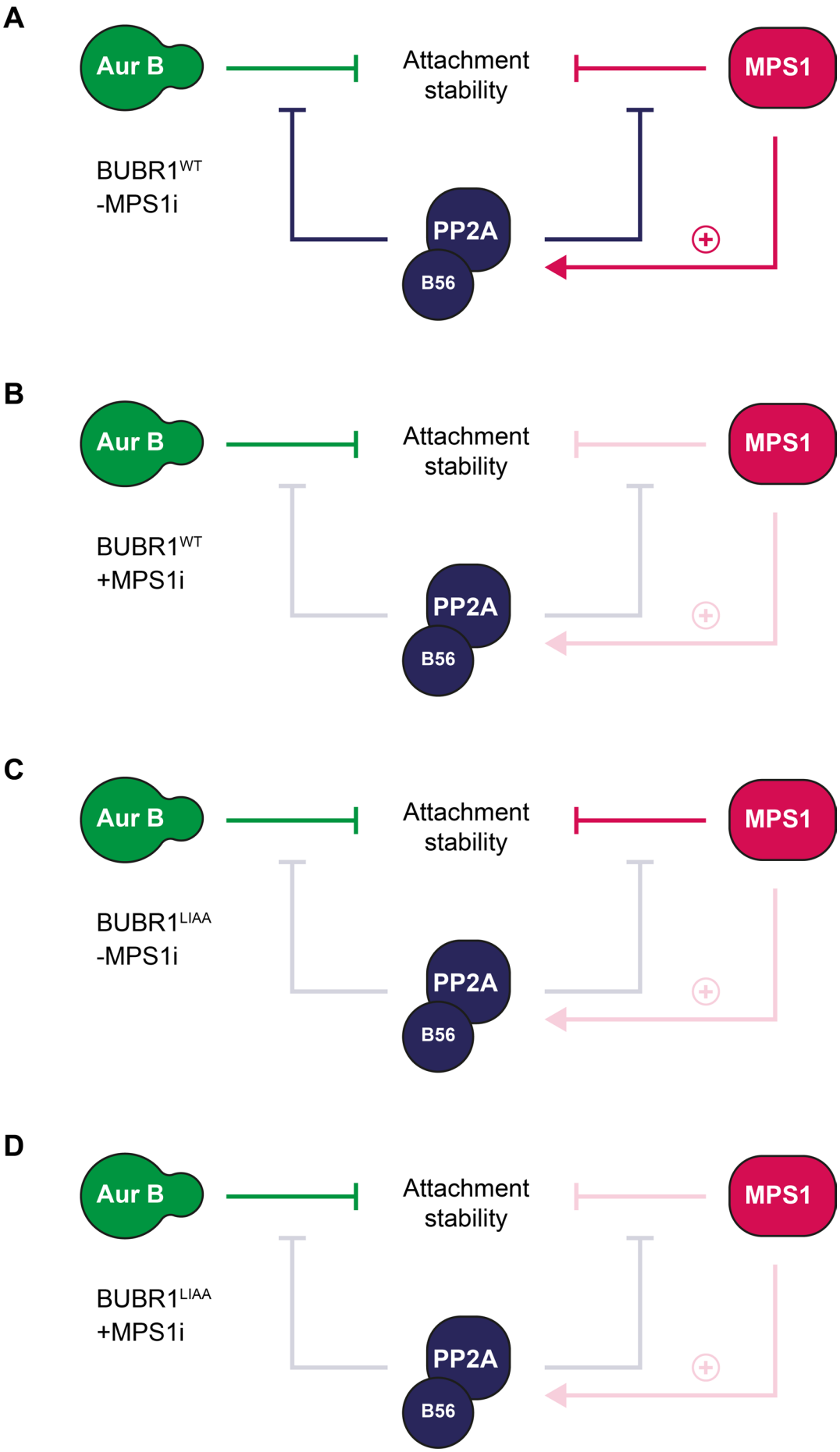
A
Aur B
Attachment
stability
MPS1
BUBR1WT
-MPS1i
PP2A
B56
B
Aur B
Attachment
stability
MPS1
BUBR1WT
+MPS1i
PP2A
B56
C
Aur B
Attachment
stability
MPS1
BUBR1LIAA
-MPS1i
PP2A
B56
D
Aur B
Attachment
stability
MPS1
BUBR1LIAA
+MPS1i
PP2A
B56

Diagram 21 – Network diagrams of the relationships between Aurora B, MPS1, and PP2-B56 regarding attachment stability. Transparent lines represent abrogated interactions. See main text for full detail.

HeLa Flp-In cells harbouring GFP-BUBR1^{WT} or GFP-BUBR1^{LIAA} were treated with siBUBR1 or siControl, and with or without doxycycline induction (Figure 35A). Endogenous BUBR1 could be efficiently replaced using this strategy. As a control for BUBR1 depletion, cells were treated with siControl or siBUBR1, arrested with monastrol, and stained for BUBR1 (Figure 35B). BUBR1 was practically undetectable in most cells upon treatment with siBUBR1, confirming the efficacy of the depletion (Figure 35B, C). To assess kinetochore-microtubule attachment stability, the number of end-on attachments were examined in a monopolar spindle (Figure 35D, F) or following monastrol washout (Figure 35E, G), with and without MPS1 inhibition.

First, the result on steady-state levels of attachments in a monopolar spindle will be described. In cells expressing endogenous BUBR1 (mock depletion and no induction) the level of Astrin-positive kinetochores was unchanged following MPS1 inhibition (Figure 35D, F). The same was true for cells depleted of endogenous BUBR1 and expressing GFP-BUBR1^{WT}, demonstrating that chemical inhibition of MPS1 has no effect on the steady-state level of end-on attachments in a monopolar spindle (Figure 35D, F). These observations are consistent with the notion that the attachment stabilising and de-stabilising activities of MPS1 are balanced.

Cells expressing GFP-BUBR1^{LIAA} displayed markedly reduced Astrin-positive kinetochores as expected [159] (Figure 35D, F). In this scenario, inhibition of MPS1 now caused a significant increase in the number of Astrin-positive kinetochores (Figure 35D, F). This observation demonstrates that MPS1 does destabilse kinetochore-microtubule attachments, and this destabilising activity is usually

counteracted by MPS1-dependent recruitment of PP2A-B56. Notably, the level of Astrin-positive kinetochores here did not reach that of GFP-BUBR1^{WT}. This may be because inhibition of MPS1 does not reduce the levels of PP2A-B56 at kinetochores as drastically as BUBR1^{LIAA}. However, this was not investigated.

Following monastrol washout, cells mock-treated or expressing GFP-BUBR1^{WT} in the absence of MPS1 inhibition efficiently made bioriented attachments to the metaphase plate as expected (Figure 35E, G). Upon MPS1 inhibition in mock-treated GFP-BUBR1^{WT}-expressing cells, a subset of unattached kinetochores accumulated at spindle poles as previously seen (Figure 35E, G, Figure 32). GFP-BUBR1^{LIAA} expression resulted in a severe decrease in the number or kinetochore-microtubule attachments, which was now increased by MPS1 inhibition (Figure 35E, G). This result was not statistically significant owning to the high variance of the level of end-on attachments made. However, the data presented here are from a single biological repeat – the addition of future repeats will likely show a statistically significant difference in phenotype. Notably, BUBR1^{WT} and BUBR1^{LIAA} did not display the same phenotype upon MPS1 inhibition (Figure 35F-H). The reason for these differences is unclear, but may come down to the residual level of PP2A-B56 at kinetochores. This remains to be investigated. Together, these observations further confirm that MPS1 does destabilise kinetochore-microtubule attachments, but this activity is opposed, and hence masked, by MPS1-dependent recruitment of PP2A-B56.

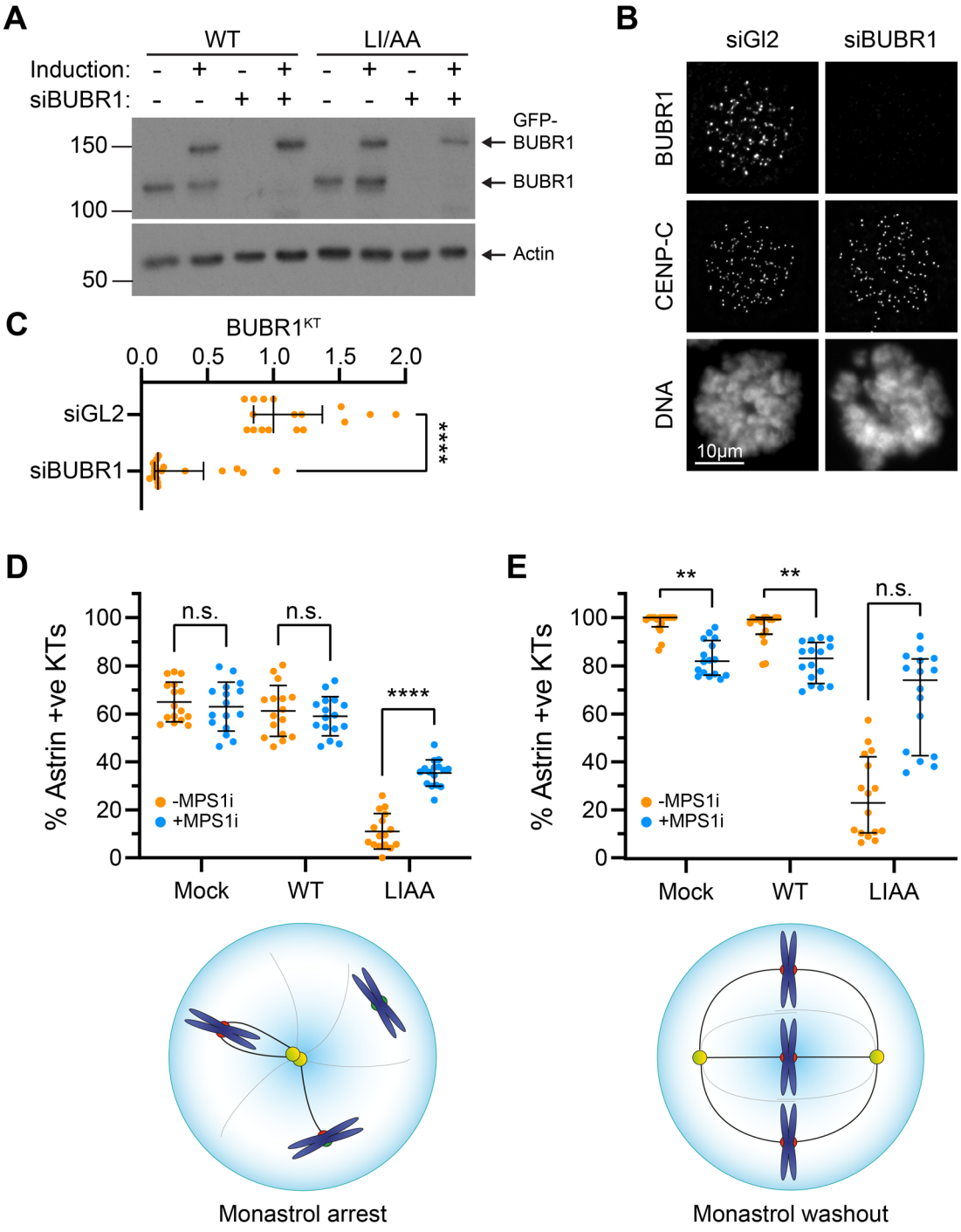
A
WT
LI/AA
Induction: - + - + - + - +
siBUBR1: - - + + - - + +
150
100
50
GFP-BUBR1
BUBR1
Actin
B
siGl2
siBUBR1
BUBR1
CENP-C
DNA
10μm
C
BUBR1KT
0.0 0.5 1.0 1.5 2.0
siGL2
siBUBR1
****
D
% Astrin +ve KTs
n.s.
n.s.
****
-MPS1i
+MPS1i
Mock
WT
LIAA
E
% Astrin +ve KTs
**
**
n.s.
-MPS1i
+MPS1i
Mock
WT
LIAA
Monastrol arrest
Monastrol washout

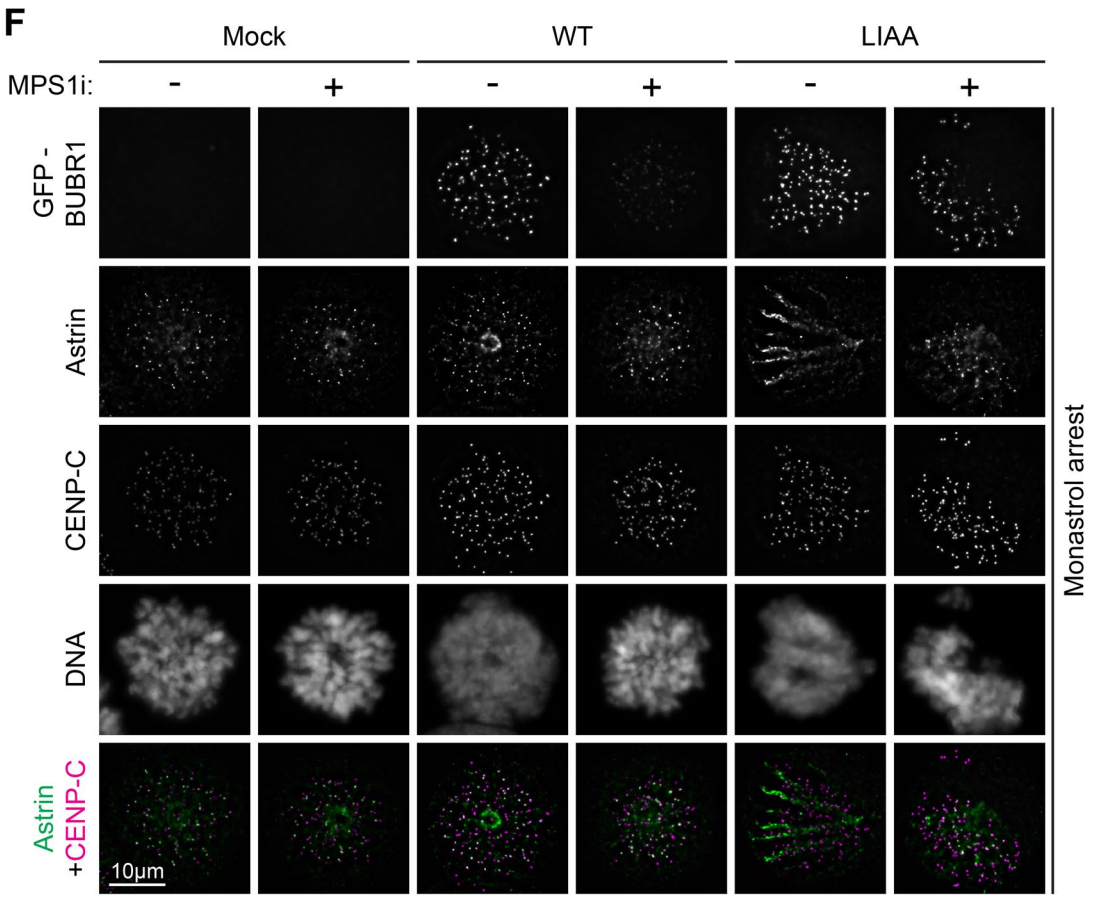
F
Mock
WT
LIAA
MPS1i:
-
+
-
+
-
+
GFP - BUBR1
Astrin
CENP-C
DNA
Astrin +CENP-C
10μm
Monastrol arrest

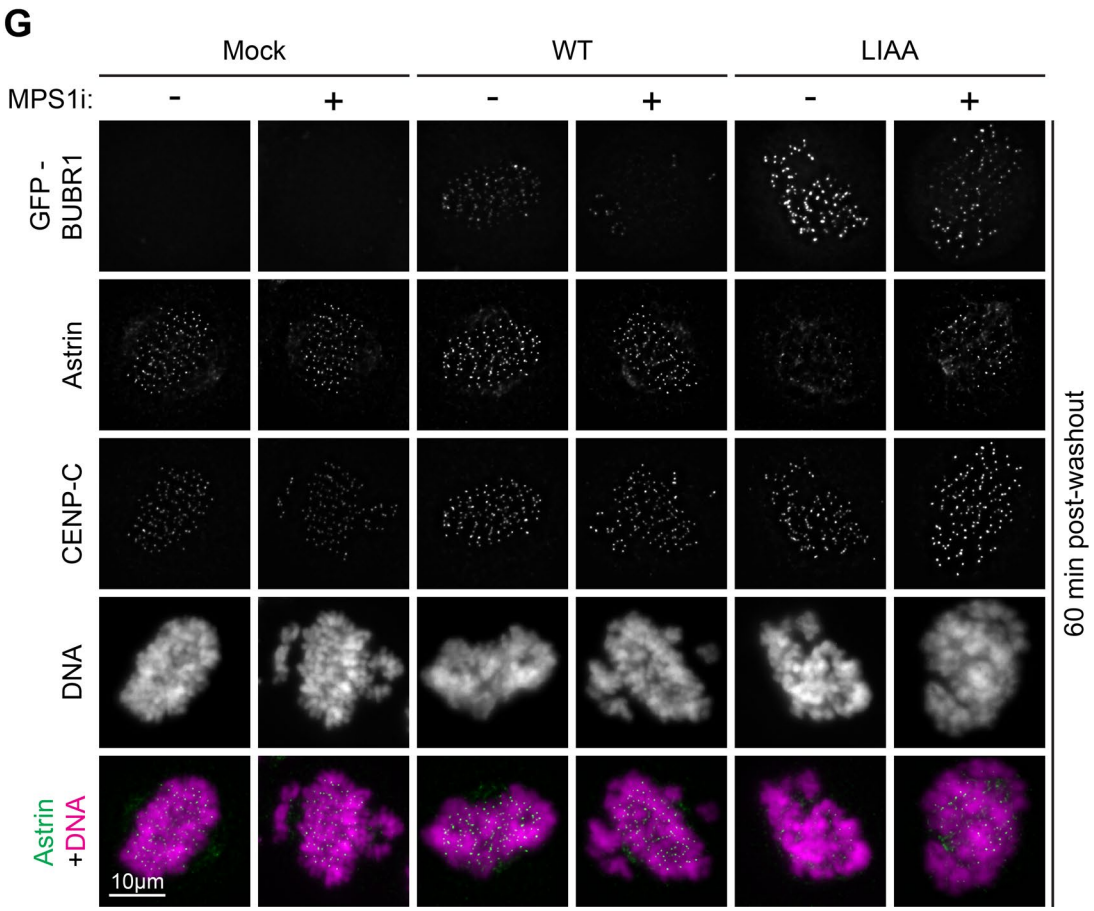
G
Mock
WT
LIAA
MPS1i:
-
+
-
+
-
+
GFP - BUBR1
Astrin
CENP-C
DNA
Astrin +DNA
10μm
60 min post-washout

Figure 35 – **MPS1 activity has a dual role in causing microtubule-kinetochore stabilisation and destabilisation**

A) Anti-BUBR1 Western blot of HeLa Flp-In TREx cells treated with siBUBR1 or siControl and ± doxycycline (2 μM) to induce GFP-BUBR1 transgene expression for 48 hours. Actin is used as a loading control.
B) HeLa Flp-In TREx cells were treated with siBUBR1 or siControl, arrested with STLC (60 min, 10 μM) and MG132 (30 min, 20 μM), fixed, and stained for BUBR1 and CENP-C.
C) Quantification of the mean amount of BUBR1 kinetochore localisation of cells in (B). Each dot represents one cell, data pooled from 3 biological repeats. Bars show median ± I.Q.R.
D) HeLa Flp-In TREx cells were treated with siControl (mock) or siBUBR1 and doxycycline (2 μM) to induce expression of GFP-BUBR1 WT or LIAA for 48 hours. Cells were arrested in monastrol (100 μM, 16 h). The proteasome was inhibited with MG132 (30 min, 20 μM) prior to the addition of DMSO or MPS1i (AZ3146, 2 μM, 60 min). Cells were fixed and stained for CENP-C, Astrin, and DNA. The percentage of kinetochores with Astrin foci are plotted. Each dot represents one cell, data from 1 biological repeat. Bars show mean ± S.D.
E) HeLa Flp-In TREx cells were treated with siControl (mock) or siBUBR1 and doxycycline (2 μM) to induce expression of GFP-BUBR1 WT or LIAA for 48 hours. Cells were arrested in monastrol (100 μM, 16 h). The proteasome was inhibited with MG132 (30 min, 20 μM) prior to several rounds of media replacement to remove the monastrol. Cells were released into media containing with or without MPS1i (AZ3146, 2 μM) and allowed to recover for 60 minutes before fixation, and staining for CENP-C, Astrin, and DNA. Each dot represents one cell, data from 1 biological repeat. Bars show median ± I.Q.R.
F) Representative cells from (D).
G) Representative cells from (E).

Discussion

Direct competition between MPS1 and microtubules is not sufficient to prevent MPS1 localising to end-on attached kinetochores

MPS1 has a crucial conserved role in initiating spindle checkpoint signalling in response to the presence of kinetochores which have not achieved end-on attachment. Ensuring that MPS1 localises to unattached kinetochores and does not bind to end-on attached kinetochores, is the basis of this function. Previous models suggest that in human cells MPS1 and microtubules compete for binding sites at the kinetochore – thus MPS1 is sterically blocked from binding the kinetochore upon end-on attachment [134,164]. This study has provided evidence in five different scenarios of robust MPS1 localisation to kinetochores with cold-stable microtubules and/or Astrin foci, indicating end-on attachment. MPS1 can be seen at attached kinetochores after; cold-treatment (Figure 1), inactivation of MPS1 (Figure 4, Figure 8, Figure 12), inhibition of PP2A/PP1 phosphatase activity (Figure 13), loss of BUBR1-bound PP2A-B56 (Figure 14), and following the ectopic recruitment of active Aurora B to the outer kinetochore (Figure 15). Together, these observations demonstrate that additional mechanisms centred around phosphorylation control if a kinetochore will localise MPS1, independent of end-on attachment [134,164] (Diagram 22). This represents a fundamental shift in the understanding of how MPS1 localisation, and thus the checkpoint-signalling status of a kinetochore, is controlled.

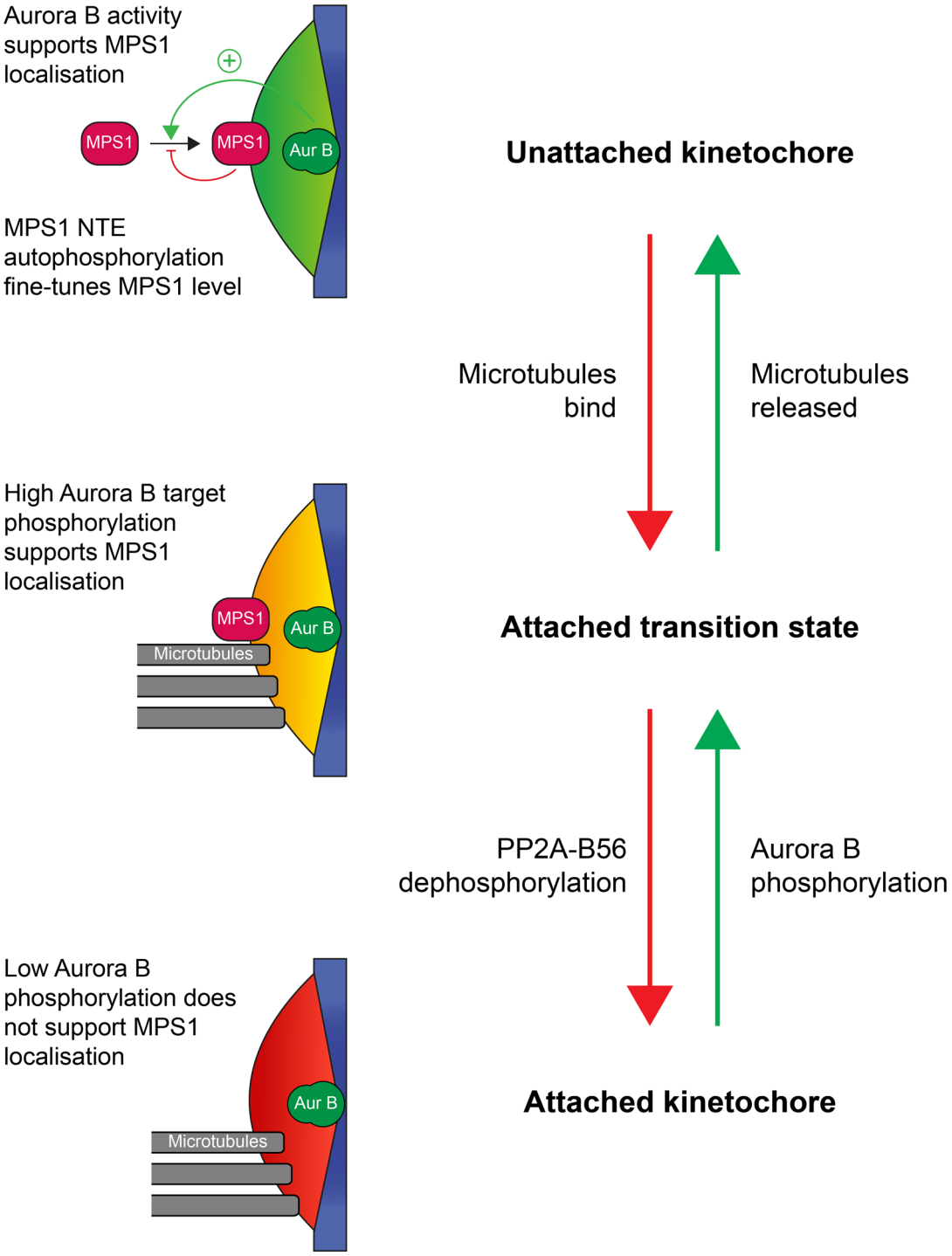

Diagram 22 – A model of changes in MPS1 localisation during end-on attachment (red arrows) and error correction (green arrows).

MPS1 activity feeds back onto MPS1 localisation behaviour through two distinct mechanisms

There are at least two separable effects on MPS1 localisation from inhibiting/inactivating MPS1 – N-terminal auto-phosphorylation, and the recruitment of BUBR1-bound PP2A-B56. Firstly, auto-phosphorylation of the N-terminus of MPS1 is responsible for fine-tuning the level to which MPS1 localises to unattached kinetochores[171] (Figure 5). Mutation of all 8 auto-phosphorylation sites in the NTE was sufficient to increase ($MPS1^{N8A}$) or decrease ($MPS1^{N8D/E}$) MPS1 localisation to unattached kinetochores, and rendered MPS1 localisation insensitive to MPS11 inhibition (Figure 5). Thus, the long-standing observation that MPS1 inhibition increases the level of MPS1 at kinetochores is explained in large part by phosphorylation of the NTE, as was previously suggested [92,124,171]. However, these mutations did not change the loss of MPS1 from kinetochores upon end-on attachment (Figure 5) or their dependency on Aurora B activity (Figure 6). This demonstrates that N-terminal auto-phosphorylation is subordinate to attachment status. These mutants thus provide a tool to examine the consequences of having different steady-state levels of MPS1 at checkpoint-active kinetochores. There was little consequence on the level of BUBR1 recruitment or mitotic progression because of having ~2.5 times as much MPS1 at unattached kinetochores. Conversely, having ~0.5x the normal level of MPS1 at unattached kinetochores did speed up progression through mitosis, but did not have a significant effect on BUBR1 recruitment to unattached kinetochores (Figure 9).

The second effect on MPS1 localisation resulting from inactivation or inhibition of MPS1 is the localisation of MPS1 to attached kinetochores (Figure 4). This suggests that some MPS1 activity-dependent mechanism beyond N-terminal

autophosphorylation feeds in to stopping MPS1 localisation to attached kinetochores. MPS1 inhibition will result in the loss of checkpoint proteins – thereby causing several changes in the local environment of the kinetochore. An attractive candidate for what is lost upon MPS1 inhibition to cause MPS1 localisation to attached kinetochores is BUBR1-bound PP2A-B56 [94–96,158,159,173]. Indeed, direct chemical inhibition of PP2A and PP1 family phosphatases caused MPS1 to localise strongly to attached kinetochores (Figure 13), as did the ablation of the B56-BUBR1 interaction via point mutation of BUBR1 (Figure 14). To directly test this hypothesis, it would be interesting to over-ride the MPS1 dependency of PP2A-B56 recruitment and see if inhibition of MPS1 still causes attached kinetochores to recruit MPS1. Perhaps this could be achieved by localising PP2A-B56 to MIS12 using the established rapamycin-dimerisation system [249]. Another difference between abrogating MPS1 activity and perturbing N-terminal autophosphorylation was that $MPS1^{KD}$ had a roughly doubled half-life compared to $MPS1^{WT/N8A}$ (Figure 9). It would be interesting to see if the half-life of MPS1 is similarly increased in the absence of BUBR1-bound PP2A-B56 by using the BUBR1 B56-binding mutants [159].

MPS1 localisation is controlled by Aurora B and PP2A-B56 downstream of microtubule attachment

Whether or not a kinetochore will recruit MPS1 is determined downstream of end-on attachment by the opposing activities of Aurora B and PP2A-B56 (Diagram 22). The inhibition of PP2A/PP1 phosphatases, or loss of the BUBR1-bound pool of PP2A-B56, caused the accumulation of MPS1 at end-on attached kinetochores (Figure 13, Figure 14). Thus, BUBR1-bound PP2A-B56, which is known to have roles in dephosphorylating Aurora B and MPS1 targets, is required for kinetochores to stop localising MPS1. As MPS1 localisation is dependent on Aurora B activity [156,157], the relevant target(s) of PP2A-B56 here are likely to be those of Aurora B. Rapidly recruiting active Aurora B to the outer kinetochore was sufficient to cause MPS1 localisation prior to the loss of end-on attachment (Figure 15). This demonstrates that Aurora B controls MPS1 localisation downstream of end-on attachment and reinforces the notion that PP2A-B56 likely dephosphorylates Aurora B targets to cause kinetochores to stop localising MPS1.

A crucial open question is what the substrate of Aurora B and PP2A-B56 is which controls MPS1 localisation. MPS1 directly binds to HEC1 and NUF2 [131,134], hence it would be reasonable to assume that these are the relevant target. In particular, phosphorylation of HEC1 by Aurora B has been proposed to increase the affinity of NDC80-C for MPS1, increasing MPS1 kinetochore localisation [134,168]. However, these observations could not be replicated by the Gruneberg group and others, as phospho-null mutation of these sites did not prevent MPS1 localisation [1,131,134]. Furthermore, these sites on HEC1 seem to be phosphorylated by Aurora A at attached kinetochores in cells, as opposed to by Aurora B at unattached kinetochores [267,268]. Therefore, HEC1 is unlikely to be the relevant target for

determining MPS1 localisation. Mutation of Aurora kinase sites in NUF2 similarly had no effect on MPS1 behaviour ([275], Gruneberg lab, unpublished). It is tempting to speculate that Aurora B could phosphorylate MPS1 directly to control its localisation. However, there is no evidence as yet that Aurora B phosphorylates MPS1, and mutation of putative Aurora B sites in MPS1 in this study caused no changes in the level of MPS1 localisation or dependency on Aurora B activity [129] (Figure 17). Therefore, it remains unclear how the MPS1 localisation is coupled to the activity of Aurora B and PP2A-B56.

Another exciting unanswered question is what aspect of end-on attachment causes changes in the balance of Aurora B and PP2A-B56 to result in the loss of MPS1 recruitment. There are multiple mechanisms which may be at play which are not mutually exclusive. Presumably an increase in PP2A-B56 levels would promote the switch of the kinetochore to a state which does not localise MPS1. However, PP2A-B56 levels are decreased at attached kinetochores following the loss of MPS1, and the subsequent decrease in BUBR1 levels (Figure 12). PP1 phosphatases are recruited to attached kinetochore by multiple pathways. However, in human cells depletion of PP1 does not cause major issues in checkpoint silencing or prevent MPS1 loss from attached kinetochores ([275], Gruneberg lab unpublished).

A drop in Aurora B activity or concentration could similarly cause the kinetochore to transition into a state in which MPS1 does not localise. A conformational change in the kinetochore which physically separates Aurora B (at the centromere) from its substrates (presumably at the outer kinetochore) could cause a drop in the local concentration of Aurora B. Indeed, microtubule binding alone is proposed to alter the conformation of HEC1 [192]. However, an attempt to simulate a decrease in Aurora B by rapidly ablating the centromeric enrichment of the CPC was insufficient

to cause kinetochores to stop MPS1 (Figure 18). Therefore, a model in which spatial separation of Aurora B from kinetochore substrate upon microtubule binding is the sole mechanism of preventing MPS1 localisation to attached kinetochores is unlikely to be true. Interestingly, the centromeric enrichment of Aurora B does seem necessary for the rapid accumulation of MPS1 at the onset of checkpoint signalling (Figure 22). This observation suggests that once kinetochores are signalling, Aurora B levels can drop to a great extent without causing kinetochores to lose MPS1. It would be interesting to see if the conformation of the kinetochore is different at those rarely-observed attached kinetochores which localise MPS1 compared to those which do not. Unfortunately, the method of trying to measure the distance between HEC1 and CENP-C used in this study was too noisy to allow this to be examined (Figure 24).

In summary, microtubule binding is coupled to MPS1 recruitment via the diametric activities of Aurora B and PP2A-B56. Upon end-on attachment, some aspect of this signalling axis must change to alter the ability of the kinetochore to recruit MPS1, but what precisely happens remains a key unanswered question.

The binding of MPS1 to the kinetochore occurs through 2 regions in an activity-dependent fashion

It is widely accepted that the interaction between the NTE and HEC1 is the predominant determinant of MPS1 kinetochore-localisation [90,131,134]. How CDK1-Cyclin B phosphorylation of the MR at S281 could be required for MPS1 localisation given reports that the MR is dispensable for MPS1 localisation was an open question [117,134]. The tendency of some studies to use MPS1 inhibitor, and others not to, when assessing how MPS1 localises to kinetochores was a major confounding variable when reconciling the published literature. By carefully re-examining the localisation of MPS1 constructs lacking the NTE or the MR, or with S281A or S281D mutations in the presence or absence of MPS1 inhibitor, a nuanced picture of MPS1 localisation has been revealed (Figure 26). Without MPS1 inhibitor the MR seems to contribute strongly to the localisation of MPS1, as does phosphorylation of the MR by CDK1. Surprisingly, in these conditions deletion of the NTE did not effect MPS1 levels – suggesting that either it is not the major kinetochore-interactor, or that the MR can compensate for the loss of the NTE (Figure 26). Conversely, upon inhibition the NTE appears to be the major kinetochore-interacting domain. Here deletion of the MR or mutation of S281 to alanine caused only a small reduction in localisation when compared to WT MPS1 (Figure 26). Given that when MPS1 is inhibited the NTE is likely to be less phosphorylated, it is possible that in these conditions the NTE can bind more strongly to the kinetochore and support MPS1 localisation despite the loss of the MR (Diagram 23). To test this hypothesis, MPS1 constructs lacking the MR and with the N-terminal sites mutated to glutamate could be used. If the NTE can support strong kinetochore-binding in the absence of the MR because it is not

phosphorylated, phospho-mimetic mutation of the NTE (to N8E) should ablate MPS1 localisation. Future work involving measuring binding between purified MPS1 and kinetochore proteins will help to fully elucidate the relationships between NTE and MR kinetochore-binding and the regulation of these interactions.

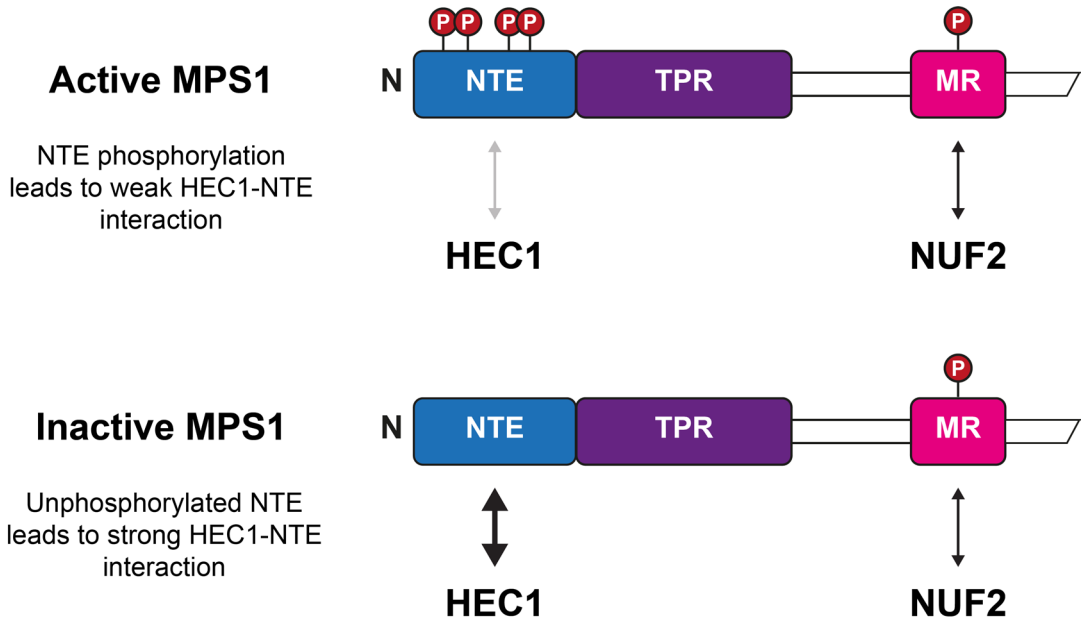

Diagram 23 – Model for how changes in activity status of MPS1 may affect the relative strengths of NTE-HEC1 and MR-NUF2 binding

MPS1 activity stabilises and destabilises microtubule attachment through different mechanisms

How MPS1 could exert error-correction functionality without binding to attached kinetochores was puzzling [134,164]. The findings in this study demonstrate that that MPS1 can bind to attached kinetochores – resolving this issue. Furthermore, at syntelic chromosomes undergoing error correction, MPS1 was observed to localise to kinetochores prior to the loss of microtubule attachment [1] (Diagram 22). This suggests that during error correction, MPS1 localises to kinetochores prior to loss of attachment to assist Aurora B in destabilising attachments. Furthermore, even after localising active Aurora B ectopically to the outer kinetochore, the kinase activity of MPS1 contributed significantly to attachment destabilisation (Figure 33). These observations corroborate the idea that MPS1 directly contributes to the resolution of incorrect attachments and the generation of unattached kinetochores. It is therefore not intuitive, why inhibition of MPS1 during error correction assays does not result in a similar phenotype to inhibition of Aurora B (stabilisation of syntelic attachments) (Figure 32) [93,165].

The feedback loop between MPS1 and PP2A-B56 can explain why MPS1 inhibition does not give a more severe phenotype during error correction assays. While inhibiting MPS1 will cause attachments to be less stable, the indirect effect of decreasing PP2A-B56 levels will cause attachment to be more stable (Diagram 20). These mechanisms result in no change in steady-state attachment levels in a monopolar spindle, and no issues with error correction in a monastrol washout upon MPS1 inhibition (Figure 35, Figure 32). By removing BUBR1-bound PP2A-B56, the role of MPS1 in destabilising attachments can be revealed (Diagram 21). Here, loss of PP2A-B56 resulted in severely decreased numbers of end-on attachments as

expected – presumably as both Aurora B and MPS1 are unopposed (Figure 35). In this scenario, the inhibition of MPS1 revealed its role in destabilising kinetochore-microtubule attachments (Figure 35).

Precisely how PP2A-B56 opposes the error correction function of MPS1 was not addressed by the assays in this study. There are multiple potential explanations for how steady-state levels of attachments are affected by the MPS1 – PP2A-B56 signalling axis:

1. The rate of attachment loss is altered
2. The rate of attachment formation is altered

In the first scenario, at kinetochores undergoing error-correction the loss of MPS1 activity should slow the destabilisation of microtubules, but the loss of PP2A-B56 could increase the rate of microtubule destabilisation by lowering the threshold of Aurora B activity required to cause microtubule turnover. In the second scenario, the loss of PP2A-B56 from unattached kinetochores may make the rate of attachment formation slower, as such kinetochores may exhibit higher levels of microtubule-destabilising Aurora B phosphorylations. These two processes, rate of attachment formation and rate of attachment destabilisation, may both be affected. Assays which directly measure these rates would be insightful.

One curious observation during the course of this study is that the process of error-correction is not solely guided by lack of tension across the chromosome. At syntelic chromosomes undergoing error correction, the recruitment of MPS1 and subsequent loss of attachment only occurred at one kinetochore of a pair [1]. How attachment of both kinetochores is sensed, and how the choice for only one kinetochore of the pair to undergo microtubule turnover is made is unclear.

Functionally the stabilisation of monotelic attachments is beneficial – as such chromosomes still have the chance to become bioriented. It is increasingly clear that inputs other than tension also feed into error correction, and the question of how this more complex decision making is made is fascinating [219].

Together, the findings presented here move the field toward a deeper understanding of the molecular underpinnings of checkpoint signalling initiation and error correction. By unpicking how MPS1 localisation is influenced by end-on attachment and dynamic phosphorylation events a new set of questions about how checkpoint signalling, and error correction are regulated have been generated. Key areas for future study are understanding how end-on attachment is coupled to MPS1 binding via Aurora B and PP2A-B56. Such an understanding will elucidate a new level of molecular detail for how MPS1 is removed from kinetochores upon microtubule attachment, and recruited to attached kinetochores to facilitate error correction.

References

1. Hayward D, Roberts E, Gruneberg U: **MPS1 localizes to end-on microtubule-attached kinetochores to promote microtubule release**. *Current Biology* 2022, **32**:5200-5208.e8.

2. Flemming W: **Zellsubstanz, Kern und Zelltheilung.** F.C.W. Vogel; 1882.

3. Strasburger E: **Die Controversen der indirecten Kerntheilung**. *Archiv für Mikroskopische Anatomie* 1883, **23**:246–304.

4. Heidenhain M: **Neue Untersuchungen über die Centralkörper und ihre Beziehungen zum Kern- und Zellen-protoplasma**. *Archiv für Mikroskopische Anatomie* 1894, **43**:423–748.

5. Gruber S, Haering CH, Nasmyth K: **Chromosomal Cohesin Forms a Ring and Smc3, all of which are conserved from yeast to humans**. *Cell* 2003, **112**:765–777.

6. Ivanov D, Nasmyth K: **A topological interaction between cohesin rings and a circular minichromosome**. *Cell* 2005, **122**:849–860.

7. Haering CH, Farcas AM, Arumugam P, Metson J, Nasmyth K: **The cohesin ring concatenates sister DNA molecules**. *Nature* 2008, **454**:297–301.

8. Waizenegger IC, Hauf S, Meinke A, Peters J-M: **Two Distinct Pathways Remove Mammalian Cohesin from Chromosome Arms in Prophase and from Centromeres in Anaphase**. *Cell* 2000, **103**:399–410.

9. Murray AW, Kirschner MW: **Cyclin synthesis drives the early embryonic cell cycle**. *Nature* 1989, **339**:275–280.

10. Minshull J, Blow JJ, Hunt' T: **Translation of Cyclin mRNA Is Necessary for Extracts of Activated Xenopus Eggs to Enter Mitosis**. *Cell* 1989, **56**:947–956.

11. Hoffmann I, Clarke PR, Marcote MJ, Karsenti E, Draetta G: **Phosphorylation and activation of human cdc25-C by cdc2-cyclin B and its involvement in the self-amplification of MPF at mitosis**. *EMBO Journal* 1993, **12**:53–63.

12. Harvey SL, Charlet A, Haas W, Gygi SP, Kellogg DR: **Cdk1-dependent regulation of the mitotic inhibitor Wee1**. *Cell* 2005, **122**:407–420.

13. Novak B, Tyson JJ: **Numerical analysis of a comprehensive model of M-phase control in Xenopus oocyte extracts and intact embryos**. *J Cell Sci* 1993, **106**:1153–1168.

14. Pomerening JR, Sontag ED, Ferrell JE: **Building a cell cycle oscillator: Hysteresis and bistability in the activation of Cdc2**. *Nat Cell Biol* 2003, **5**:346–351.

15. Sha W, Moore J, Chen K, Lassaletta AD, Yi C-S, Tyson JJ, Sible JC: **Hysteresis drives cell-cycle transitions in Xenopus laevis egg extracts**. *PNAS* 2003, **100**:975–980.

16. Dephoure N, Zhou C, Villé J, Beausoleil SA, Bakalarski CE, Elledge SJ, Gygi SP: **A quantitative atlas of mitotic phosphorylation**. *PNAS* 2008, **105**:10762–10767.

17. Dohadwala M, Da Cruz EF, Silva E, Hall FL, Williams RT, Carbonaro-Hall DA, Nairn AC, Greengard P, Berndt N: **Phosphorylation and Inactivation of Protein Phosphatase 1 by Cyclin-Dependent Kinases**. *PNAS* 1994, **91**:6408–6412.

18. Vigneron S, Gharbi-Ayachi A, Raymond A-A, Burgess A, Labbé J-C, Labesse G, Monsarrat B, Lorca T, Castro A: **Characterization of the Mechanisms Controlling Greatwall Activity**. *Mol Cell Biol* 2011, **31**:2262–2275.

19. Blake-Hodek KA, Williams BC, Zhao Y, Castilho P V., Chen W, Mao Y, Yamamoto TM, Goldberg ML: **Determinants for Activation of the Atypical AGC Kinase Greatwall during M Phase Entry**. *Mol Cell Biol* 2012, **32**:1337–1353.

20. Mochida S, Maslen SL, Skehel M, Hunt T: **Greatwall Phosphorylates an Inhibitor of Protein Phosphatase 2A That Is Essential for Mitosis**. *Science (1979)* 2010, **330**:1670–1673.

21. Gharbi-Ayachi A, Labbe J-C, Burgess A, Vigneron S, Strub J-M, Brioudes E, Van-Dorsselaer A, Castro A, Lorca T: **The Substrate of Greatwall Kinase, Arpp19, Controls Mitosis by Inhibiting Protein Phosphatase 2A**. *Science (1979)* 2007, **330**:1673–1677.

22. Murray AW, Solomon MJ, Kirschner MW: **The role of cyclin synthesis and degradation in the control of maturation promoting factor activity**. *Nature* 1989,

23. Glotzer M, Murray AW, Kirschner MW: **Cyclin is degraded by the ubiquitin pathway**. *NATURE ·* 1991, **349**.

24. Hershko A, Ganoth D, Pehrson J, Palazzo RE, Cohen LH: **Methylated Ubiquitin Inhibits Cyclin Degradation in Clam Embryo Extracts***. *THE JOURNAL OF BIOLOGICAL CHEMISTRY (c)* 1991, **266**:16376–16373.

25. Cohen-Fix O, Peters JM, Kirschner MW, Koshland D: **Anaphase initiation in Saccharomyces cerevisiae is controlled by the APC-dependent degradation of the anaphase inhibitor Pds1p.** *Genes Dev* 1996, **10**:3081–3093.

26. Sudakin V, Ganoth D, Dahan A, Heller H, Hershko J, Luca FC, Ruderman J V, Hershko A: **The Cyclosome, a Large Complex Containing Cyclin-Selective Ubiquitin Ligase Activity, Targets Cyclins for Destruction at**

the End of Mitosis Cyclin destruction results in the release of. *Mol Biol Cell* 1995, **6**:185–198.

27. King RW, Peters J-M, Tugendreich S, Rolfe M, Hieter P, Kirschnert MW: **A 20S Complex Containing CDC27 and CDC16 Catalyzes the Mitosis-Specific Conjugation of Ubiquitin to Cyclin B**. *Cell* 1995, **81**:279–288.

28. Gorr IH, Boos D, Stemmann O: **Mutual inhibition of separase and Cdk1 by two-step complex formation**. *Mol Cell* 2005, **19**:135–141.

29. Ciosk R, Zachariae W, Michaelis C, Shevchenko A, Mann M, Nasmyth K: **An ESP1/PDS1 Complex Regulates Loss of Sister Chromatid Cohesion at the Metaphase to Anaphase Transition in Yeast**. *Cell* 1998, **93**:1067–1076.

30. Uhlmann F, Lottspeich F, Nasmyth K: **Sister-chromatid separation at anaphase onset is promoted by cleavage of the cohesin subunit Scc1**. *Nature* 1999, **400**.

31. Cundell MJ, Bastos RN, Zhang T, Holder J, Gruneberg U, Novak B, Barr FA: **The BEG (PP2A-B55/ENSA/Greatwall) Pathway Ensures Cytokinesis follows Chromosome Separation**. *Mol Cell* 2013, **52**:393–405.

32. Cundell MJ, Hutter LH, Bastos RN, Poser E, Holder J, Mohammed S, Novak B, Barr FA: **A PP2A-B55 recognition signal controls substrate dephosphorylation kinetics during mitotic exit**. *Journal of Cell Biology* 2016, **214**:539–554.

33. Holder J, Mohammed S, Barr FA: **Ordered dephosphorylation initiated by the selective proteolysis of cyclin B drives mitotic exit**. *Elife* 2020, **9**:1–33.

34. Holder J, Poser E, Barr FA: **Getting out of mitosis: spatial and temporal control of mitotic exit and cytokinesis by PP1 and PP2A**. *FEBS Lett* 2019, **593**:2908–2924.

35. Fujimitsu K, Grimaldi M, Yamano H: **Cyclin-dependent kinase 1-dependent activation of APC/C ubiquitin ligase**. *Science (1979)* 2016, **352**:1121–1124.

36. Zhang S, Chang L, Alfieri C, Zhang Z, Yang J, Maslen S, Skehel M, Barford D: **Molecular mechanism of APC/C activation by mitotic phosphorylation**. *Nature* 2016, **533**:260–264.

37. Qiao R, Weissmann F, Yamaguchi M, Brown NG, VanderLinden R, Imre R, Jarvis MA, Brunner MR, Davidson IF, Litos G, et al.: **Mechanism of APC/CCDC20 activation by mitotic phosphorylation**. *Proc Natl Acad Sci U S A* 2016, **113**:E2570–E2578.

38. D'Angiolella V, Mari C, Nocera D, Rametti L, Grieco D: **The spindle checkpoint requires cyclin-dependent kinase activity**. *Genes Dev* 2003, **17**:2520–2525.

39. Yudkovsky Y, Shteinberg M, Listovsky T, Brandeis M, Hershko A: **Phosphorylation of Cdc20/Fizzy negatively regulates the mammalian cyclosome/APC in the mitotic checkpoint**. *Biochem Biophys Res Commun* 2000, **271**:299–304.

40. Jokelainen PT: **The Ultrastructure and Spatial Organization of the Metaphase Kinetochore in Mitotic Rat Cells**. *J ULTRASTRUCTURE RESEARCH* 1967, **19**:19–44.

41. Foltz DR, Jansen LET, Black BE, Bailey AO, Yates JR, Cleveland DW: **The human CENP-A centromeric nucleosome-associated complex**. *Nat Cell Biol* 2006, **8**:458–469.

42. Blower MD, Sullivan BA, Karpen GH: **Conserved organization of centromeric chromatin in flies and humans**. *Dev Cell* 2002, **2**:319–330.

43. Carroll CW, Milks KJ, Straight AF: **Dual recognition of CENP-A nucleosomes is required for centromere assembly**. *Journal of Cell Biology* 2010, **189**:1143–1155.

44. Kato H, Jiang J, Zhou B-R, Rozendaal M, Feng H, Ghirlando R, Xiao TS, Straight AF, Bai Y: **A Conserved Mechanism for Centromeric Nucleosome Recognition by Centromere Protein CENP-C**. *Science (1979)* 2013, **340**:1110–1113.

45. Yatskevich S, Muir KW, Bellini D, Zhang Z, Yang J, Tischer T, Predin M, Dendooven T, McLaughlin SH, Barford D: **Structure of the human inner kinetochore bound to a centromeric CENP-A nucleosome**. *Science (1979)* 2022, **376**:844–852.

46. Pesenti ME, Raisch T, Conti D, Walstein K, Hoffmann I, Vogt D, Prumbaum D, Vetter IR, Raunser S, Musacchio A: **Structure of the human inner kinetochore CCAN complex and its significance for human centromere organization**. *Mol Cell* 2022, **82**:2113-2131.e8.

47. Hori T, Haraguchi T, Hiraoka Y, Kimura H, Fukagawa T: **Dynamic behavior of Nuf2-Hec1 complex that localizes to the centrosome and centromere and is essential for mitotic progression in vertebrate cells**. *J Cell Sci* 2003, **116**:3347–3362.

48. Cheeseman IM, Niessen S, Anderson S, Hyndman F, Yates JR, Oegema K, Desai A: **A conserved protein network controls assembly of the outer kinetochore and its ability to sustain tension**. *Genes Dev* 2004, **18**:2255–2268.

49. Emanuele MJ, Lan W, Jwa M, Miller SA, Chan CSM, Stukenberg PT: **Aurora B kinase and protein phosphatase 1 have opposing roles in modulating kinetochore assembly**. *Journal of Cell Biology* 2008, **181**:241–254.

50. Rago F, Gascoigne KE, Cheeseman IM: **Distinct organization and regulation of the outer kinetochore KMN network downstream of CENP-C and CENP-T**. *Current Biology* 2015, **25**:671–677.

51. Gascoigne KE, Cheeseman IM: **CDK-dependent phosphorylation and nuclear exclusion coordinately control kinetochore assembly state**. *Journal of Cell Biology* 2013, **201**:23–32.

52. Suzuki A, Badger BL, Salmon ED: **A quantitative description of Ndc80 complex linkage to human kinetochores**. *Nat Commun* 2015, **6**.

53. Rieder CL: **The Formation, Structure, and Composition of the Mammalian Kinetochore and Kinetochore Fiber**. 1982:1–58.

54. Cheeseman IM, Chappie JS, Wilson-kubalek EM, Desai A: **The Conserved KMN Network Constitutes the Core Microtubule-Binding Site of the Kinetochore**. *Cell* 2006, **127**:983–997.

55. DeLuca JG, Musacchio A: **Structural organization of the kinetochore-microtubule interface**. *Curr Opin Cell Biol* 2012, **24**:48–56.

56. DeLuca JG, Moree B, Hickey JM, Kilmartin J V., Salmon ED: **hNuf2 inhibition blocks stable kinetochore-microtubule attachment and induces mitotic cell death in HeLa cells**. *Journal of Cell Biology* 2002, **159**:549–555.

57. Ciferri C, Pasqualato S, Screpanti E, Varetti G, Santaguida S, Dos Reis G, Maiolica A, Polka J, De Luca JG, De Wulf P, et al.: **Implications for Kinetochore-Microtubule Attachment from the Structure of an Engineered Ndc80 Complex**. *Cell* 2008, **133**:427–439.

58. Wei RR, Al-Bassam J, Harrison SC: **The Ndc80/HEC1 complex is a contact point for kinetochore-microtubule attachment**. *Nat Struct Mol Biol* 2007, **14**:54–59.

59. Kiewisz R, Fabig G, Conway W, Baum D, Needleman D, Müller-Reichert T: **Three-dimensional structure of kinetochore-fibers in human mitotic spindles**. *Elife* 2022, **11**.

60. O'Toole E, Morphew M, Richard McIntosh J: **Electron tomography reveals aspects of spindle structure important for mechanical stability at metaphase**. *Mol Biol Cell* 2020, **31**:184–195.

61. Jokelainen PT: **The ultrastructure and spatial organization of the metaphase kinetochore in mitotic rat cells**. *J Ultrastruct Res* 1967, **19**:19–44.

62. Hoffman DB, Pearson CG, Yen TJ, Howell BJ, Salmon ED: **Microtubule-dependent Changes in Assembly of Microtubule Motor Proteins and Mitotic Spindle Checkpoint Proteins at PtK1 Kinetochores**. *Mol Biol Cell* 2001, **12**:1995–2009.

63. Thrower DA, Jordan MA, Wilson L: **Modulation of CENP-E organization at kinetochores by spindle microtubule attachment**. *Cell Motil Cytoskeleton* 1996, **35**:121–133.

64. Wordeman L, Steuer ER, Sheetz MP, Mitchison T: **Chemical subdomains within the kinetochore domain of isolated CHO mitotic chromosomes.** *J Cell Biol* 1991, **114**:285–294.

65. Cooke CA, Schaar B, Yen TJ, Earnshaw WC: **Localization of CENP-E in the fibrous corona and outer plate of mammalian kinetochores from prometaphase through anaphase**. *Chromosoma* 1997, **106**:446–455.

66. Basto R, Scaerou F, Mische S, Wojcik E, Lefebvre C, Gomes R, Hays T, Karess R: **In Vivo Dynamics of the Rough Deal Checkpoint Protein during Drosophila Mitosis**. *Current Biology* 2004, **14**:56–61.

67. Starr DA, Williams BC, Hays TS, Goldberg ML: **ZW10 Helps Recruit Dynactin and Dynein to the Kinetochore**. *J Cell Biol* 1998, **142**:763–774.

68. Rattner JB, Rao A, Fritzler MJ, Valencia DW, Yen TJ: **CENP-F is a ca 400 kDa kinetochore protein that exhibits a cell-cycle dependent localization**. *Cell Motil Cytoskeleton* 1993, **26**:214–226.

69. Moyle MW, Kim T, Hattersley N, Espeut J, Cheerambathur DK, Oegema K, Desai A: **A Bub1-Mad1 interaction targets the Mad1-Mad2 complex to unattached kinetochores to initiate the spindle checkpoint**. *Journal of Cell Biology* 2014, **204**:647–657.

70. Shrestha RL, Draviam VM: **Lateral to end-on conversion of chromosome-microtubule attachment requires kinesins CENP-E and MCAK**. *Current Biology* 2013, **23**:1514–1526.

71. Koshland DE, Mitchison TJ, Kirschner MW: **Polewards chromosome movement driven by microtubule depolymerization in vitro**. *Nature* 1988, **331**:499–504.

72. Coue M, Lombillo VA, McIntosh JR: **Microtubule depolymerization promotes particle and chromosome movement in vitro.** *J Cell Biol* 1991, **112**:1165–1175.

73. Mitchison TJ, Salmon ED: **Poleward kinetochore fiber movement occurs during both metaphase and anaphase-A in newt lung cell mitosis.** *J Cell Biol* 1992, **119**:569–582.

74. Kapoor TM, Lampson MA, Hergert P, Cameron L, Cimini D, Salmon ED, McEwen BF, Khodjakov A: **Chromosomes Can Congress to the Metaphase Plate Before Biorientation**. *Science (1979)* 2006, **311**:388–391.

75. Cai S, O'Connell CB, Khodjakov A, Walczak CE: **Chromosome congression in the absence of kinetochore fibres**. *Nat Cell Biol* 2009, **11**:832–838.

76. McEwen BF, Chan GKT, Zubrowski B, Savoian MS, Sauer MT, Yen TJ: **CENP-E Is Essential for Reliable Bioriented Spindle Attachment, but Chromosome Alignment Can Be Achieved via Redundant Mechanisms in Mammalian Cells**. *Mol Biol Cell* 2001, **12**:2776–2789.

77. Rieder CL, Cole RW, Khodjakov A, Sluder G: **The Checkpoint Delaying Anaphase in Response to Chromosome Monoorientation Is Mediated by an Inhibitory Signal Produced by Unattached Kinetochores**. *J Cell Biol* 1995, **130**:941–948.

78. Sudakin V, Chan GKT, Yen TJ: **Checkpoint inhibition of the APC/C in HeLa cells is mediated by a complex of BUBR1, BUB3, CDC20, and MAD2**. *Journal of Cell Biology* 2001, **154**:925–936.

79. Izawa D, Pines J: **Mad2 and the APC/C compete for the same site on Cdc20 to ensure proper chromosome segregation**. *Journal of Cell Biology* 2012, **199**:27–37.

80. Zhang Y, Lees E: **Identification of an Overlapping Binding Domain on Cdc20 for Mad2 and Anaphase-Promoting Complex: Model for Spindle Checkpoint Regulation**. *Mol Cell Biol* 2001, **21**:5190–5199.

81. Burton JL, Solomon MJ: **Mad3p, a pseudosubstrate inhibitor of APCCdc20 in the spindle assembly checkpoint**. *Genes Dev* 2007, **21**:655–667.

82. Lara-Gonzalez P, Scott MIF, Diez M, Sen O, Taylor SS: **Bubr1 blocks substrate recruitment to the APC/C in a KEN-box-dependent manner**. *J Cell Sci* 2011, **124**:4332–4345.

83. Chao WCH, Kulkarni K, Zhang Z, Kong EH, Barford D: **Structure of the mitotic checkpoint complex**. *Nature* 2012, **484**:208–213.

84. Izawa D, Pines J: **The mitotic checkpoint complex binds a second CDC20 to inhibit active APC/C**. *Nature* 2015, **517**:631–634.

85. Hoyt MA, Totis L, Roberts BT: **S. cerevisiae Genes Required for Cell Cycle Arrest in Response to Loss of Microtubule Function**. *Cell* 1991, **66**:507–517.

86. Li R, Murray AW: **Feedback Control of Mitosis in Budding Yeast**. *Cell* 1991, **66**:519–531.

87. Hartwell LH, Culotti J, Reidt B: **Genetic Control of the Cell-Division Cycle in Yeast, I. Detection of Mutants**. *Proceedings of the National Academy of Sciences* 1970, **66**:352–359.

88. Hartwell LH, Mortimer RK, Culotti J, Culotti M: **GENETIC CONTROL OF THE CELL DIVISION CYCLE IN YEAST: V. GENETIC ANALYSIS OF *cdc* MUTANTS**. *Genetics* 1973, **74**:267–286.

89. Weiss E, Winey M: **The Saccharomyces cerevisiae spindle pole body duplication gene MPS1 is part of a mitotic checkpoint**. *Journal of Cell Biology* 1996, **132**:111–123.

90. Maciejowski J, George KA, Terret ME, Zhang C, Shokat KM, Jallepalli P V.: **Mps1 directs the assembly of Cdc20 inhibitory complexes during interphase and mitosis to control M phase timing and spindle checkpoint signaling**. *Journal of Cell Biology* 2010, **190**:89–100.

91. Schmidt JC, Kiyomitsu T, Hori T, Backer CB, Fukagawa T, Cheeseman IM: **Aurora B kinase controls the targeting of the Astrin-SKAP complex to bioriented kinetochores**. *Journal of Cell Biology* 2010, **191**:269–280.

92. Hewitt L, Tighe A, Santaguida S, White AM, Jones CD, Musacchio A, Green S, Taylor SS: **Sustained Mps1 activity is required in mitosis to recruit O-Mad2 to the Mad1-C-Mad2 core complex**. *Journal of Cell Biology* 2010, **190**:25–34.

93. Santaguida S, Tighe A, D'Alise AM, Taylor SS, Musacchio A: **Dissecting the role of MPS1 in chromosome biorientation and the spindle checkpoint through the small molecule inhibitor reversine**. *Journal of Cell Biology* 2010, **190**:73–87.

94. Shepperd LA, Meadows JC, Sochaj AM, Lancaster TC, Zou J, Buttrick GJ, Rappsilber J, Hardwick KG, Millar JBA: **Phosphodependent recruitment of Bub1 and Bub3 to Spc7/KNL1 by Mph1 kinase maintains the spindle checkpoint**. *Current Biology* 2012, **22**:891–899.

95. Yamagishi Y, Yang CH, Tanno Y, Watanabe Y: **MPS1/Mph1 phosphorylates the kinetochore protein KNL1/Spc7 to recruit SAC components**. *Nat Cell Biol* 2012, **14**:746–752.

96. London N, Ceto S, Ranish JA, Biggins S: **Phosphoregulation of Spc105 by Mps1 and PP1 regulates Bub1 localization to kinetochores**. *Current Biology* 2012, **22**:900–906.

97. Overlack K, Primorac I, Vleugel M, Krenn V, Maffini S, Hoffman I, Kops GJPL, Musacchio A: **A molecular basis for the differential roles of Bub1 and BubR1 in the spindle assembly checkpoint.** *Elife* 2014, **4**:1–24.

98. Krenn V, Overlack K, Primorac I, Van Gerwen S, Musacchio A: **KI motifs of human Knl1 enhance assembly of comprehensive spindle checkpoint complexes around MELT repeats**. *Current Biology* 2014, **24**:29–39.

99. Sironi L, Melixetian M, Faretta M, Prosperini E, Helin K, Musacchio A: **Mad2 binding to Mad1 and Cdc20, rather than oligomerization, is required for the spindle checkpoint**. *EMBO J* 2001, **20**:6371–6382.

100. Sironi L, Marina M, Knapp S, De Antoni A, Jeang J-T, Musacchio A: **Crystal structure of the tetrameric Mad1-Mad2 core complex: implications of a "safety belt" binding mechanism for the spindle checkpoint**. *EMBO J* 2002, **21**:2496–2506.

101. Rodriguez-Rodriguez JA, Lewis C, McKinley KL, Sikirzhytski V, Corona J, Maciejowski J, Khodjakov A, Cheeseman IM, Jallepalli P V.: **Distinct Roles of RZZ and Bub1-KNL1 in Mitotic Checkpoint Signaling and Kinetochore Expansion**. *Current Biology* 2018, **28**:3422-3429.e5.

102. Silió V, McAinsh AD, Millar JB: **KNL1-Bubs and RZZ Provide Two Separable Pathways for Checkpoint Activation at Human Kinetochores**. *Dev Cell* 2015, **35**:600–613.

103. Qian J, García-Gimeno MA, Beullens M, Manzione MG, Van der Hoeven G, Igual JC, Heredia M, Sanz P, Gelens L, Bollen M: **An Attachment-Independent Biochemical Timer of the Spindle Assembly Checkpoint**. *Mol Cell* 2017, **68**:715–730.

104. Ji Z, Gao H, Jia L, Li B, Yu H: **A sequential multi-target Mps1 phosphorylation cascade promotes spindle checkpoint signaling**. *Elife* 2017, **6**:1–23.

105. Zhang G, Kruse T, López-Méndez B, Sylvestersen KB, Garvanska DH, Schopper S, Nielsen ML, Nilsson J: **Bub1 positions Mad1 close to KNL1 MELT repeats to promote checkpoint signalling**. *Nat Commun* 2017, **8**.

106. London N, Biggins S: **Mad1 kinetochore recruitment by Mps1-mediated phosphorylation of Bub1 signals the spindle checkpoint**. *Genes Dev* 2014, **28**:140–152.

107. Hardwick KG, Weiss E, Luca FC, Winey M, Murray AW: **Activation of the budding yeast spindle assembly checkpoint without mitotic spindle disruption**. *Science (1979)* 1996, **273**:953–956.

108. DiFiore B, Davey NE, Hagting A, Izawa D, Mansfeld J, Gibson TJ, Pines J: **The ABBA Motif binds APC/C activators and is shared by APC/C substrates and regulators**. *Dev Cell* 2015, **32**:358–372.

109. Piano V, Alex A, Stege P, Maffini S, Stoppiello GA, Huis in ’t Veld PJ, Vetter IR, Musacchio A: **CDC20 assists its catalytic incorporation in the mitotic checkpoint complex**. *Science (1979)* 2021, **371**:67–71.

110. Lara-Gonzalez P, Kim T, Oegema K, Corbett K, Desai A: **A tripartite mechanism catalyzes Mad2-Cdc20 assembly at unattached kinetochores**. *Science (1979)* 2021, **371**:64–67.

111. Fischer ES, Yu CWH, Hevler JF, McLaughlin SH, Maslen SL, Heck AJR, Freund SMV, Barford D: **Juxtaposition of Bub1 and Cdc20 on phosphorylated Mad1 during catalytic mitotic checkpoint complex assembly**. *Nat Commun* 2022, **13**.

112. Faesen AC, Thanasoula M, Maffini S, Breit C, Müller F, Van Gerwen S, Bange T, Musacchio A: **Basis of catalytic assembly of the mitotic checkpoint complex**. *Nature* 2017, **542**:498–502.

113. Simonetta M, Manzoni R, Mosca R, Mapelli M, Massimiliano L: **The influence of catalysis on Mad2 activation dynamics**. *PLoS Biol* 2009, **7**:e1000010.

114. Antoni A De, Pearson CG, Cimini D, Canman JC, Sala V, Nezi L, Mapelli M, Sironi L, Faretta M, Salmon ED, et al.: **The Mad1/Mad2 Complex as a Template for Mad2 Activation in the Spindle Assembly Checkpoint**. *Current Biology* 2005, **15**:214–225.

115. Alfonso-Pérez T, Hayward D, Holder J, Gruneberg U, Barr FA: **MAD1-dependent recruitment of CDK1-CCNB1 to kinetochores promotes spindle checkpoint signaling**. *J Cell Biol* 2019, **218**:1108–1117.

116. Jackman M, Marcozzi C, Barbiero M, Pardo M, Yu L, Tyson AL, Choudhary JS, Pines J: **Cyclin B1-Cdk1 facilitates MAD1 release from the nuclear pore to ensure a Robust spindle checkpoint**. *Journal of Cell Biology* 2020, **219**.

117. Hayward D, Alfonso-Pérez T, Cundell MJ, Hopkins M, Holder J, Bancroft J, Hutter LH, Novak B, Barr FA, Gruneberg U: **CDK1-CCNB1 creates a spindle checkpoint–permissive state by enabling MPS1 kinetochore localization**. *J Cell Biol* 2019, **218**:1182–1199.

118. Wong OK, Fang G: **Cdk1 phosphorylation of BubR1 controls spindle checkpoint arrest and Plk1-mediated formation of the 3F3/2 epitope**. *J Cell Biol* 2007, **179**:611–617.

119. Qi W, Tang Z, Yu H: **Phosphorylation- and Polo-Box–dependent Binding of Plk1 to Bub1 Is Required for the Kinetochore Localization of Plk1**. *Mol Biol Cell* 2006, **17**:3705–3716.

120. Elowe S, Hümmer S, Uldschmid A, Li X, Nigg EA: **Tension-sensitive Plk1 phosphorylation on BubR1 regulates the stability of kinetochore–microtubule interactions**. *Genes Dev* 2007, **21**:2205–2219.

121. Cordeiro MH, Smith RJ, Saurin AT: **Kinetochore phosphatases suppress autonomous Polo-like kinase 1 activity to control the mitotic checkpoint**. *Journal of Cell Biology* 2020, **219**.

122. von Schubert C, Cubizolles F, Bracher JM, Sliedrecht T, Kops GJPL, Nigg EA: **Plk1 and Mps1 Cooperatively Regulate the Spindle Assembly Checkpoint in Human Cells**. *Cell Rep* 2015, **12**:66–78.

123. Ikeda M, Tanaka K: **Plk1 bound to Bub1 contributes to spindle assembly checkpoint activity during mitosis**. *Sci Rep* 2017, **7**.

124. Jelluma N, Dansen TB, Sliedrecht T, Kwiatkowski NP, Kops GJPL: **Release of Mps1 from kinetochores is crucial for timely anaphase onset**. *Journal of Cell Biology* 2010, **191**:281–290.

125. Winey M, Goetsch L, Baum P, Byers B: **MPS1 and MPS2: Novel yeast genes defining distinct steps of spindle pole body duplication**. *Journal of Cell Biology* 1991, **114**:745–754.

126. Lindberg RA, Fischer WH, Hunter T: **Characterization of a Human Protein Threonine Kinase Isolated by Screening an Expression Library with Antibodies to Phosphotyrosine**. *Oncogene* 1993, **8**:351–359.

127. Mills GB, Schmandt R, McGill M, Amendola A, Hill M, Jacobs K, May C, Rodricks AM, Campbell S, Hogg D: **Expression of TTK, a novel human protein kinase, is associated with cell proliferation**. *Journal of Biological Chemistry* 1992, **267**:16000–16006.

128. Espeut J, Lara-Gonzalez P, Sassine M, Shiau AK, Desai A, Abrieu A: **Natural Loss of Mps1 Kinase in Nematodes Uncovers a Role for Polo-like Kinase 1 in Spindle Checkpoint Initiation**. *Cell Rep* 2015, **12**:58–65.

129. Dou Z, von Schubert C, Körner R, Santamaria A, Elowe S, Nigg EA: **Quantitative Mass Spectrometry Analysis Reveals Similar Substrate Consensus Motif for Human Mps1 Kinase and Plk1**. *PLoS One* 2011, **6**:e18793.

130. Hennrich ML, Marino F, Groenewold V, Kops GJPL, Mohammed S, Heck AJR: **Universal quantitative kinase assay based on diagonal SCX chromatography and stable isotope dimethyl labeling provides high-definition kinase consensus motifs for pka and human mps1**. *J Proteome Res* 2013, **12**:2214–2224.

131. Nijenhuis W, Von Castelmur E, Littler D, De Marco V, Tromer E, Vleugel M, Van Osch MHJ, Snel B, Perrakis A, Kops GJPL: **A TPR domain-containing N-terminal module of MPS1 is required for its kinetochore localization by Aurora B**. *Journal of Cell Biology* 2013, **201**:217–231.

132. Lee S, Thebault P, Freschi L, Beaufils S, Blundell TL, Landry CR, Bolanos-Garcia VM, Elowe S: **Characterization of spindle checkpoint kinase mps1 reveals domain with functional and structural similarities to tetratricopeptide repeat motifs of Bub1 and BubR1 checkpoint kinases**. *Journal of Biological Chemistry* 2012, **287**:5988–6001.

133. Thebault P, Chirgadze DY, Dou Z, Blundell TL, Elowe S, Bolanos-Garcia VM: **Structural and functional insights into the role of the N-terminal Mps1 TPR domain in the SAC (spindle assembly checkpoint)**. *Biochemical Journal* 2012, **448**:321–328.

134. Ji Z, Gao H, Yu H: **Kinetochore attachment sensed by competitive Mps1 and microtubule binding to Ndc80C**. *Science (1979)* 2015, **348**:1260–1264.

135. Wang W, Yang Y, Gao Y, Xu Q, Wang F, Zhu S, Old W, Resing K, Ahn N, Lei M, et al.: **Structural and mechanistic insights into Mps1 kinase activation**. *J Cell Mol Med* 2009, **13**:1679–1694.

136. Stucke VM, Silljé HHW, Arnaud L, Nigg EA: **Human Mps1 kinase is required for the spindle assembly checkpoint but not for centrosome duplication**. *EMBO Journal* 2002, **21**:1723–1732.

137. Abrieu A, Magnaghi-Jaulin L, Kahana JA, Peter M, Castro A, Vigneron S, Lorca T, Cleveland DW, Labbé JC: **Mps1 is a kinetochore-associated kinase essential for the vertebrate mitotic checkpoint**. *Cell* 2001, **106**:83–93.

138. He X, Jones MH, Winey M, Sazer S: **mph1, a member of the Mps1-like family of dual specificity protein kinases, is required for the spindle checkpoint in S. pombe**. *J Cell Sci* 1998, **111**:1635–1647.

139. Fisk HA, Mattison CP, Winey M: **Human Mps1 protein kinase is required for centrosome duplication and normal mitotic progression**. *Proceedings of the National Academy of Sciences* 2003, **100**:14875–14880.

140. Stucke VM, Baumann C, Nigg EA: **Kinetochore localization and microtubule interaction of the human spindle checkpoint kinase Mps1**. *Chromosoma* 2004, **113**:1–15.

141. Schmidt M, Budirahardja Y, Klompmaker R, Medema RH: **Ablation of the spindle assembly checkpoint by a compound targeting Mps1**. *EMBO Rep* 2005, **6**:866–872.

142. Kwiatkowski N, Jelluma N, Filippakopoulos P, Soundararajan M, Manak MS, Kwon M, Choi HG, Sim T, Deveraux QL, Rottmann S, et al.: **Small-molecule kinase inhibitors provide insight into Mps1 cell cycle function**. *Nat Chem Biol* 2010, **6**:359–368.

143. Jones MH, Huneycutt BJ, Pearson CG, Zhang C, Morgan G, Shokat K, Bloom K, Winey M: **Chemical Genetics Reveals a Role for Mps1 Kinase in Kinetochore Attachment during Mitosis**. *Current Biology* 2005, **15**:160–165.

144. Jemaà M, Galluzzi L, Kepp O, Senovilla L, Brands M, Boemer U, Koppitz M, Lienau P, Prechtl S, Schulze V, et al.: **Characterization of novel MPS1 inhibitors with preclinical anticancer activity**. *Cell Death Differ* 2013, **20**:1532–1545.

145. Tighe A, Staples O, Taylor S: **Mps1 kinase activity restrains anaphase during an unperturbed mitosis and targets Mad2 to kinetochores**. *Journal of Cell Biology* 2008, **181**:893–901.

146. Kang J, Chen Y, Zhao Y, Yu H: **Autophosphorylation-dependent activation of human Mps1 is required for the spindle checkpoint**. *Proceedings of the National Academy of Sciences* 2007, **104**:20232–20237.

147. Liu S, Chan GKT, Hittle JC, Fujii G, Lees E, Yen TJ: **Human MPS1 Kinase Is Required for Mitotic Arrest Induced by the Loss of CENP-E from Kinetochores**. 2003, **14**:1638–1651.

148. Fisk HA, Winey M: **The Mouse Mps1p-like Kinase Regulates Centrosome Duplication**. *Cell* 2001, **106**:95–104.

149. Howell BJ, Moree B, Farrar EM, Stewart S, Fang G, Salmon ED: **Spindle Checkpoint Protein Dynamics at Kinetochores in Living Cells**. *Current Biology* 2004, **14**:953–964.

150. Hoffman DB, Pearson CG, Yen TJ, Howell BJ, Salmon ED: **Microtubule-dependent Changes in Assembly of Microtubule Motor Proteins and Mitotic Spindle Checkpoint Proteins at PtK1 Kinetochores**. *Mol Biol Cell* 2001, **12**:1995–2009.

151. Etemad B, Kuijt TEF, Kops GJPL: **Kinetochore-microtubule attachment is sufficient to satisfy the human spindle assembly checkpoint**. *Nat Commun* 2015, **6**:1–8.

152. Kuhn J, Dumont S: **Spindle assembly checkpoint satisfaction occurs via end-on but not lateral attachments under tension**. *Journal of Cell Biology* 2017, **216**:1533–1542.

153. Jelluma N, Brenkman AB, McLeod I, Yates JR, Cleveland DW, Medema RH, Kops GJPL: **Chromosomal instability by inefficient Mps1 auto-activation due to a weakened mitotic checkpoint and lagging chromosomes**. *PLoS One* 2008, **3**:1–8.

154. Mattison CP, Old WM, Steiner E, Huneycutt BJ, Resing KA, Ahn NG, Winey M: **Mps1 activation loop autophosphorylation enhances kinase activity**. *Journal of Biological Chemistry* 2007, **282**:30553–30561.

155. Hayward D, Bancroft J, Mangat D, Alfonso-Pérez T, Dugdale S, McCarthy J, Barr FA, Gruneberg U: **Checkpoint signaling and error correction require regulation of the MPS1 T-loop by PP2A-B56**. *J Cell Biol* 2019, **218**:3188–3199.

156. Saurin AT, Van Der Waal MS, Medema RH, Lens SMA, Kops GJPL: **Aurora B potentiates Mps1 activation to ensure rapid checkpoint establishment at the onset of mitosis**. *Nat Commun* 2011, **2**.

157. Santaguida S, Vernieri C, Villa F, Ciliberto A, Musacchio A: **Evidence that Aurora B is implicated in spindle checkpoint signalling independently of error correction**. *EMBO Journal* 2011, **30**:1508–1519.

158. Suijkerbuijk SJE, Vleugel M, Teixeira A, Kops GJPL: **Integration of Kinase and Phosphatase Activities by BUBR1 Ensures Formation of Stable Kinetochore-Microtubule Attachments**. *Dev Cell* 2012, **23**:745–755.

159. Kruse T, Zhang G, Larsen MSY, Lischetti T, Streicher W, Nielsen TK, Bjørn SP, Nilsson J: **Direct binding between BubR1 and B56-PP2A phosphatase complexes regulate mitotic progression**. *J Cell Sci* 2013, **126**:1086–1092.

160. Espert A, Uluocak P, Bastos RN, Mangat D, Graab P, Gruneberg U: **PP2A-B56 opposes Mps1 phosphorylation of Knl1 and thereby promotes spindle assembly checkpoint silencing**. *Journal of Cell Biology* 2014, **206**:833–842.

161. Liu D, Vleugel M, Backer CB, Hori T, Fukagawa T, Cheeseman IM, Lampson MA: **Regulated targeting of protein phosphatase 1 to the outer kinetochore by KNL1 opposes Aurora B kinase**. *Journal of Cell Biology* 2010, **188**:809–820.

162. Nijenhuis W, Vallardi G, Teixeira A, Kops GJPL, Saurin AT: **Negative feedback at kinetochores underlies a responsive spindle checkpoint signal**. *Nat Cell Biol* 2014, **16**:1257–1264.

163. Martin-Lluesma S, Stucke VM, Nigg EA: **Role of Hec1 in Spindle Checkpoint Signaling and Kinetochore Recruitment of Mad1/Mad2**. *Science (1979)* 2002, **297**:2267–2270.

164. Hiruma Y, Sacristan C, Pachis ST, Adamopoulos A, Kuijt T, Ubbink M, Von Castelmur E, Perrakis A, Kops GJPL: **Competition between MPS1 and microtubules at kinetochores regulates spindle checkpoint signaling**. *Science (1979)* 2015, **348**:1264–1267.

165. Dou Z, Liu X, Wang W, Zhu T, Wang X, Xu L, Abrieu A, Fu C, Hill DL, Yao X: **Dynamic localization of Mps1 kinase to kinetochores is essential for accurate spindle microtubule attachment**. *Proceedings of the National Academy of Sciences* 2015, **112**:E4546–E4555.

166. Pachis ST, Hiruma Y, Tromer EC, Perrakis A, Kops GJPL: **Interactions between N-terminal Modules in MPS1 Enable Spindle Checkpoint Silencing**. *Cell Rep* 2019, **26**:2101–2112.

167. Combes G, Barysz H, Garand C, Gama Braga L, Alharbi I, Thebault P, Murakami L, Bryne DP, Stankovic S, Eyers PA, et al.: **Mps1 Phosphorylates Its N-Terminal Extension to Relieve Autoinhibition and Activate the Spindle Assembly Checkpoint**. *Current Biology* 2018, **28**:872–883.

168. Zhu T, Dou Z, Qin B, Jin C, Wang X, Xu L, Wang Z, Zhu L, Liu F, Gao X, et al.: **Phosphorylation of microtubule-binding protein hec1 by mitotic kinase aurora b specifies spindle checkpoint kinase mps1 signaling at the kinetochore**. *Journal of Biological Chemistry* 2013, **288**:36149–36159.

169. Daub H, Olsen J V., Bairlein M, Gnad F, Oppermann FS, Körner R, Greff Z, Kéri G, Stemmann O, Mann M: **Kinase-Selective Enrichment Enables Quantitative Phosphoproteomics of the Kinome across the Cell Cycle**. *Mol Cell* 2008, **31**:438–448.

170. Tyler RK, Chu MLH, Johnson H, McKenzie EA, Gaskell SJ, Eyers PA: **Phosphoregulation of human Mps1 kinase**. *Biochemical Journal* 2009, **417**:173–181.

171. Wang X, Yu H, Xu L, Zhu T, Zheng F, Fu C, Wang Z, Dou Z: **Dynamic Autophosphorylation of Mps1 Kinase Is Required for Faithful Mitotic Progression**. *PLoS One* 2014, **9**:e104723.

172. Koch LB, Opoku KN, Deng Y, Barber A, Littleton AJ, London N, Biggins S: **Autophosphorylation is sufficient to release Mps1 kinase from native kinetochores**. 2019, doi:10.1073/pnas.1901653116.

173. Xu P, Raetz EA, Kitagawa M, Virshup DM, Lee SH: **BUBR1 recruits PP2A via the B56 family of targeting subunits to promote chromosome congression**. *Biol Open* 2013, **2**:479–486.

174. Kruse T, Zhang G, Larsen MSY, Lischetti T, Streicher W, Nielsen TK, Bjørn SP, Nilsson J: **Direct binding between BubR1 and B56-PP2A phosphatase complexes regulate mitotic progression**. *J Cell Sci* 2013, **126**:1086–1092.

175. Alfieri C, Chang L, Barford D: **Mechanism for remodelling of the cell cycle checkpoint protein MAD2 by the ATPase TRIP13**. *Nature* 2018, **559**:274–278.

176. Eytan E, Wang K, Miniowitz-Shemtov S, Sitry-Shevah D, Kaisari S, Yen TJ, Liu ST, Hershko A: **Disassembly of mitotic checkpoint complexes by the joint action of the AAA-ATPase TRIP13 and p31comet**. *Proc Natl Acad Sci U S A* 2014, **111**:12019–12024.

177. Westhorpe FG, Tighe A, Lara-Gonzalez P, Taylor SS: **p31 comet-mediated extraction of Mad2 from the MCC promotes efficient mitotic exit**. *J Cell Sci* 2011, **124**:3905–3916.

178. Xia G, Luo X, Habu T, Rizo J, Matsumoto T, Yu H: **Conformation-specific binding of p31comet antagonizes the function of Mad2 in the spindle checkpoint**. *EMBO Journal* 2004, **23**:3133–3143.

179. Wang K, Sturt-Gillespie B, Hittle JC, Macdonald D, Chan GK, Yen TJ, Liu ST: **Thyroid hormone receptor interacting protein 13 (TRIP13) AAA-ATPase is a novel mitotic checkpoint-silencing protein**. *Journal of Biological Chemistry* 2014, **289**:23928–23937.

180. Yoo TY, Choi JM, Conway W, Yu CH, Pappu R V., Needleman DJ: **Measuring NDC80 binding reveals the molecular basis of tension-dependent kinetochore-microtubule attachments**. *Elife* 2018, **7**:1–34.

181. Vázquez-Novelle MD, Petronczki M: **Relocation of the chromosomal passenger complex prevents mitotic checkpoint engagement at anaphase**. *Current Biology* 2010, **20**:1402–1407.

182. Koch LB, Opoku KN, Deng Y, Barber A, Littleton AJ, London N, Biggins S, Asbury CL: **Autophosphorylation is sufficient to release Mps1 kinase from native kinetochores**. *Proc Natl Acad Sci U S A* 2019, **116**:17355–17360.

183. Howell BJ, McEwen BF, Canman JC, Hoffman DB, Farrar EM, Rieder CL, Salmon ED: **Cytoplasmic dynein/dynactin drives kinetochore protein transport to the spindle poles and has a role in mitotic spindle checkpoint inactivation**. *Journal of Cell Biology* 2001, **155**:1159–1172.

184. Wojcik E, Basto R, Serr M, Scaërou F, Karess R, Hays T: **Kinetochore dynein: its dynamics and role in the transport of the Rough deal checkpoint protein**. *Nat Cell Biol* 2001, **3**:1001–1007.

185. Gassmann R, Holland AJ, Varma D, Wan X, Çivril F, Cleveland DW, Oegema K, Salmon ED, Desai A: **Removal of Spindly from microtubule-attached kinetochores controls spindle checkpoint silencing in human cells**. *Genes Dev* 2010, **24**:957–971.

186. Maresca TJ, Salmon ED: **Intrakinetochore stretch is associated with changes in kinetochore phosphorylation and spindle assembly checkpoint activity**. *Journal of Cell Biology* 2009, **184**:373–381.

187. Uchida KSK, Takagaki K, Kumada K, Hirayama Y, Noda T, Hirota T: **Kinetochore stretching inactivates the spindle assembly checkpoint**. *Journal of Cell Biology* 2009, **184**:383–390.

188. Wan X, O'Quinn RP, Pierce HL, Joglekar AP, Gall WE, DeLuca JG, Carroll CW, Liu ST, Yen TJ, McEwen BF, et al.: **Protein Architecture of the Human Kinetochore Microtubule Attachment Site**. *Cell* 2009, **137**:672–684.

189. Tauchman EC, Boehm FJ, DeLuca JG: **Stable kinetochore–microtubule attachment is sufficient to silence the spindle assembly checkpoint in human cells**. *Nat Commun* 2015, **6**:10036.

190. Magidson V, He J, Ault JG, O'Connell CB, Yang N, Tikhonenko I, McEwen BF, Sui H, Khodjakov A: **Unattached kinetochores rather than intrakinetochore tension arrest mitosis in taxol-treated cells**. *Journal of Cell Biology* 2016, **212**:307–319.

191. Aravamudhan P, Goldfarb AA, Joglekar AP: **The kinetochore encodes a mechanical switch to disrupt spindle assembly checkpoint signalling**. *Nat Cell Biol* 2015, **17**:868–879.

192. Roscioli E, Germanova TE, Smith CA, Embacher PA, Erent M, Thompson AI, Burroughs NJ, McAinsh AD: **Ensemble-Level Organization of Human Kinetochores and Evidence for Distinct Tension and Attachment Sensors**. *Cell Rep* 2020, **31**:107535.

193. Kufer TA, Silljé HHW, Körner R, Gruss OJ, Meraldi P, Nigg EA: **Human TPX2 is required for targeting Aurora-A kinase to the spindle**. *J Cell Biol* 2002, **158**:617–623.

194. Carmena M, Wheelock M, Funabiki H, Earnshaw WC: **The chromosomal passenger complex (CPC): from easy rider to the godfather of mitosis**. *Nat Rev Mol Cell Biol* 2012, **13**:789–803.

195. Kimmins S, Crosio C, Kotaja N, Hirayama J, Monaco L, Höög C, van Duin M, Gossen JA, Sassone-Corsi P: **Differential Functions of the Aurora-B and Aurora-C Kinases in Mammalian Spermatogenesis**. *Molecular Endocrinology* 2007, **21**:726–739.

196. Tang C-JC, Lin C-Y, Tang TK: **Dynamic localization and functional implications of Aurora-C kinase during male mouse meiosis**. *Dev Biol* 2006, **290**:398–410.

197. Sessa F, Mapelli M, Ciferri C, Tarricone C, Areces LB, Schneider TR, Stukenberg PT, Musacchio A: **Mechanism of Aurora B Activation by INCENP and Inhibition by Hesperadin**. *Mol Cell* 2005, **18**:379–391.

198. Klein UR, Nigg EA, Gruneberg U: **Centromere targeting of the chromosomal passenger complex requires a ternary subcomplex of borealin, survivin, and the N-terminal domain of INCENP**. *Mol Biol Cell* 2006, **17**:2547–2558.

199. Jeyaprakash AA, Klein UR, Lindner D, Ebert J, Nigg EA, Conti E: **Structure of a Survivin-Borealin-INCENP Core Complex Reveals How Chromosomal Passengers Travel Together**. *Cell* 2007, **131**:271–285.

200. Kelly AE, Ghenoiu C, Xue JZ, Zierhut C, Kimura H, Funabiki H: **Survivin Reads Phosphorylated Histone H3 Threonine 3 to Activate the Mitotic Kinase Aurora B**. *Science (1979)* 2010, **330**:235–239.

201. Wang F, Dai J, Daum JR, Niedzialkowska E, Banerjee B, Stukenberg PT, Gorbsky GJ, Higgins JMG: **Histone H3 Thr-3 Phosphorylation by Haspin Positions Aurora B at Centromeres in Mitosis**. *Science (1979)* 2010, **330**:231–235.

202. Yamagishi Y, Honda T, Tanno Y, Watanabe Y: **Two Histone Marks Establish the Inner Centromere and Chromosome Bi-Orientation**. *Science (1979)* 2010, **330**:239–243.

203. Tsukahara T, Tanno Y, Watanabe Y: **Phosphorylation of the CPC by Cdk1 promotes chromosome bi-orientation**. *Nature* 2010, **467**:719–723.

204. Kawashima SA, Yamagishi Y, Honda T, Ishiguro K, Watanabe Y: **Phosphorylation of H2A by Bub1 Prevents Chromosomal Instability Through Localizing Shugoshin**. *Science (1979)* 2010, **327**:172–177.

205. Serena M, Bastos RN, Elliott PR, Barr FA: **Molecular basis of MKLP2-dependent Aurora B transport from chromatin to the anaphase central spindle**. *Journal of Cell Biology* 2020, **219**.

206. Wheelock MS, Wynne DJ, Tseng BS, Funabiki H: **Dual recognition of chromatin and microtubules by INCENP is important for mitotic progression**. *Journal of Cell Biology* 2017, **216**:925–941.

207. Gruneberg U, Neef R, Honda R, Nigg EA, Barr FA: **Relocation of Aurora B from centromeres to the central spindle at the metaphase to anaphase transition requires MKlp2**. *J Cell Biol* 2004, **166**:167–172.

208. Dietz R: **Multiple Geschlechtschromosomen bei den cypriden Ostracoden, ihre Evolution und ihr Teilungsverhalten**. *Chromosoma* 1957, **9**:359–440.

209. Nicklas RB, Koch CA: **CHROMOSOME MICROMANIPULATION**. *J Cell Biol* 1969, **43**:40–50.

210. Tanaka TU, Rachidi N, Janke C, Pereira G, Galova M, Schiebel E, Stark MJR, Nasmyth K: **Evidence that the Ipl1-Sli15 (Aurora Kinase-INCENP) complex promotes chromosome bi-orientation by altering kinetochore-spindle pole connections**. *Cell* 2002, **108**:317–329.

211. Hauf S, Cole RW, LaTerra S, Zimmer C, Schnapp G, Walter R, Heckel A, Van Meel J, Rieder CL, Peters JM: **The small molecule Hesperadin reveals a role for Aurora B in correcting kinetochore-microtubule attachment and in maintaining the spindle assembly checkpoint**. *Journal of Cell Biology* 2003, **161**:281–294.

212. Welburn JPI, Vleugel M, Liu D, Yates JR, Lampson MA, Fukagawa T, Cheeseman IM: **Aurora B Phosphorylates Spatially Distinct Targets to Differentially Regulate the Kinetochore-Microtubule Interface**. *Mol Cell* 2010, **38**:383–392.

213. Cheeseman IM, Anderson S, Jwa M, Green EM, Kang J-S, Yates Iii JR, Chan CSM, Drubin DG, Barnes G: **Phospho-Regulation of Kinetochore-Microtubule Attachments by the Aurora Kinase Ipl1p will require the identification of any remaining kineto-chore proteins. Given the central role that kinetochore-microtubule**. *Cell* 2002, **111**:163–172.

214. DeLuca JG, Gall WE, Ciferri C, Cimini D, Musacchio A, Salmon ED: **Kinetochore Microtubule Dynamics and Attachment Stability Are Regulated by Hec1**. *Cell* 2006, **127**:969–982.

215. Miller SA, Johnson ML, Stukenberg PT: **Kinetochore Attachments Require an Interaction between Unstructured Tails on Microtubules and Ndc80Hec1**. *Current Biology* 2008, **18**:1785–1791.

216. Guimaraes GJ, Dong Y, McEwen BF, DeLuca JG: **Kinetochore-Microtubule Attachment Relies on the Disordered N-Terminal Tail Domain of Hec1**. *Current Biology* 2008, **18**:1778–1784.

217. Liu D, Vader G, Vromans MJM, Lampson MA, Lens SMA: **Sensing Chromosome Bi-Orientation by Spatial Separation of Aurora B Kinase from Kinetochore Substrates**. *Science (1979)* 2009, **323**:1350–1353.

218. Lampson MA, Cheeseman IM: **Sensing centromere tension: Aurora B and the regulation of kinetochore function**. *Trends Cell Biol* 2011, **21**:133–140.

219. McVey SL, Cosby JK, Nannas NJ: **Aurora b tension sensing mechanisms in the kinetochore ensure accurate chromosome segregation**. *Int J Mol Sci* 2021, **22**.

220. Akiyoshi B, Sarangapani KK, Powers AF, Nelson CR, Reichow SL, Arellano-Santoyo H, Gonen T, Ranish JA, Asbury CL, Biggins S: **Tension directly stabilizes reconstituted kinetochore-microtubule attachments**. *Nature* 2010, **468**:576–579.

221. Tanaka TU: **Bi-orienting chromosomes: acrobatics on the mitotic spindle**. *Chromosoma* 2008, **117**:521–533.

222. Baumann C, Körner R, Hofmann K, Nigg EA: **PICH, a Centromere-Associated SNF2 Family ATPase, Is Regulated by Plk1 and Required for the Spindle Checkpoint**. *Cell* 2007, **128**:101–114.

223. Taveras C, Liu C, Mao Y: **A tension-independent mechanism reduces Aurora B-mediated phosphorylation upon microtubule capture by CENP-E at the kinetochore**. *Cell Cycle* 2019, **18**:1349–1363.

224. Sandall S, Severin F, McLeod IX, Yates JR, Oegema K, Hyman A, Desai A: **A Bir1-Sli15 Complex Connects Centromeres to Microtubules and Is Required to Sense Kinetochore Tension**. *Cell* 2006, **127**:1179–1191.

225. Asai Y, Matsumura R, Hasumi Y, Susumu H, Nagata K, Watanabe Y, Terada Y: **SET/TAF1 forms a distance-dependent feedback loop with Aurora B and Bub1 as a tension sensor at centromeres**. *Sci Rep* 2020, **10**:15653.

226. Asai Y, Fukuchi K, Tanno Y, Koitabashi-Kiyozuka S, Kiyozuka T, Noda Y, Matsumura R, Koizumi T, Watanabe A, Nagata K, et al.: **Aurora B kinase activity is regulated by SET/TAF1 on Sgo2 at the inner centromere**. *Journal of Cell Biology* 2019, **218**:3223–3236.

227. Broad AJ, DeLuca KF, DeLuca JG: **Aurora B kinase is recruited to multiple discrete kinetochore and centromere regions in human cells**. *Journal of Cell Biology* 2020, **219**.

228. Hadders MA, Hindriksen S, Truong MA, Mhaskar AN, Pepijn Wopken J, Vromans MJM, Lens SMA: **Untangling the contribution of Haspin and Bub1 to Aurora B function during mitosis**. *Journal of Cell Biology* 2020, **219**.

229. Broad AJ, DeLuca JG: **The right place at the right time: Aurora B kinase localization to centromeres and kinetochores**. *Essays Biochem* 2020, **64**:299–311.

230. Maure JF, Kitamura E, Tanaka TU: **Mps1 Kinase Promotes Sister-Kinetochore Bi-orientation by a Tension-Dependent Mechanism**. *Current Biology* 2007, **17**:2175–2182.

231. Jelluma N, Brenkman AB, van den Broek NJF, Cruijsen CWA, van Osch MHJ, Lens SMA, Medema RH, Kops GJPL: **Mps1 Phosphorylates**

Borealin to Control Aurora B Activity and Chromosome Alignment. *Cell* 2008, **132**:233–246.

232. Kapoor TM, Mayer TU, Coughlin ML, Mitchison TJ: **Probing Spindle Assembly Mechanisms with Monastrol, a Small Molecule Inhibitor of the Mitotic Kinesin, Eg5**. *J Cell Biol* 2000, **150**:975–988.

233. Khodjakov A, Copenagle L, Gordon MB, Compton DA, Kapoor TM: **Minus-end capture of preformed kinetochore fibers contributes to spindle morphogenesis**. *J Cell Biol* 2003, **160**:671–683.

234. Lampson MA, Renduchitala K, Khodjakov A, Kapoor TM: **Correcting improper chromosomes-spindle attachments during cell division**. *Nat Cell Biol* 2004, **6**:232–237.

235. Maciejowski J, Drechsler H, Grundner-Culemann K, Ballister ER, Rodriguez-Rodriguez JA, Rodriguez-Bravo V, Jones MJK, Foley E, Lampson MA, Daub H, et al.: **Mps1 Regulates Kinetochore-Microtubule Attachment Stability via the Ska Complex to Ensure Error-Free Chromosome Segregation**. *Dev Cell* 2017, **41**:143-156.e6.

236. Zhang Q, Sivakumar S, Chen Y, Gao H, Yang L, Yuan Z, Yu H, Liu H: **Ska3 Phosphorylated by Cdk1 Binds Ndc80 and Recruits Ska to Kinetochores to Promote Mitotic Progression**. *Current Biology* 2017, **27**:1477-1484.e4.

237. Helgeson LA, Zelter A, Riffle M, MacCoss MJ, Asbury CL, Davis TN: **Human Ska complex and Ndc80 complex interact to form a load-bearing assembly that strengthens kinetochore–microtubule attachments**. *Proc Natl Acad Sci U S A* 2018, **115**:2740–2745.

238. Gaitanos TN, Santamaria A, Jeyaprakash AA, Wang B, Conti E, Nigg EA: **Stable kinetochore-microtubule interactions depend on the Ska complex and its new component Ska3/C13Orf3**. *EMBO Journal* 2009, **28**:1442–1452.

239. Cheerambathur DK, Prevo B, Hattersley N, Lewellyn L, Corbett KD, Oegema K, Desai A: **Dephosphorylation of the Ndc80 Tail Stabilizes Kinetochore-Microtubule Attachments via the Ska Complex**. *Dev Cell* 2017, **41**:424-437.e4.

240. Thein KH, Kleylein-Sohn J, Nigg EA, Gruneberg U: **Astrin is required for the maintenance of sister chromatid cohesion and centrosome integrity**. *Journal of Cell Biology* 2007, **178**:345–354.

241. Kern DM, Monda JK, Su K-C, Wilson-Kubalek EM, Cheeseman IM: **Astrin-SKAP complex reconstitution reveals its kinetochore interaction with microtubule-bound Ndc80**. *Elife* 2017, **6**.

242. Dunsch AK, Linnane E, Barr FA, Gruneberg U: **The astrin-kinastrin/SKAP complex localizes to microtubule plus ends and facilitates chromosome alignment**. *Journal of Cell Biology* 2011, **192**:959–968.

243. Manning AL, Bakhoum SF, Maffini S, Correia-Melo C, Maiato H, Compton DA: **CLASP1, astrin and Kif2b form a molecular switch that regulates kinetochore-microtubule dynamics to promote mitotic progression and fidelity**. *EMBO Journal* 2010, **29**:3531–3543.

244. Foley EA, Maldonado M, Kapoor TM: **Formation of stable attachments between kinetochores and microtubules depends on the B56-PP2A phosphatase**. *Nat Cell Biol* 2011, **13**:1265–1271.

245. Conti D, Song X, Shrestha RL, Braun D, Draviam VM: **Cells protect chromosome-microtubule attachments, independent of biorientation, using an Astrin-PP1 and CyclinB-CDK1 feedback loop**. *bioRxiv* 2020,

246. Alfonso-Pérez T, Hayward D, Holder J, Gruneberg U, Barr FA: **MAD1-dependent recruitment of CDK1-CCNB1 to kinetochores promotes spindle checkpoint signaling**. *J Cell Biol* 2019, **218**:1108–1117.

247. Hayward D, Bancroft J, Mangat D, Alfonso-Pérez T, Dugdale S, McCarthy J, Barr FA, Gruneberg U: **Checkpoint signaling and error correction require regulation of the MPS1 T-loop by PP2A-B56**. *J Cell Biol* 2019, **218**:3188–3199.

248. Tighe A, Johnson VL, Taylor SS: **Truncating APC mutations have dominant effects on proliferation, spindle checkpoint control, survival and chromosome stability**. *J Cell Sci* 2004, **117**:6339–6353.

249. Ballister ER, Riegman M, Lampson MA: **Recruitment of Mad1 to metaphase kinetochores is sufficient to reactivate the mitotic checkpoint.** *J Cell Biol* 2014, **204**:901–8.

250. Natsume T, Kiyomitsu T, Saga Y, Kanemaki MT: **Rapid Protein Depletion in Human Cells by Auxin-Inducible Degron Tagging with Short Homology Donors**. *Cell Rep* 2016, **15**:210–218.

251. Schindelin J, Arganda-Carreras I, Frise E, Kaynig V, Longair M, Pietzsch T, Preibisch S, Rueden C, Saalfeld S, Schmid B, et al.: **Fiji: an open-source platform for biological-image analysis.** *Nat Methods* 2012, **9**:676–82.

252. Li CH, Lee CK: **Minimum cross entropy thresholding**. *Pattern Recognit* 1993, **26**:617–625.

253. RStudio Team: **RStudio: Integrated Development Environment for R**. 2015,

254. Wickham H, Averick M, Bryan J, Chang W, McGowan L, François R, Grolemund G, Hayes A, Henry L, Hester J, et al.: **Welcome to the Tidyverse**. *J Open Source Softw* 2019, **4**:1686.

255. Kuhn J, Dumont S: **Mammalian kinetochores count attached microtubules in a sensitive and switch-like manner**. *J Cell Biol* 2019, **218**:3583–3596.

256. Rieder CL: **The Structure of the Cold-stable Kinetochore Fiber in Metaphase PtK1 Cells**. *Chromosoma (Berl)* 1981, **84**:145–158.

257. De Brabander MJ, Van de Veire RM, Aerts FE, Borgers M, Janssen PA: **The effects of methyl (5-(2-thienylcarbonyl)-1H-benzimidazol-2-yl) carbamate, (R 17934; NSC 238159), a new synthetic antitumoral drug interfering with microtubules, on mammalian cells cultured in vitro.** *Cancer Res* 1976, **36**:905–16.

258. Rock KL, Gramm C, Rothstein L, Clark K, Stein R, Dick L, Hwang D, Goldberg AL: **Inhibitors of the proteasome block the degradation of most cell proteins and the generation of peptides presented on MHC class I molecules**. *Cell* 1994, **78**:761–771.

259. Skoufias DA, DeBonis S, Saoudi Y, Lebeau L, Crevel I, Cross R, Wade RH, Hackney D, Kozielski F: **S-trityl-L-cysteine is a reversible, tight binding inhibitor of the human kinesin Eg5 that specifically blocks mitotic progression.** *J Biol Chem* 2006, **281**:17559–69.

260. Wang X, Yu H, Xu L, Zhu T, Zheng F, Fu C, Wang Z, Dou Z: **Dynamic Autophosphorylation of Mps1 Kinase Is Required for Faithful Mitotic Progression**. *PLoS One* 2014, **9**:e104723.

261. Hsu J-Y, Sun Z-W, Li X, Reuben M, Tatchell K, Bishop DK, Grushcow JM, Brame CJ, Caldwell JA, Hunt DF, et al.: **Mitotic Phosphorylation of Histone H3 Is Governed by Ipl1/aurora Kinase and Glc7/PP1 Phosphatase in Budding Yeast and Nematodes**. *Cell* 2000, **102**:279–291.

262. Kawashima SA, Yamagishi Y, Honda T, Ishiguro K, Watanabe Y: **Phosphorylation of H2A by Bub1 prevents chromosomal instability through localizing shugoshin.** *Science* 2010, **327**:172–7.

263. Bonner MK, Haase J, Saunders H, Gupta H, Li BI, Kelly AE: **The Borealin dimerization domain interacts with Sgo1 to drive Aurora B-mediated spindle assembly.** *Mol Biol Cell* 2020, **31**:2207–2218.

264. Chen C, Whitney IP, Banerjee A, Sacristan C, Sekhri P, Kern DM, Fontan A, Kops GJPL, Tyson JJ, Cheeseman IM, et al.: **Ectopic Activation of the Spindle Assembly Checkpoint Signaling Cascade Reveals Its Biochemical Design**. *Current Biology* 2019, **29**:104-119.e10.

265. Qian X, McDonald A, Zhou H-J, Adams ND, Parrish CA, Duffy KJ, Fitch DM, Tedesco R, Ashcraft LW, Yao B, et al.: **Discovery of the First Potent and Selective Inhibitor of Centromere-Associated Protein E: GSK923295.** *ACS Med Chem Lett* 2010, **1**:30–4.

266. Silljé HHW, Nagel S, Körner R, Nigg EA: **HURP is a Ran-importin beta-regulated protein that stabilizes kinetochore microtubules in the vicinity of chromosomes.** *Curr Biol* 2006, **16**:731–42.

267. Sobajima T, Kowalczyk KM, Skylakakis S, Hayward D, Fulcher LJ, Neary C, Batley C, Kurlekar S, Roberts E, Gruneberg U, et al.: **PP6 regulation of**

Aurora A–TPX2 limits NDC80 phosphorylation and mitotic spindle size. *Journal of Cell Biology* 2023, **222**.

268. DeLuca KF, Meppelink A, Broad AJ, Mick JE, Peersen OB, Pektas S, Lens SMA, DeLuca JG: **Aurora A kinase phosphorylates Hec1 to regulate metaphase kinetochore-microtubule dynamics**. *Journal of Cell Biology* 2018, **217**:163–177.

269. Matsuda A, Schermelleh L, Hirano Y, Haraguchi T, Hiraoka Y: **Accurate and fiducial-marker-free correction for three-dimensional chromatic shift in biological fluorescence microscopy**. *Sci Rep* 2018, **8**:7583.

270. Matsuda A, Koujin T, Schermelleh L, Haraguchi T, Hiraoka Y: **High-Accuracy Correction of 3D Chromatic Shifts in the Age of Super-Resolution Biological Imaging Using Chromagnon**. *Journal of Visualized Experiments* 2020, doi:10.3791/60800.

271. Gambarotto D, Zwettler FU, Le Guennec M, Schmidt-Cernohorska M, Fortun D, Borgers S, Heine J, Schloetel J-G, Reuss M, Unser M, et al.: **Imaging cellular ultrastructures using expansion microscopy (U-ExM)**. *Nat Methods* 2019, **16**:71–74.

272. Schmidt JC, Arthanari H, Boeszoermenyi A, Dashkevich NM, Wilson-Kubalek EM, Monnier N, Markus M, Oberer M, Milligan RA, Bathe M, et al.: **The Kinetochore-Bound Ska1 Complex Tracks Depolymerizing Microtubules and Binds to Curved Protofilaments**. *Dev Cell* 2012, **23**:968–980.

273. Chen GY, Renda F, Zhang H, Gokden A, Wu DZ, Chenoweth DM, Khodjakov A, Lampson MA: **Tension promotes kinetochore–microtubule release by aurora B kinase**. *Journal of Cell Biology* 2021, **220**.

274. Maciejowski J, Drechsler H, Grundner-Culemann K, Ballister ER, Rodriguez-Rodriguez JA, Rodriguez-Bravo V, Jones MJK, Foley E, Lampson MA, Daub H, et al.: **Mps1 Regulates Kinetochore-Microtubule Attachment Stability via the Ska Complex to Ensure Error-Free Chromosome Segregation**. *Dev Cell* 2017, **41**:143-156.e6.

275. Bancroft J, Holder J, Geraghty Z, Alfonso-Pérez T, Murphy D, Barr FA, Gruneberg U: **PP1 promotes cyclin b destruction and the metaphase-anaphase transition by dephosphorylating cdc20**. *Mol Biol Cell* 2020, **31**:2315–2330.